

PULSATING FLOW OF NON-NEWTONIAN FLUIDS IN PIPES

by

© ESSAME E.F. EL-SAYED, B.Sc.(Eng.), M.Sc. (Eng.)

A Thesis

Submitted to the School of Graduate Studies
in Partial Fulfillment of the Requirements

for the Degree

Doctor of Philosophy

McMaster University

February 1984

PULSATING FLOW OF NON-NEWTONIAN FLUIDS IN PIPES

DOCTOR OF PHILOSOPHY (1984)
(Mechanical Engineering)

McMaster University
Hamilton, Ontario

TITLE: Pulsating Flow of Non-Newtonian Fluids in Pipes

AUTHOR: Essam E.F. El-Sayed, B.Sc., M.Sc.(Eng.) (Al-Azhar University)

SUPERVISOR: Dr. G.F. Round

NUMBER OF PAGES xvii, 211

ABSTRACT

The first part of this thesis contains a theoretical formulation and solution for unsteady flows (pulsatile and start-up flows) of non-Newtonian time-independent fluids through rigid pipes. The approach was based on the use of the equation of motion for axisymmetric unsteady flow of fluids in cylindrical coordinates. In the case of pulsating flow, the unsteady behaviour of the pressure gradient was considered to be described by a periodic function of time, of sinusoidal form, added to a stationary pressure gradient, while for start-up flow the fluid was assumed to start its transient motion from rest due to instantaneous and sudden imposition of a stationary pressure gradient. The constitutive equation of generalized Bingham fluids was used since it represents the majority of time-independent fluids.

A grid was imposed on the flow field in order to obtain a system of equations in finite difference form. The use of finite difference techniques provided detailed information about the time deformation of the pulsating and start-up velocity profiles as well as valuable information about energy consumption and flowrates under different pulsating flow conditions. The results are presented in the most general form so that they are widely applicable to any case where the assumptions and the boundary conditions are all satisfied. The main conclusion which can be drawn from the theoretical results is that the hydraulic power required to transport a fluid in pulsating flow is never less than that required for the same flowrate under steady flow conditions for all fluids except those which exhibit yield stress, i.e., Bingham fluids.

On the experimental side, an investigation of pulsating flow of solid-liquid mixtures is presented. Solid-liquid mixtures are divided into two types, homogeneous suspensions and pseudohomogeneous/heterogeneous slurries. The terms homogeneous and pseudohomogeneous are used when solids concentration gradient along pipe vertical axis is

constant for homogeneous flows and almost constant for pseudohomogeneous flows; while the term heterogeneous represents the cases where appreciable solids gradient along pipe vertical axis exists.

The experiments were carried out for two types of solid-liquid mixtures. The first was a bentonite clay-water suspension with weight concentration ranges from 2.97% to 11.2%, while the second has coal/water slurry with weight concentrations between 5.34% - 53.7%.

The main aim of the experimental rig was to create a sinusoidal pressure gradient. The experimental set-up allowed different ranges of different flow parameters to be adopted, these were:

1. Pulsing frequency ranging between 0-1.25 Hz.
2. Pulsing amplitude (axial deformation of rubber bellows) of 34.6, 52.1 and 76.2 mm.
3. Average flow velocity at 1.63, 2.18, and 2.63 m/sec.

The effect of different combinations of these parameters on the ratio of the hydraulic power in pulsating flow to that in steady flow for the same throughput was studied.

ACKNOWLEDGEMENTS

The author wishes to express his sincere gratitude and indebtedness to his supervisor, Dr. G.F. Round, whose helpful advice, valuable discussions and continuous encouragement made the completion of this work possible..

Thanks are extended to the men of the McMaster University Machine Shop for the construction of the test rig.

For his assistance during the construction of the microcomputer, Mr. J. Verhaeghe receives the author's deepest gratitude.

Thanks also are due to the McMaster University Engineering Word Processing Centre for typing the manuscript.

The financial support provided by the Natural Sciences and Engineering Research Council of Canada is acknowledged.

Finally, I would like to express my special appreciation to my wife Kefah for her support and encouragement during this work.

LIST OF CONTENTS

	<u>Page</u>
Abstract	iii
Acknowledgements	v
List of Contents	vi
List of Figures	ix
List of Tables	xiv
Nomenclature	xv
Chapter 1 INTRODUCTION	1
Chapter 2 LITERATURE REVIEW	6
2.1 Introduction	6
2.2 Steady Flow of Homogeneous Non-Newtonian Fluids	7
2.3 Unsteady (Pulsatile and Oscillatory) Flow of Newtonian and Non-Newtonian Fluids	11
2.3.1 Pulsatile Flow of Newtonian Fluids	11
2.3.2 Pulsatile Flow of Non-Newtonian Fluids	26
2.4 Steady Flow of Heterogeneous Slurries	29
2.5 Pulsatile Flow of Heterogeneous Slurries	34
Chapter 3 SCOPE OF INVESTIGATION	39
Chapter 4 A THEORETICAL TREATMENT OF UNSTEADY LAMINAR FLOWS IN PIPES USING A GENERALIZED BINGHAM MODEL	41
4.1 Introduction	41
4.2 Derivation of Steady Flow Correlation	42

4.3	Velocity Distribution in Steady Laminar Flow	50
4.4	Mathematical Formulation for Unsteady Laminar Flow	52
4.4.1	Governing Equations	52
4.4.2	Determination of Flow Patterns	53
4.4.3	Determination of Flowrate	58
4.4.4	Determination of Power Requirements	59
4.5	Finite Difference Formulation	61
Chapter 5 EXPERIMENTAL PROCEDURE		63
5.1	Introduction	63
5.2	Description of the Installation	64
5.2.1	The Pipeline	64
5.2.2	Steady Flow System	66
5.2.3	Pulsing Equipment	66
5.2.4	Measuring Instrumentation and the Microcomputer	69
5.3	Bentonite Clay-Water Suspension	70
5.4	Coal-Water Slurry	73
5.5	Calibration of Measuring Instruments	73
5.5.1	Calibration of Pressure Transducer	78
5.5.2	Calibration of Flowmeter	78
5.6	Programming the Microcomputer	81
5.7	Experimental Procedures	81
Chapter 6 RESULTS OF FINITE DIFFERENCE SOLUTION AND DISCUSSION		84
6.1	Pulsating Flow	84
6.1.1	Velocity Profiles	84
6.1.2	Flowrates	93
6.1.3	Hydraulic Power Requirements	97
6.1.4	Phase Angles	99
6.2	Start-up Flow	99

Chapter 7	EXPERIMENTAL RESULTS AND DISCUSSION	105
7.1	Bentonite Clay-Water Suspension	105
7.1.1	Pulsing Frequency and Pulsing Amplitude	105
7.1.2	Effect of Solids Concentration	117
7.1.3	Effect of Average Flow Velocity	118
7.2	Coal-Water Slurry	121
7.2.1	Effect of Pulsing Frequency	122
7.2.2	Effect of Pulsing Amplitude	133
7.2.3	Effect of Average Flow Velocity	134
7.2.4	Effect of Solids Concentration	135
7.3	Limitations	138
Chapter 8	CONCLUSIONS AND RECOMMENDATIONS	140
8.1	Conclusions	140
8.2	Suggestions for Further Studies	143
	REFERENCES	146
APPENDIX A	DETAILS OF PULSING EQUIPMENT	152
APPENDIX B	PULSATING FLOW DATA OF BENTONITE CLAY-WATER SUSPENSION	158
APPENDIX C	PULSATING FLOW DATA OF COAL-WATER SLURRY	170
APPENDIX D	COMPUTER PROGRAM FOR FINITE DIFFERENCE CALCULATIONS	195
APPENDIX E	MICROCOMPUTER PROGRAM FOR EXPERIMENTAL DETERMINATION OF HYDRAULIC POWER	208
APPENDIX F	ERROR ANALYSIS OF EXPERIMENTAL DATA	211

LIST OF FIGURES

<u>Figure</u>	<u>Title</u>	<u>Page</u>
2.1	Pressure gradient vs. flow velocity for homogeneous suspensions	8
2.2	Transitions of velocity profiles for pulsating flows. From Muto and Nakane [37].	16
2.3	Critical Reynolds number vs. dimensionless velocity. From Gilbrech and Combs [42].	18
2.4	Critical Reynolds number vs. velocity amplitude for various values of frequency parameter α (harmonic oscillation). From Sarpkaya [44].	19
2.5	Comparison of measured with theoretical results in an oscillating pipe flow (Run 1). From Ohmi and Iguchi [51].	24
2.6	Comparison of measured with theoretical results in an oscillating pipe flow (Run 2). From Ohmi and Iguchi [51].	25
2.7	Comparison of measured with theoretical results in an oscillating pipe flow (Run 3). From Ohmi and Iguchi [51].	25
2.8	Increase of flowrate by pulsations for aqueous solutions of polyacrylamide. From Barnes <u>et al.</u> [1].	27
2.9	Velocity profiles - numerical and experimental results for sodium carboxymethylcellulose concentration 0.5%. From Bousquet <u>et al.</u> [53].	30
2.10	Velocity profiles - numerical and experimental results for sodium carboxymethylcellulose concentration 1%. From Bousquet <u>et al.</u> [53].	30
2.11	Increase in flowrate at different pulsing frequencies for visco- elastic fluid. From Walters and Townsend [2].	31
2.12	Pressure gradient vs. flow velocity for heterogeneous slurries.	36
2.13	Formation of particle-free layer in pulsating flow of heterogeneous slurries.	36
2.14	Ratio of hydraulic energy of pulsating flow to that of steady flow as a function of pulsing frequency for sand-water slurries. From Round [5].	38
4.1	τ - $\dot{\gamma}$ relation for a generalized Bingham fluid.	43

4.2	Flow of a Bingham fluid in a circular pipe.	43
4.3	Solution of equation (4.12) - for $n = 0.5, 1.0, 1.5$ and 2.0 .	47
4.4	Comparison of experimental data for laminar flow with equation (4.12). Top bracketed data from ref. [9]; bottom bracketed data from ref. [86].	48
4.5	Finite difference network.	62
5.1	Schematic diagram of experimental pipe loop.	65
5.2	Schematic diagram of pulse generating mechanism.	68
5.3	Shear stress vs. shear rate for bentonite clay-water suspensions at different solids weight concentrations (obtained by Haake viscometer).	71
5.4	Coal particle size distribution.	74
5.5	Photomicrograph of a coal sample.	75
5.6	Pressure transducer calibration curve.	79
5.7	Flowmeter calibration curve.	80
6.1	Theoretical predictions of velocity profiles for pulsating flows of (a) Newtonian, (b) power law $n = 0.7$, (c) ideal Bingham $\tau_0/\tau_w = 0.32$. Results at $\zeta = 5.0$ and $\epsilon = 1$.	85
6.1cont.	(d) generalized Bingham $n = 0.7$ and $\tau_0/\tau_w = 0.32$, (e) ideal Bingham $\tau_0/\tau_w = 0.44$, (f) generalized Bingham $n = 0.7$ and $\tau_0/\tau_w = 0.44$. Results at $\zeta = 5.0$ and $\epsilon = 1$.	86
6.2	Theoretical predictions of velocity profiles for pulsating flows of an ideal Bingham fluid at different frequencies. (a) $\zeta = 4.0$, (b) $\zeta = 7.0$, (c) $\zeta = 10$ Results at $\tau_0/\tau_w = 0.44$ and $\epsilon = 1$.	89
6.3	Theoretical predictions of velocity profiles for pulsating flows of a generalized Bingham fluid at different frequencies. (a) $\zeta = 4.0$, (b) $\zeta = 7.0$, (c) $\zeta = 10$ Results at $n = 0.7$, $\tau_0/\tau_w = 0.44$ and $\epsilon = 1$.	90

6.4	Theoretical predictions of velocity profiles for pulsating flows of a generalized Bingham fluid at different amplitudes. (a) $\varepsilon = 0.5$, (b) $\varepsilon = 1.$, (c) $\varepsilon = 1.5$, (d) $\varepsilon = 2$. Results at $n = 0.7$, $\tau_0/\tau_w = 0.32$ and $\zeta = 7$.	92
6.5	Theoretical predictions of dimensionless pulsating flowrates S vs. dimensionless frequency ζ ($\varepsilon = 1$).	94
6.6	Theoretical predictions of dimensionless pulsating hydraulic power requirements E vs. dimensionless frequency ζ ($\varepsilon = 1$).	96
6.7	Theoretical predictions of phase angle ϕ vs. dimensionless frequency ζ ($\varepsilon = 1$).	98
6.8	Theoretical predictions of velocity profiles for start-up flow for a Newtonian (middle) and two-power law fluids $n = 0.7$ (bottom) and 1.4 (top).	100
6.9	Theoretical predictions of velocity profiles for start-up flow for an ideal Bingham (top) and a generalized Bingham fluid (bottom), $\tau_0/\tau_w = 0.32$, $n = 0.7$.	101
6.10	Theoretical predictions of velocity profiles for start-up flow for an ideal Bingham (top) and a generalized Bingham fluid (bottom), $\tau_0/\tau_w = 0.44$, $n = 0.7$.	102
6.11	Velocity development as a function of dimensionless time T on the pipe centerline for start-up flows of Newtonian and non-Newtonian fluids.	104
7.1	Output signals from the pressure transducer at different pulsing frequencies ($A = 52.1$ mm)	106
7.2	Hydraulic power ratio of pulsating to steady flow vs. pulsing frequency. Experimental results for bentonite clay-water suspension ($C_w = 2.97\%$).	109
7.3	Hydraulic power ratio of pulsating to steady flow vs. dimensionless velocity amplitude. Experimental results for bentonite clay-water suspension ($C_w = 2.97\%$).	110
7.4	Hydraulic power ratio of pulsating to steady flow vs. pulsing frequency. Experimental results for bentonite clay-water suspension ($C_w = 4.47\%$).	111

7.5	Hydraulic power ratio of pulsating to steady flow vs. dimensionless velocity amplitude. Experimental results for bentonite clay-water suspension ($C_w = 4.47\%$).	112
7.6	Hydraulic power ratio of pulsating to steady flow vs. pulsing frequency. Experimental results for bentonite clay-water suspension ($C_w = 7.63\%$).	113
7.7	Hydraulic power ratio of pulsating to steady flow vs. dimensionless velocity amplitude. Experimental results for bentonite clay-water suspension ($C_w = 7.63\%$).	114
7.8	Hydraulic power ratio of pulsating to steady flow vs. pulsing frequency. Experimental results for bentonite clay-water suspension ($C_w = 11.2\%$).	115
7.9	Hydraulic power ratio of pulsating to steady flow vs. dimensionless velocity amplitude. Experimental results for bentonite clay-water suspension ($C_w = 11.2\%$).	116
7.10	Hydraulic power ratio of pulsating to steady flow vs. pulsing frequency. Experimental results for coal-water slurry ($C_w = 5.34\%$).	124
7.11	Hydraulic power ratio of pulsating to steady flow vs. pulsing frequency. Experimental results for coal-water slurry ($C_w = 8.9\%$).	125
7.12	Hydraulic power ratio of pulsating to steady flow vs. pulsing frequency. Experimental results for coal-water slurry ($C_w = 14.25\%$).	126
7.13	Hydraulic power ratio of pulsating to steady flow vs. pulsing frequency. Experimental results for coal-water slurry ($C_w = 19.59\%$).	127
7.14	Hydraulic power ratio of pulsating to steady flow vs. pulsing frequency. Experimental results for coal-water slurry ($C_w = 24.93\%$).	128
7.15	Hydraulic power ratio of pulsating to steady flow vs. pulsing frequency. Experimental results for coal-water slurry ($C_w = 30.27\%$).	129
7.16	Hydraulic power ratio of pulsating to steady flow vs. pulsing frequency. Experimental results for coal-water slurry ($C_w = 37.5\%$).	130

7.17	Hydraulic power ratio of pulsating to steady flow vs. pulsing frequency. Experimental results for coal-water slurry ($C_w = 44.64\%$).	131
7.18	Hydraulic power ratio of pulsating to steady flow vs. pulsing frequency. Experimental results for coal-water slurry ($C_w = 53.7\%$).	132
7.19	Hydraulic power ratio of pulsating to steady flow vs. solids weight concentration. Experimental results for coal-water slurry. Experimental results at pulsing amplitude $A = 34.6$ mm, average flow velocity $V = 1.63$ m/s and pulsing frequency $\lambda = 0.3$ Hz.	136

LIST OF TABLES

	<u>TableTitle</u>	<u>Page</u>
5.1	Physical properties of bentonite clay-water suspensions at different weight concentrations.	72
5.2	Coal particle size distribution.	76
5.3	Coal chemical analysis.	77
5.4	Density of coal-water slurry at different solids weight concentrations.	77
6.1	Velocity profiles during the first six cycles for a generalized Bingham material with $n = 0.7$, $\tau_0/\tau_w = 0.32$; and at $\zeta = 10$, $\varepsilon = 1.0$.	87
7.1	Values of Reynolds number and Plasticity number at different flow velocities and solids weight concentrations.	119

NOMENCLATURE

English:

A	pulse amplitude
a	pipe radius
C_1, C_2, C_3	variable functions of n
C_v	volume solids concentration
C_w	weight solids concentration
D	bellows diameter
d	pipe diameter
E	ratio of hydraulic power in pulsating flow to that in steady flow for the same mean pressure gradient
f	pipe friction coefficient
G	ratio in equation (4.19)
g	gravity acceleration
He	Hedström number, $\tau_0 d^2 \rho / \eta_p^2$
He'	generalized Hedström number, $\tau_0 d^{2n} V^{2-2n} \rho / (K' 8^{n-1})^2$
J	hydraulic power
J_p	hydraulic power in pulsating flow
J_s	hydraulic power in steady flow
K	consistency factor for non-Newtonian fluids
K'	modified consistency factor for non-Newtonian fluids, $K(1 + 3n/4n)^n$
k	characteristic parameter, $\sqrt{\omega/N}$
L	length

M	modulus of pressure gradient, equation (2.4)
n	non-Newtonian index
P	pressure
Pe	Plasticity number, $\tau_0 d / \eta_p V$
Pe'	generalized Plasticity number, $\tau_0 d^n / K' g^{n-1} V^n$
Q	volumetric flowrate
Q_n	instantaneous flowrate of nth harmonic
Q_p	instantaneous flowrate in pulsating flow
Q_s	flowrate in steady flow
R	dimensionless radius, r/a
r	radial distance from pipe axis
r_p	solid particle mean radius
Re	Reynolds number, $V d \rho / \mu$
Re'	generalized Reynolds number, $V^{2-n} d^n \rho / K' g^{n-1}$
Re_p	particle Reynolds number, $r_p (r_p/a)^2 V \rho / \mu$
S	ratio of flowrate in pulsating flow to that in steady flow at the same mean pressure gradient
T	dimensionless time
t	time
U	dimensionless axial flow velocity, u/V
u	axial velocity, function of radius and time
u_0	oscillating axial velocity component
u_s	steady axial velocity component

V average flow velocity
 x, y, z coordinates

Greek:

α non-dimensional characteristic parameter, $a\sqrt{\omega/\nu}$
 β velocity amplitude, u_0/V
 γ shear rate, $\partial u/\partial r$
 δ particle-free layer thickness
 ϵ pressure amplitude, $(dP/dx)_0/(dP/dx)_s$
 ζ frequency parameter, $(\omega/2\pi)(d/V)Re'$
 η_p plastic viscosity
 λ frequency, Hz
 μ dynamic viscosity
 μ_a apparent viscosity
 ν kinematic viscosity
 ρ density
 ϕ phase angle
 ω angular frequency, rad/sec

CHAPTER 1

INTRODUCTION

An understanding of the characteristics of pulsating flows in closed conduits is of considerable interest in many areas of science and engineering. Examples that may be cited are the uses of pulsed flow to increase the efficiency of heat exchangers; extraction columns and interphase mass transfer in chemical reactors, studies on blood circulation in the human cardiovascular system, and hydraulic and pneumatic-control systems.

One of the major applications of pulsating flows is in fluid and fluid-solid transport. It has been recognized [1-7] that the application of controlled pulsations, that is, of specific amplitude, frequency and symmetry have beneficial effects as far as hydraulic power savings are concerned. Usually the frequencies considered in these applications are of the order of 1 Hz.

The majority of solid-liquid suspensions or slurries exhibit non-Newtonian behaviour, i.e., the shear stress is not linearly related to the rate of strain. In many cases non-Newtonian behaviour is time-independent. In some cases thixotropy and viscoelasticity cannot be ignored.

Workers in this field have used the terms homogeneous and pseudohomogeneous flow and heterogeneous flow to distinguish between different types of slurry behaviour. A criterion is required to quantify, in some manner, the point of separation between nearly homogeneous or pseudohomogeneous flow and heterogeneous flow. In a strict sense, a homogeneous flow is one which does not exhibit a measurable concentration gradient of solids along the vertical pipe axis. However, in a practical sense, a better definition would be that it refers to a flow in which the inertial effects of the suspended particles are relatively minor.

On the other hand, in heterogeneous flow the relative magnitude of the inertial forces compared with the viscous and/or the turbulent forces are large and cannot be neglected. From the preceding consideration, it follows that between the pseudo-homogeneous flow condition and the heterogeneous flow condition there is a region in which both mechanisms are of approximately equal order. In this intermediate region the system will be extremely sensitive to slight changes in flow conditions. It is, however, possible to relate flow condition, i.e., homogeneous, pseudohomogeneous, or heterogeneous to the relationship between drag coefficient and particle Reynolds number. A system whose particles are governed by Stokes law is conveyed in pseudohomogeneous flow, while a system whose particles are governed by Newton's law is markedly heterogeneous.

Homogeneous non-Newtonian suspensions are classified according to their response to the application of shear stress. The most common classification is:

- I) power law fluids;
- II) ideal Bingham fluids; and
- III) generalized Bingham fluids.

Correlations have been developed to relate the friction factor to Reynolds number in a conventional form for the first two types of fluids [8,9]. In the present thesis, however, a general correlation has been developed to apply for all three types of fluids (refer to Chapter 4 for the mathematical derivation).

As far as pulsating flow is concerned, it is believed that in homogeneous non-Newtonian suspensions; superposition of an oscillating flow component on steady flow may have beneficial effects [1, 2, 7, 10-12]. Some studies [1, 2] have shown experimentally that the flowrate can be considerably increased, for the same mean pressure gradient, by applying pulsations to the flow. Such an increase in the flowrate may be the result of a significant reduction in the apparent viscosity of the fluid due to the instantaneous high shear stress

occurring in the accelerating phase of each pulse. This reduction in the apparent viscosity occurs only if the fluid being pumped is shear thinning, i.e., if the fluid exhibits pseudo-plastic or Bingham-like behaviour.

A theoretical attack on the problem of pulsating flow using the generalized Bingham model is presented in Chapter 4. The approach is based on the assumption that the velocity gradient is zero where the shear stress is less in magnitude than the yield stress. In this approach, the pressure gradient is of sinusoidal form. The results obtained are presented in Chapter 6 in general dimensionless form so that they may apply to any case as long as the assumptions and the boundary conditions are justified.

In the mathematical treatment of the problem, presented in Chapter 4, the case of start-up flows is also included. The solution of start-up flow is important in an understanding of the phenomenon of transient flow which occurs due to sudden and instantaneous imposition of a pressure gradient.

On the other hand, the steady flow of heterogeneous slurries is a complex problem. Theoretical treatments are very limited and have many questionable assumptions. An experimental approach seems to be much more efficient and more practical since the parameters affecting heterogeneous flow are numerous and interdependent. Some of these parameters are:

1. Solid particle size distribution;
2. Solid particle shape;
3. Solid specific gravity;
4. Solid volume or weight concentration;
5. Average flow velocity;
6. Physical properties of the carrier fluid;
7. Pipe size and geometry.

One of the main objectives of the present study is to present more detailed information about the behaviour of heterogeneous slurries under pulsating flow conditions. The experimental part of the present investigation includes both homogeneous and heterogeneous types of flows. Bentonite clay-water suspension is used to typify a homogeneous non-Newtonian fluid. At high concentrations it behaves as generalized Bingham fluid. Coal-water slurry is used as a representative for heterogeneous flow. Pulse generating equipment was designed and manufactured for this particular investigation. The design allowed the pulse frequency and amplitude to be changed easily. One of the effects of superposing a controlled oscillating flow component onto steady heterogeneous flow is to enhance inward radial migration of solid particles from the pipe wall. Radial migration of solid particles has been observed in steady laminar heterogeneous flows. It has also been previously verified experimentally [13] that the rate of inward radial migration may possibly be increased by harmonically oscillating the flow. The result is the formation of a particle-free layer adjacent to the pipe wall, which acts as lubricating layer. Since the major part of hydraulic power in horizontal pipeline transport is consumed in overcoming friction between the flowing substance and the pipe wall, the formation of such a particle-free layer could be of great advantage. The reduction in local shear stress at the pipe wall due to the formation of a particle-free layer depends on the pulsing frequency, amplitude, and wave shape in combination with all the other parameters in steady heterogeneous flows. In the present study four of these parameters were investigated, these were:

1. Pulse amplitude;
2. Pulse frequency;
3. Average flow velocity;
4. Solids weight concentration.

Chapter 5 includes detailed information about the experimental instrumentation and procedure. Comparison of hydraulic power requirement in pulsating flow to that in steady flow at the same throughput demonstrates the effect of the flow parameters.

CHAPTER 2

LITERATURE REVIEW

2.1 Introduction

Steady-state incompressible viscous flow in rigid pipes is a classical problem. An exact solution can be obtained from the Navier-Stokes equations (Schlichting [14]). In such a case, there is only one controlling parameter, i.e., the Reynolds number. Both the velocity profile and the volumetric flowrate can be easily determined from the static pressure gradient at the pipe wall. The limit of applicability of the solution, or in other words, the transition from laminar to turbulent flow is well known experimentally in terms of the single parameter, Reynolds number ($Re \approx 2100$).

For the more general and also more realistic case of arbitrary, time-dependent, viscous incompressible fluid flow in rigid pipes, the situation is very different. It is much more difficult to relate instantaneous velocity profiles and the volumetric flowrate to instantaneous pressure gradient. It is also more difficult to specify the limits of applicability of the Navier-Stokes equations for such a general case.

In practice, the majority of fluids are found to be non-Newtonian. Unlike Newtonian fluids, non-Newtonian fluids respond very differently to the application of a shear stress in terms of shear rate. Moreover, in some cases, the shear stress/shear rate relation may be function of time -- as in thixotropic and/or rheopectic fluids. These fluids are excluded from consideration in the present study; but this is not a serious limitation.

It is perhaps important to state at this point that time-independent non-Newtonian fluids can be categorized as "homogeneous" and "heterogeneous". This categorization is merely used for convenience and it is not the only one in use. For

suspensions, some authors [15] prefer to differentiate between fluids with the terms "settling" and "non-settling". So-called "settling" suspensions may become nearly homogeneous or so-called "pseudo-homogeneous" under conditions of high velocity and high concentration and to behave as heterogeneous fluids at low velocity and low concentration. While it must be accepted that a truly homogeneous slurry does not exist, the fact that many suspensions closely approach homogeneity makes the pseudo-homogeneous/heterogeneous classification very convenient.

The following different cases are considered:

1. steady flows of homogeneous non-Newtonian fluids;
2. unsteady (pulsatile or oscillatory) flows of homogeneous non-Newtonian fluids;
3. steady flows of heterogeneous slurries;
4. unsteady (pulsatile or oscillatory) flows of heterogeneous slurries.

In the present chapter, a review of previous studies which have significance are summarized with emphasis on (2) and (4) above.

2.2 Steady Flow of Homogeneous Non-Newtonian Fluids

A homogeneous fluid (or suspension) is the one which does not exhibit a measurable concentration gradient of solids along the vertical axis of a pipe. In a more practical sense, it is a slurry in which the inertia of the suspended particles (the relative velocity between the suspended particles and the carrier fluid) is relatively minor and can be neglected.

A typical pressure gradient/velocity response of a homogeneous fluid (suspension) is given in Figure 2.1. In the low velocity range, the flow is laminar and the variation in the pressure gradient as a function of the velocity is a flat curve. As the velocity increases, a point is reached where the flow changes from laminar to turbulent; this point is the viscous

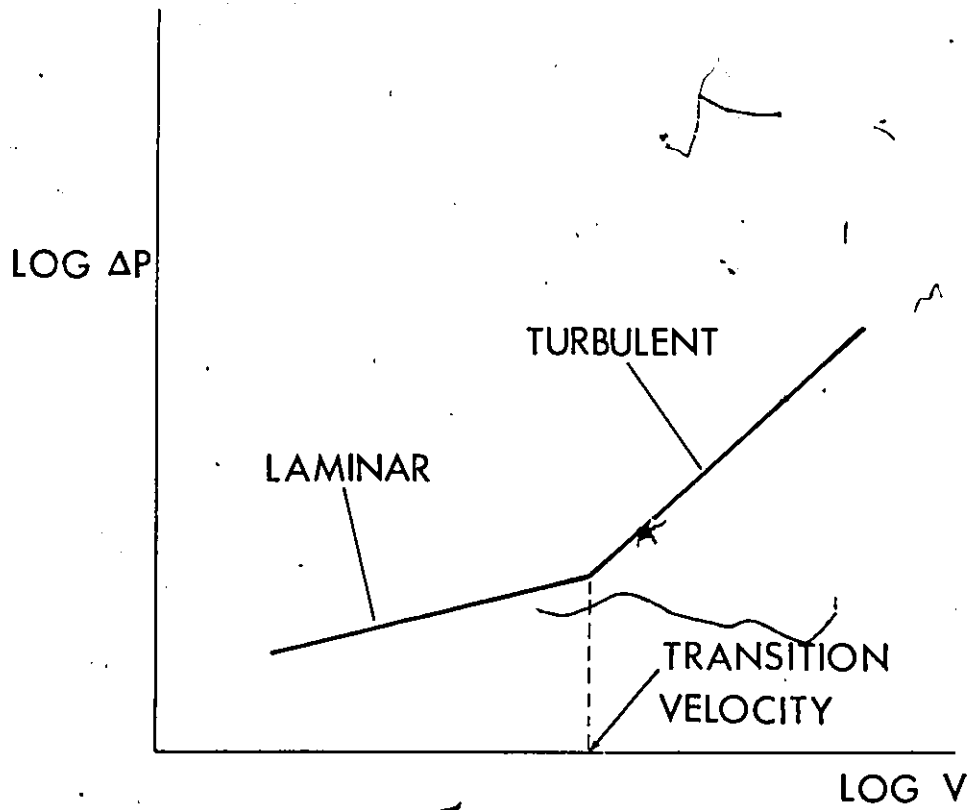


Figure 2.1 Pressure gradient vs. flow velocity for homogeneous suspensions

transition velocity. In the higher velocity range, the flow is turbulent as indicated by the steep linear curve. Prior to considering the laminar, transition and turbulent flow regimes, it is necessary to review the rheological models used in the literature to characterize the fluids concerned.

There are a large number of equations that have been developed in the past to describe the rheological behaviour of time-independent homogeneous non-Newtonian fluids.

These may conveniently be divided into three models [9, 16-21]:

- power law flow,
- ideal Bingham flow,
- generalized Bingham flow.

The power law model is the most common for representing pseudoplastics and dilatant fluids. Its form is generally

$$\tau = K \dot{\gamma}^n \quad (2.1)$$

Ideal Bingham fluids are usually represented by the idealized equation,

$$\tau = \tau_0 + \eta_p \dot{\gamma} \quad \text{when } |\tau| \geq \tau_0 \quad (2.2)$$

and

$$\dot{\gamma} = 0 \quad \text{when } |\tau| < \tau_0$$

The third model is the most general one. It can be represented by the relationship,

$$\tau = \tau_0 + K \dot{\gamma}^n \quad \text{when } |\tau| \geq \tau_0 \quad (2.3)$$

and

$$\dot{\gamma} = 0 \quad \text{when } |\tau| < \tau_0$$

These equations are known as constitutive equations. K and n are the consistency factor and the non-Newtonian index respectively. In equation(2.2), τ_0 is the yield stress of the fluid and η_p is the fluid plastic viscosity. Classification of fluids into the above is critical for certain flow conditions. It has been shown [8,22,23] that the classification into which a fluid falls, and

even the numerical values assigned its rheological properties, is dependent upon the experimental conditions under which the measurements are made. For example, under certain narrow ranges of shear rate, a given fluid may clearly appear to behave as an ideal Bingham flow; at slightly different rates of shear, the power law model may closely be followed, and at higher shear rates, the same material may appear almost Newtonian.

The consequence of the foregoing is that methods have been developed which are widely applicable to the simplification of the pressure gradient- flowrate relationships. Several attempts at generalization have been reported in the literature [17,19,24,25]. These are either limited because of their empirical nature or because they require the assumption of equations relating the fluid shear rate to the shear stress which do not always correlate fluid properties with adequate precision. Another limitation of these methods is their inability to predict the onset of turbulence accurately.

Other attempts of more significance have been reported [8,9,26,27]. For power law fluids, Metzner and Reed [8] introduced the concept and terminology of the generalized Reynolds number in order to eliminate the problem of defining an apparent viscosity for each particular flow model. Their main objective was to generalize the standard friction factor-Reynolds number correlation for all flow regimes so that it was applicable for all Newtonian and all fluids exhibiting power law behaviour. Their approach was derived from an expression given by Mooney [28] for wall shear stress. Consequently, the rheological properties needed should be related to the walls (e.g., using a capillary-tube viscometry). Hanks [29] has examined the generalized Reynolds number concept and has drawn attention to some definite limitations concerning the widespread use of the generalized Reynolds number as defined by Metzner and Reed [8].

In the case of flow of ideal Bingham plastics in pipes, exact solutions of the Buckingham equation are available due to McMillen [30] and, in particular, Hedström [9].

Hedström assumed a functional form by which he proposed two dimensionless groups. Plastic viscosity η_p and yield stress τ_0 were involved in both groups. These are known as plasticity number and Hedström number. One conclusion that was reached for the turbulent flow region was that from an experimental viewpoint, the conventional friction factor versus Reynolds number curves of purely Newtonian fluids were also applicable to ideal Bingham plastics.

A survey of the available literature indicates that no correlation has been developed for the flow of a generalized Bingham plastic. A mathematical derivation of such a correlation is included in the next chapter.

2.3 Unsteady (Pulsatile and Oscillatory) Flow of Newtonian and Non-Newtonian Fluids

An understanding of the characteristics of pulsating and oscillating flows in closed conduits has been and still is of interest to many workers in the field of fluid dynamics and hemodynamics. It is of considerable technological interest since unsteady flow in tubes and pipelines plays a major role in hydraulic and pneumatic control systems, hydrotransportation systems, blood, extracorporeal circulatory systems, and elsewhere.

2.3.1 Pulsatile Flow of Newtonian Fluids

A review of the available literature inevitably starts with Womersley's work [31]. In his analysis of pulsating flow, he applied a technique which made possible the expression of a complex wave shape in terms of a Fourier series. The Navier-Stokes equations were solved for one-dimensional incompressible viscous time-independent pipe flow by assuming a sinusoidal pressure gradient. This approach allowed the computation of the instantaneous flow rate for any complex pulse on a term-by-term basis, the sum of which was the resultant flow wave. Each component (or element) of the summation could be considered as an

individual flow problem having its own amplitude, frequency and phase, and being characterized by its own Reynolds number and Stokes number. The final form was a type of Bessel's equation where a non-dimensional characteristic parameter α was introduced. α is a function of pipe radius, frequency and fluid kinematic viscosity (proportional to square root of the Stokes number). The final form for the instantaneous flowrate is:

$$Q_n = \frac{n a^4}{\mu} \frac{M'_n}{\alpha_n^2} [(A_n \sin \phi'_n - B_n \cos \phi'_n) \cos n\omega t + (A_n \cos \phi'_n + B_n \sin \phi'_n) \sin n\omega t] \quad (2.4)$$

where

$$A_n = M \cos \phi, \text{ and}$$

$$B_n = M \sin \phi$$

are Fourier coefficients (ϕ is the phase angle of pressure gradient pulse). Tabulations of M'/α^2 and ϕ' , the phase angle complement between flow and pressure gradient, have been compiled and presented by Womersley [31] for values of α from 0 to 10 or Stokes number from 0 to 400. In addition, he derived asymptotic expressions for M' and ϕ' for values of α greater than 10. Summing the steady and pulsating flow components results in the total instantaneous flow ratio

$$\frac{Q}{Q_s} = 1 + \sum_{n=1}^n \frac{Q_n}{Q_s} \quad (2.5)$$

where

Q is the total flowrate,

Q_s is the steady (mean) flow component,

Q_n is the alternating flow component, and

n is the number of Fourier harmonics.

Uchida [32] found that the fundamental equation of motion for incompressible viscous time-dependent pipe flow could be linearized by introducing the assumption of axially parallel flow which may be allowed for in the expression of principal characteristics of

pulsating flows. By the property of linearity, elements of the periodic part of the solution were given in an identical form as that of Sexl's solution [33]. A non-dimensional expression of velocity was obtained in the form:

$$\frac{u}{V} = \frac{u_s}{V} + \frac{u_o}{V},$$

$$\frac{u_s}{V} = 2 \left(1 - \frac{r^2}{a^2} \right),$$

$$\begin{aligned} \frac{u_o}{V} = & \sum_{n=1}^{\infty} \frac{\kappa_{cn}}{\kappa_o} \left\{ \frac{8B}{(ka)^2} \cos \omega t + \frac{8(1-A)}{(ka)^2} \sin \omega t \right\} \\ & + \sum_{n=1}^{\infty} \frac{\kappa_{sn}}{\kappa_o} \left\{ \frac{8B}{(ka)^2} \sin \omega t + \frac{8(1-A)}{(ka)^2} \sin \omega t \right\} \end{aligned} \quad (2.6)$$

where

$$A = \frac{\text{ber } ka \text{ ber } kr + \text{bei } ka \text{ bei } kr}{\text{ber}^2 ka + \text{bei}^2 ka},$$

$$B = \frac{\text{bei } ka \text{ ber } kr - \text{ber } ka \text{ bei } kr}{\text{ber}^2 ka + \text{bei}^2 ka},$$

$$k = \sqrt{\frac{\omega}{\nu}}$$

The above expression corresponds to a pressure gradient of the form:

$$-\frac{2a}{\nu^2} \frac{\partial p}{\partial x} = \frac{64}{\text{Re}} \left[1 + \sum_{n=1}^{\infty} \frac{\kappa_{cn}}{\kappa_o} \cos \omega t + \sum_{n=1}^{\infty} \frac{\kappa_{sn}}{\kappa_o} \sin \omega t \right] \quad (2.7)$$

where

$$\text{Re} = \frac{2aV}{\nu},$$

κ_{c_n}/κ_0 and κ_{s_n}/κ_0 are ratios of amplitude of periodic variation of pressure gradients to that of average one, a is the pipe radius.

Uchida [32] used the above expressions to calculate the instantaneous velocity distribution, the relationship between mass flow and necessary pressure gradient, and loss of energy by dissipation caused by the components of periodic motion and must be overcome by excess work from the exterior.

On the experimental side, Lindford and Ryan [34] among other workers, using a reciprocating piston arrangement, successfully matched Womersleys [31] theory with test data at zero mean flowrate, i.e., purely sinusoidal oscillating flow, and at limited Stokes number. Because the Navier-Stokes equations are non-linear, the superposition of a steady flow affects the time-dependent solution and therefore Linford and Ryan [34] were not able to verify experimentally Womersley's theory [31]. Bettner [35] investigated sinusoidal oscillating flow; his objective was to verify experimentally the theories of Uchida [32] and Chang and Atabek [36].

Muto and Nakane [37] have studied the velocity distribution of oscillating and pulsating flow through rigid circular tubes. In their theoretical analysis, they assumed axisymmetric and parallel flow of an incompressible fluid. Using this assumption, the Navier-Stokes equations for unsteady, viscous, incompressible flow were simplified. Non-slip boundary conditions at the wall were introduced and the Laplace transform of the resulting velocity distribution was obtained. The input velocity was assumed to be the sum of a steady flow component and an oscillating flow component in the form:

$$\bar{u}(t) = V + u_0 \sin \omega t = V(1 + \beta \sin \omega t) \quad (2.8)$$

An equation which describes a velocity distribution was then derived after taking the inverse Laplace transform. The result was as follows:

$$\begin{aligned}
 U = \frac{u(r,t)}{V} = & \left[2(1-R^2) + 2 \sum_{n=1}^{\infty} \left\{ \frac{J_0(\alpha_n R) - J_0(\alpha_n)}{\alpha_n J_1(\alpha_n)} \cdot \exp\left(-\frac{\alpha_n^2 v}{a^2} t\right) \right\} \right] \\
 & + \beta \left[\left\{ \frac{J_0(i^{3/2} AR) - J_0(i^{3/2} A)}{J_2(i^{3/2} A)} e^{i\omega t} \right\} - 4 \sum_{n=1}^{\infty} \left\{ \frac{\alpha_n A^2}{\alpha_n^4 + A^4} \cdot \frac{J_0(\alpha_n R) - J_0(\alpha_n)}{J_1(\alpha_n) - J_3(\alpha_n)} \exp\left(-\frac{\alpha_n^2 \omega}{A^2} t\right) \right\} \right] \quad (2.9)
 \end{aligned}$$

where $J_0 - J_3$ are Bessel functions of the first kind, $i = \sqrt{-1}$, α_n are the successive positive roots of $J_0(\alpha) = 0$, and R , A and B are defined

$$R = \frac{r}{a}, \quad A = a\sqrt{\omega/v}, \quad \beta = \frac{u_0}{V}$$

as non-dimensional quantities, respectively. The terms in the first and second brackets on the right-hand side in equation (2.9) correspond to the steady and oscillatory flow components for the solution of pulsating flow, respectively. The first and the second terms in each bracket represent the steady-state and the transient-state solutions, respectively, which together form a total solution. Muto and Nakane [37] then analyzed the problem experimentally in the region of fully developed laminar flow. Transitions of velocity distribution with respect to time were measured by a flow-visualization method using aluminum powder suspended in the fluid. Many particle tracks were photographed for differing periods of time. The velocity distribution was then obtained by measuring the length of pathlines. A comparison between the theory and their experimental data established the validity of the theory. Figure 2.2 shows some of the results obtained by Muto and Nakane [37] for different values of the frequency parameter A and different values of velocity amplitude β according to the definitions mentioned above.

Klimes, Korenar, and Toman [38] presented a brief summary of their theoretical analysis for the problem of pulsating flow of a viscous incompressible fluid which was based on assumptions similar to those of Muto and Nakane [37]. The derived analytical expressions provided detailed information about the velocity profiles of pulsating flow. Measurements of

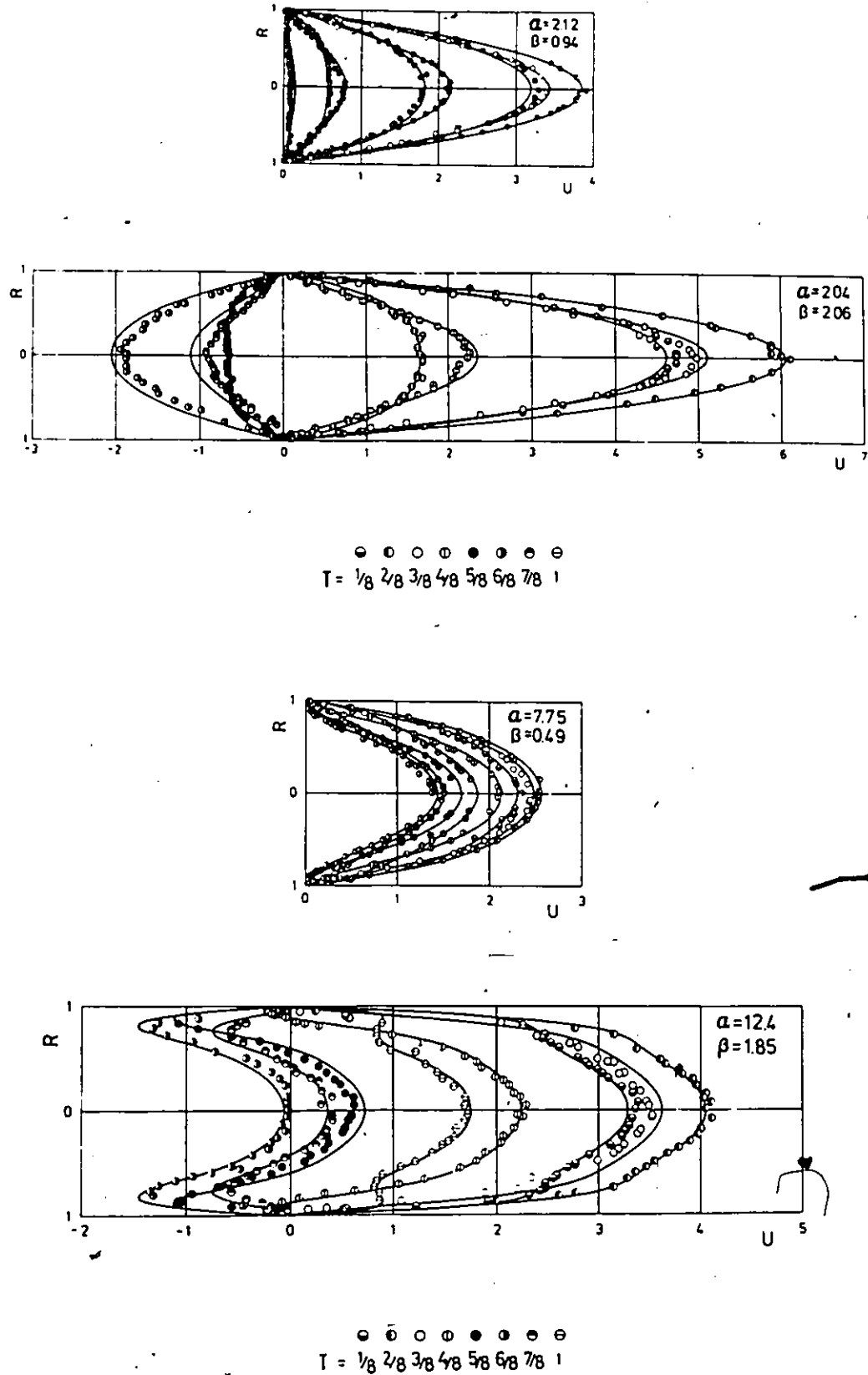


Figure 2.2 Transitions of velocity profiles for pulsating flows. From Muto and Nakane [37].

velocity profiles of oscillatory and pulsating flows by means of a Laser-Doppler Anemometer were also given. Their measurements have indicated that very good agreement between theory and experiment was achieved only at low frequencies.

So far, the majority of studies have only dealt with unsteady laminar flow. There are fewer reports dealing with unsteady turbulent flow and the transition from laminar to turbulent flow.

Binnie [39] observed the transition process by injecting a dye solution in a liquid column oscillating harmonically, but no definite conclusions have been drawn because of the limited range of the frequency parameter. Darling [40] found that the transition Reynolds number dropped from 2500 in steady flow to 1500 in pulsating flow. Kastner and Shih [41] measured the transition Reynolds number for the pulsating flow of air between two parallel flat plates and they have found a decrease in the value of the critical Reynolds number from that of steady flow. Gilbrech and Combs [42,43] investigated laminar/turbulent transition in pulsating flow. In their arrangement, they used water as the working fluid and determined the characteristics of turbulent bursts from photocell signal recordings. The experimental data indicated that critical values of the Reynolds number in pulsating flow through smooth pipes increased to a maximum and then decreased as the amplitude of the pulsations was increased. The value of the dimensionless velocity amplitude at which the maximum critical Reynolds number occurred appeared to decrease with increasing values of the frequency. This is indicated clearly in Figure 2.3, in which values of critical Reynolds number are plotted against dimensionless velocity amplitude at different values of the frequency parameter.

Sarpkaya [44] reported that for the same mean pressure gradient, the critical Reynolds numbers for pulsating flow are higher than the critical Reynolds numbers for steady Poiseuille flow. He showed that the critical Reynolds number depended on both the Stokes

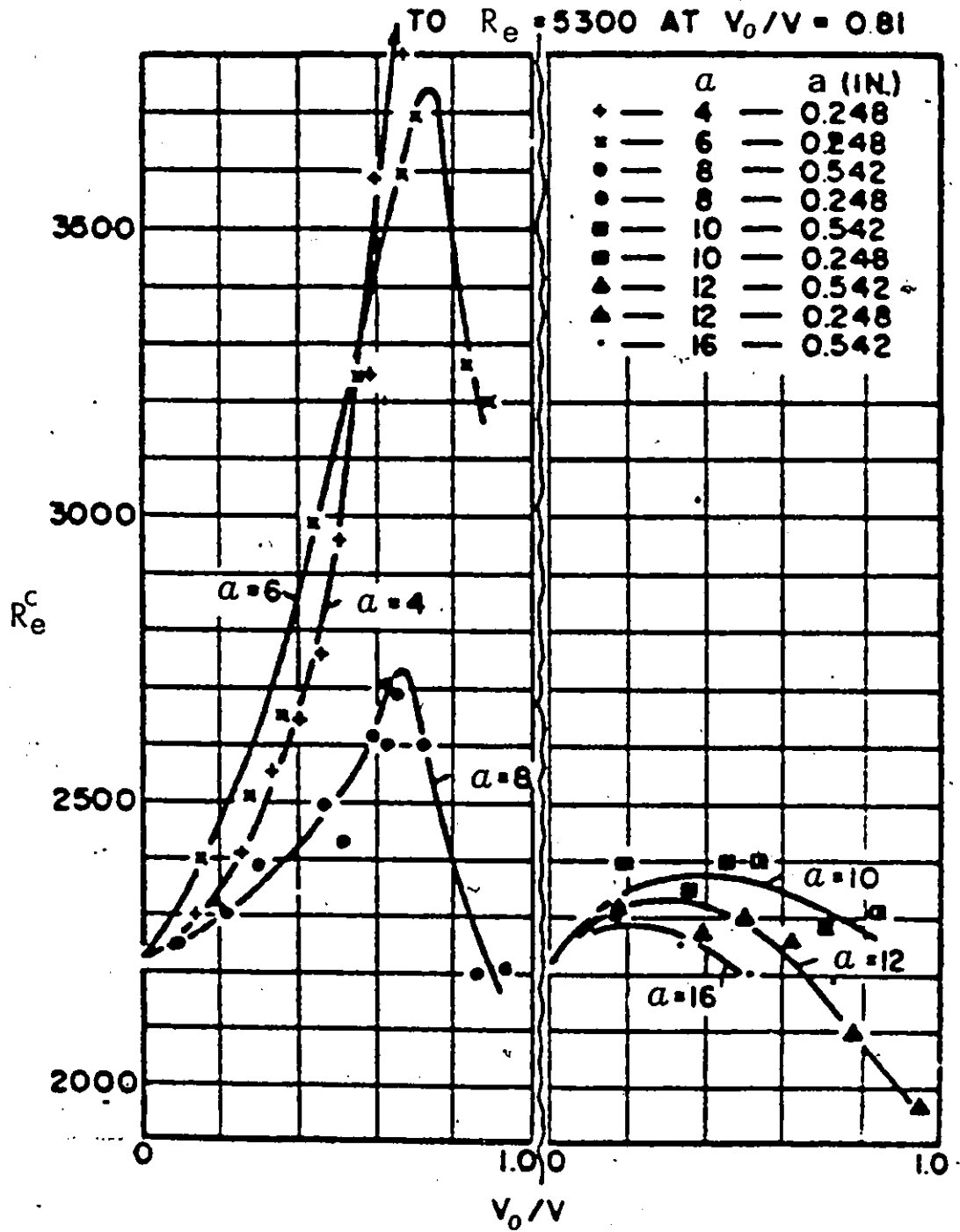


Figure 2.3

Critical Reynolds number vs. dimensionless velocity.
From Gilbrech and Combs (42).

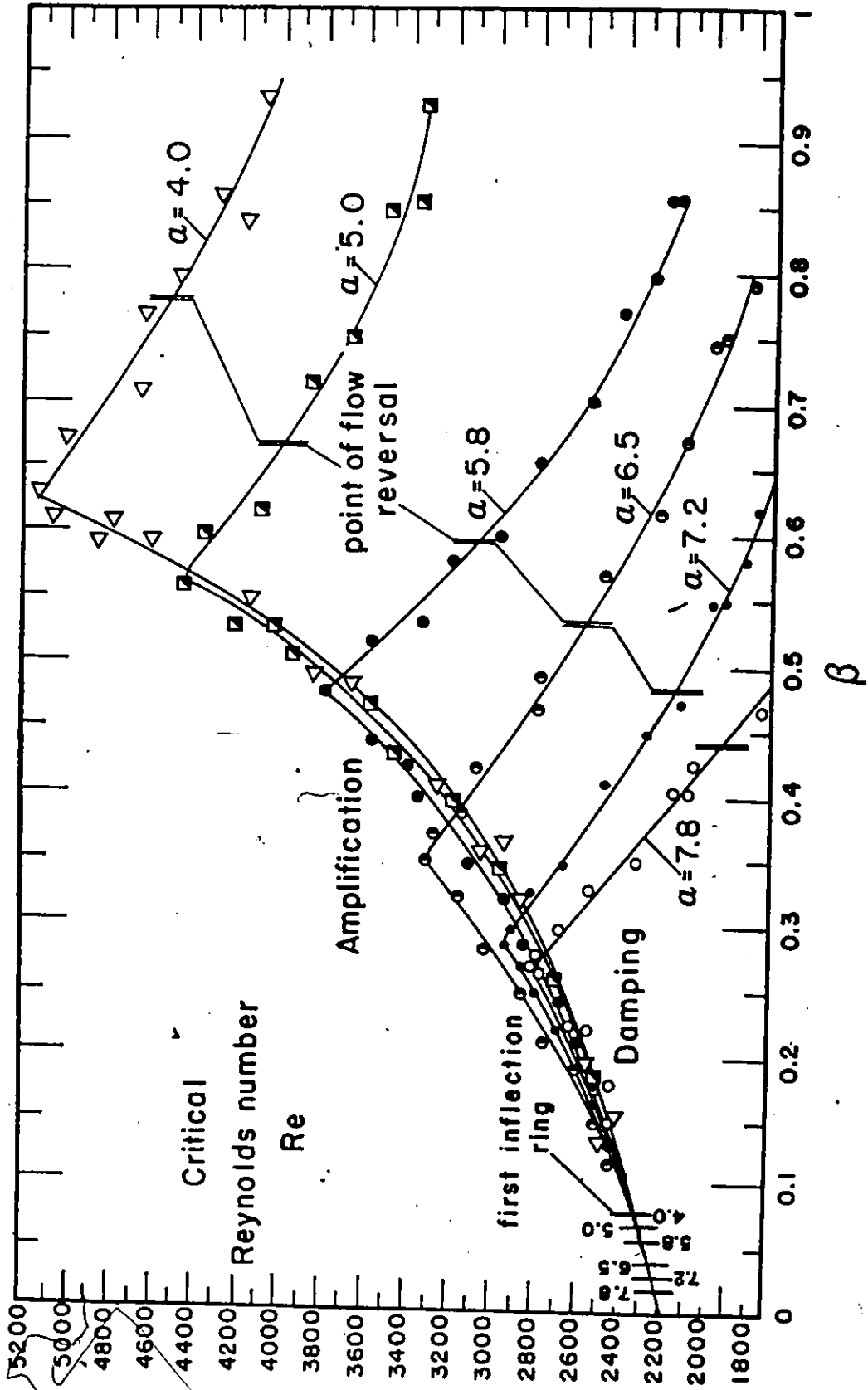


Figure 2.4 Critical Reynolds number vs. velocity amplitude for various values of frequency parameter α (harmonic oscillation).

number and on the flow velocity amplitude ratio. The main conclusion of Sarpkaya's work is that laminar flow can be maintained at much higher mean flowrates if the flow is harmonically oscillating than if the flow is steady. This conclusion can be seen in Figure 2.4.

In a recent research series by Ohmi and Iguchi [45-51], the flow patterns and friction losses in turbulent pulsating pipe flow and the transition to turbulence in pulsating pipe flow were studied in detail. In this experimental work, the oscillating component of a pulsatile flow was generated by means of a blower and a piston-crank mechanism. The experimental arrangement allowed the control of pulsation frequency and velocity amplitude. The velocity measurements were made by using a hot wire anemometer probe radially movable. The pressure drop measurements were made with two semiconductor-type transducers placed at two ends of the test section.

The effect of pulsation frequency on the turbulent flow pattern and on the turbulent frictional losses were studied. The pulsating turbulent pipe flow was measured at a time-averaged value of Reynolds number of about 5.7×10^4 and over wide ranges of both frequency and velocity amplitude. The momentum balance equation was obtained by integrating the cross-sectional mean equation of motion for the incompressible fluid in a pipe over a certain length which was given in the form:

$$\rho \frac{dv}{dt} + \frac{2}{a} \tau_w = \frac{\Delta P}{L} \quad (2.10)$$

A finite Fourier expansion was applied to the experimental waveforms of the pressure gradient, the cross-sectional mean velocity, and the wall shear stress. In order to evaluate the individual terms in the momentum balance equation, quantitatively, four characteristic parameters describing the flow pattern in a pulsating flow were introduced. The flow patterns were classified into three types: quasi-steady, intermediate, and inertia-dominant with respect to the dimensionless frequency level. According to Ohmi and Iguchi [46], the instantaneous friction factor and the quasi-steady friction factor were almost equal in the

quasi-steady region. As the dimensionless frequency increased, the instantaneous friction factor became smaller than the quasi-steady friction factor in the first part and larger in the rest of the accelerating phase, this was reversed over the decelerating phase. In addition, the time-averaged friction factor, as a function of dimensionless frequency; time-averaged Reynolds number; and velocity amplitude, was larger than the steady flow friction factor at the same time-averaged mean cross-sectional velocity. The experimental values compared favourably with their estimated values.

In the fourth and fifth reports, Ohmi and Iguchi [48,49] continued their study on flow patterns and frictional losses as well as the transition to turbulence but for an oscillating pipe flow. In order to clarify the flow patterns and the frictional losses in an oscillating pipe flow, velocity and pressure drop were measured as before. According to their observations, they suggested a flow classification into five regions with respect to Reynolds number. These are:

- (I) laminar flow;
- (II) small amplitude perturbations appear in the early stage of accelerating phase at the central portion of the pipe;
- (III) small amplitude perturbations exist in the higher velocity phase;
- (IV) turbulent bursts occur in the decelerating phase; and
- (V) turbulent bursts occur in the accelerating phase as well as in the decelerating phase.

The limits between the second and third regions were not well defined. Also, the limit between the fourth and the fifth region was not clear either. On the other hand, the limits between first two regions and between regions III and IV were found to be in good agreement with other workers. Furthermore, when Reynolds number based on the amplitude of the cross-sectional mean velocity is larger than the critical Reynolds number (indicating the limit

above which turbulent bursts occur, i.e. when the flow is in region IV or V), turbulence appears most of the time except at the early stage of the accelerating phase and the last stage of the decelerating phase. At the phase when turbulence appears, the instantaneous velocity distribution was found to follow the 1/7 power law.

The last two reports of research series by Ohmi and Iguchi [50,51] provide more information about the transition to turbulence in a pulsating pipe flow and also in some way in an oscillating pipe flow. In these two reports, a solution for the transient laminar pulsatile pipe flow was obtained by first considering the equation of motion of an incompressible fluid in a fully developed laminar unsteady pipe flow. A Laplace transformation was performed with initial conditions of zero axial velocity and the boundary conditions of zero velocity at the pipe wall and zero radial velocity gradient at the pipe centreline. The cross-sectional mean velocity was expressed in the form:

$$V(t) = 0 \quad t < 0$$

$$V(t) = V(A + \beta \sin \omega t) \quad t \geq 0$$
(2.11)

where $A = 0$ for oscillating pipe flow and $A = 1$ for a pulsating pipe flow. This equation was substituted into the equation of motion and the inverse transformation of the resulting expression yielded

$$\frac{u}{V} = 2(1 - R^2)(A + \beta \sin \omega t) + \sum_{i=1}^{\infty} \frac{4}{\alpha_i^2} \left[\frac{J_0(\alpha_i R)}{J_0(\alpha_i)} - 1 \right] \left\{ \frac{\beta \frac{a^2 \omega}{v} \alpha_i^2}{\alpha_i^4 + \frac{a^4 \omega^2}{v^2}} \cos \omega t \right.$$

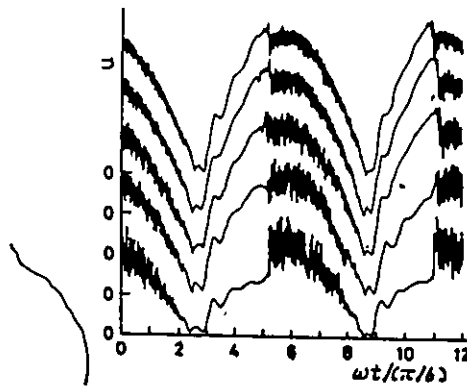
$$\left. + \frac{\beta \frac{a^2 \omega}{v}}{\alpha_i^4 + \frac{a^4 \omega^2}{v^2}} \sin \omega t + \left[A - \frac{\beta \frac{a^2 \omega}{v} \alpha_i^2}{\alpha_i^4 + \frac{a^4 \omega^2}{v^2}} \right] e^{-\frac{\alpha_i^2 vt}{a^2}} \right\}$$
(2.12)

where α_i is the i th zero of the first kind of Bessel function of order 2. The wall shear stress was given by

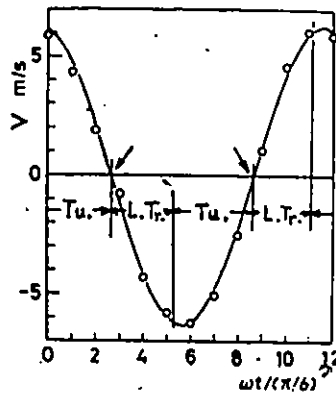
$$\tau_w = -\mu \left(\frac{\partial u}{\partial r} \right)_{r=a}$$

where $(\partial u / \partial r)_{r=a}$ could be obtained from equation (2.12). The measurements were made over a range of time-averaged Reynolds number from 0 up to about 2.4×10^4 . Some interesting observations were reported. These included the observation, that in a pulsating flow which did not only alter its direction but also was accompanied by a relaminarization in one cycle, the fluid began to accelerate under the laminar state from rest at the same time over the whole cross-section of the pipe and suddenly bursts of turbulence occurred. Such a series of events were observed in every cycle. This phenomenon was significant in purely oscillating pipe flow with zero mean component as well as in pulsating flow in which reversal and relaminarization of flow were taking place in one cycle. Accordingly, in such cases, the velocity distribution in the phase where turbulence did not appear could be well represented by the solution for transient pulsatile laminar pipe flow, i.e. equation (2.12), while in the phase where turbulence occurred, it was well represented by the 1/7 power law. There was also a case observed in which the axial velocity vanished at nearly the same time over the whole pipe cross-section. This case was also noticed in the theoretical solution for Bingham fluids given in the present work. This point will be discussed later in Chapter 6. Figures 2.5 to 2.7 are examples of the results obtained by Ohmi and Iguchi [51]. Oscillating flows accompanied by the occurrence of turbulence bursts in the decelerating phase on the velocity wave forms are shown at three different dimensionless frequencies. The velocity waveforms, the cross-sectional mean velocity and the velocity profiles in each example are shown in (a), (b) and (c), respectively, of each figure.

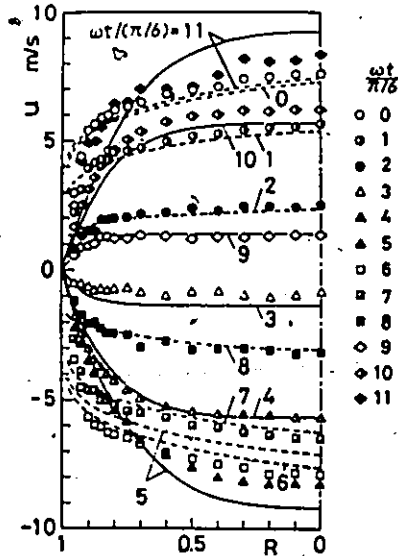
Hino, Sawamoto and Takasu [52], in their experimental investigations, agreed in general, with the observations of Ohmi and Iguchi concerning the transition to turbulence in



(a) Velocity wave forms from top to bottom measured at $R = 0, 0.3, 0.6, 0.8,$ and 0.95



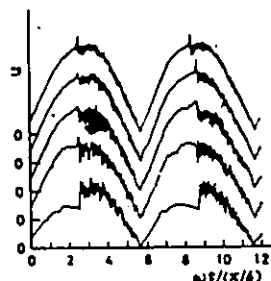
(b) Cross-sectional mean velocity (o : measured, — : finite Fourier expansion having fundamental wave)



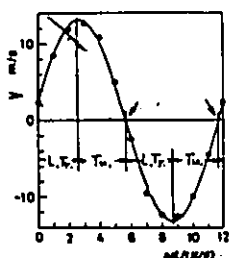
(c) Axial velocity distribution (— : solution for transient pulsatile laminar flow, - - - : 1/7 power law)

Figure 2.5

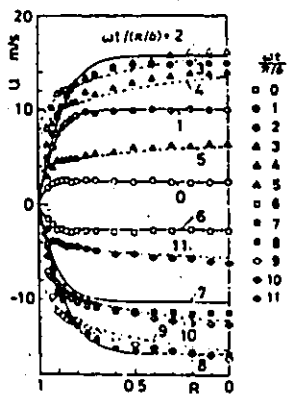
Comparison of measured with theoretical results in an oscillating pipe flow (Run 1). From Ohmi and Iguchi [51].



(a) Velocity wave forms from top to bottom measured at $R = 0, 0.3, 0.6, 0.8,$ and 0.95

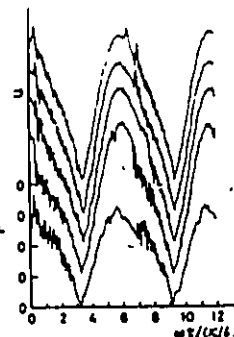


(b) Cross-sectional mean velocity (o: measured, —: finite Fourier expansion having fundamental wave)

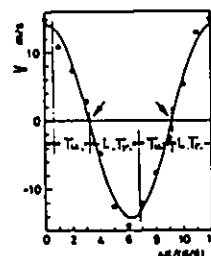


(c) Axial velocity distribution (—: solution for transient pulsatile laminar flow, ---: 1/7 power law)

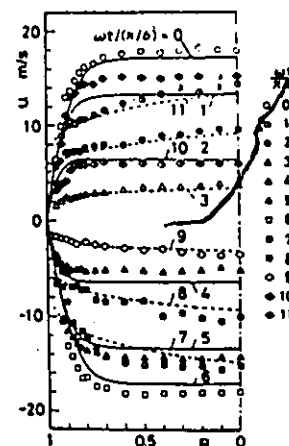
Figure 2.6 Comparison of measured with theoretical results in an oscillating pipe flow (Run 2). From Ohmi and Iguchi [51].



(a) Velocity wave forms from top to bottom measured at $R = 0, 0.3, 0.6, 0.8,$ and 0.95



(b) Cross-sectional mean velocity (o: measured, —: finite Fourier expansion having fundamental wave)



(c) Axial velocity distribution (—: solution for transient pulsatile laminar flow, ---: 1/7 power law)

Figure 2.7 Comparison of measured with theoretical results in an oscillating pipe flow (Run 3). From Ohmi and Iguchi [51].

an oscillatory pipe flow. Three types of turbulent flow have been detected during their investigations, these were: weakly turbulent flow, conditionally turbulent flow, and fully turbulent flow. Determination of the flow regime was dependent on frequency of oscillations and velocity amplitude. The critical velocity amplitude of the first transition was found to decrease as the frequency increased. In the conditionally turbulent flow, turbulence was observed to be generated suddenly over the decelerating phase while dramatic change in the velocity profiles was taking place. In the accelerating phase, the flow was recovered to laminar flow.

2.3.2 Pulsatile Flow of Non-Newtonian Fluids

The available literature on pulsatile flow of non-Newtonian fluids is very limited. In some papers [1,10,13], attention has been drawn to possible power saving for pipeline pumping by superimposing an oscillatory component on the steady pressure gradient with a carefully adjusted amplitude and frequency.

Barnes et al. [1] presented a theoretical analysis of the problem of pulsating flow of a non-Newtonian fluid. Rheological data obtained experimentally from steady pipe flow were used directly in the calculations. Increases in the flowrate were predicted on the addition of an oscillating flow component to the steady pressure gradient, above that of purely steady flow at the same mean value of pressure gradient. In the same paper, experimental data were presented on the pulsating flow of non-Newtonian aqueous polyacrylamide solutions through a rigid tube at low frequency (0.14 Hz) and at low amplitude of oscillatory pressure gradient to a steady pressure gradient (0.2). Experimental data compared favourably with theoretical predictions. Increases in the flowrate of about 20% for a 1.5% solution and about 8% for a 1% solution were observed. These results are indicated in Figure 2.8. However, it may be noted at this point that this does not necessarily imply that the power requirements are lowered.

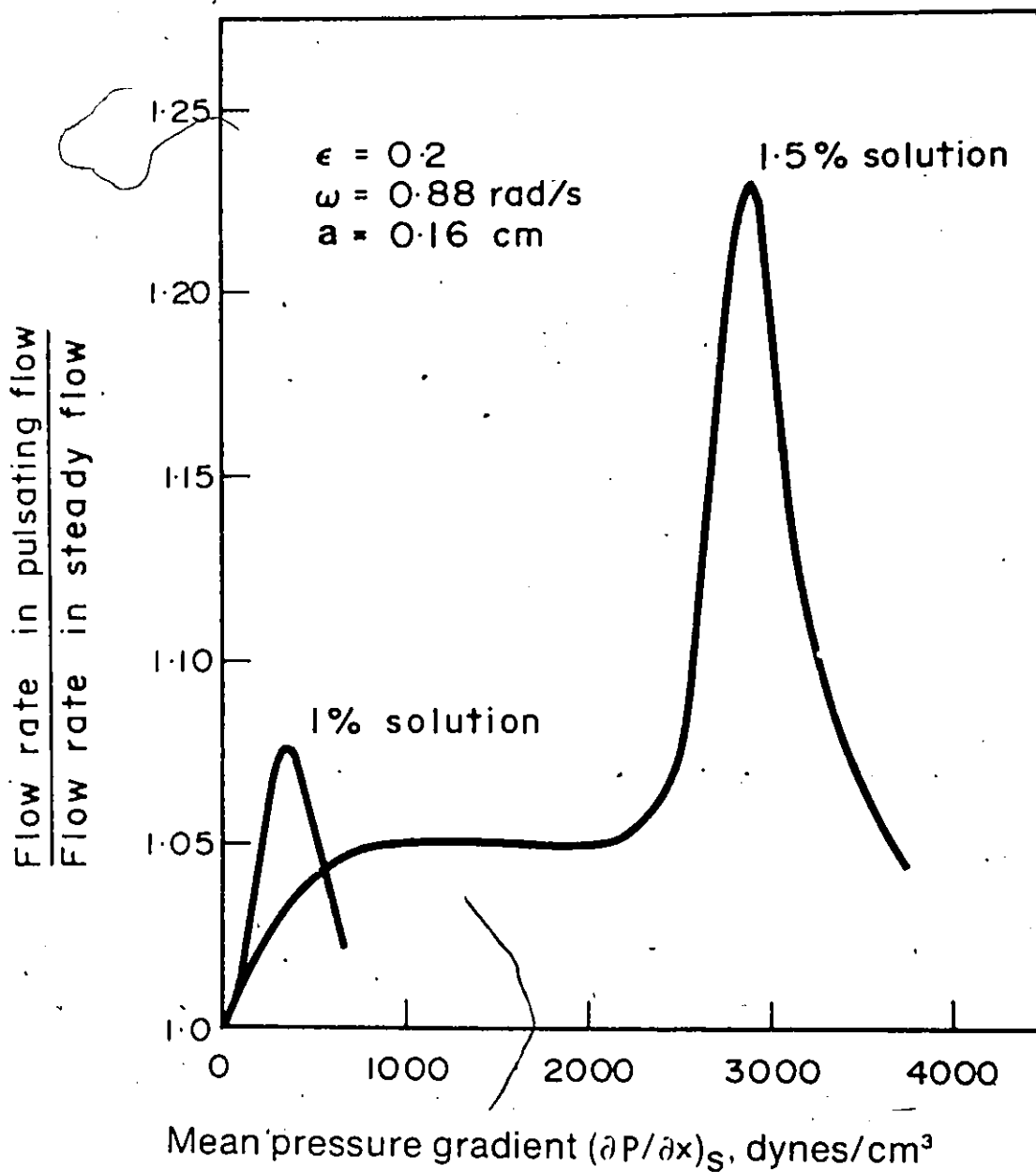


Figure 2.8

Increase of flowrate by pulsations for aqueous solutions of polyacrylamide. From Barnes *et al.* [1].

Edwards, Nellist and Wilkinson [10-12] presented a theoretical approach to the pulsating flow of non-Newtonian fluids represented by the power law model, equation (2.1). In their method, they put the equation of motion of unsteady pipe flow in finite difference form. In this formulation, they substituted for the viscous term by equation (2.1), and for the pressure gradient by: (a) a step function of pressure gradient; (b) oscillating pressure gradient of zero mean; and (c) an oscillating pressure gradient component added to a steady pressure gradient. Thus, they have obtained solutions for three different cases. The transient velocity profiles for these three cases were obtained for laminar pipe flows of power law non-Newtonian fluids. Flowrates and power requirements were also predicted for pulsating pipe flow of power law fluids. It was found for pseudoplastic fluids that the flowrate could be increased by the addition of an oscillatory pressure gradient to a steady pressure gradient, while the converse was true for dilatant fluids. Also, it was found for all power law fluids that the power requirements for the fluid to flow under a pulsating pressure gradient was always equal to or higher than that required for the fluid to flow under a steady pressure gradient at the same flowrate.

In later reports [53,54] studies were undertaken by Bousquet et al. on unsteady laminar pipe flows of power law non-Newtonian fluids. In their studies they have used aqueous solutions of high polymers which exhibited pseudoplastic rheological behaviour. The chosen parameters in their studies were of two types: (a) rheological characteristics of a fluid, i.e. consistency factor K and non-Newtonian power index n , (b) parameters relative to the sinusoidal variations of the pressure gradient. The velocity profiles were determined at regular intervals during the period of a cycle for each group of values of the parameters. Velocity profiles were obtained both theoretically and experimentally. The first experimental method was based on the use of the laser anemometry. This method is flexible and precise but it can only be employed when the fluid being considered is transparent or translucent. The

second method used was a photographic method which enabled fluid particles to be observed by photographing hydrogen bubbles at definite instants within the period of a cycle. One of the main conclusions was that the velocities at different points of the same cross-section of a pipe and at different instants were very sensitive to any variations of the consistency factor K , while they did not appear to be affected very much by the variations of the non-Newtonian index n . However, n and K are interdependent. Also, it was observed that variations of the frequency have a qualitatively similar influence due to increases in the consistency of the fluid. Some of the results obtained by Bellet and Bousquet [53,54] are shown in Figures 2.9 and 2.10.

Other investigations concerned with viscoelastic materials have been reported [55-57]. In these studies, purely oscillating flows in rigid pipes were analyzed and observations were reported, the chief of which was that the maximum velocity amplitude did not necessarily occur at the pipe centreline as in the steady flow case. Also, as the frequency increased, the point of the maximum velocity amplitude was found to move away from the pipe centre toward the pipe walls. These observations are similar to those of purely Newtonian fluids. A more comprehensive study by Walters and Townsend [2] for viscoelastic fluids has shown that pulsations could increase or decrease the mean flowrate; such a change depended on the type of fluid as well as the flow conditions. At a particular frequency and pressure gradient a resonance effect could take place and cause a significant increase in the flowrate. Figure 2.11 shows some of these results.

2.4 Steady Flow of Heterogeneous Slurries

A heterogeneous slurry is the one which exhibits an appreciable gradient of solids concentration across the vertical diameter of a pipe. When dealing with a slurry, one must

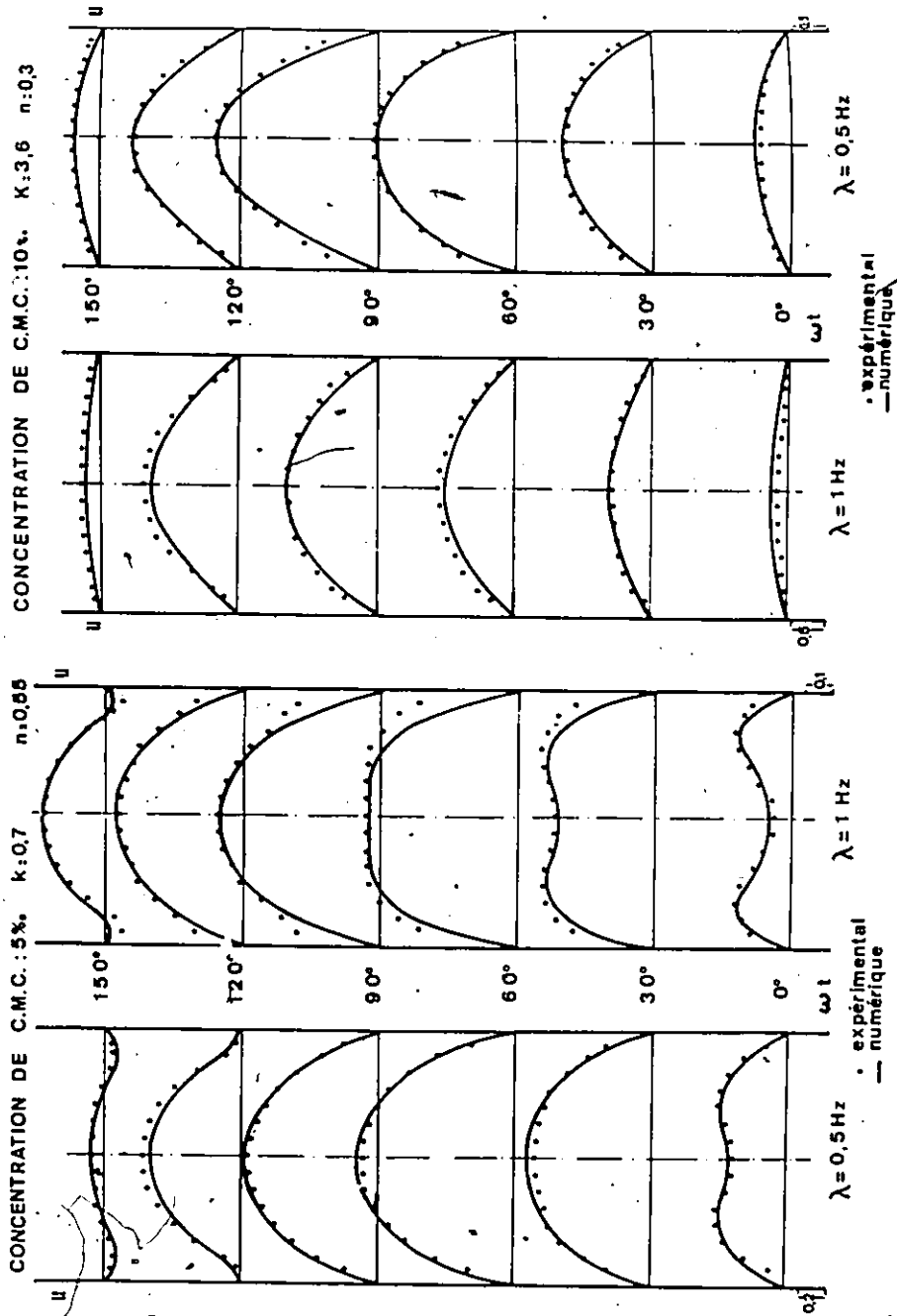


Figure 2.10 Velocity profile - numerical and experimental results for sodium carboxymethylcellulose concentration 1%. From Bousquet et al [53].

Figure 2.9 Velocity profiles - numerical and experimental results for sodium carboxymethylcellulose concentration 0.5%. From Bousquet et al [53].

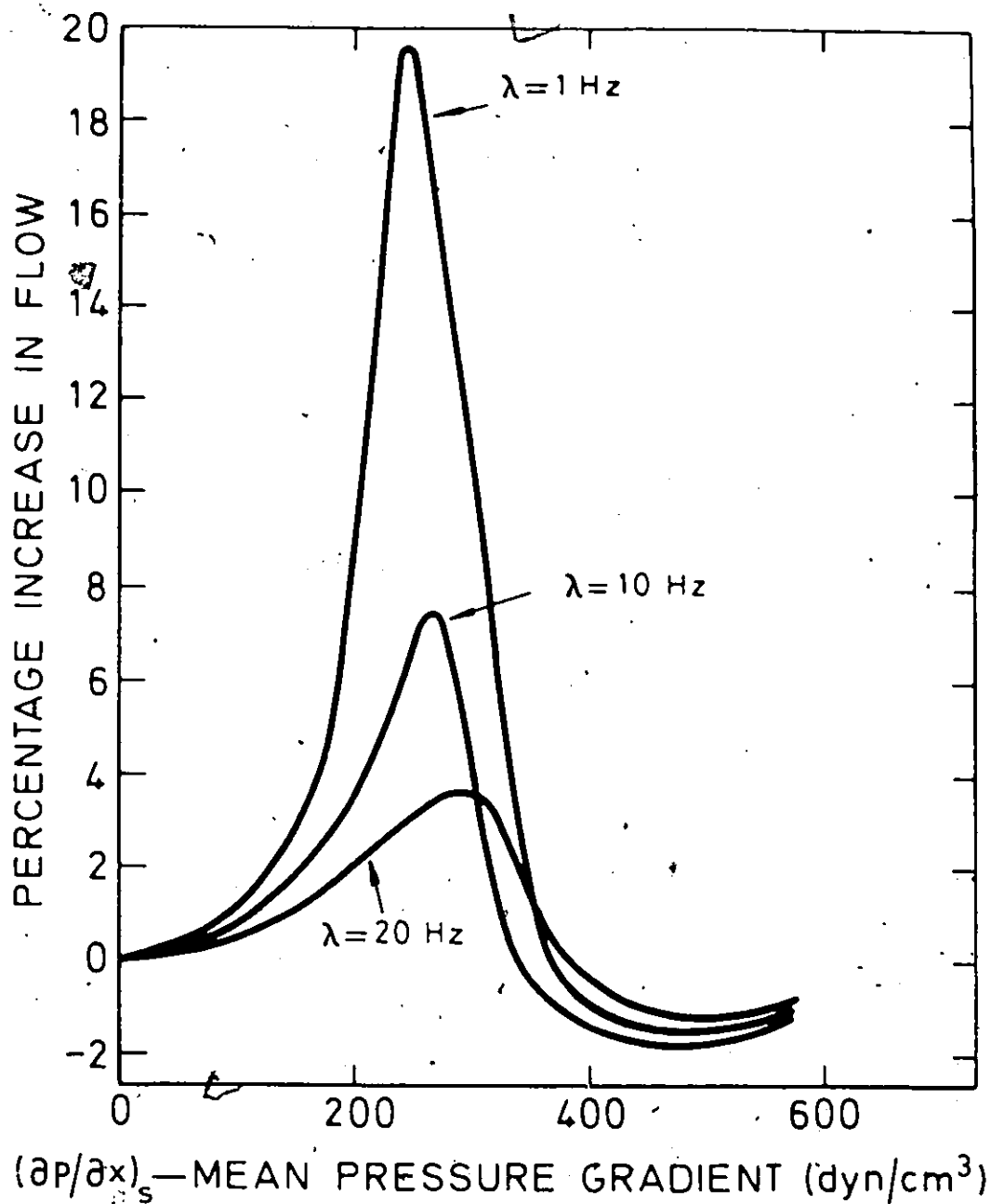


Figure 2.11 Increase in flow rate at different pulsing frequencies for viscoelastic fluid. From Walters and Townsend [2].

recognize that, unlike homogeneous slurries, the orientation of the pipe axis is important due to the influence of gravity force on the solid particles.

A typical pressure gradient-velocity response for a horizontal pipe flow of a heterogeneous slurry is shown in Figure 2.12. There are certain differences from the typical homogeneous response given in Figure 2.1. At higher velocities, i.e. point A, the pressure gradient-velocity response tends asymptotically toward a position parallel to the carrier fluid, which means that as the velocity increases, the solids concentration gradient across the vertical pipe diameter becomes less pronounced and the system tends toward homogeneity. On the other hand, as the velocity is decreased, i.e. below point A, the gradient of solids concentration becomes more and more pronounced until, at a point generally at point B, a layer of sliding or stationary solid particles is reached. For systems containing uniformly sized solid particles, point B coincides with the minimum in the pressure gradient-velocity curve. If the velocity is further reduced beyond point B, a bed of solids begins to build up in the pipe and consequently, the flow area is reduced which causes further increases in friction losses. In fact, this region of flow is unstable and the exact location of the Δp -V curve may be time-dependent. Point B is known as the limit deposit velocity; at this point, the tendency of the particle to settle under gravitational forces just exceeds the turbulence forces helping to maintain the particle suspension.

In practice, operating velocities lower than the deposit velocity are impractical. In addition to the obvious risk of pipeline blockage, there is also a possibility of the pipeline acting as a classifier, i.e. larger particles being deposited at the bottom of the pipe with smaller particles remaining in suspension. For a slurry pipeline, the intent is always to transport solids in suspension. Thus, a knowledge of deposit velocities is very important for heterogeneous slurry pipelines. Since this aspect is not specifically relevant to the present

study, a detailed review will not be included in the thesis but the reader may refer to [58-65] for more details.

The other aspect which seems to be of considerable interest in the present study is the radial migration of solid particles in pipe flow. For some time, it had been thought that when a mixture of solid particles and a fluid are caused to flow through a pipe, the particles would tend to accumulate in a region near the axis of the pipe. Young [66] observed that in some cases, in addition to the axial accumulation, the particles tended to congregate at a position near the wall of the pipe under certain circumstances. Segré and Silberberg [67] reported that neutrally buoyant particles would migrate away from both the axis and the wall at low Reynolds numbers (approximately up to 700), and would accumulate at a position midway between the axis and the wall of the pipe. Although particle migration has been observed with spheres, rods, discs, ellipsoids and particles of other shapes [68], most of the available research on migration has been concerned only with spherical particles.

Young [66], Oliver [69], Jeffrey [70], and several others have observed that when the solid particles moved downstream faster than the fluid, they tended to migrate towards the pipe wall. On the other hand, when particles move downstream slower than the fluid, they tend to migrate towards the pipe axis. Oliver [69] also found that neutrally buoyant particles, which were eccentrically buoyant so that they could not rotate, tended to reach an equilibrium position much closer to the tube axis. Theodor [71] found that no measurable difference in the lift force could be detected when the particles were constrained from rotation. These two observations are contradictory to each other, but it must be understood that the experimental conditions in the two cases were significantly different. Oliver's data have shown that the equilibrium positions attained by neutrally buoyant spherical particles were dependent on the ratio between particle and pipe diameters. Smaller particles were found

closer to the pipe wall when particle rotation was not inhibited, while they were found closer to the pipe axis when they were constrained.

Other studies [72,73] have also dealt with radial migration of solid particles in pipe flows, and data have been presented indicating that, when a solid particle tends to lead the fluid, it migrates toward the pipe wall; and when it tends to lag the fluid, it migrates toward the pipe centreline. When a particle is neutrally buoyant, it reaches an equilibrium position between pipe wall and axis. These results agree with the previously mentioned observations of Young [66], Oliver [69], and Jeffrey [70].

The radial migration of solid particles is basically related to three causes:

- (a) interaction between particles,
- (b) entrance effect, and
- (c) lift force acting on the particles.

Experiments [69,70,74,75] have shown that single particles also experienced radial migration which means that particle interaction cannot be the reason or at least the sole reason for migration. Furthermore, the work conducted by Segré and Silberberg [67] showed radial migration of solid particles far downstream of the entrance region. Hence, entrance effect is not the main cause. This leaves only the lift force as the major cause of radial migration -- this was first proposed by Young [66]. Saffman [76] has studied the motion of a sphere relative to an unbounded shear flow and he obtained an expression relating the lift force to the relative velocity between the solid particle and the fluid.

2.5 Pulsatile Flow of Heterogeneous Slurries

The main idea of pulsatile pipe flow of heterogeneous slurries is to make advantageous use of the phenomenon of radial migration of solid particles. It has obviously been noted in Section 2.4 that when a suspension of solid particles flows in steady flow

through a pipe, an appreciable migration of particles away from the wall toward the pipe axis occurs. In pulsating flow, similar effects were observed and the rates of radial migration were believed to be increased. Shizgal and Goldsmith [13] conducted some experiments on viscous suspensions containing between 5% to 20% by volume of polystyrene spheres in water, and a particle to tube diameter ratio of .035. After five minutes of oscillations at certain frequency, they have found that a particle-free layer ranging from .25 to .5 mm was developed. When the steady flow was recommenced with the 20% concentration, a flow situation was established in which a central core of slurry moved as a plug on a lubricating layer of solid-free liquid. This is shown in Figure 2.13. This flow situation may possibly result in reduction in hydraulic power consumption. In that paper [13], the velocity of the plug was expressed in the form

$$u = u_s + u_o e^{i(\omega t + \phi)} \quad (2.13)$$

where u_s was the steady flow velocity component of the plug, u_o was the oscillating component of the velocity, and ω was the angular frequency. The hydraulic power consumption per unit length was evaluated as the sum of a steady flow component and an oscillating component by averaging over one cycle the product of the velocity of the plug and the shear force acting on the plug. The following expression was obtained with the assumption that the thickness of the lubricating layer δ is small with respect to the pipe radius,

$$J_p = \frac{2\pi\mu}{\delta} \left(u_s^2 + \frac{1}{2} u_o^2 \right) \quad (2.14)$$

The first term of the above expression is the steady flow component, while the second term is the oscillating component which produces no net flow but it may increase the lubricating layer thickness δ . Since the power is inversely proportional to δ , there may be situations at which an input of oscillatory power can increase δ sufficiently enough to cause a net reduction in the total power per unit length at a given flowrate.

Other papers are available [3-5] showing the possibility for large hydraulic energy savings in slurry pipelines by superimposing a low frequency periodic pulse on a steady flow.

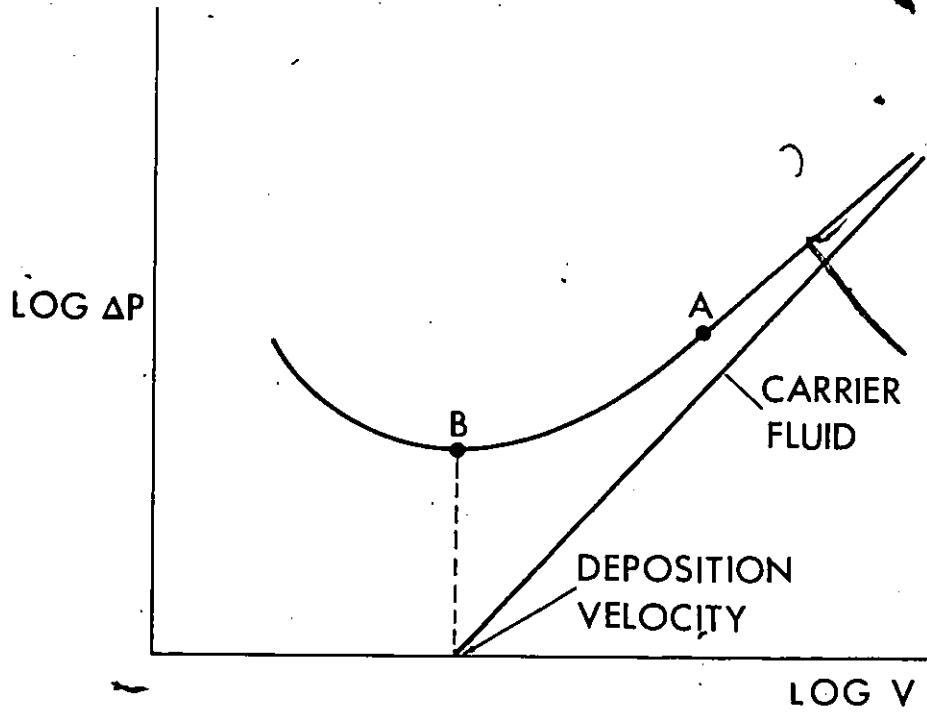


Figure 2.12 Pressure gradient vs. flow velocity for heterogeneous slurries.

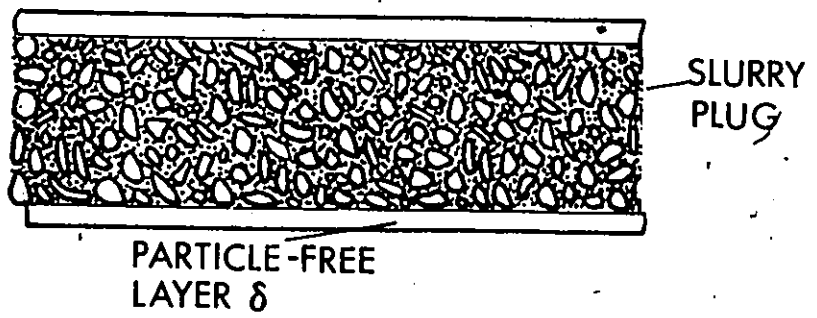


Figure 2.13 Formation of particle-free layer in pulsating flow of heterogeneous slurries.

In the third report of the above three, Round has presented experimental studies using laboratory-scale pipelines involving flow systems using periodic total interruption of the flow and an air pulsating device. The experiments were carried out using sand-water slurries with concentrations up to 20% by volume. It has been concluded through these experiments that the ratio of power requirements in pulsing flow to that in steady flow for a given flowrate was function of frequency and the solids concentration in the liquid. Points of maximum amount of energy saving were found at certain frequencies and at certain concentrations for the two types of experimental arrangements used. Figure 2.14 shows the points of maximum energy saving. Although the work presented by Round [5] has indicated clearly quantitative reductions in the friction losses due to pulsating pipe flow, the study did not involve the effect of amplitude of oscillations, and also the ranges of the parameters were limited.

Other experimental data are also available [6] for sand-water slurries in pulsating pipe flow: these also indicate significant reductions of power compared to steady flow. The highest reductions in hydraulic power were observed at low frequencies and low amplitudes and at certain concentrations depending on the mean particle size.

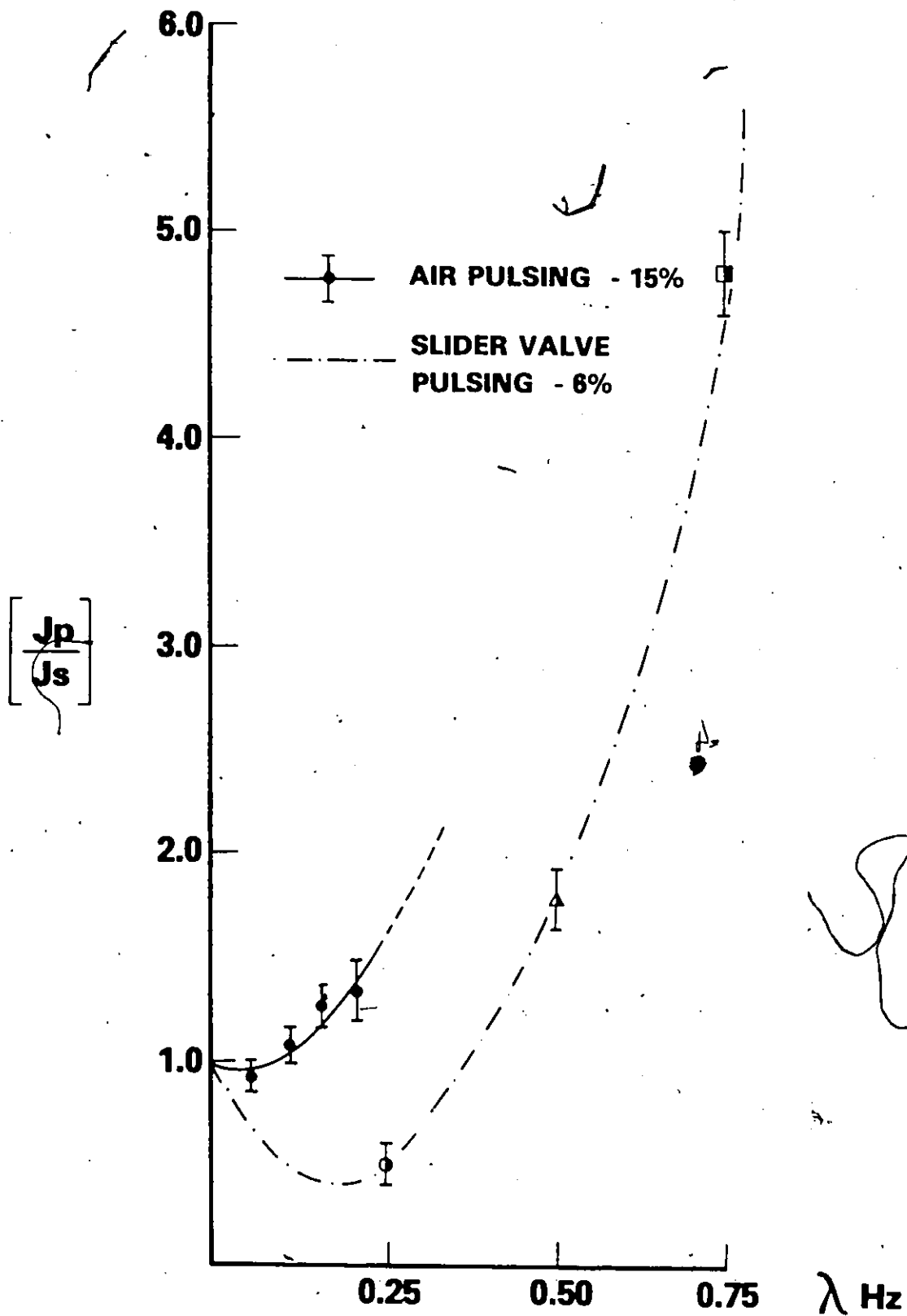


Figure 2.14

Ratio of hydraulic energy of pulsating flow to that of steady flow as a function of pulsing frequency for sand-water slurries. From Round [5].

CHAPTER 3

SCOPE OF INVESTIGATION

The literature review presented in Chapter 2 has indicated that flowrates of time-independent homogeneous fluids can be increased by superimposing an oscillating flow component on the steady flow. But no studies have yet indicated whether hydraulic power can be reduced accordingly.

Furthermore, pulsating flow of blood is a problem of fundamental interest in hemodynamics. Studies in this field are numerous, but they are frequently very fragmentary. Almost none of the available studies has treated blood as a non-Newtonian fluid despite the fact that blood has a small yield stress [31,32,53,77-85].

In Chapter 2, it was also mentioned that, in heterogeneous pipe flows, migration of solid particles in the radial direction was observed and different reasons advanced to explain it. This phenomenon was thought to be advantageous in pulsating flows. The few papers available have indicated reductions in hydraulic power requirements due to pulsating flows, but these are limited in their ranges and no definite conclusion may be drawn.

These facts have prompted the present research, which, for convenience, may be divided into two parts:

- 1) The first part is a theoretical treatment of the problem of time-dependent flows in pipes. The approach here is based on the use of the constitutive equation of a general non-Newtonian material. In this part, two types of time-dependent pipe flows are solved, these are (a) pulsating flow, and (b) start-up flow.

The solutions given in this theoretical part are in a very general form, so that they are widely applicable. Solutions at different frequencies and at different amplitudes in dimensionless forms are given and can easily be obtained by using

the computer program listed in Appendix D. Predictions of the flowrates, power requirements, and phase angles are also included in dimensionless forms. Other important conclusions, such as the effects of changes in pipe diameter, flow velocity and fluid properties, can be drawn from the general results.

- 2) In the second part, the possibility of reducing the hydraulic power requirements is examined. It is understood, however, that the mechanisms of pulsating flow in homogeneous and in heterogeneous flows are not alike. In homogeneous non-Newtonian fluids, changes in the rheological properties are expected due to the time-dependent changes in the pressure gradient and, consequently, in the flowrate. This may result in increases or decreases in the power requirements. On the other hand, the main idea in the case of pulsed heterogeneous fluids is to enhance the radial migration of solid particles from the pipe wall towards the pipe centre, so that a particle-free layer is formed. This particle-free layer works as a lubricating layer of fluid and may result in considerable reduction in friction pressure losses.

Two types of slurries were examined experimentally. Bentonite clay-water suspension was used as an example for homogeneous flow, while coal-water slurry was used for heterogeneous flow. A pulsing device was constructed for this particular investigation and attached to an existing pipeline. Details of the experimental model and procedure are contained in Chapter 5. Wide ranges of solid concentration in water, average flow velocity, pulsating frequency, and pulsating amplitude were covered in the experiments. The results are arranged in a condensed form and presented with a detailed discussion in Chapter 7.

CHAPTER 4

A THEORETICAL TREATMENT OF UNSTEADY LAMINAR FLOWS IN PIPES USING A GENERALIZED BINGHAM MODEL

4.1 Introduction

Two aspects of unsteady, laminar motion of non-Newtonian fluids in pipes are concerned in this chapter. These are:

- a) Pulsatile flow in which a periodic pressure gradient having a non-zero mean is applied to the fluid and there is a net flow of fluid through the pipe.
- b) Startup flow in a pipe following sudden imposition of an axial pressure gradient to the fluid which starts its transient motion from rest.

The second of the above, that is start-up flow, is of considerable industrial importance, particularly for large diameter pipelines and in the analysis of the performance of hydraulic systems. On the other hand, the first point is of interest to researchers in hydrotransport, control systems, hemodynamics, mining industries, and elsewhere.

A survey of the available literature has indicated that much of the work done was with pulsatile flow and has been done by investigators interested in physiology. For simplicity, blood was treated in all of the known studies as a Newtonian fluid. Analytical solutions were obtainable due to the simple linear relationship between shear stress and shear rate (Newton's law of viscosity).

Homogeneous time-independent non-Newtonian fluids may conveniently be divided into three types. These are:

- a) power law fluids,
- b) ideal Bingham fluids.

c) generalized Bingham fluids.

The last one of these three is a model which has good general applicability.

The flow curve of a general Bingham material, as shown in Figure 4.1, starts at some point on the shear stress axis corresponding to the yield stress and is not a straight line. This flow curve can be represented by the relationship given by equation (2.3).

Unlike Newtonian fluids, analytical solution of unsteady flow using the generalized Bingham model is difficult if not impossible. The alternative is the use of numerical techniques, in this case a finite difference technique. But, in order to solve the problem of a fluid undergoing time-dependent flow, it is necessary first to solve the steady flow problem of such a fluid.

Thus the main thrust in the present Chapter is, first, to develop a general form of the relationship between the flowrate and the pressure gradient as well as to determine the velocity distribution for a steady pipe flow in a laminar region. Such a correlation will be applicable to all commonly met time-independent homogeneous fluids. Secondly, a mathematical treatment and a method of solution of the pulsatile flow and start-up flow problems are to be presented in a general form in terms of generalized flow parameters such as Reynolds number, plasticity number, dimensionless time, dimensionless frequency, dimensionless amplitude, and finally the non-Newtonian index. The mathematical model of the pulsatile flow will provide valuable information about the instantaneous velocity profiles, flowrate, power requirements all in convenient dimensionless forms.

4.2 Derivation of Steady Flow Correlation

In equation (2.3), when the shear stress exceeds the value of yield stress, i.e. $|\tau_r| \geq$

$$\tau_r = \tau_0 + K\dot{\gamma}^n \quad (4.1)$$

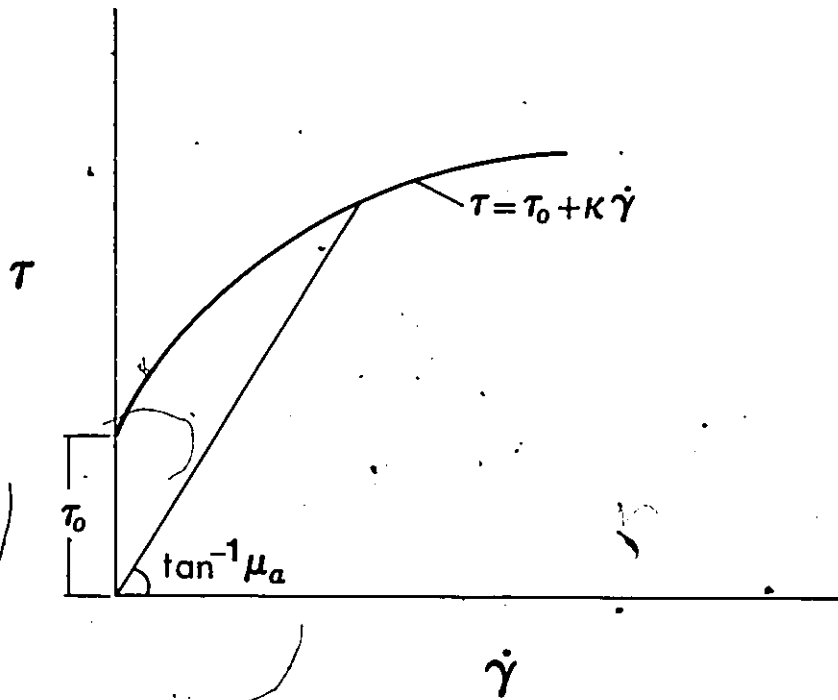


Figure 4.1 τ - $\dot{\gamma}$ relation for a generalized Bingham fluid.

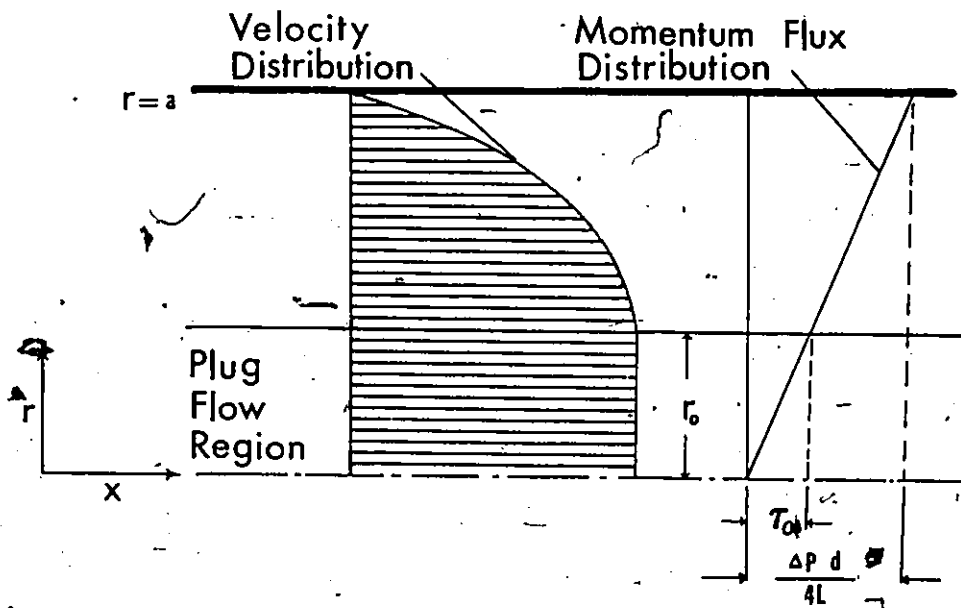


Figure 4.2 Flow of a Bingham fluid in a circular pipe.

where τ_0 , K and n are the rheological properties of the fluid. In the above equation, the shear rate $\dot{\gamma}$ can be expressed in the form:

$$\dot{\gamma} = \left[\frac{\tau_r - \tau_0}{K} \right]^{\frac{1}{n}} = f(\tau_r) \quad (4.2)$$

For a given pipe of a length L and diameter d , the shear stress at the pipe wall is given by:

$$\tau_w = \frac{\Delta P d}{4L} \quad (4.3)$$

where ΔP is the axial pressure drop over length L . The volumetric flowrate is given by:

$$Q = 2\pi \int_0^{d/2} u_r r dr \quad (4.4)$$

where u_r is the fluid axial velocity at radius r . The ratio between the shear stress τ_r and the shear stress at the pipe wall τ_w is the same as the radius ratio [16], i.e.

$$\frac{\tau_r}{\tau_w} = \frac{2r}{d} \quad (4.5)$$

Substituting for $r = (d/2)\tau_r/\tau_w$ into equation (4.4), and integrating yields

$$\frac{8Q}{\pi d^3} = \frac{1}{\tau_w^3} \int_0^{\tau_w} \tau_r^2 f(\tau_r) d\tau_r \quad (4.6)$$

This is a well-known expression for the pipe volumetric flowrate. In this expression $f(\tau_r)$ is a function of the rheological characteristics of the fluid.

Proceeding with $f(\tau_r)$ as it has been defined in equation (4.2), equation (4.6) becomes

$$\frac{8Q}{\pi d^3} = \frac{1}{\tau_w^3} \int_0^{\tau_w} \tau_r^2 \left[\frac{\tau_r - \tau_0}{K} \right]^{\frac{1}{n}} d\tau_r \quad (4.7)$$

This equation can be integrated and the result can be arranged in the form:

$$\frac{8Q}{\pi d^3} = \left(\frac{\tau_w - \tau_0}{K} \right)^{\frac{1}{n}} \left[\frac{\left(\frac{\tau_0}{\tau_w} \right)^2 \left(1 - \frac{\tau_0}{\tau_w} \right)}{1+n} + \frac{2 \frac{\tau_0}{\tau_w} \left(1 - \frac{\tau_0}{\tau_w} \right)^2}{1+2n} + \frac{\left(1 - \frac{\tau_0}{\tau_w} \right)^3}{1+3n} \right] \quad (4.8)$$

Equation (4.8) holds for general time-independent non-Newtonian materials with the absence of thixotropy and rheopexy. Substitution of $n = 1$ and $K = \eta_p$, where η_p is the plastic

viscosity of an ideal Bingham fluid, yields the Buckingham equation

$$\frac{8V}{d} = \frac{\tau_w}{\eta_p} \left[1 - \frac{4}{3} \frac{\tau_o}{\tau_w} + \frac{1}{3} \left(\frac{\tau_o}{\tau_w} \right)^4 \right] \quad (4.9)$$

While for Newtonian fluids $n = 1$, $K = \mu$ and $\tau_o = 0$, equation (4.8) becomes the Hagen-Poiseuille equation

$$Q = \frac{\pi d^4 \Delta P}{128 L \mu} \quad (4.10)$$

It can be seen from equation (4.8) that the variables involved are the yield stress τ_o , pressure drop ΔP , fluid properties ρ , K and n , pipe geometry d and L , and the average velocity V . A dimensional analysis of these variables yields:

$$\frac{\Delta P d^{n+1}}{L K V^n} = \psi \left(\frac{\tau_o d^n}{K V^n}, n \right) \quad (4.11)$$

It may be noticed in the above form that; the dimensionless quantity on the right hand side of equation (4.11), $\tau_o d^n / K V^n$ is very similar to the plasticity number given by Hedsröm [9].

Equation (4.8) can be manipulated into a more practical form according to equation (4.11), thus

$$\left[16 C_1 \left(\frac{\tau_o d^n}{K' 8^{n-1} V^n} / \frac{\Delta P d^{n+1}}{L K' 8^{n-1} V^n} \right)^2 + 4 C_2 \left(\frac{\tau_o d^n}{K' 8^{n-1} V^n} / \frac{\Delta P d^{n+1}}{L K' 8^{n-1} V^n} \right) + 1 \right]^{1/n} \left[1 - 4 \left(\frac{\tau_o d^n}{K' 8^{n-1} V^n} / \frac{\Delta P d^{n+1}}{L K' 8^{n-1} V^n} \right) \right]^{n+1} \left(\frac{\Delta P d^{n+1}}{L K' 8^{n-1} V^n} \right) = 32 \quad (4.12)$$

where

$$C_1 = \frac{2n^2}{(1+n)(1+2n)}$$

$$C_2 = \frac{2n}{1+2n}$$

and

$$K' = K \left(\frac{1 + 3n}{4n} \right)^n$$

Equation (4.12) is a function of three different dimensionless quantities,

$$\frac{\tau_0 d^n}{K' 8^{n-1} V^n}, \quad \frac{\Delta P d^{n+1}}{L K' 8^{n-1} V^n}$$

and n . This equation holds for any positive value of n . Figure 4.3 shows a logarithmic plot for the solution of equation (4.12) for $0 < n \leq 2$. It was found that a computer plot could not differentiate between values of $n = 0.5, 1.0, 1.5$ and 2.0 . In fact the curve shown in Figure 4.3 was drawn for the above four values of n . Hence, equation (4.11) may be rewritten as:

$$\frac{\Delta P d^{n+1}}{L K' 8^{n-1} V^n} = \psi' \left(\frac{\tau_0 d^n}{K' 8^{n-1} V^n} \right) \quad (4.13)$$

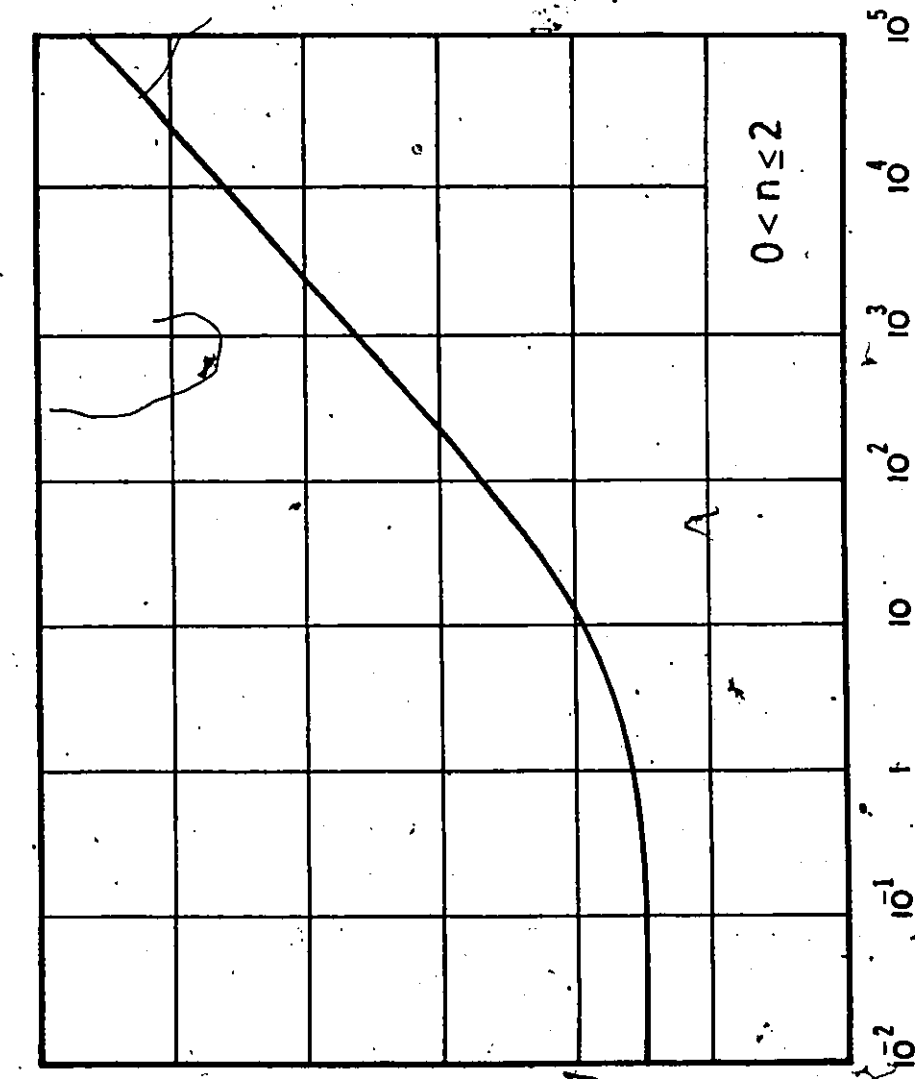
The importance of this equation is that it represents a universal relationship between the frictional pressure drop along a defined length of a pipe and the flowrate through the pipe for all fluids represented by equations (2.1), (2.2) and (2.3). Equation (4.13) also assumes rheological properties which are constant over a very wide range of shear stress, given by equation (4.1). In other words, experimental data given by rotational viscometry can be used without reservation as long as the absence of thixotropy and rheopexy is justified.

In order to verify and confirm the validity of the above relation in equation (4.13), data from the experimental work of Davidson [86] have been used here. These experimental data were obtained for bentonite clay suspensions at different concentrations by using a capillary tube technique. Figure 4.4 shows good agreement between the available experimental data and equation (4.13) over quite a wide range of rheological properties.

The friction factor in pipe flow is usually defined as

$$f = \frac{\Delta P d}{L \rho V^2 / 2}$$

Reynolds number in a generalized form was introduced for the first time by Metzner and Reed [8] and will be used here in the form



$$\frac{\Delta P d^{n+1}}{LK'V^n 8^{n-1}} \cdot 10^3$$

$$\frac{\tau_0 d^n}{K'V^n 8^{n-1}}$$

Solution of equation (4.12) - for n = 0.5, 1.0, 1.5 and 2.0.

Figure 4.3

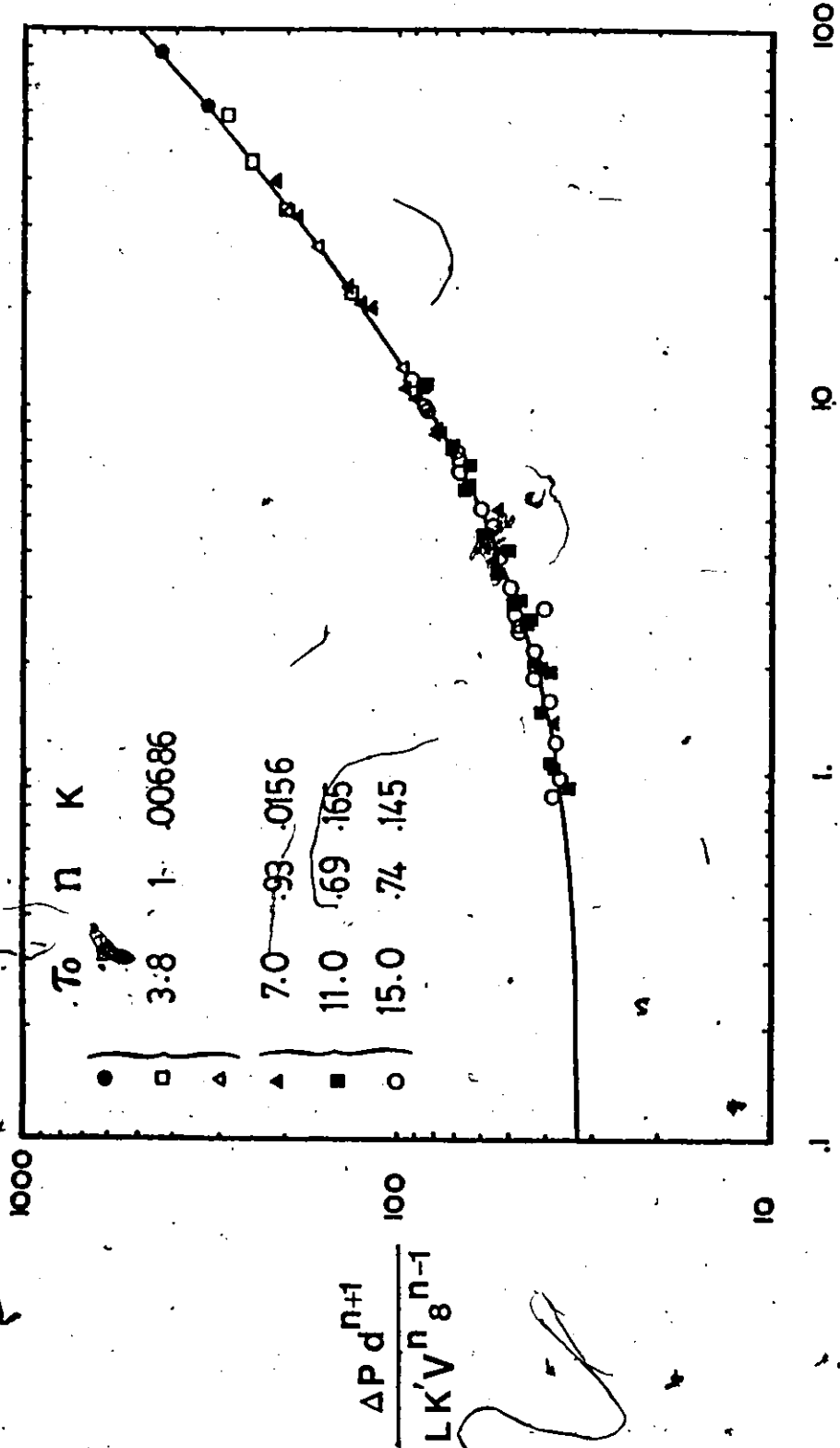


Figure 4.4 Comparison of experimental data for laminar flow with equation (4.12). Top bracketed data from ref. [9]; bottom bracketed data from ref. [86].

$$Re' = \frac{V^{2-n} d^n \rho}{K' \delta^{n-1}}$$

Therefore equation (4.13) can be rewritten in the form

$$f = \phi \left[\frac{V^{2-n} d^n \rho}{K' \delta^{n-1}}, \frac{\tau_0 d^n}{K' \delta^{n-1} V^n} \right] \quad (4.14)$$

Here, the dimensionless quantity

$$\frac{\tau_0 d^n}{K' \delta^{n-1} V^n}$$

may be called a generalized plasticity number.

In the corresponding case of an ideal Bingham plastic, the dimensionless group known as Hedström number [9] is defined as:

$$\frac{\tau_0 d^2 \rho}{\eta_p^2} = \left(\frac{V d \rho}{\eta_p} \right) \left(\frac{\tau_0 d}{\eta V} \right) \quad (4.15)$$

i.e.

$$H_e = R_e \cdot Pl$$

Therefore, applying the same type of relationship for the present case, a generalized form of Hedström number can be obtained as:

$$He' = Re' \cdot Pl' = \frac{\tau_0 d^{2n} V^{2-2n} \rho}{(K' \delta^{n-1})^2} \quad (4.16)$$

It may be noted that when $n = 1$, $Pl' \rightarrow Pl$ and $He' \rightarrow He$. It may be important to explain at this point that another form of Hedström number can be obtained which does not include the velocity in the group, and consequently another group for the plasticity number will also be

obtained. But the disadvantage in this case is that equation (4.13) is no longer valid, i.e., the solution is not unique and there is a solution for each particular value of n .

Using the above definitions of generalized Hedström number and generalized plasticity number, equation (4.14) may be written in the form

$$f = \phi'(Re', Pl')$$
(4.17)

and

$$f = \phi''(Re', He')$$
(4.18)

It has been shown in Figure 4.2 that ψ of equation (4.11) can be represented by a single curve. According to equations (4.17) and (4.18) both ϕ' and ϕ'' are represented by a family of curves, each curve represents an $f-Re'$ relationship for a certain value of Pl' or He' whichever is in use. Both ϕ' and ϕ'' are represented analytically in terms of

$$\frac{64}{Re'} = f[1-G]^{n+1} [C_1 G^2 + C_2 G + 1]^n$$
(4.19)

$$G = \frac{8Pl'}{fRe'} \text{ for } \phi'$$

and

$$G = \frac{8He'}{f(Re')^2} \text{ for } \phi''$$

This is the final form of the universal correlation. It correlates the frictional pressure gradient with the flowrate in pipelines for steady laminar flow of all commonly met time-independent non-Newtonian fluids defined above and, of course, Newtonian fluids,

4.3 Velocity Distribution in Steady Laminar Flow

The equation of motion for a steady fully developed laminar pipe flow is

$$\frac{r}{L} \frac{r}{2} = \tau_r$$
(4.20)

where τ_r is the shear stress at a radius r and $0 < r \leq D/2$. But the shear stress τ_r is given by equation (4.1) for general non-Newtonian. Hence,

$$\frac{\Delta P}{L} \frac{r}{2} = \tau_0 + K \left(\frac{d\tau_r}{dr} \right)^n \quad (4.21)$$

Two dimensionless quantities may be introduced at this point for convenience:

$$U = u_r/V \text{ and } R = 2r/d$$

where V is an average velocity and d is a pipe diameter. Therefore equation (4.21) becomes

$$\frac{\Delta P}{L} \frac{d}{4} R = \tau_0 + K \frac{(2V)^n}{d^n} \left(- \frac{dU}{dR} \right)^n \quad (4.22)$$

or alternately,

$$\frac{\Delta P}{L} \frac{d}{4} \frac{d^n}{K(2V)^n} R = \frac{\tau_0 d^n}{K(2V)^n} + \left(- \frac{dU}{dR} \right)^n \quad (4.23)$$

This is a dimensionless form of the equation of motion. Making use of the friction factor, generalized Reynolds number, and the generalized plasticity number as they have been defined above, and after rearranging the terms and integrating, equation (4.23) can be obtained in its final form

$$U = \frac{1+3n}{1+n} \left(\frac{f \cdot Re'}{64} \right)^{\frac{1}{n}} \left[\left(1 - \frac{8P\ell'}{f \cdot Re'} \right)^{\frac{1+n}{n}} - \frac{8P\ell'}{f \cdot Re'} \right]^{\frac{1+n}{n}} \quad (4.24)$$

for

$$R \geq \frac{8P\ell'}{f \cdot Re'}$$

while

$$U = \frac{1+3n}{1+n} \left(\frac{f \cdot Re'}{64} \right)^{\frac{1}{n}} \left(1 - \frac{8P\ell'}{f \cdot Re'} \right)^{\frac{1+n}{n}} \quad (4.25)$$

for

$$R \leq \frac{8P\ell'}{f \cdot Re'}$$

According to the constitutive equation, equation (2.3), the flow of this type of materials is hypothetically divided into two regions. The first region is at the centre of the

pipe where the fluid flows as a non-deformed rigid core, i.e., the velocity gradient in the radial direction is zero. The velocities at all points of the cross-section of the core are equal and given by equation (4.25). The radius of the core, r_0 , is simply given by

$$\frac{r_0}{a} = \frac{\tau_0}{\tau_w} = \frac{8P\ell'}{f \cdot Re'} \quad (4.26)$$

In the second region, outside the core, the shear stress exceeds the value of yield stress, and the velocity at any radius, where $r_0 \leq r \leq d/2$, can be obtained in dimensionless form (equation (4.24)). Those two regions are illustrated in Figure 4.2.

From the above discussion, it can be seen that the constitutive equation forces a discontinuity of the fluid at the edge of the core, i.e. at r_0 . This assumption cannot of course be true but for low loading rates it is justifiable.

4.4 Mathematical Formulation for Unsteady Laminar Flow

4.4.1 Governing Equations:

Unsteady laminar flows of fluids in long pipes where entrance or exit effects are negligible, may be described by the equation of motion of axially symmetric time-dependent parallel flow in cylindrical coordinates [14]

$$\rho \frac{\partial u_r}{\partial t} = - \frac{\partial P}{\partial x} - \frac{1}{r} \frac{\partial}{\partial r} (r \tau_r) \quad (4.27)$$

In this equation, u_r and τ_r are functions of time as well as the radial position. $\partial P/\partial x$ is a function of time only and serves as the source of momentum for the flow.

The constitutive equation for laminar flow of generalized Bingham materials is given here in the form, see [16,87],

$$\tau_r = \tau_0 + K \left(- \frac{\partial u_r}{\partial r} \right) \left| \frac{\partial u_r}{\partial r} \right|^{n-1} \quad \text{for } |\tau_r| \geq \tau_0 \quad (4.28a)$$

$$\frac{\partial u_r}{\partial r} = 0 \quad \text{for } |\tau_r| < \tau_0 \quad (4.28b)$$

This equation is the same as (4.1), but the modulus is introduced here to avoid mathematical complexity which arises due to the -ve sign when $n \neq 1$.

For pulsating flow the pressure gradient consists of a stationary component with a superposed oscillatory component of a certain amplitude and frequency. A sinusoidal form for the oscillatory component is assumed, thus:

$$-\frac{\partial P}{\partial x} = \left(\frac{dP}{dx}\right)_s + \left(\frac{dP}{dx}\right)_o \sin \omega t \quad (4.29)$$

where $(dP/dx)_s$ is the stationary component, $(dP/dx)_o$ is the maximum amplitude of the oscillatory component, and ω is the angular frequency. In the case of start-up flow problem the fluid is assumed to start its transient motion from rest due to instantaneous and sudden imposition of a stationary pressure gradient, i.e.

$$-\frac{\partial P}{\partial x} = 0 \quad \text{for } t < 0 \quad (4.30a)$$

$$-\frac{\partial P}{\partial x} = \frac{dP}{dx} \quad \text{for } t \geq 0 \quad (4.30b)$$

where dP/dx is the pressure gradient required to maintain a fully developed laminar steady flow.

4.4.2 Determination of Flow Patterns:

The above equations can be combined together to form two sets of equations, one is applicable to the case of pulsating flow, while the other set of equations is for the start-up flow problem. Thus,

a) for pulsating flow:

$$\rho \frac{\partial u_r}{\partial t} = \left(\frac{dP}{dx}\right)_s + \left(\frac{dP}{dx}\right)_o \sin \omega t - \frac{\tau_0}{r} + \left[\frac{K}{r} \frac{\partial u_r}{\partial r} \right]$$

$$\left| \frac{\partial u_r}{\partial r} \right|^{n-1} + K \frac{\partial^2 u_r}{\partial r^2} \left| \frac{\partial u_r}{\partial r} \right|^{n-1} \left\{ 1 + (n-1) \text{sign} \left(\frac{\partial u_r}{\partial r} \right) \text{sign} \left(\frac{\partial^2 u_r}{\partial r^2} \right) \right\} \quad \text{for } \frac{d}{2} > r \geq r_0 \quad (4.31a)$$

$$\rho \frac{\partial u_r}{\partial t} = \left(\frac{dP}{dx} \right)_s + \left(\frac{dP}{dx} \right)_o \sin \omega t - \frac{4\tau_0}{d} + \left\{ \frac{4K}{d} \left(\frac{\partial u_r}{\partial r} \right) \right\}_{r=\frac{d}{2}}$$

$$\left| \frac{\partial u_r}{\partial r} \right|_{r=\frac{d}{2}}^{n-1} \quad \text{for } r_0 > r \geq 0 \quad (4.31b)$$

b) for start-up flow

$$\rho \frac{\partial u_r}{\partial t} = \frac{dP}{dx} - \frac{\tau_0}{r} + \frac{K}{r} \left| \frac{\partial u_r}{\partial r} \right| \left| \frac{\partial u_r}{\partial r} \right|^{n-1} +$$

$$K \frac{\partial^2 u_r}{\partial r^2} \left| \frac{\partial u_r}{\partial r} \right|^{n-1} \left\{ 1 + (n-1) \text{sign} \left(\frac{\partial u_r}{\partial r} \right) \text{sign} \left(\frac{\partial^2 u_r}{\partial r^2} \right) \right\}$$

$$\text{sign} \left(\frac{\partial^2 u_r}{\partial r^2} \right) \quad \text{for } \frac{d}{2} > r \geq r_0 \quad (4.32a)$$

$$\rho \frac{\partial u_r}{\partial t} = \frac{dP}{dx} - \frac{4\tau_0}{d} + \frac{4K}{d} \left(\frac{\partial u_r}{\partial r} \right)_{r=\frac{d}{2}} \left| \frac{\partial u_r}{\partial r} \right|_{r=\frac{d}{2}}^{n-1} \quad \text{for } r_0 > r \geq 0 \quad (4.32b)$$

where d is the pipe diameter. It can be seen that there are two equations in each case with each of these equations being applied to a limited region in the pipe. This is a natural consequence of the constitutive relation (4.28) which has been noted before (section 4.3).

It is convenient at this point to introduce a dimensionless radius R and velocity U as well as a dimensionless pressure amplitude

$$\varepsilon = \left(\frac{dP}{dx} \right)_0 / \left(\frac{dP}{dx} \right)_s$$

Therefore, equations (4.31) and (4.32) become

a) for pulsating flow:

$$\rho V \frac{\partial U}{\partial t} = \left(\frac{dP}{dx} \right)_s (1 + \varepsilon \sin \omega t) - \frac{2\tau_0}{d} \frac{1}{R} + \frac{2K}{d} \left(\frac{2V}{d} \right)^n \frac{1}{R} \left| \frac{\partial U}{\partial R} \right| \left| \frac{\partial U}{\partial R} \right|^{n-1} + \frac{2K}{d} \left(\frac{2V}{d} \right)^n \frac{\partial^2 U}{\partial R^2} \left| \frac{\partial U}{\partial R} \right|^{n-1} \left\{ 1 + (n-1) \operatorname{sign} \left(\frac{\partial U}{\partial R} \right) \operatorname{sign} \left(\frac{\partial^2 U}{\partial R^2} \right) \right\}$$

for $1 > R \geq R_0$

(4.33a)

$$\rho V \frac{\partial U}{\partial t} = \left(\frac{dP}{dx} \right)_s (1 + \varepsilon \sin \omega t) - \frac{4\tau_0}{d} + \left\{ \frac{4K}{d} \left(\frac{2V}{d} \right)^n \left(\frac{\partial U}{\partial R} \right)_{R=1} \left| \frac{\partial U}{\partial R} \right|_{R=1}^{n-1} \right\} \text{ for } R_0 > R \geq 0$$

(4.33b)

b) for start-up flow:

$$\rho V \frac{\partial U}{\partial t} = \frac{dP}{dx} - \frac{2\tau_0}{d} \frac{1}{R} + \frac{2K}{d} \left(\frac{2V}{d} \right)^n \frac{1}{R} \left| \frac{\partial U}{\partial R} \right| \left| \frac{\partial U}{\partial R} \right|^{n-1} + \frac{2K}{d} \left(\frac{2V}{d} \right)^n \frac{\partial^2 U}{\partial R^2} \left| \frac{\partial U}{\partial R} \right|^{n-1} \left\{ 1 + (n-1) \operatorname{sign} \left(\frac{\partial U}{\partial R} \right) \operatorname{sign} \left(\frac{\partial^2 U}{\partial R^2} \right) \right\}$$

for $1 > R \geq R_0$

(4.34a)

$$\rho V \frac{\partial U}{\partial t} = \frac{dP}{dx} - \frac{4\tau_0}{d} + \frac{4K}{d} \left(\frac{2V}{d} \right)^n \left(\frac{\partial U}{\partial R} \right)_{R=1} \left| \frac{\partial U}{\partial R} \right|_{R=1}^{n-1} \text{ for } R_0 > R \geq 0$$

(4.34b)

where $R_0 = r_0/(d/2)$. Each of the above equations has to be solved separately with suitable boundary conditions. But, there are two unknowns in each of these equations, these are, the velocity U and the pressure gradient dP/dx . A relation between the axial pressure gradient and the cross-sectional average velocity of steady flow is necessary to reduce the number of unknowns to one. Such a correlation has already been obtained in section 4.2, in terms of the friction factor f , generalized Reynolds number Re' , and generalized plasticity number $P\ell'$ or generalized Hedström number He' . Furthermore, a dimensionless time T and dimensionless frequency ζ can be defined as:

a) for pulsating flow:

$$T = \frac{\omega t}{2\pi} \quad (4.35)$$

$$\zeta = \frac{\omega}{2\pi} \cdot \frac{d}{V} \cdot Re'$$

b) for start-up flow:

$$T = \frac{t \cdot V}{d Re'} \quad (4.36)$$

Hence, equations (4.33) and (4.34) can be rearranged to take the following general form,

a) for pulsating flow:

$$\begin{aligned} \zeta \left(\frac{1+3n}{4n} \right)^n \frac{\partial U}{\partial T} &= \frac{Re' \cdot f}{2} \left(\frac{1+3n}{4n} \right)^n (1 + \epsilon \sin 2\pi T) \\ &- 2P\ell' \left(\frac{1+3n}{4n} \right)^n \frac{1}{R} + 4^{2-n} \frac{1}{R} \frac{\partial U}{\partial R} \left| \frac{\partial U}{\partial R} \right|^{n-1} \\ &+ 4^{2-n} \frac{\partial^2 U}{\partial R^2} \left| \frac{\partial U}{\partial R} \right|^{n-1} \left\{ 1 + (n-1) \text{sign} \left(\frac{\partial U}{\partial R} \right) \text{sign} \left(\frac{\partial^2 U}{\partial R^2} \right) \right\} \end{aligned}$$

for $l > R \geq R_0$

(4.37a)

$$\zeta \left(\frac{1+3n}{4n} \right)^n \frac{\partial U}{\partial T} = \frac{Re' \cdot f}{2} \left(\frac{1+3n}{4n} \right)^n (1 + \varepsilon \sin 2nT)$$

$$- 4P\ell' \left(\frac{1+3n}{4n} \right)^n + 2^{5-2n} \left(\frac{\partial U}{\partial R} \right)_{R=1} \left| \frac{\partial U}{\partial R} \right|_{R=1}^{n-1}$$

for $R_0 > R \geq 0$

(4.37b)

b) for start-up flow:

$$\left(\frac{1+3n}{4n} \right)^n \frac{\partial U}{\partial T} = \frac{Re' \cdot f}{2} \left(\frac{1+3n}{4n} \right)^n - 2P\ell' \left(\frac{1+3n}{4n} \right)^n \frac{1}{R}$$

$$+ 4^{2-n} \frac{1}{R} \frac{\partial U}{\partial R} \left| \frac{\partial U}{\partial R} \right|^{n-1} + \left[4^{2-n} \frac{\partial^2 U}{\partial R^2} \left| \frac{\partial U}{\partial R} \right|^{n-1} \right]$$

$$\left[1 + (n-1) \text{sign} \left(\frac{\partial U}{\partial R} \right) \text{sign} \left(\frac{\partial^2 U}{\partial R^2} \right) \right]$$

for $1 > R \geq R_0$

(4.38a)

$$\left(\frac{1+3n}{4n} \right)^n \frac{\partial U}{\partial T} = \frac{Re' \cdot f}{2} \left(\frac{1+3n}{4n} \right)^n - 4P\ell' \left(\frac{1+3n}{4n} \right)^n$$

$$+ 2^{5-2n} \left(\frac{\partial U}{\partial R} \right)_{R=1} \left| \frac{\partial U}{\partial R} \right|_{R=1}^{n-1}$$

for $R_0 > R \geq 0$

(4.38b)

The friction factor f in these equations is obtainable from equation (4.19) by setting values for the flow parameters Re' and $P\ell'$. Again, the difference in the definitions of the dimensionless

time should be noted since they are not the same for both cases. Also, it may be noted here that R_0 is a function of time and is not an independent parameter.

The boundary conditions which apply to the above sets of equations are:

$$U = 0 \text{ at } T = 0 \text{ for } 0 \leq R \leq 1 \quad (4.39)$$

$$U = 0 \text{ at } R = 1 \text{ at all } T \quad (4.40)$$

In the case of solving for a fluid which has a zero yield stress, i.e. $P\ell' = 0$, equations (4.37b) and (4.38b) will vanish and equations (4.37a) and (4.38a) must be solved for the range $0 \leq R \leq 1$ subject to the same boundary conditions (4.39) and (4.40). However, in this particular case, a modified form of equations (4.37a) and (4.38a) must be used at $R = 0$ in order to avoid the term R in the denominators. This necessary modification can be achieved by using L'Hopital's rule. Therefore,

a) for pulsating flow:

$$\zeta \left(\frac{1+3n}{4n} \right)^n \frac{\partial U}{\partial T} = \frac{Re \cdot f}{2} \left(\frac{1+3n}{4n} \right)^n (1 + \varepsilon \sin 2\pi T) +$$

$$2^{5-2n} \frac{\partial^2 U}{\partial R^2} \left| \frac{\partial U}{\partial R} \right|^{n-1} \left\{ 1 + (n-1) \text{sign} \left(\frac{\partial U}{\partial R} \right) \text{sign} \left(\frac{\partial^2 U}{\partial R^2} \right) \right\} \quad (4.41)$$

b) for start-up flow:

$$\left(\frac{1+3n}{4n} \right)^n \frac{\partial U}{\partial T} = \frac{Re \cdot f}{2} \left(\frac{1+3n}{4n} \right)^n + \left[2^{5-2n} \frac{\partial^2 U}{\partial R^2} \left| \frac{\partial U}{\partial R} \right|^{n-1} \right.$$

$$\left. \left\{ 1 + (n-1) \text{sign} \left(\frac{\partial U}{\partial R} \right) \text{sign} \left(\frac{\partial^2 U}{\partial R^2} \right) \right\} \right] \quad (4.42)$$

4.4.3 Determination of Flowrate:

In this part, the objective is to derive an expression for the ratio of flowrate due to pulsating flow to the flowrate due to steady flow with one condition, that is both flows have the same mean pressure gradient.

Designating the instantaneous flow rate in pulsating flow by Q_p , then

$$Q_p = 2\pi \int_0^{d/2} u_r r dr \quad (4.43)$$

In a dimensionless form, this equation can be modified to

$$Q_p = 2\pi V \frac{d^2}{4} \int_0^1 UR dR \quad (4.44)$$

The average flowrate under pulsating flow conditions may then be given as

$$\bar{Q}_p = 2\pi V \frac{d^2}{4} \frac{\omega}{2\pi} \int_0^{2\pi} \int_0^1 UR dR dt \quad (4.45)$$

or in a dimensionless form

$$S = \frac{\bar{Q}_p}{\pi V \frac{d^2}{4}} = 2 \int_0^1 \int_0^1 UR dR dT \quad (4.46)$$

In this equation S is the ratio of the flowrate under the pulsating flow conditions to a steady flowrate of the same mean pressure gradient. The dimensionless velocity U in equation (4.46) is obtained from equations (4.37) by using a finite difference technique as will be explained later. The integrals in this equation are to be performed by using suitable numerical techniques in parallel with the finite difference solution.

4.4.4 Determination of power requirements:

Similarly, in this part, the aim is to obtain an expression to compare the power requirements in pulsating flow to that of steady flow for the same flow rate.

The instantaneous value of the power required per unit length in pulsating flow is given by

$$J_p = \left(- \frac{\partial P}{\partial x} \right) \cdot Q_p \quad (4.47)$$

The pressure gradient is given by equation (4.29) and the instantaneous flowrate is given by equation (4.43), therefore

$$J_p = 2\pi \left(\frac{dP}{dx} \right)_s \int_0^{d/2} (1 + \epsilon \sin \omega t) u_r r dr \quad (4.48)$$

The average power requirements can then be obtained by integrating over one cycle of the pulsation

$$\bar{J}_p = 2\pi \left(\frac{dP}{dx} \right)_s \frac{\omega}{2\pi} \int_0^{2\pi} \int_0^{d/2} (1 + \epsilon \sin \omega t) u_r r dr dt \quad (4.49)$$

The average power requirement, per unit length per unit volumetric throughput under pulsating flow conditions can be obtained from \bar{J}_p / \bar{Q}_p , where \bar{J}_p and \bar{Q}_p are obtainable from equations (4.49) and (4.45) respectively.

In order to achieve proper comparison this power requirement has to be compared with the power required to maintain the same volumetric throughput \bar{Q}_p under steady flow conditions. In other words a steady pressure gradient corresponding to \bar{Q}_p has to be obtained.

This steady pressure gradient is designated by $(dP/dx)_s'$. The power requirement per unit length is designated J_s' and can be expressed as

$$J_s' = \left(\frac{\partial P}{\partial x} \right)_s' \cdot \bar{Q}_p \quad (4.50)$$

The power requirement per unit length per unit volumetric throughput is

$$\frac{J_s'}{\bar{Q}_p} = \left(\frac{\partial P}{\partial x} \right)_s' \quad (4.51)$$

In steady laminar flow, according to equation (4.8)

$$\frac{\partial P}{\partial x} \propto Q^n \quad (4.52)$$

Therefore,

$$\left(\frac{dP}{dx} \right)_s' / \left(\frac{dP}{dx} \right)_s = S^n \quad (4.53)$$

Thus the ratio of power requirement in pulsating flow to that of steady flow at the same volumetric flowrate can be given in the dimensionless form

$$E = \frac{\bar{J}_p / \bar{Q}_p}{\left(\frac{dP}{dx}\right)_s} = \frac{2}{S^{n+1}} \int_0^1 \int_0^1 \left\{ (1 + \epsilon \sin \omega t) \cdot U \cdot R \cdot dR \cdot dT \right\} \quad (4.54)$$

In this equation S is obtained from equation (4.46) and U is obtained from equations (4.37). As it has been mentioned before that U is calculated by using a finite difference technique while S is calculated by using the numerical integration technique. Also the integrals above in equation (4.54) will be performed in parallel by the same numerical techniques used for the calculation of S .

4.5 Finite Difference Formulation

Equations (4.37) and (4.38) are non linear second order partial differential equations. Analytical solution of such systems is virtually impossible. Thus a finite difference technique is used here. But, due to the modulus existing in the above equations, only an explicit finite difference scheme is permissible [88, 89].

For an explicit numerical scheme a grid is imposed on the flow field as shown in Figure 4.5. The velocity at each grid point is $U_{i,j}$ where i indicates the position in the radial direction and j indicates the time level. A forward difference form is used for $\partial U / \partial T$, while a central difference form is used for $\partial U / \partial R$. Hence,

$$\frac{\partial U}{\partial T} = \frac{U_{i,j+1} - U_{i,j}}{\Delta T}$$

$$\frac{\partial U}{\partial R} = \frac{U_{i+1,j} - U_{i-1,j}}{2\Delta R} \quad (4.55)$$

$$\frac{\partial^2 U}{\partial R^2} = \frac{U_{i+1,j} + U_{i-1,j} - 2U_{i,j}}{(\Delta R)^2}$$

The main difficulty here is to overcome the numerical instability. Usually, in similar problems stability can be examined, but due to the nonlinearity of the present system such examination becomes exceedingly difficult [88]. However, a skillful control over the step size of both the time and the radius would produce stable numerical solution and convergence toward the exact solution may be achieved.

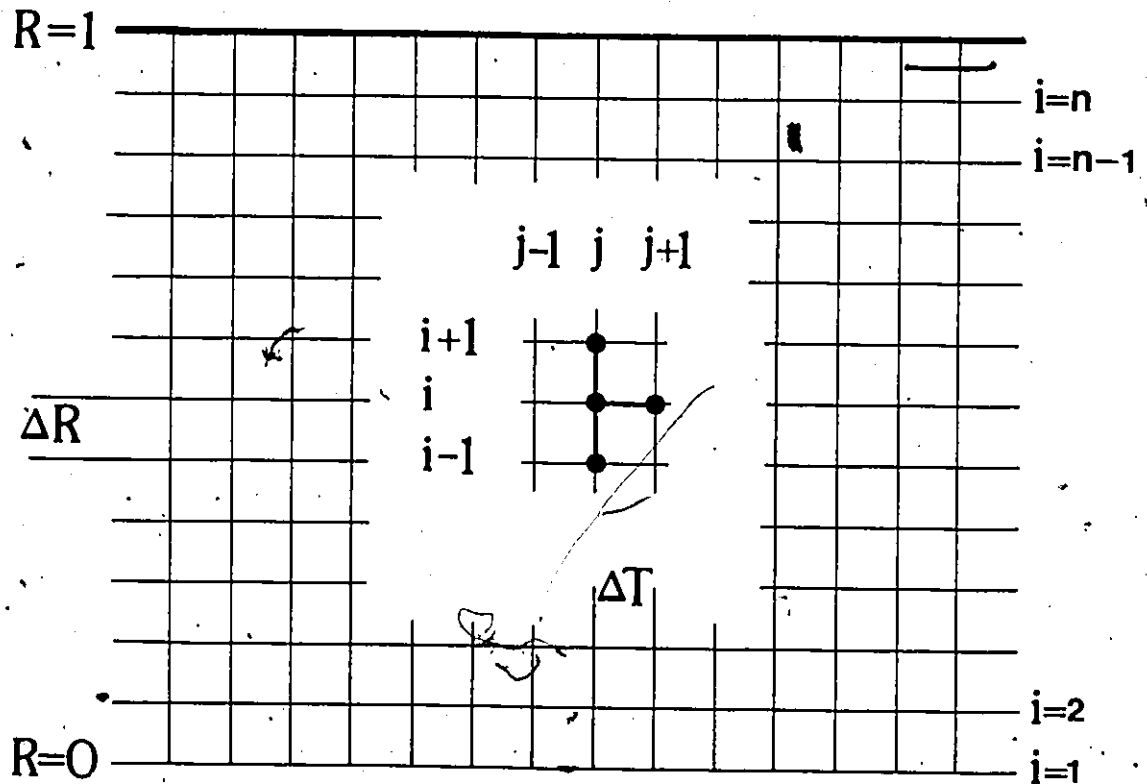


Figure 4.5 Finite difference network

CHAPTER 5

EXPERIMENTAL PROCEDURE

5.1 Introduction

The present study was initiated in the first place to examine the possibility of reducing the hydraulic power requirements in solid-liquid slurry transportation, by superposing an oscillating flow component over the main steady flow component. Accordingly, measuring the hydraulic power under different flow conditions is the major subject as far as the experimental side is concerned.

Two types of slurry or suspension were experimentally examined, these are:

- a) bentonite clay-water slurry which flows homogeneously even at very low velocities;
- b) coal-water slurry which, under the experimental conditions in the present investigation, behaved as heterogeneous flow.

The parameters under investigation here may be summarized as:

1. Solid particles concentration in the mixture;
2. Average flow velocity;
3. Pulsating frequency, i.e. the rate at which the pulsing equipment travels,
4. Amplitude of pulsations, which is the maximum displacement of the pulsing device. This, in combination with the frequency, results in a dimensionless velocity amplitude as will be shown later on.

There are, however, other parameters that may significantly affect the subject under investigation here. Some of these are: solid particle size distribution; the ratio between solid particle size and the pipe diameter; the ratio between the solid density and the density of

the carrier fluid; the form of the pulsating wave; and many more. The present investigation was restricted to the four parameters mentioned above.

5.2 Description of the Installation

The main aim of the experimental model was to create a sinusoidal axial velocity component superimposed on a steady axial velocity component. The installation used consisted of: a pipeline, a steady flow system, pulsing equipment, and measuring instruments associated with a pre-programmed microcomputer. A schematic diagram of the flow loop is shown in Figure 5.1.

5.2.1 The Pipeline

The overall length of the laboratory scaled pipeline was 35 m with an ID of 5.08 cm. The length of the test section over which the measurements were taken was 4.57 m. The test section was placed on the return side of the pipeline and it was preceded by an adequate length of pipeline to insure elimination of entrance effects. Also, the test section was built in one piece with no joints to avoid any disturbances to the flow which might affect the measurements. Two pressure taps were placed at the two ends of the test section to allow measurement of the pressure drop over the given length. A 61 Cm QVF glass pipe, of same ID, was fitted at the end of the test section to allow visualization of the flow and checking if there was air trapped in the system.

The pipes used in building the pipeline, including the test section, were schedule 40 commercial steel and it was joined together with necessary fittings, elbows, and valves of gate type.

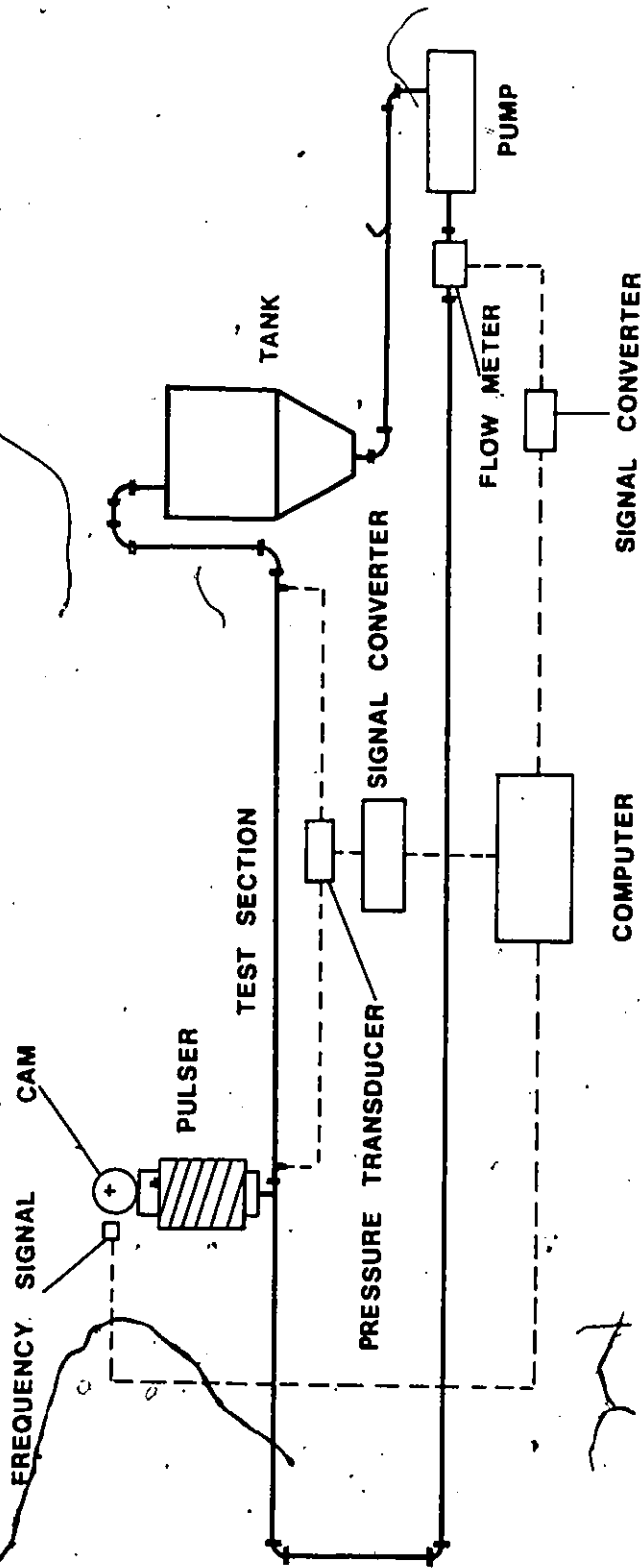


Figure 5.1 Schematic diagram of experimental pipe loop.

5.2.2 Steady Flow System

The different steady flows were obtained by a pump which was connected on the return circuit. The pump was a progressive cavity Moyno type CDR with 3L8 frame. The pump had a maximum capacity of about 0.45 cubic meter per minute at 900 r.p.m. The static head at the maximum pump capacity was about 103 kPa. The pump was driven by a 15 kW AC induction motor of 1160 r.p.m., Brook type DP and frame K286T, provided with a 32 cm diameter Lovejoy spring-loaded pulley and ribbed V-belt arrangement. The pump speed could be changed by using three different pulleys keyed onto the pump driving shaft, one for each speed. These changes were possible by moving the motor on its base toward or away from the pump which could then accommodate the changes in the lengths of the belts. By this arrangement, three different pump speeds could be achieved resulting in three different flowrates. The pump delivery line was 5.08 cm ID and was connected to the pipe line by a flexible rubber pipe of same ID and 1.22 m long. This helped to reduce transmission of vibration to the pipeline and provided flexibility when changes were needed.

A circulating tank was connected to the suction side of the pump by an approximately 5 m long section of the pipeline. The tank had an approximate maximum capacity of 150 liters and was provided with a scale on its side, taking into consideration the total volume of fluid in the whole system for convenience. The bottom part of the tank was conically shaped to prevent accumulation of solid particles and was connected to the suction pipe by an ordinary steel reducer.

5.2.3 Pulsing Equipment

The pulsing equipment was designed and manufactured so that it transformed the rotational movement of a variable speed motor into a sinusoidal translation movement. The basic idea was to convert this translational motion to fully controlled deformations of a

collapsible bellows-type tube." Thus, a rubber bellows of 12.7 cm nominal diameter and of approximately 46 cm relaxed length was placed firmly between a moving piston and a fixed flange attached to the pipeline via a reducer and a Y-lateral. A simple cam mechanism, shown schematically in Figure 5.2, was designed to drive the moving piston between three special steel guide rods. Full control over the amplitude of the sinusoidal translation movement of the piston was achieved by moving a pin in a slot, i.e. alteration of the centre of rotation of the connecting rod. On the other hand, the frequency was controlled by changing the speed of the driving DC motor which drove the cam via a reduction gear system. Three compression springs were placed parallel to the bellows tube, and coaxial with the guide rods, to provide continuous upward force for full contact between the cam and the cam follower.

The sinusoidal vertical reciprocating motion of the piston caused the bellows to collapse and relax identically. Thus, as the piston was forced downward, the fluid that had previously filled the chamber inside the bellows was injected into the pipeline causing a time-dependent increase in the flowrate. In the reverse stroke, the piston was pushed upwards and a negative pressure was generated inside the expanding chamber causing the fluid, of an equal amount to that previously injected ~~into the pipeline~~, to fill into it back from the pipeline and result in a time-dependent decrease in the flowrate.

An acrylic smooth pipe 13 cm ID x 30 cm long was fixed coaxially with the bellows tube to the base in order to prevent undesirable lateral bending to occur occasionally, which could result in considerable changes in the wave shape as well as changes in the amplitude of the pulses.

Detailed drawings for the construction of the pulser mechanism are given in Appendix A.

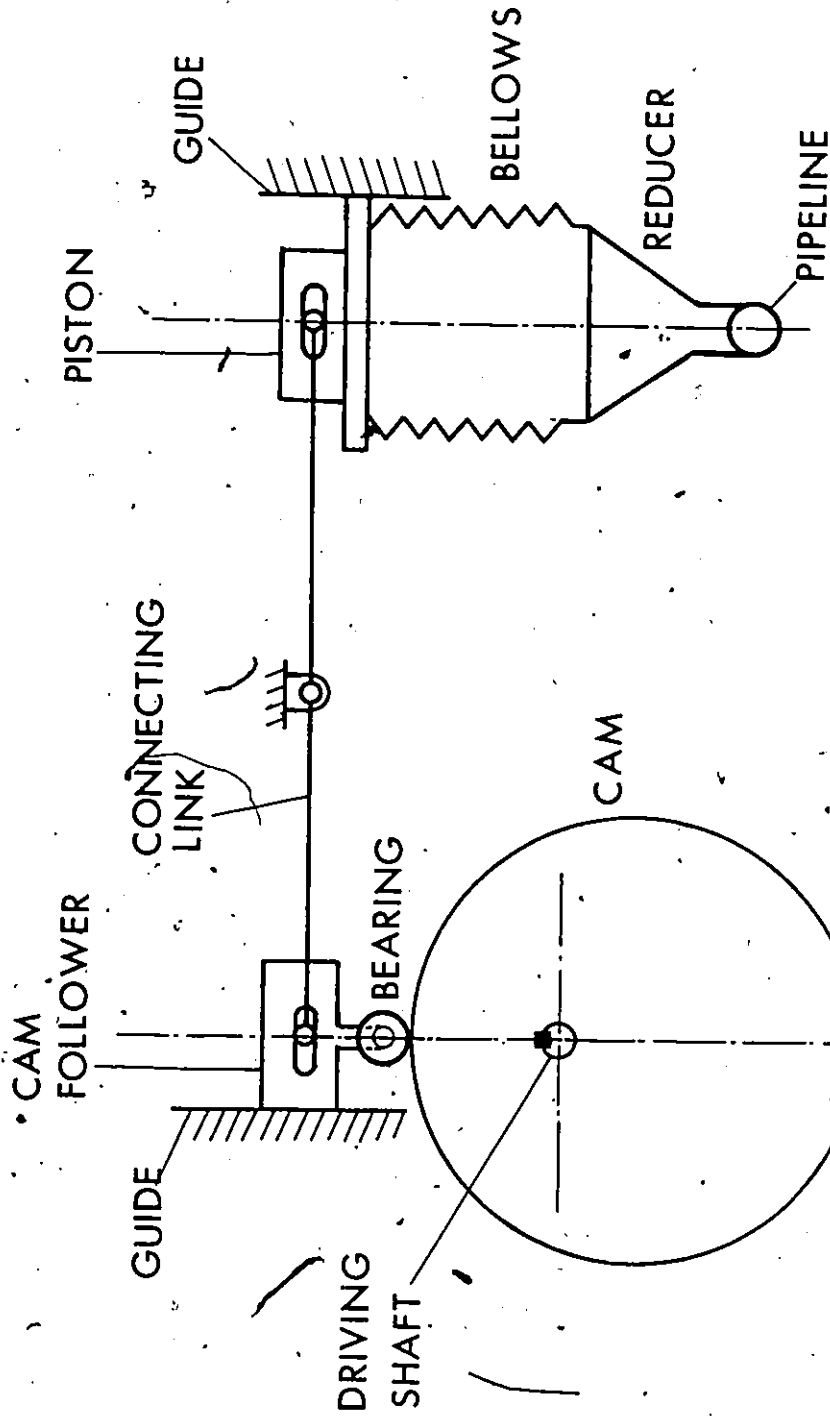


Figure 5.2 Schematic diagram of pulse generating mechanism.

5.2.4 Measuring Instrumentation and the Microcomputer

Measurements of the pressure drop over a defined pipe length and of the flowrate of the flowing fluid are essential for calculating the hydraulic power requirements. A differential pressure transducer was used to measure the pressure drop across the test section. The transducer used was a Celesco Variable Reluctance type, model VP7D. The pressure transducer was connected to a signal converter - Celesco model CD-25A. The signal converter had facility to convey the pressure signal to the microcomputer as well as displaying it as a percentage reading of certain maximum value which could be changed to increase the degree of sensitivity.

The fluid or the slurry flowrate was measured by a flowmeter which was contained on the delivery line of the pump. The flowmeter was a Brooks electromagnetic type model 7100/7200. The output of the flowmeter was taken to a signal converter, Brooks model 7300. The signal converter was also connected to the microcomputer and it displayed the flowrate reading as a percentage of a maximum capacity of 180 USGPM which corresponds to 0.6184 m³/min.

The frequency of pulsations was determined by measuring the average time of a single cycle. An electronic photocell was attached to the cam follower while a thin metal blade was fixed to the pulser frame so that it passed through the photocell beam only when it was at its lowest position. The photocell reached its lowest position once each cycle; consequently, the blade cut the light beam and caused a signal once each cycle. These signals were conveyed to the microcomputer to calculate the average time of a single cycle, i.e. the frequency.

The microcomputer itself was built, programmed and installed for specific calculations. The mathematical bases on which the microcomputer was programmed are explained in detail in a following section, 5.6.

5.3 Bentonite Clay-Water Suspension

The clay-water suspension was produced by accurately weighing out the required amount of bentonite powder and accurately measuring the required amount of tap water to achieve the desired concentration. The bentonite powder was pre-mixed with enough water in a separate tank to disperse it into highly concentrated mixture which was then carefully poured into the circulating tank to be mixed with the flowing water while stirring vigorously by keeping the pump running at moderate speed. This prevented the clay powder from flocculating and also prevented possible plugging of the system.

The bentonite powder used was very fine. Up to 94% of the clay particles were finer than 5 microns, while 96% were finer than 45 microns. The average particle size was estimated about 2.25 microns. The specific gravity and the pH value were 2.7 and 8.5-10, respectively.

Four different clay-water suspension concentrations were examined in this investigation. Samples were taken from each concentration for accurate determination of density and also for testing the rheological behaviour of the suspension at such concentration.

The density of the suspension was measured by taking three random samples directly from the pressure taps, which were provided with switching valves to release the air trapped in the system. The samples were taken in a measuring cylinder of 100 cc and were then weighed to an accuracy of ± 0.01 g. It was found that the density of each sample remained essentially the same, irrespective of the flowrate.

Other samples were taken for rheological tests. The rheological analysis was obtained by using a Haake viscometer. The rheograms given by the viscometry tests are shown in Figure 5.3, and the other physical properties are given in Table 5.1.

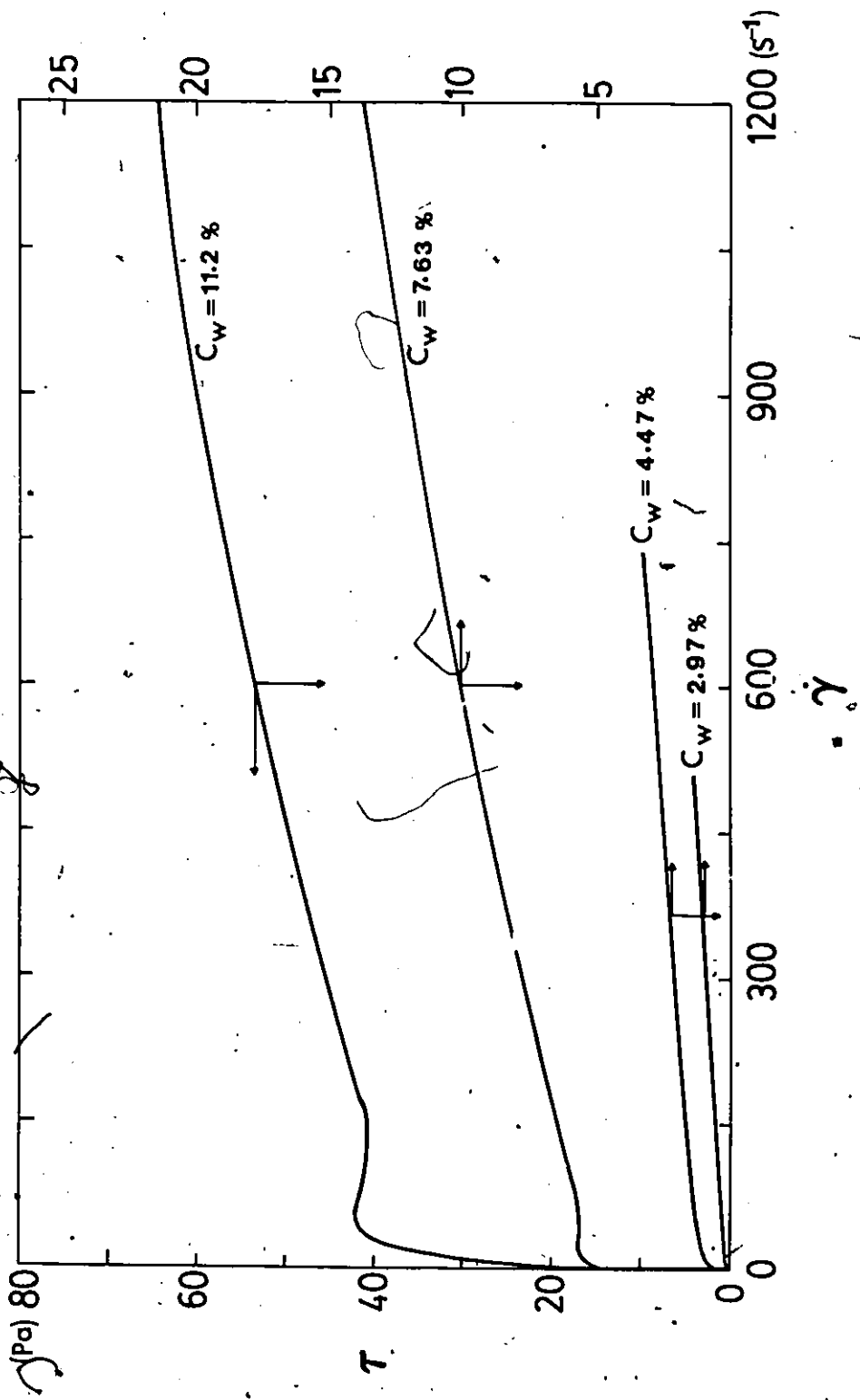


Figure 5.3 Shear stress vs. shear rate for bentonite clay-water suspensions at different solids weight concentrations (obtained by Haake viscometer).

Table 5.1

Physical properties of bentonite clay-water suspensions at different weight concentrations

$C_w\%$	$\rho(\text{Kg/m}^3)$	$\tau_0(\text{Pa})$	$K(\text{Pa}\cdot\text{s}^n)$	n
2.97	1018.5	0.0	0.00193	1.0
4.47	1033.8	1.14	0.00256	0.9890
7.63	1053.3	4.83	0.01140	0.9362
11.20	1061.5	33.81	0.03963	0.9432

5.4 Coal-Water Slurry

The coal was used as received from the supplier. It was a bituminous coal from Butler County, Pennsylvania. Three samples were taken from different packages and were carefully weighed and screened using standard screen sieves. The size was found to range from 45 to 880 microns, with a mean of 260 microns. The size distribution is presented in Table 5.2 and Figure 5.4. A sample was microphotographed. Figure 5.5 is such a microphotograph of the coal used. The particles were very angular and plate-like in form and had the distinct appearance of crushed rock.

The specific gravity and the pH value for the coal as received, were 1.28 and 2.7-2.9, respectively. Chemical analysis of the coal is given in Table 5.3.

The slurry was prepared by following the same procedures mentioned above, as in clay-water suspension. Samples of 100 cc from each concentration were taken directly from the pipe which delivered into the circulating tank. The samples were then accurately weighed and the density was obtained for each concentration. These values are given in Table 5.4.

5.5 Calibration of Measuring Instruments

Two terms always appear in calculating hydraulic energy or power consumption. These are: the pressure drop over a known length, and the volumetric flowrate. It has already been noted in section 5.2.4 that a differential pressure transducer and an electromagnetic flowmeter were used for measuring such quantities. The signals from these measurements had to be conveyed to the microcomputer for processing at high rates. Therefore, accurate calibrations of the differential pressure transducer and the flowmeter were necessary.

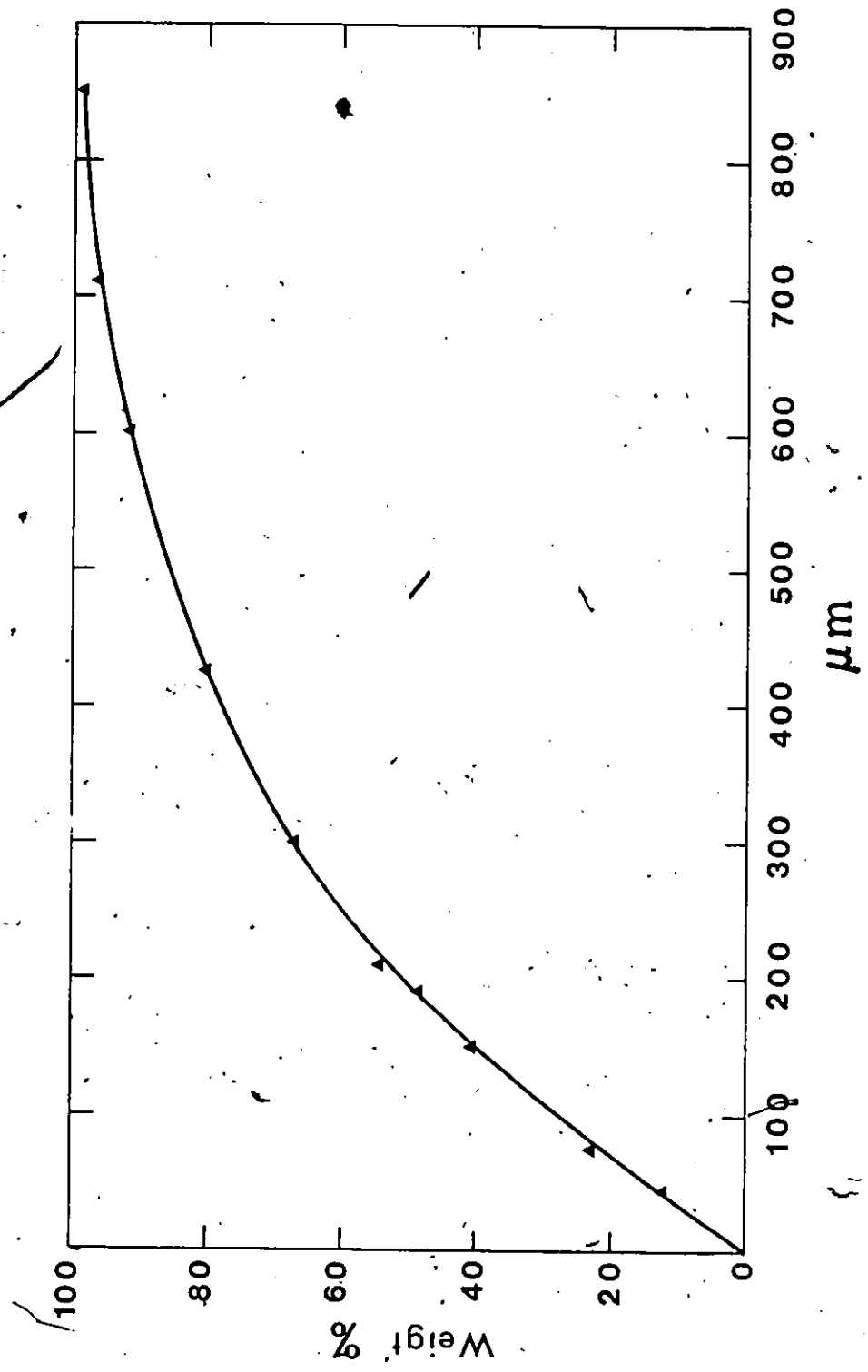


Figure 5.4 Coal particle size distribution.

0 0.5 1. mm



Figure 5.5 Photomicrograph of a coal sample.

Table 5.2

Coal particle size distribution

Mesh	Size μm	Weight%
-325	<45	12.60
-200, +325	75-45	10.11
-100, +200	150-75	17.61
-80, +100	180-150	7.84
-65, +80	212-180	6.42
-48, +65	300-212	12.38
-35, +48	425-300	13.12
-28, +35	600-425	11.56
-24, +28	710-600	4.32
-20, +24	850-710	2.74
+20	>850	1.30

Table 5.3

Coal chemical analysis

Moisture	2%
Ash	10%
Volatile	34%
Fixed Carbon	54%
Sulphur	2.7%

Table 5.4

Density of coal-water slurry at different solids weight concentrations

$C_w\%$	5.34	8.9	14.25	19.59	24.93	30.27	37.5	44.64	53.7
$\rho(\text{Kg/m}^3)$	1010.9	1019.0	1031.3	1036.1	1057.0	1070.3	1088.9	1101.7	1127.6

5.5.1 Calibration of Pressure Transducer

The pressure transducer was first adjusted so that zero voltage was indicated at zero pressure difference. A pressure head of 34.5 kPa was then applied using a dead-weight apparatus and the signal converter was adjusted so that the corresponding output voltage was $10 \text{ v} \pm 5 \text{ mV}$ and the display reading was 100%.

A mercury U-tube manometer was connected to the transducer and to the oil-filled dead-weight apparatus via a T-connection. The U-tube manometer was used here because the dead-weight apparatus did not have the facility to indicate values of pressure less than 34.5 kPa. As the pressure was decreased from 34.5 kPa by reasonable increments, 10% on the display, the height of mercury in the manometer as well as the corresponding voltage were recorded. Figure 5.6 shows the voltmeter readings plotted against the manometer and the display readings. The relationship is a straight line passing through the origin indicating a linear response of the transducer with respect to the applied pressure.

5.5.2 Calibration of the Flowmeter

In this case, the flowmeter was turned on and allowed to warm up for about 1 h. The flowrate was measured in two ways: first, by collecting a certain amount of the fluid in a measuring tank and recording the corresponding time; and secondly, by multiplying the percentage reading from the display by a conversion factor of $0.6814 \text{ m}^3/\text{min}$. The output of the signal converter was connected to the voltmeter yields recording of the corresponding voltage. Figure 5.7 shows the voltmeter readings plotted against the flowmeter and the manually measured flowrate. Again here, the relationship is a straight line passing through the origin which indicates a linear response of the flowmeter.

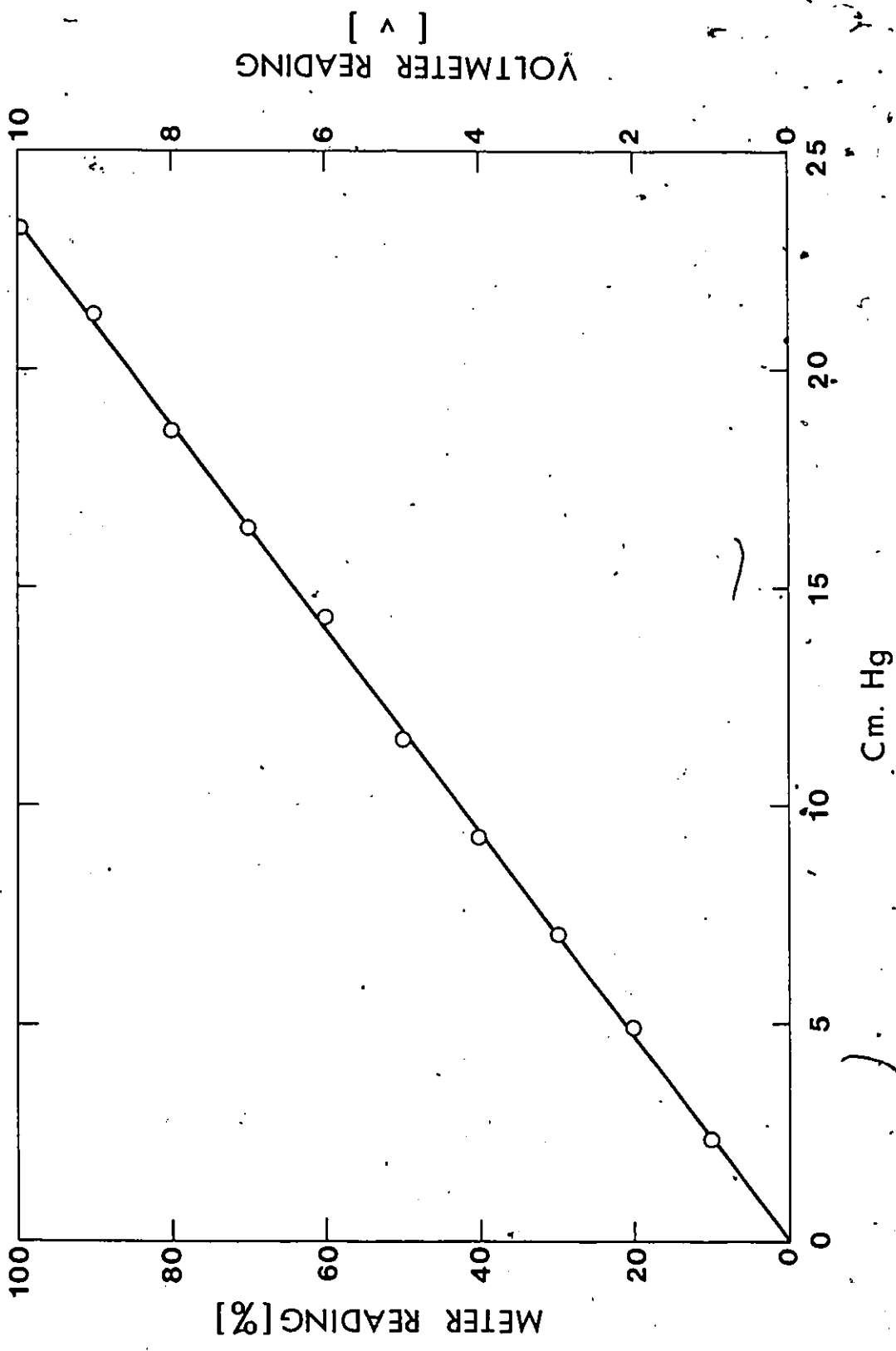


Figure 5.6 Pressure transducer calibration curve.

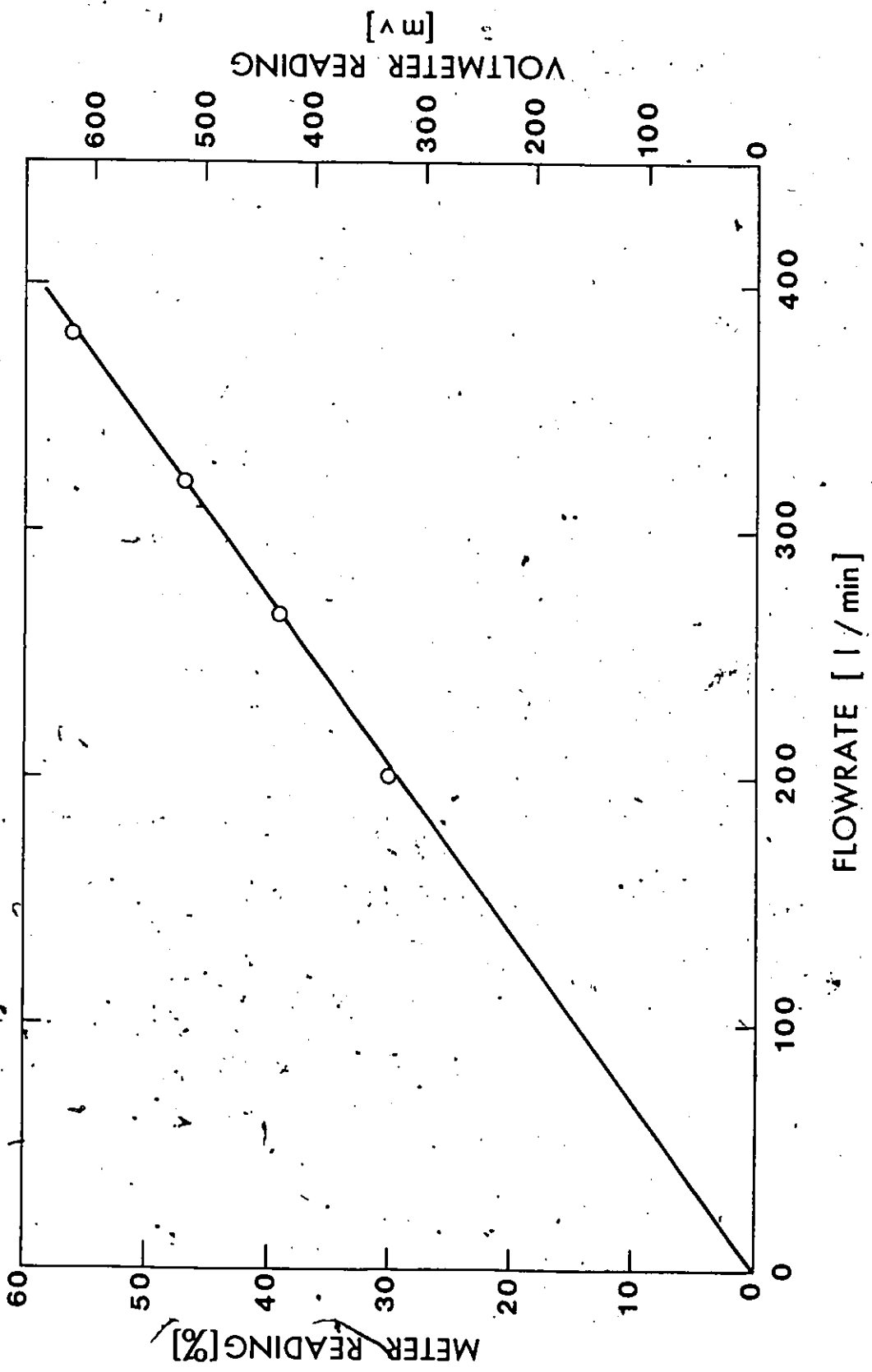


Figure 5.7 Flowmeter calibration curve.

5.6 Programming the Microcomputer

The microcomputer, in fact, had a very important role to play in this investigation. Values of the pressure drop across the test section and the flowrate had to be recorded and stored for calculations at high sampling rates.

The microcomputer was programmed so that first, it calculated the average frequency over 20 cycles. The hydraulic energy consumed in the test section under pulsating flows in one cycle was given by

$$J_p = \lambda \int_0^{1/\lambda} \frac{\Delta P}{L} Q dt \quad (5.1)$$

where, J_p is the hydraulic power per unit length under pulsating flow conditions, λ is the frequency as number of cycles per unit time. This integration was carried out numerically by using Simpson's rule. 150 samples per cycle were conveyed to the microcomputer for the values of the pressure differential and same for the flowrate. This number of samples was tested and found to be adequate for obtaining accurate results. The calculations were then carried out, and a value of J_p was obtained and stored by the computer. This process was repeated over 35 cycles. The 35 values of J_p were then averaged mathematically and the result was one average value for J_p corresponding to a certain frequency, certain amplitude, certain average flow velocity and certain slurry concentration. 35 cycles was also found to be reasonable for obtaining accurate value of J_p . In the case of steady flow, i.e. J_s , a total number of samples of 300 at a rate of 30 samples per second was found to be satisfactory.

A list of the program in Fortran-IV is given in Appendix E.

5.7 Experimental Procedures

As mentioned before, two types of solid-liquid mixtures were examined in this investigation at different concentrations, frequencies, amplitudes and flowrates. The

experiments were designed in such a way that only one parameter was changed at a time while keeping all the others fixed.

The experimental procedures adopted in the present investigation may be summarized as follows:

1. The system was filled with a predetermined quantity of tap water which could give the desired slurry concentration.
2. The flowmeter and the signal converters of both the flowmeter and the pressure transducer were turned on about one hour before running the experiments for warming up.
3. The pump was set at the required speed and turned on.
4. The prepared slurry was added gradually and carefully into the circulating tank. The amount of water which have been used in preparing the slurry was originally taken from the predetermined quantity of water.
5. The system was left running for enough time to attain thermal stability.
6. The pulsing device was set at the desired amplitude and frequency and was turned on. Signals from the pressure transducer were monitored on the screen of an oscilloscope. When the steady state of pulsating flow was reached, the microcomputer received a signal to start running its program to evaluate J_p as it has been explained in section 5.6.
7. The pulsing frequency was then changed to its next value. The range of the frequency was from zero up to about 1.25 Hz.
8. Another amplitude was then obtained by moving a pin in a slot. Three amplitudes were investigated; these were 34.6, 52.1 and 76.2 mm. The amplitudes here are given as measurable axial deflection of the bellows tube.

9. Steps 6 to 8 were repeated after changing the pump speed. Three average flowrates, i.e. three average velocities were included in the present study. They were 1.63, 2.18 and 2.63 m/s.

10. Steps from 4 to 9 were then repeated for another slurry concentration.

All the above steps from 1 to 10 were followed for the two solid liquid mixtures, the clay-water suspension and the coal-water slurry.

CHAPTER 6

RESULTS OF FINITE DIFFERENCE SOLUTION AND DISCUSSION

Typical computed results for pulsating flows and start-up flows are presented in this chapter. The results are shown in terms of dimensionless velocity profiles for both cases, while they are shown as predictions of flowrate, power requirement, and phase angle only for pulsating flows. Analysis and discussion of the results are also included in this chapter.

6.1 Pulsating Flow

6.1.1 Velocity Profiles

Computed velocity profiles in pulsating flow are presented in Figures 6.1 to 6.4 for different fluids and at different flow parameters. These results were obtained after the decay of the initial transient, i.e. after the motion had equilibrated to its steady cycling behaviour. The number of cycles required to achieve this steady cycling behaviour depended on the frequency parameter and type of fluid. For example, fewer cycles are required for a Bingham fluid compared to Newtonian fluid, while a higher number is needed as n becomes less than unity. This is explained by referring to the results of start-up flow. On the other hand, a higher number of cycles are required to achieve the steady cycling mode at higher values of the frequency parameter, whilst much less are required at lower frequencies.

Comparison of the velocities at equivalent times during two consecutive cycles shows almost complete decay of the initial transient. Typical results illustrating the decay of this transient are presented in Table 6.1 where values of the velocity are given for equivalent times during the first six cycles.

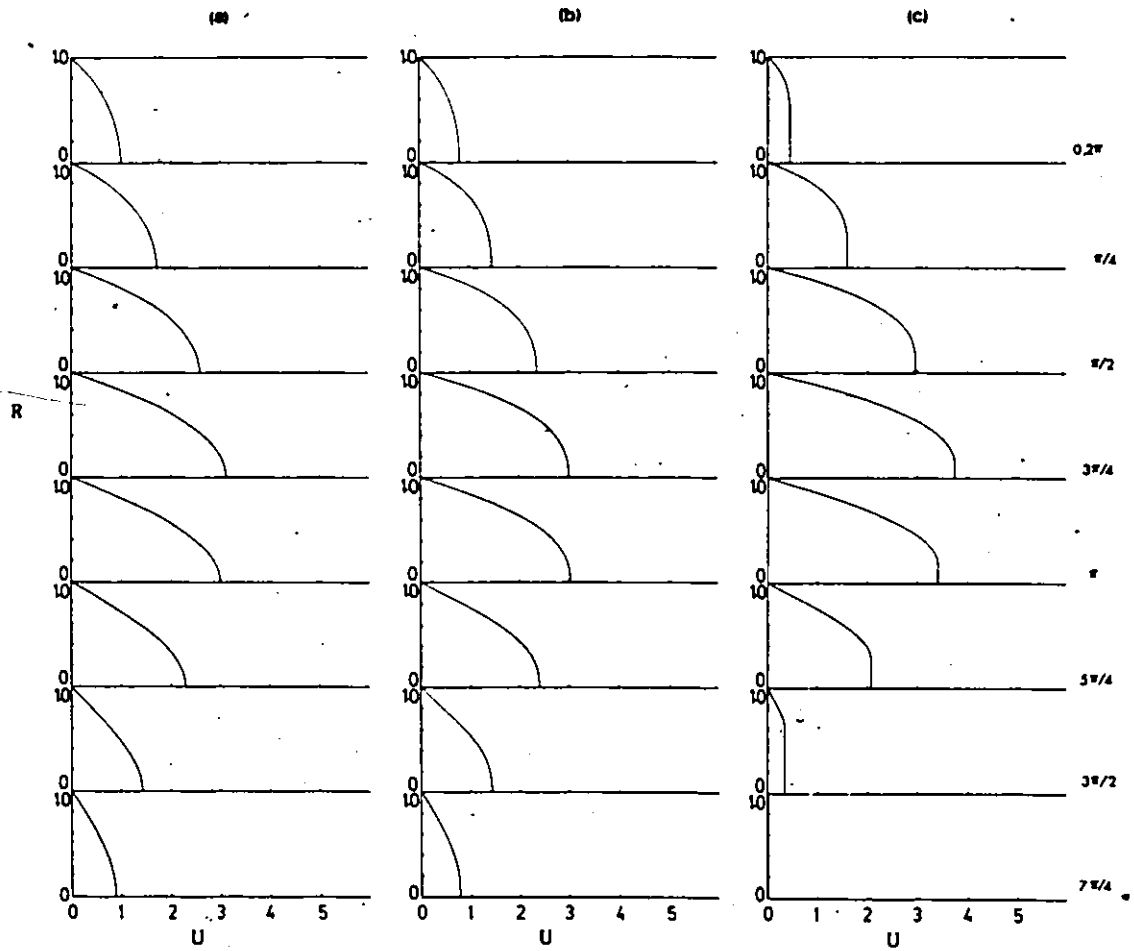


Figure 6.1

Theoretical predictions of velocity profiles for pulsating flows of

(a) Newtonian,

(b) power law $n = 0.7$,

(c) ideal Bingham $\tau_0/\tau_w = 0.32$.

Results at $\zeta = 5.0$ and $\epsilon = 1$.

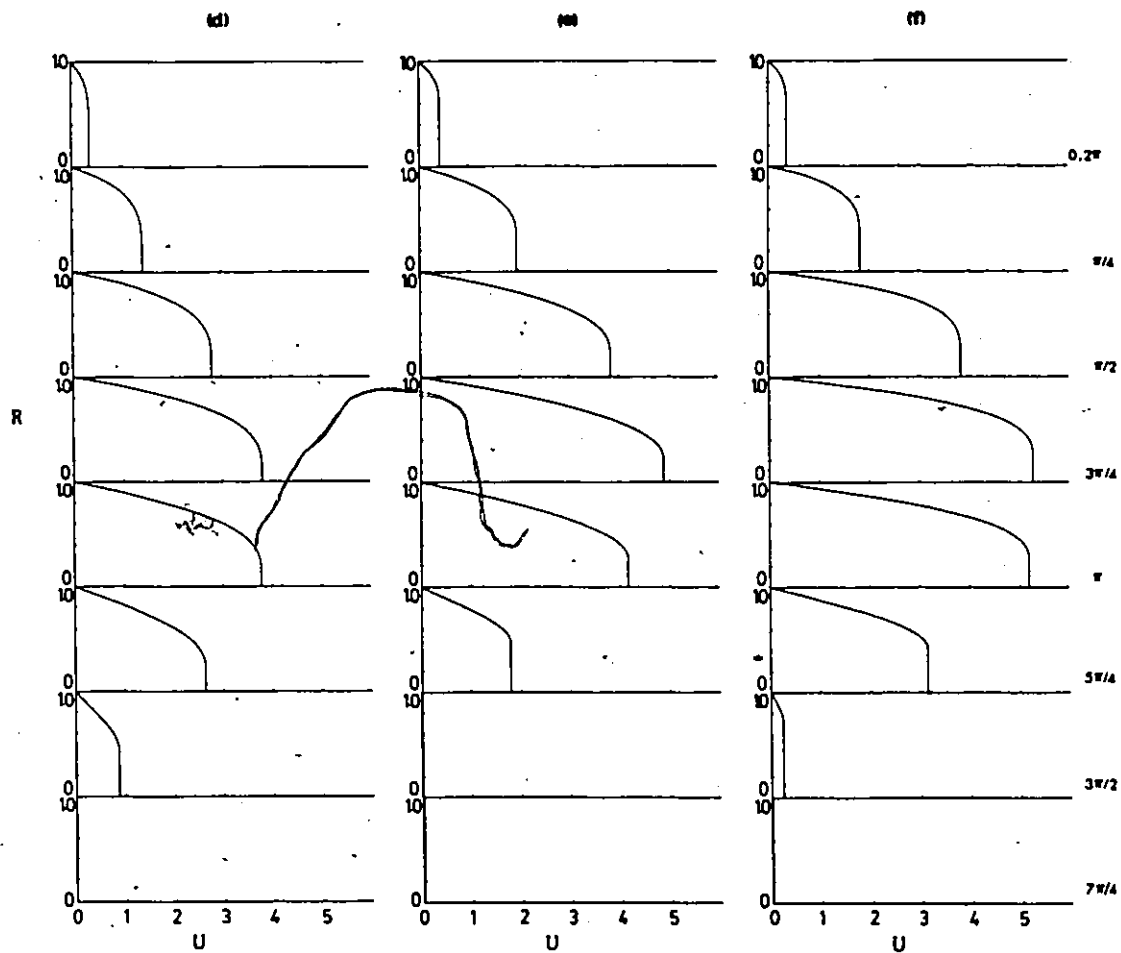


Figure 6.1cont. (d) generalized Bingham $n = 0.7$ and $\tau_0/\tau_w = 0.32$,
 (e) ideal Bingham $\tau_0/\tau_w = 0.44$,
 (f) generalized Bingham $n = 0.7$ and $\tau_0/\tau_w = 0.44$.
 Results at $\zeta = 5.0$ and $\epsilon = 1$.

Table 6.1

Velocity profiles during the first 6 cycles for a generalized Bingham material

with $n=0.7$; $\tau_0/\tau_w = 0.32$, and at $\zeta = 10$, $\varepsilon = 1.0$

$\begin{matrix} R \\ T \end{matrix}$.9	.8	.7	.6	.5	.4	.3	.2	.1	0.0
0.5	.7572	1.3668	1.8228	2.1423	2.3500	2.4712	2.5296	2.5490	2.5490	2.5490
1.5	.8080	1.4660	1.9644	2.3184	2.5518	2.6901	2.7579	2.7803	2.7803	2.7083
2.5	.8145	1.4788	1.9828	2.3412	2.5780	2.7186	2.7876	2.8104	2.8104	2.8104
3.5	.8155	1.4807	1.9854	2.3445	2.5818	2.7227	2.7919	2.8147	2.8147	2.8147
4.5	.8156	1.4809	1.9858	2.3449	2.5823	2.7233	2.7925	2.8154	2.8154	2.8154
5.5	.8156	1.4810	1.9858	2.3450	2.5824	2.2733	2.7926	2.8155	2.8155	2.8155

The velocity profiles in Figures 6.1 to 6.4 are shown at equal intervals of $\pi/4$ of the pressure-wave and across one-half of the pipe cross-section. Figure 6.1 shows computed values of the instantaneous velocity profiles for Newtonian, power law, ideal Bingham, and generalized Bingham fluids at a frequency parameter $\zeta = 5$ and at pressure amplitude $\varepsilon = 1.0$. In this figure, the effect of the fluid properties is illustrated. The effect of yield stress can be seen in (a), (c) and (e), or in (b), (d) and (f). Increases in the ratio of yield stress to wall shear stress is accompanied by increases in the velocity amplitude, and consequently increases in the rate at which the velocity profile deforms. A comparison between a Newtonian fluid (a) and Bingham fluids (c) and (e) shows higher rates of velocity profile deformation for Bingham fluids over that of Newtonian fluids in the accelerating phase. This difference is more pronounced over the decelerating phase. Over the last portion of the decelerating phase, the Bingham fluid has a velocity profile with shape differing very little from zero. This situation may be a result of the relatively high plastic viscosity of the fluid - the pressure in this phase is not adequate to overcome the yield stress. It was pointed out previously, in section 2.3, that this phenomenon was observed by Ohmi and Iguchi [50,51] during their investigation for pulsating laminar pipe flow.

In the same Figure 6.1, a comparison between (c) and (d), or between (e) and (f) illustrates the effect of n being less than unity, i.e. the fluid is much more shear thinning. For $n < 1$ and in the region where $R > R_0$, the shear stress is higher near the wall and the values of the velocity are higher than those corresponding to $n = 1$. This means that a significant change in the form of the velocity profile is expected, due to the change of n . Furthermore, a significant increase of the instantaneous flowrate is expected as n becomes less than unity.

The effect of frequency parameter ζ is illustrated in Figures 6.2 and 6.3, where the results are given for an ideal Bingham fluid and a generalized Bingham fluid, respectively.

The frequency parameter $\zeta = 4, 7$ and 10 for (a), (b) and (c), respectively in both cases.

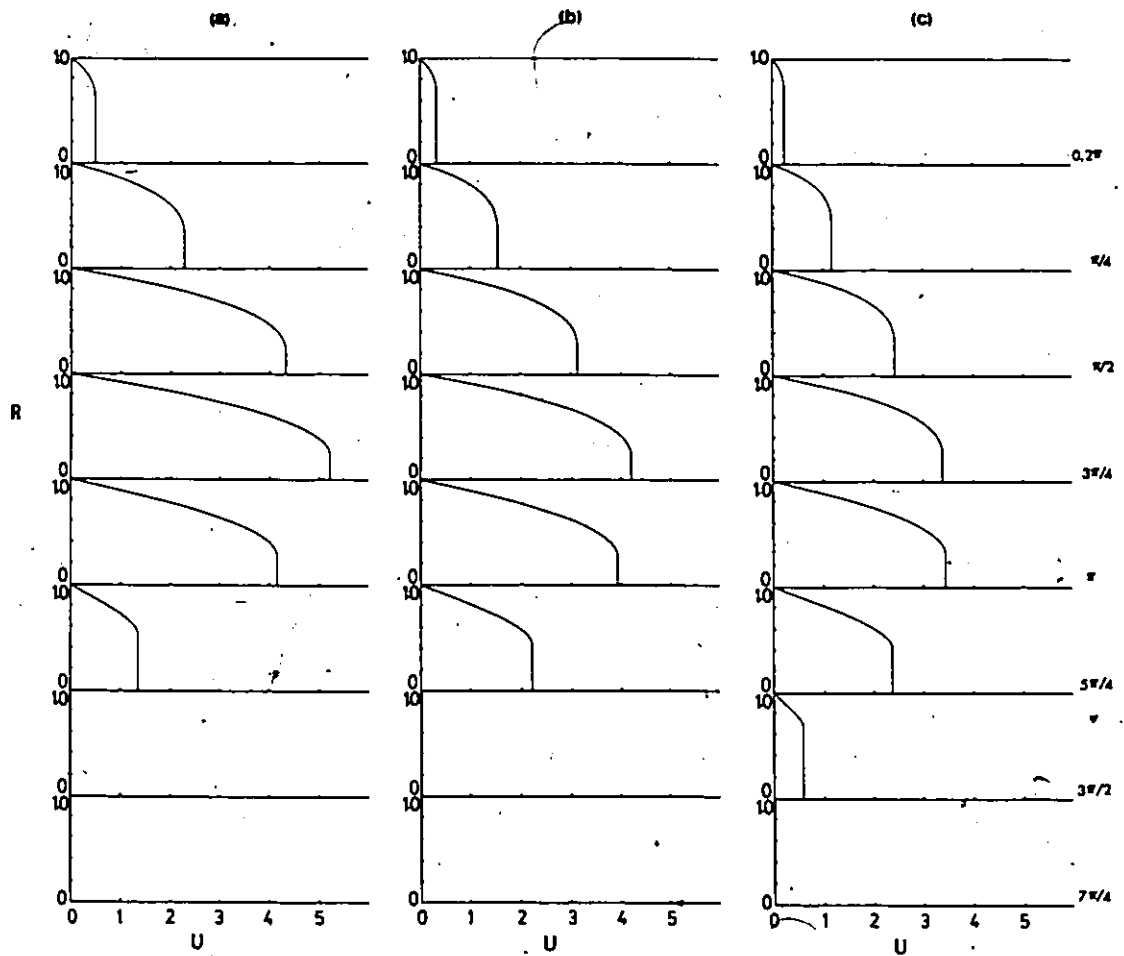


Figure 6.2

Theoretical predictions of velocity profiles for pulsating flows of an ideal Bingham fluid at different frequencies.

(a) $\zeta = 4.0$,

(b) $\zeta = 7.0$,

(c) $\zeta = 10$

Results at $\tau_0/\tau_w = 0.44$ and $\varepsilon = 1$.

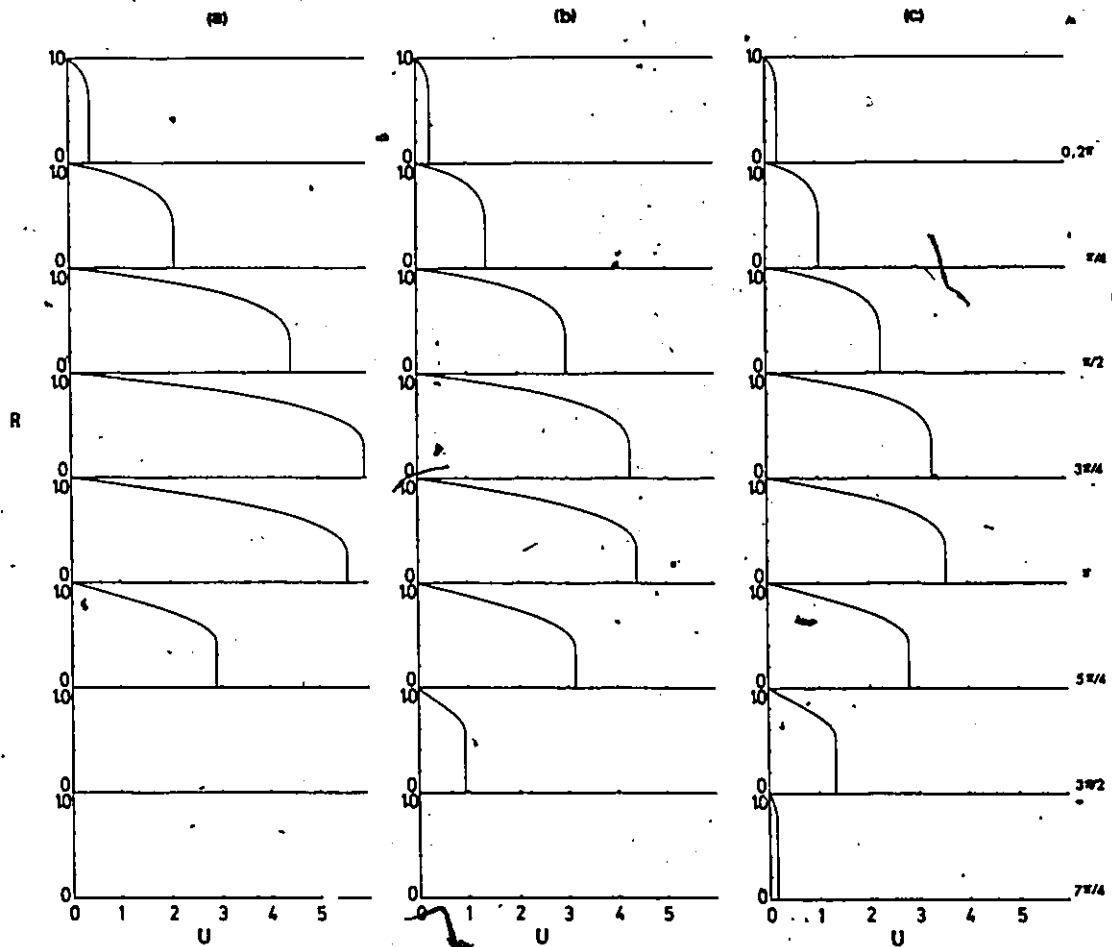


Figure 6.3

Theoretical predictions of velocity profiles for pulsating flows of a generalized Bingham fluid at different frequencies.

(a) $\zeta = 4.0$,

(b) $\zeta = 7.0$,

(c) $\zeta = 10$

Results at $n = 0.7$, $\tau_0/\tau_w = 0.44$ and $\varepsilon = 1$.

Examination of the results in these two figures demonstrates that for a fixed pressure amplitude ($\epsilon = 1.0$), changing the frequency parameter significantly affects the velocity amplitude as well as the minimum value of R_0 . As the frequency increases, the velocity amplitude decreases until $\zeta > 30$, thereafter the change is insignificant. The converse is also true as Figures 6.2 and 6.3 indicate; at low frequencies, the velocity amplitude is much higher and the size of the central core, i.e. R_0 approaches values smaller than those at higher frequencies. This can be explained by the fact that the mass of the fluid is accelerating and decelerating due to the oscillating pressure gradient which is acting as the source of momentum in this case, and therefore, the fluid takes time to achieve its maximum and its minimum velocities while at high frequencies that time becomes smaller and smaller.

Figure 6.4 shows the effect of variations in the pressure amplitude ϵ at a value of the frequency parameter of 7.0 for a generalized Bingham fluid. The values of ϵ range from .5 to 2.0. It is clear that variations in ϵ have direct effect on the velocity amplitude, the minimum value of R_0 , and the shape of the velocity profile itself. No significant flow reversal is achieved, even for $\epsilon = 2.0$. Flow reversal may be achieved at very low values of ζ . Such values are not included in the results presented here because it is believed that these are impractical. Additionally, the numerical calculations become exceedingly difficult for $\zeta < 1.0$. The minima of the velocity profile is not affected as much as the maxima is affected by the variation of ϵ . For example, the value of U at $R = 0$, $\omega t = 7\pi/4$ and at $\epsilon = 0.5$ is nearly 1.1, while the equivalent value at $\epsilon = 2.0$ is about -0.01. On the other hand, these values at $\omega t = \pi$ are about 2.5 and 5.2, respectively. Also, the situation in which the velocity almost approaches zero at all points at the same time is more pronounced as the value of ϵ increases.

Examination of all the above results for Bingham fluids demonstrates the variation of R_0 over a complete cycle. In some cases, R_0 approaches 1 as a maximum. This, however, may not be true in practice since fluids of this type have a finite relaxation time; in other

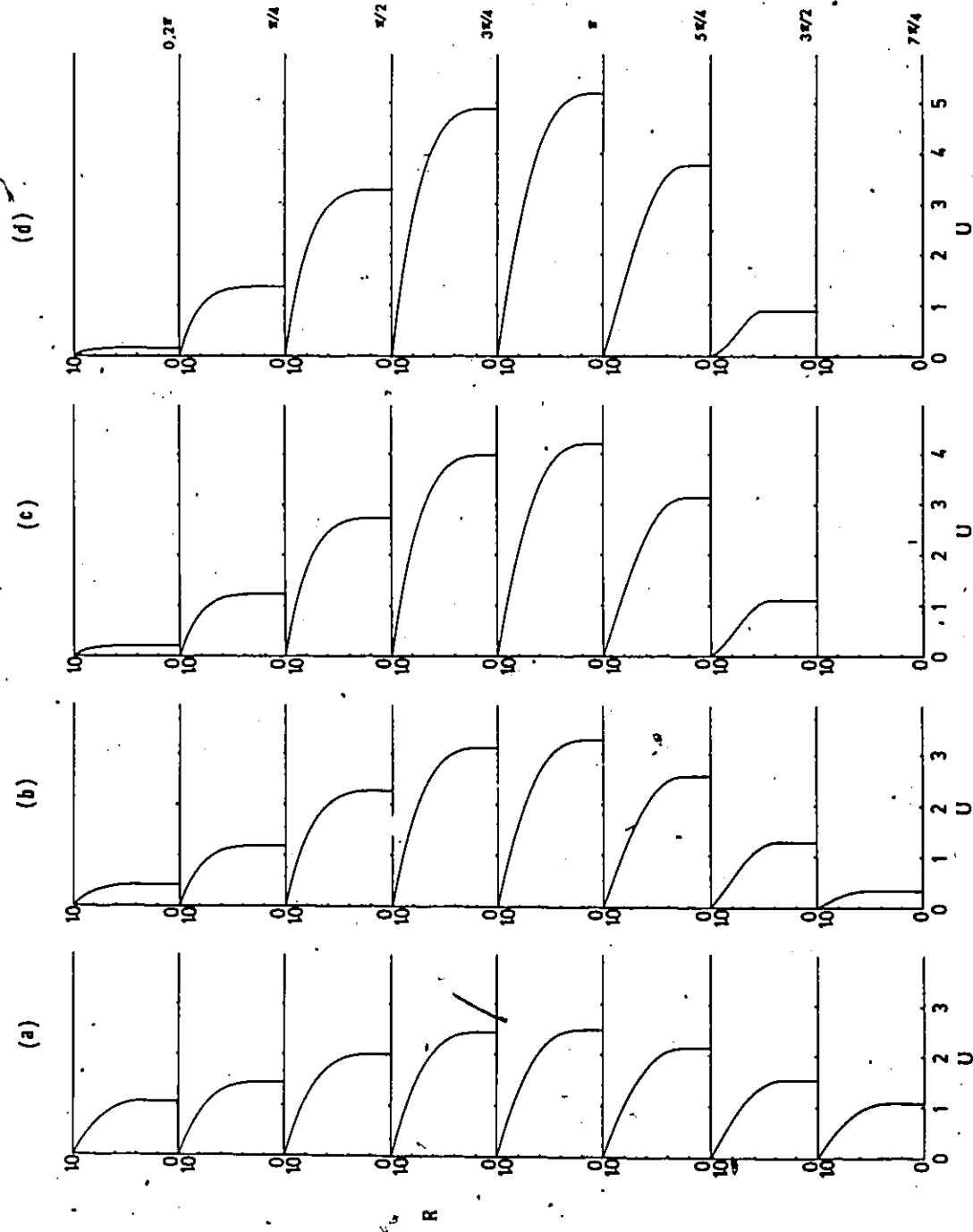


Figure 6.4
 Theoretical predictions of velocity profiles for pulsating flows of a generalized Bingham fluid at different amplitudes.

- (a) $\epsilon = 0.5$,
- (b) $\epsilon = 1$,
- (c) $\epsilon = 1.5$,
- (d) $\epsilon = 2$.

Results at $n = 0.7$, $\tau_0/\tau_w = 0.32$ and $\zeta = 7$.

words, when such a fluid is stressed, it deforms accordingly and after the stress is removed, it takes some time to reform back. This fact is not taken into consideration in the constitutive equation (4.1); and therefore, the fluid shows immediate response to variations in stress.

6.1.2 Flowrates

Computed values of the ratio S of the flowrate in pulsating flow to that in steady flow of the same mean pressure gradient are presented as functions of the frequency parameter ζ in Figure 6.5. The results are given for Newtonian, power law, ideal Bingham and generalized Bingham fluids at a constant value of pressure amplitude $\epsilon = 1.0$.

In Figure 6.5, each curve represents each type of the aforementioned fluids (with $n = 0.7$, and $\tau_0/\tau_w = .44$). In the case of a Newtonian fluid, the curve is a horizontal straight line at a value of $S = 1.0$, which indicates that no change in the flowrate is expected due to pulsating flow at any value of the frequency parameter. Unlike the case of Newtonian fluid, the curves of non-Newtonian fluids approach $S = 1$ asymptotically in two regions. One is where $\zeta \rightarrow 0$ in which the flow is steady or nearly steady, and eventually S approaches unity and the other at values of ζ ranging between 10 and 20 or higher, depending on the type and rheological properties of the fluid. It is clear from the definition of S that at $\zeta = 0$, S must equal unity. Unfortunately, at very low values of ζ , a numerical solution is practically impossible to obtain. Assumption of quasi-steady flow may be introduced by neglecting the inertia term in the equation of motion (4.37) because it is very small in comparison with the viscous term. This yields a value of S which is independent of ζ and nearly equals unity regardless of the type of fluid. There is, however, a small gap between the minimum value of ζ at which a numerical solution can be obtained and the point at which quasi-steady flow can be assumed. Such a point is not very well defined and it may vary from one fluid to another, but this is not a serious deficiency for two reasons: first, this range of frequency is far from a

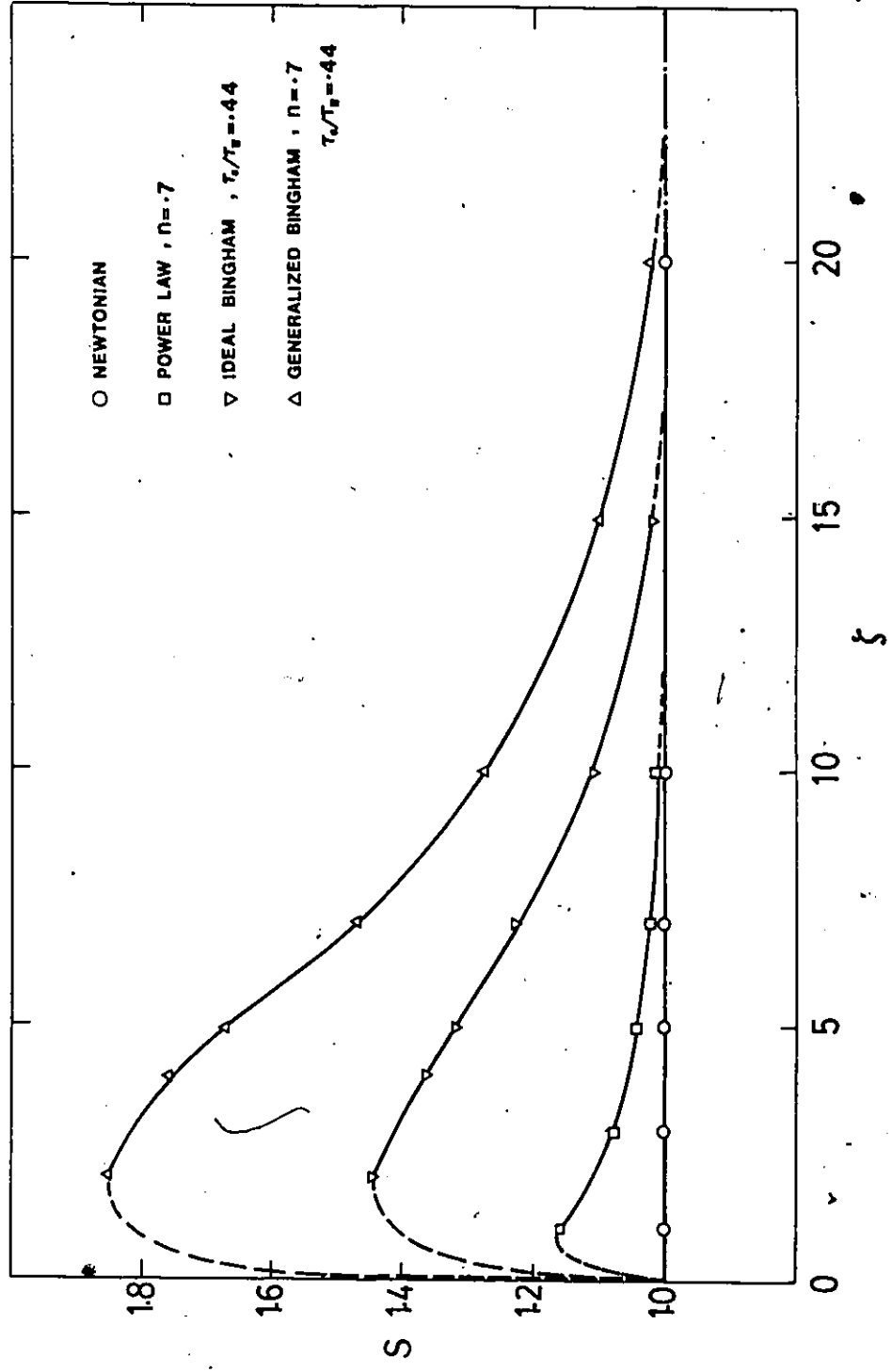


Figure 6.5 Theoretical predictions of dimensionless pulsating flowrates S vs. dimensionless frequency ζ ($c = 1$).

practical range and secondly, quasi-steady flow assumption does not yield values of S very much different from the steady flow, i.e. $S \approx 1$.

The other limiting region that can be seen in Figure 6.5 occurs at large values of ζ . For such values, it has been demonstrated previously that the velocity profile fluctuates by only a very small amount about the steady flow velocity profile. Consequently, it can be concluded that at large values of ζ , the pulsating flowrate Q_p approaches the steady flowrate Q_s , or in other words, S approaches unity.

Between the above two limiting regions, non-Newtonian fluids behave very differently from Newtonian fluids. The solution in this transition region may be obtained by the use of finite difference analysis.

It is clear that increases in the flowrate are possible for power law fluids (where $n < 1.0$) as well as ideal and generalized Bingham fluids (also where $n \leq 1.0$). There is a value of ζ at which a peak in S occurs for each type of fluid. As ζ increases, the values of S start to drop gradually until it approach unity, as described above.

A comparison between these theoretical findings with the data of Barnes *et al.* [1], given in Figure 2.8, and the data of Walters and Townsend [2], given in Figure 2.11, shows that they all basically agree about the existence of a peak in S .

The major reason for these increases in flowrate for fluids of $n < 1$ is that these fluids are shear thinning materials and significant increases in the velocity, particularly in the region near the wall, occur due to the high shear stress which is generated during the accelerating phase of each pulse -- causing the apparent viscosity to reduce accordingly. The other reasons which applies to Bingham materials is the reduction in the size of the central core. This may be seen clearly in the velocity profiles given in Figures 6.1 to 6.4.

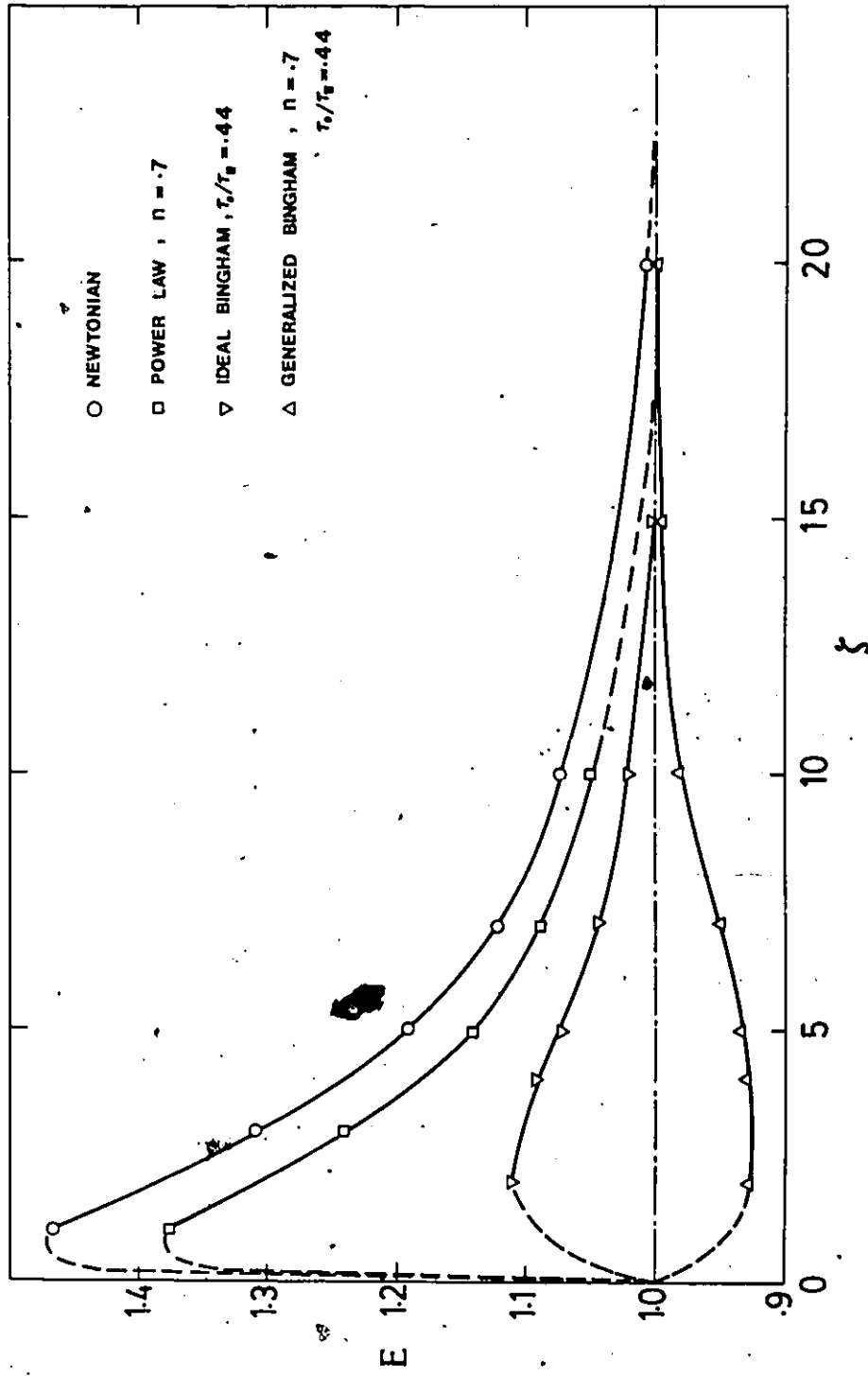


Figure 6.6 Theoretical predictions of dimensionless pulsating hydraulic power requirements E vs. dimensionless frequency ζ ($\epsilon = 1$).

6.1.3 Hydraulic Power Requirements

The ratio of the power requirement per unit length for pulsating flow to that for steady flow at the same flowrate is presented in Figure 6.6 as a function of the frequency parameter ζ for different fluids. Results are shown for Newtonian, power law, ideal Bingham and generalized Bingham fluids for an amplitude of $\epsilon = 1.0$.

The same asymptotic behaviour is also observed for the ratio E , at very low values and at high values of ζ . As it has been explained previously, as $\zeta \rightarrow 0$, the flow is steady or nearly steady and according to the definition of E , its value must equal unity. On the other hand, at large values of ζ , the instantaneous pulsating velocity profiles oscillate with very small amplitude about the steady flow velocity profile, i.e. $Q_p \rightarrow \bar{Q}_p \rightarrow Q_s$. Thus, the hydraulic power requirement in pulsating flow becomes

$$\bar{J}_p = \frac{\omega}{2\pi} \int_0^{2\pi/\omega} Q_s \left(\frac{dP}{dx} \right)_s (1 + \epsilon \sin \omega t) dt \quad (6.1)$$

i.e.

$$\bar{J}_p = Q_s \cdot \left(\frac{dP}{dx} \right)_s = J_s \quad (6.2)$$

The result given by this equation in addition to the fact that $\bar{Q}_p = Q_s$ is that as ζ becomes large, E approaches unity.

Computed values of E within the range $1.0 \leq \zeta \leq 20$ are given for different types of fluids. In this range, the solution given for Newtonian fluids is compared with a known solution (Uchida [32]). Such a comparison indicates that the discrepancy between the computed values and the analytical values [32] is less than 1%. All fluids, except the Bingham type show values of E higher than unity. This indicates that hydraulic pumping power for the transport of power law and Newtonian fluids is minimum in steady flow. However, this is not the case for a generalized Bingham fluid. It may be seen in Figure 6.6 that the curve for such a fluid (with $n = 0.7$, and $\tau_0/\tau_w = 0.44$) indicates values of E less than

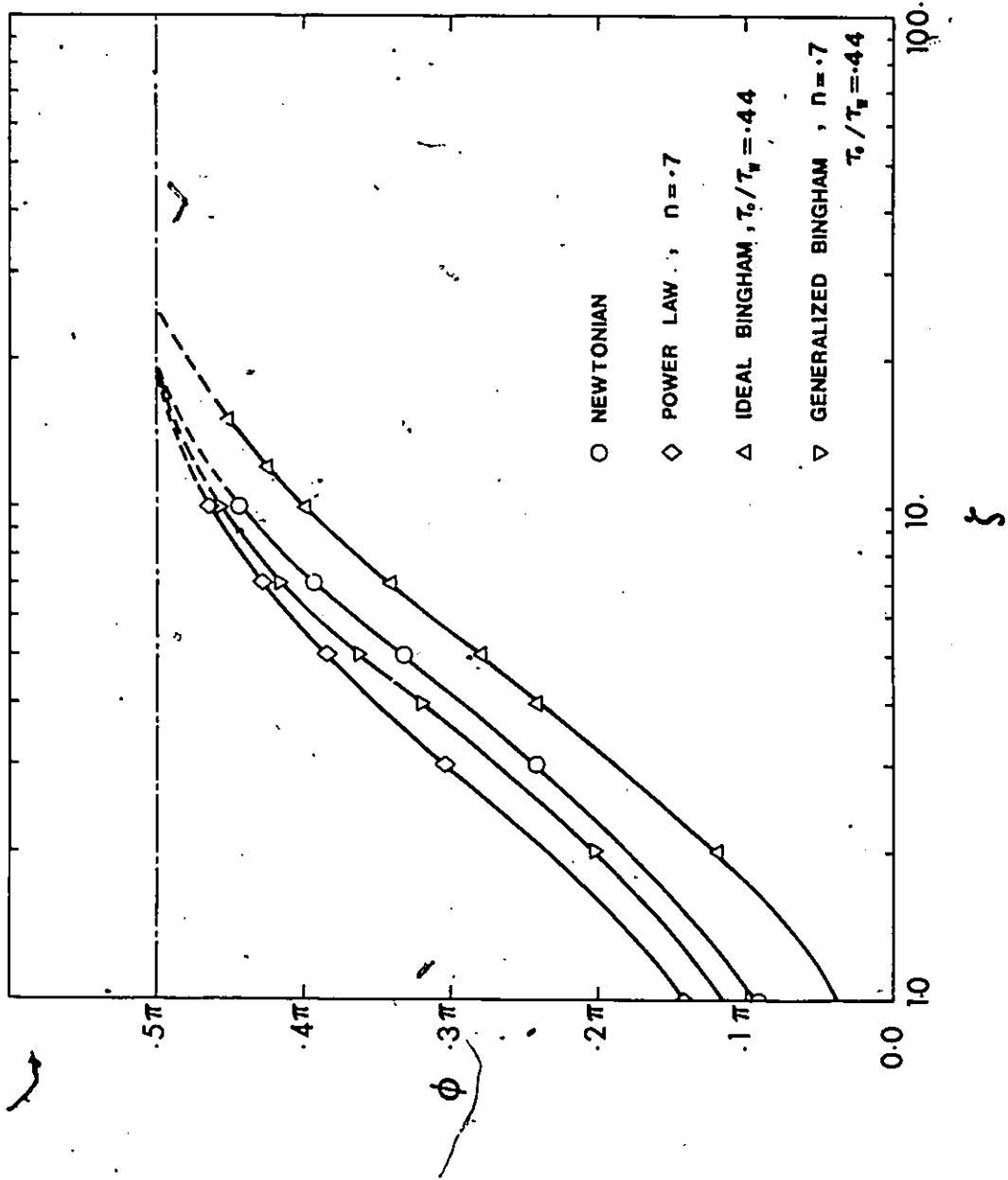


Figure 6.7 Theoretical predictions of phase angle ϕ vs. dimensionless frequency ζ ($\epsilon = 1$).

unity. A minimum value of $E \approx 0.93$ is observed in the range of $\zeta = 2-5$ for $n = 0.7$ and $\tau_0/\tau_w = 0.44$.

6.1.4 Phase Angles

Results from the finite difference calculations of the velocity profiles yield complete information about the phase angle between the pressure-wave and the velocity-wave. The phase angle reaches its maximum value under certain flow conditions, after the flow has completely achieved steady state pulsating behaviour. Also, the phase angle is always maximum at the pipe centerline, i.e. $R = 0$. Values of phase angle ϕ for different fluids are presented in Figure 6.7 as functions of the frequency parameter ζ at $R = 0$. It can be seen that the type of fluid has no significant effect on the variation ϕ with respect to ζ . Asymptotic approach to $\phi = 90^\circ$ is observed at high frequency, while eventually $\phi \rightarrow 0$ when $\zeta \rightarrow 0$. Fluids of the power law and ideal Bingham type show values of ϕ higher than those for Newtonian fluids. Only generalized Bingham fluids exhibit values of ϕ lower than those of Newtonian fluid.

6.2 Start-Up Flow

Figures 6.8 to 6.10 show the computed values of the instantaneous velocity profiles for different fluids. In Figure 6.8, the velocity profiles of a Newtonian and two power law fluids ($n = .7$ and 1.4) are given. The velocity profiles for an ideal Bingham and a generalized Bingham with $n = 0.7$ and $\tau_0/\tau_w = 0.32$ are presented in Figure 6.9, while in Figure 6.10, they are presented for $\tau_0/\tau_w = 0.44$. In these diagrams, a dimensionless velocity U is plotted as a function of the radial position R for various values of dimensionless time T . For Newtonian and power law fluids ($n = 0.7$ and 1.4), the results are in excellent agreement with results of

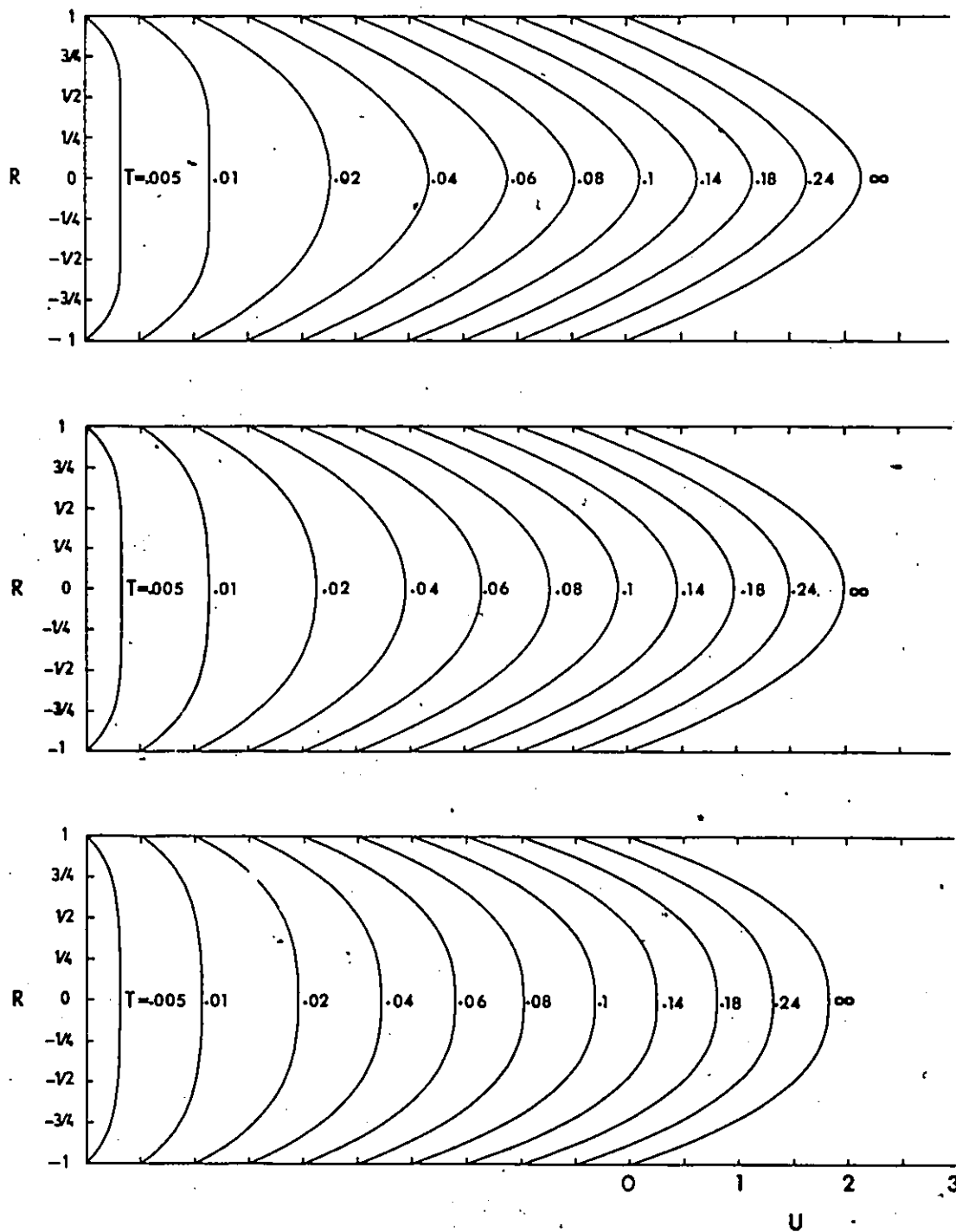


Figure 6.8

Theoretical predictions of velocity profiles for start-up flow for a Newtonian (middle) and two-power law fluids $n = 0.7$ (bottom) and 1.4 (top).

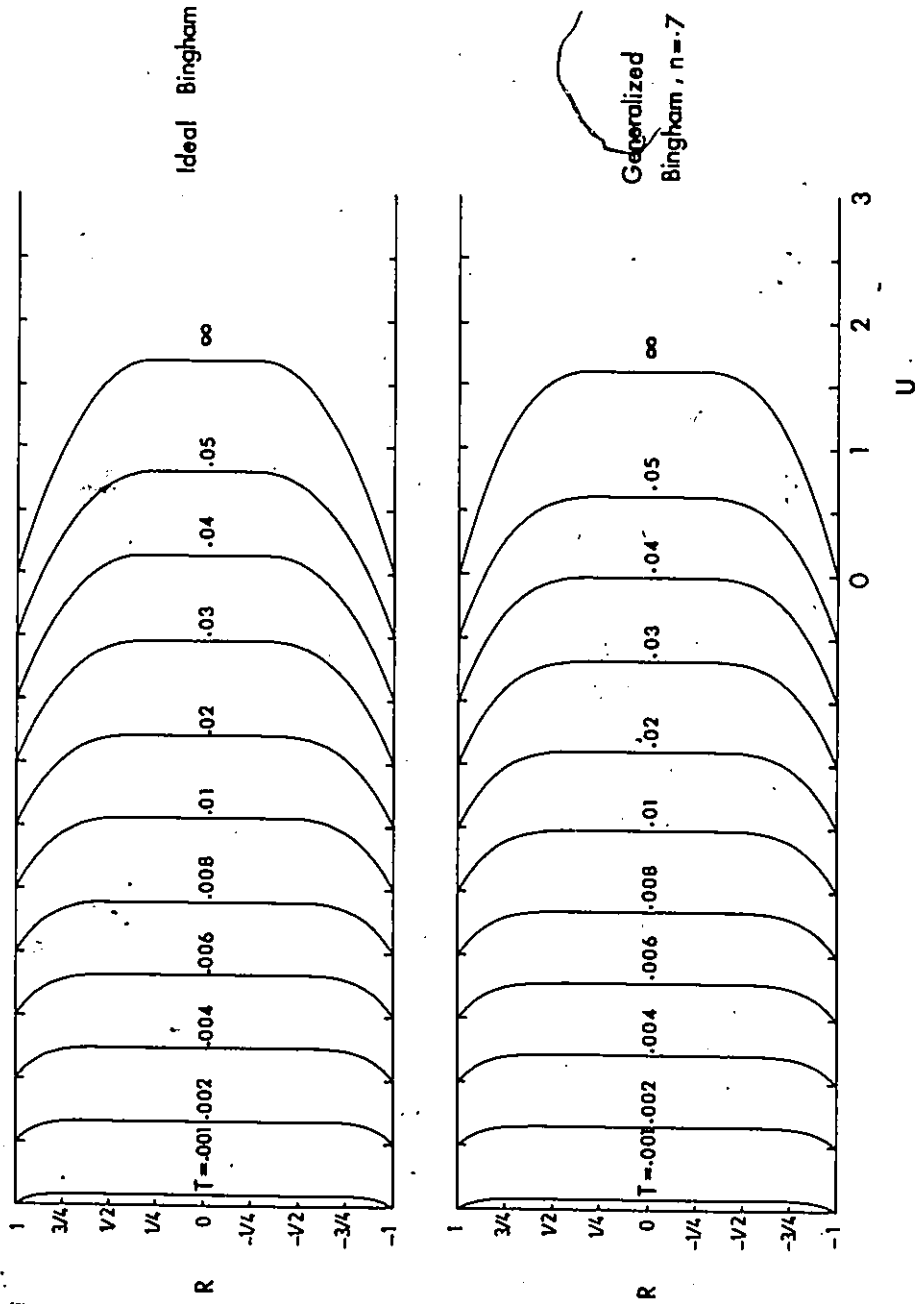


Figure 6.9 Theoretical predictions of velocity profiles for start-up flow for an ideal Bingham (top) and a generalized Bingham fluid (bottom), $\tau_0/\tau_w = 0.32, n = 0.7$.

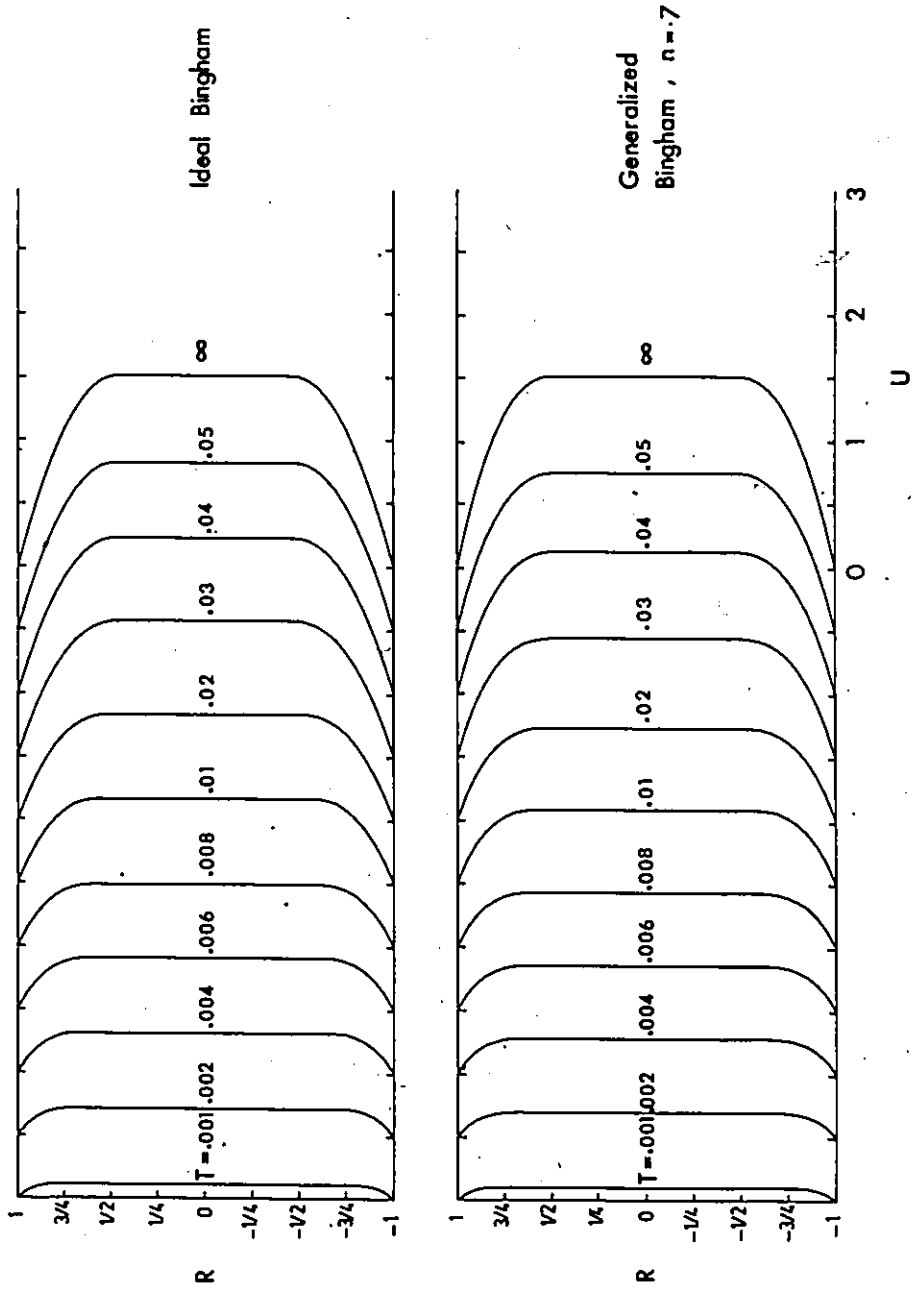


Figure 6.10 Theoretical predictions of velocity profiles for start-up flow for an ideal Bingham (top) and a generalized Bingham fluid (bottom), $\tau_0/\tau_w = 0.44$, $n = 0.7$.

Szymanski [90], who solved the Newtonian start-up flow problem analytically, and with results obtained numerically for the power law start-up flow by Edwards et al. [11].

It may be noticed in Figures 6.8 to 6.10 that the rate of approach of the velocity to the equilibrium value, in terms of the dimensionless time, depends on the radial position, the non-Newtonian index and the value of yield stress. In Figure 6.11, the rate of approach of the velocity to the equilibrium value is presented at the centre of the pipe for different values of the non-Newtonian index and the yield stress. It can be seen that such rates can be increased significantly by an increase in the yield stress of the fluid. On the other hand, fluids exhibiting n less than unity show a slower approach rate to equilibrium. It also appears that the effect of n on the rate of approach decreases when the fluids have a yield stress.

According to the constitutive equation (4.1), the flow is hypothetically separated into two regions at $R = R_0$. In deriving equations (4.38a) and (4.38b), it is assumed that velocity, stress and pressure gradient are continuous across $R = R_0$. This assumption, however, is not satisfied since

$$\left(\frac{\partial \tau_r}{\partial r}\right)_{r=r_{0+}} \neq \left(\frac{\partial \tau_r}{\partial r}\right)_{r=r_{0-}}$$

This is a natural consequence of the assumption of a rigid body behaviour for the region $0 < R < R_0$. For accelerating and decelerating flows, elasticity of the core, i.e. $0 < R < R_0$, has to be considered. Although relative displacements in this region are very small, depending on the loading rate, corresponding relative velocities inside this region may exist. However, introduction of the elastic behaviour of the core will cause both the problems of pulsating flow and start-up flow to become exceedingly and unnecessarily complex. Some error may therefore arise, but it is insignificant and can be accepted for low to moderate loading rates, i.e. those investigated in the present research.

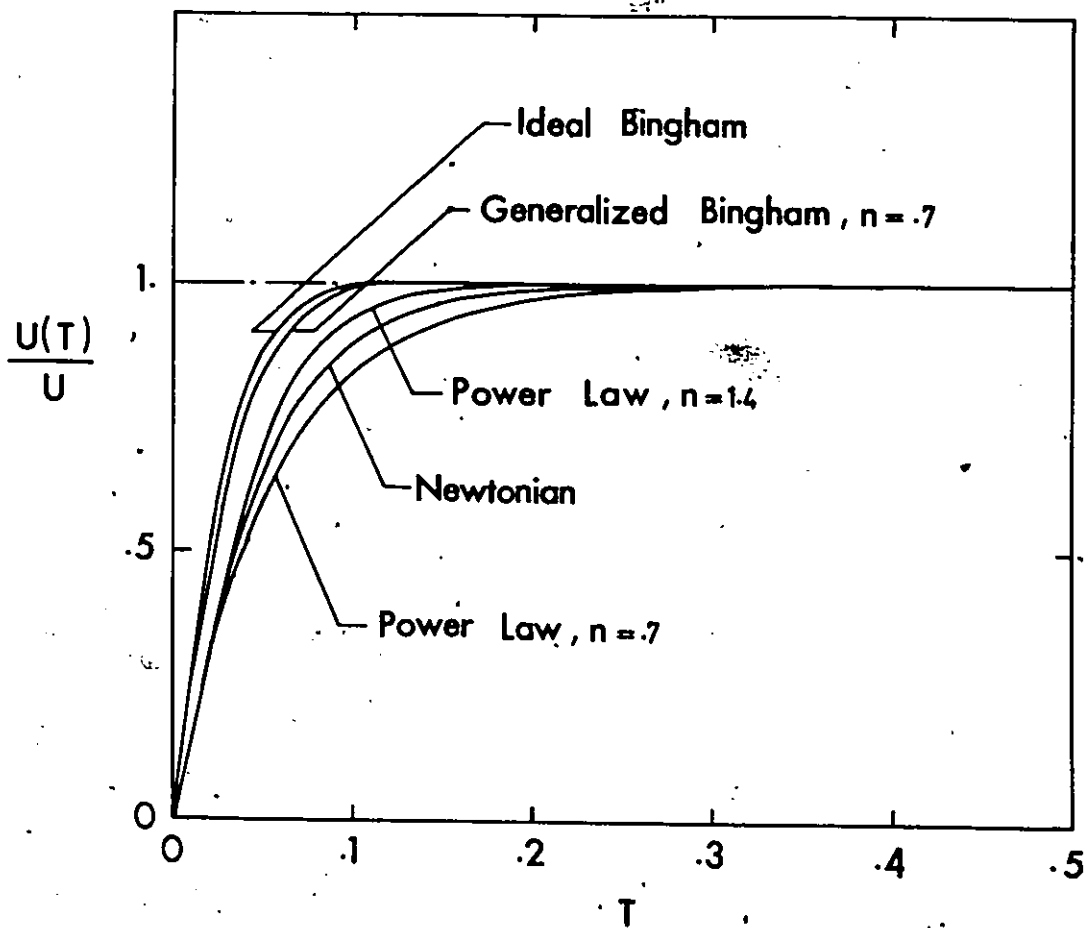


Figure 6.11

Velocity development as a function of dimensionless time T on the pipe centerline for start-up flows of Newtonian and non-Newtonian fluids.

CHAPTER 7

EXPERIMENTAL RESULTS AND DISCUSSION

In this chapter the results of pulsating flow measurements are presented in terms of hydraulic power requirement. The measurements were obtained for two types of solid-liquid suspension or slurry.

- (i) bentonite clay-water; as a homogeneous suspension
- (ii) coal-water; as a heterogeneous slurry.

The results are presented as a ratio between the hydraulic power requirement of pulsating flow to that of steady flow at the same throughput and at different pulsing frequency, pulsing amplitude, average flow velocity, and solids concentration.

7.1 Bentonite Clay-Water Suspension:

Values of the ratio of pulsating to steady hydraulic power J_p/J_s can be obtained from the measurements of steady and pulsating flows. Such measurements are tabulated and presented in Appendix B. Figures 7.2 to 7.9 contain the values obtained for the ratio J_p/J_s as functions of different flow parameters. In all cases the value of J_p/J_s equals unity when the flow is steady, i.e. pulsing frequency $\lambda = 0$. The effect of each of the adopted parameters on J_p/J_s is discussed below.

7.1.1 Pulsing Frequency and Pulsing Amplitude:

Typical pressure-wave forms traced by an X-Y recorder are shown in Figure 7.1. For different values of pulsing frequency λ and at pulsing amplitude $A = 52.1$ mm. In this Figure it is clear that the pressure-waves are of sinusoidal-like form and the pressure amplitude is changing with alterations in both pulsing frequency and pulsing amplitude.

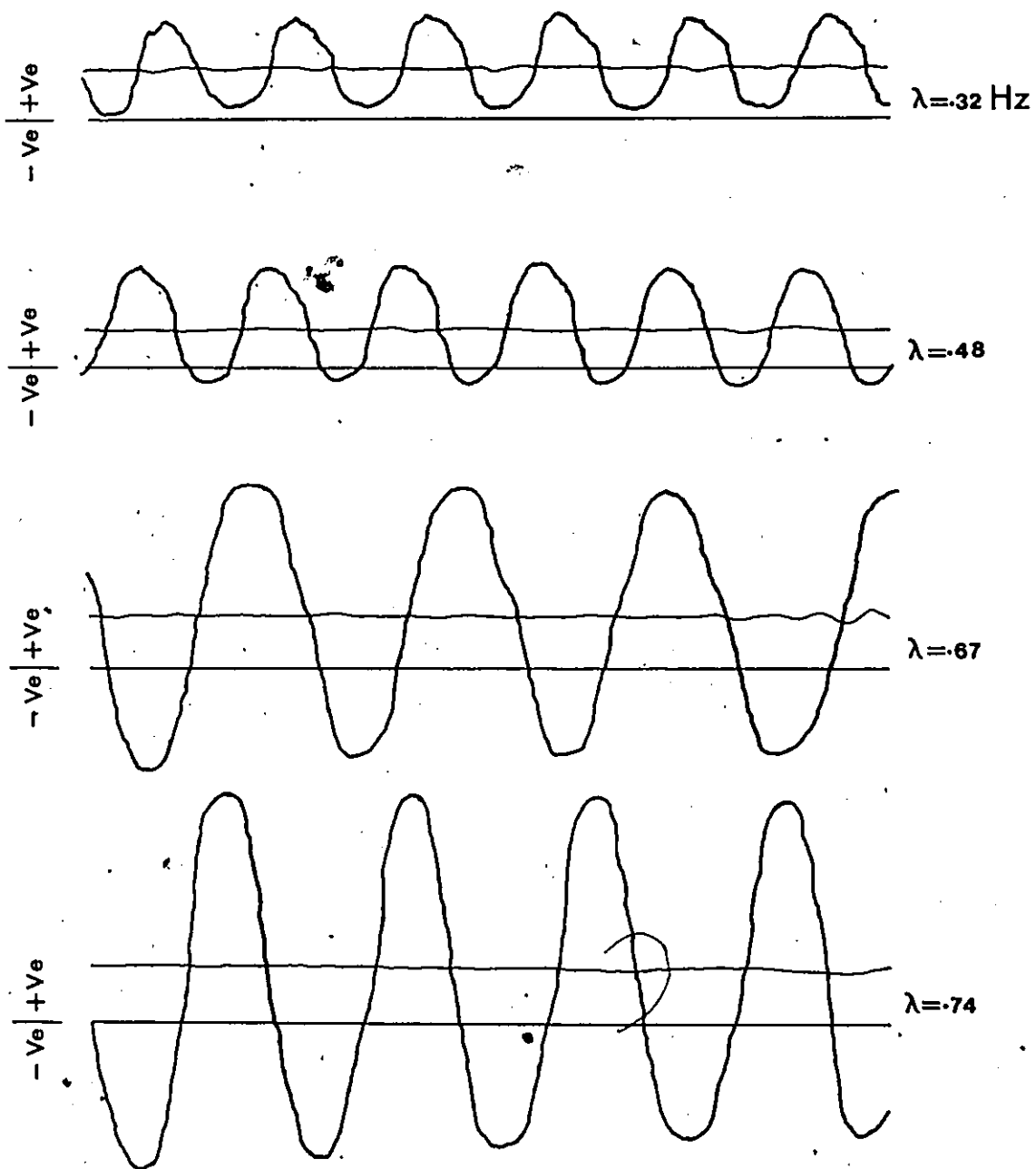


Figure 7.1

Output signals from the pressure transducer at different pulsing frequencies ($A = 52.1$ mm)

From a mathematical viewpoint, the compressed volume of the bellows must equal the amount of fluid injected into the pipeline, i.e.

$$\frac{\pi}{4} D^2 A = \int_0^{n/\omega} \left\{ (u_0 \sin \omega t) \frac{\pi}{4} d^2 \right\} dt \quad (7.1)$$

The term on the right hand side of this equation is the volume of fluid due to the oscillating component in the accelerating part of one pulse. Integration of such equation yields

$$u_0 = A \left(\frac{D}{d} \right)^2 \frac{\omega}{2} \quad (7.2)$$

But,

$$\lambda = \frac{\omega}{2\pi}$$

therefore,

$$u_0 = \pi A \left(\frac{D}{d} \right)^2 \lambda \quad (7.3)$$

In a dimensionless form

$$\frac{u_0}{V} = \frac{\pi A \left(\frac{D}{d} \right)^2}{V} \lambda \quad (7.4)$$

This is an expression for dimensionless velocity amplitude. In this expression it can be seen that the velocity amplitude is function of the frequency λ as well as of A . In other words any alteration in λ is in fact an alteration in two flow parameters at the same time; namely, pulsing frequency and pressure or velocity amplitude. It should be emphasized here that the phenomenon is very much dependent on the experimental equipment being used. Because of the pulse generating mechanism used in this investigation, the effect of pulsing frequency cannot be separated from the effect of pressure amplitude. However, there is no question that the response of the hydraulic power to changes in frequency and in pressure or velocity amplitude remains the same irrespective of the equipment.

Examination of Figures 7.2, 7.4, 7.6, and 7.8 demonstrates the effect of λ on J_p/J_s at different flow conditions. Each curve in the figures shows a minimum in the ratio J_p/J_s

occurring at different values of λ . It can be seen that the minima of J_p/J_s occur at lower values of λ as A increases, and at higher values of λ as C_w increases.

Figures 7.4 and 7.6, where $C_w = 4.47\%$ and 7.63% respectively, show in the region of $\lambda = 0 - 0.3$ Hz a slight decrease in values of J_p/J_s as A increases for the same value of λ . This means that in such a range of λ , the decrease in J_p/J_s is not only due to increasing frequency but also due to increase in the velocity amplitude. As the value of λ exceeds the point at which minima in J_p/J_s occur, the effect of A on J_p/J_s is reversed and becomes more and more pronounced. An increase in the pulsing amplitude A , at a fixed value of λ where $\lambda > 0.3$, results in a considerable increase in J_p/J_s . On the other hand, for a certain value of A , increasing λ is accompanied by an increase in J_p/J_s . It may be concluded therefore that the actual effect of pulsing frequency is indirect in that it affects the pulsing amplitude. This point however is not too serious as it might appear because from a practical point of view, it is unlikely that a pulser can be designed in which pulsing amplitude and frequency are non-interdependent.

The above discussion applies also to Figure 7.8 except that the minimum in J_p/J_s is different in magnitude and in position with respect to λ . In this figure, $C_w = 11.2\%$, the value of λ at which a minimum in J_p/J_s occurs is $\lambda \approx 0.4$ Hz. The dimensionless velocity amplitude at this point, where $A = 34.6$ mm and $V = 1.63$ m/sec., is 0.17. The theoretical value of J_p/J_s at such amplitude and frequency is about 0.967 while the experimental value is about 0.95. This difference may be due to the fact that such a fluid has a finite relaxation time - this is not allowed for in the theoretical solution. Although the comparison between theoretical calculations and the experimental measurements given here is difficult due to the limitations discussed in section 7.3, it is clear that overall agreement in the general behaviour is achieved and there is no contradiction between the theoretical prediction and experimental observations.

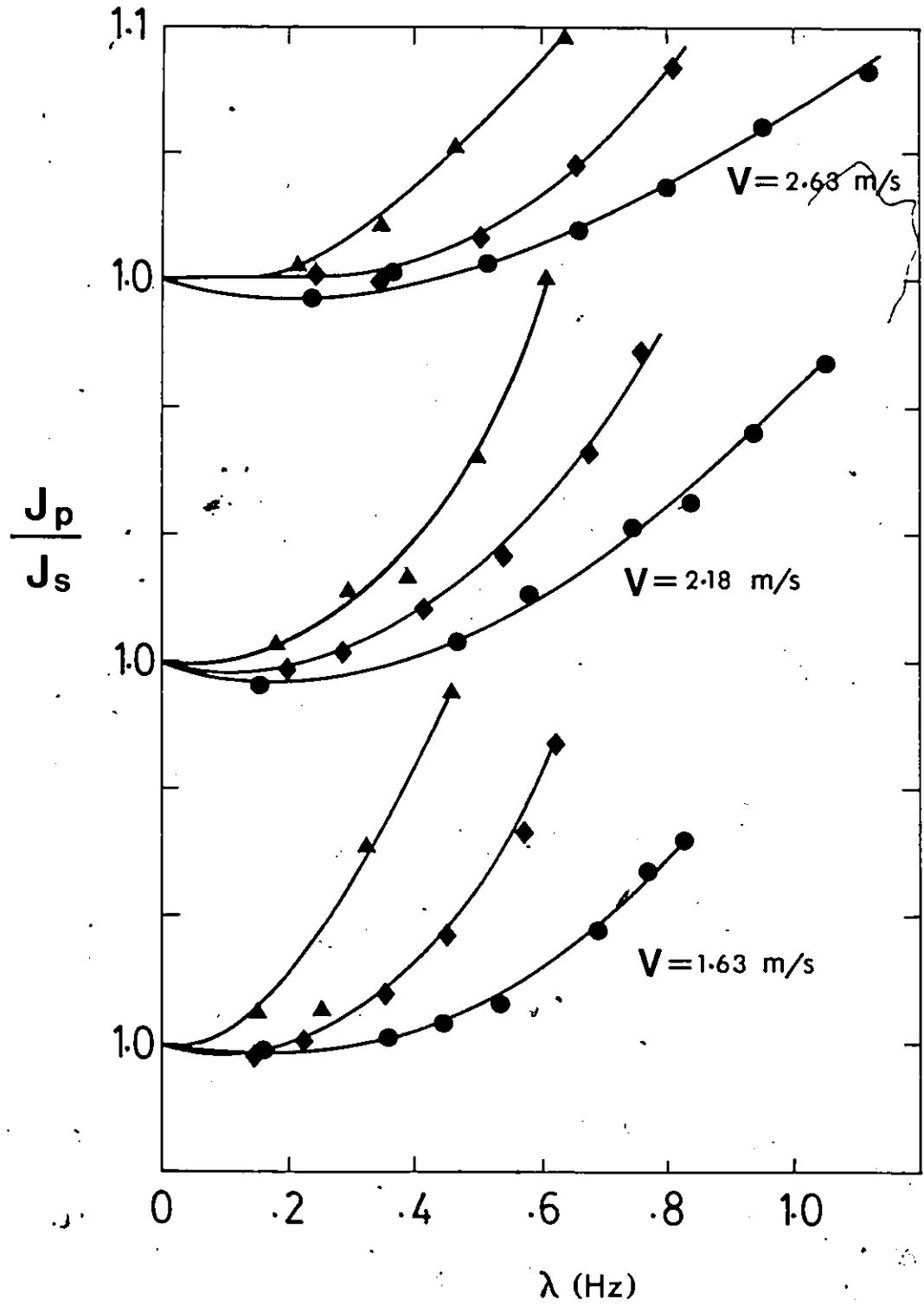


Figure 7.2

Hydraulic power ratio of pulsating to steady flow vs. pulsing frequency. Experimental results for bentonite clay-water suspension ($C_w = 2.97\%$).

● $A = 34.6$ mm, ◆ $A = 52.1$ mm, ▲ $A = 76.2$ mm.

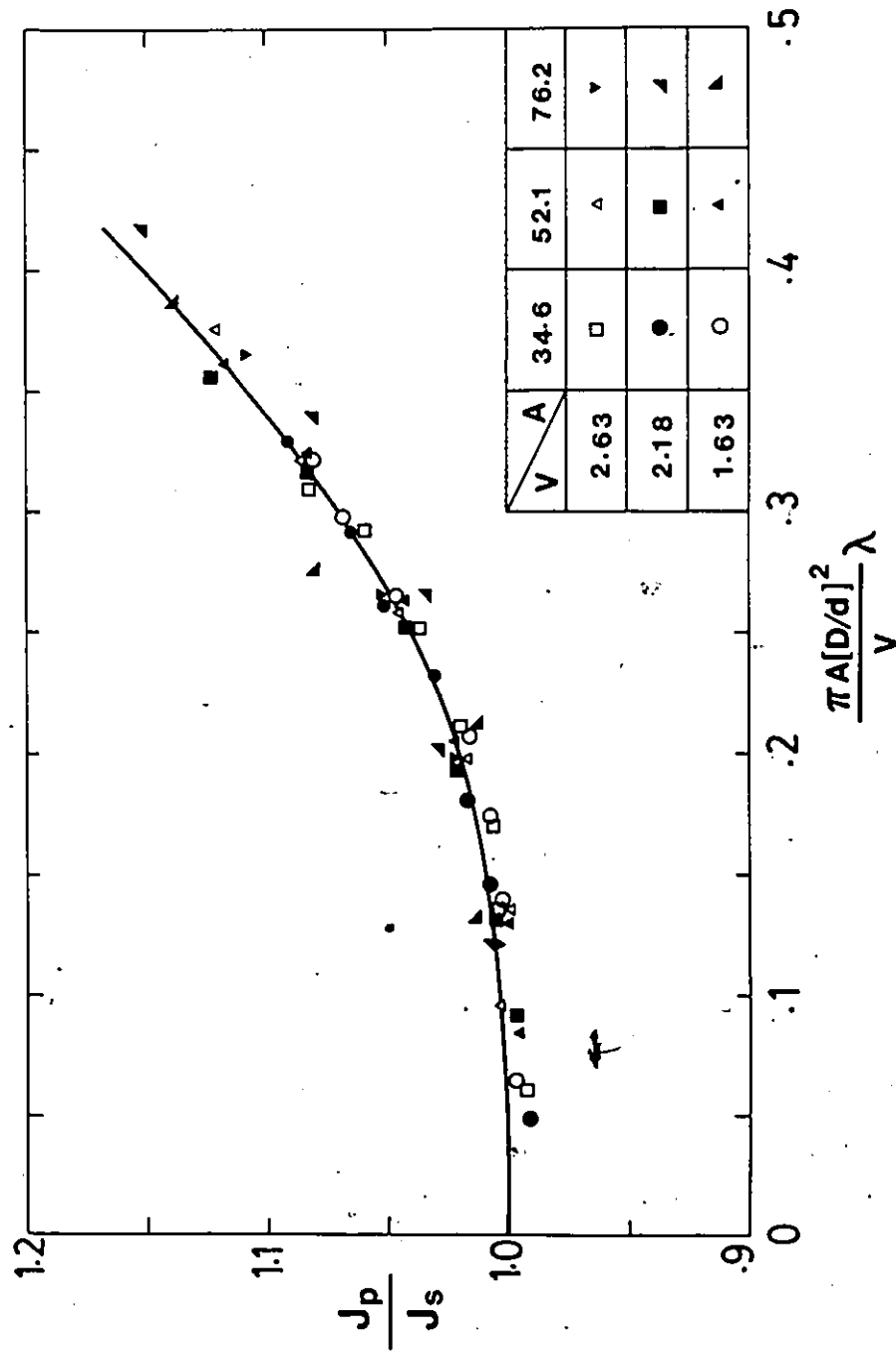


Figure 7.3 Hydraulic power ratio of pulsating to steady flow vs. dimensionless velocity amplitude. Experimental results for bentonite clay-water suspension ($C_w = 2.97\%$).

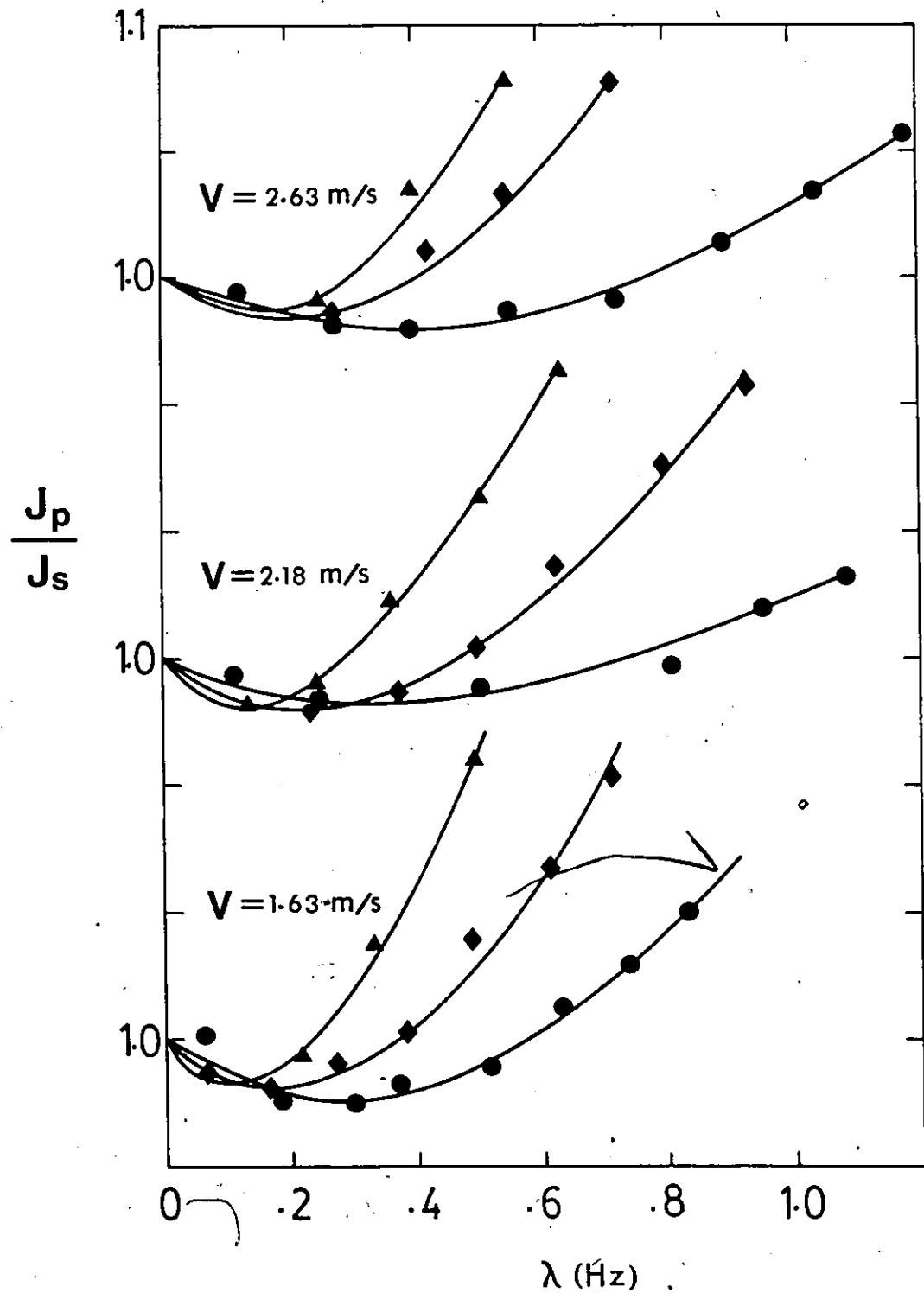


Figure 7.4

Hydraulic power ratio of pulsating to steady flow vs. pulsing frequency. Experimental results for bentonite clay-water suspension ($C_w = 4.47\%$).

● $A = 34.6$ mm, ◆ $A = 52.1$ mm, ▲ $A = 76.2$ mm.

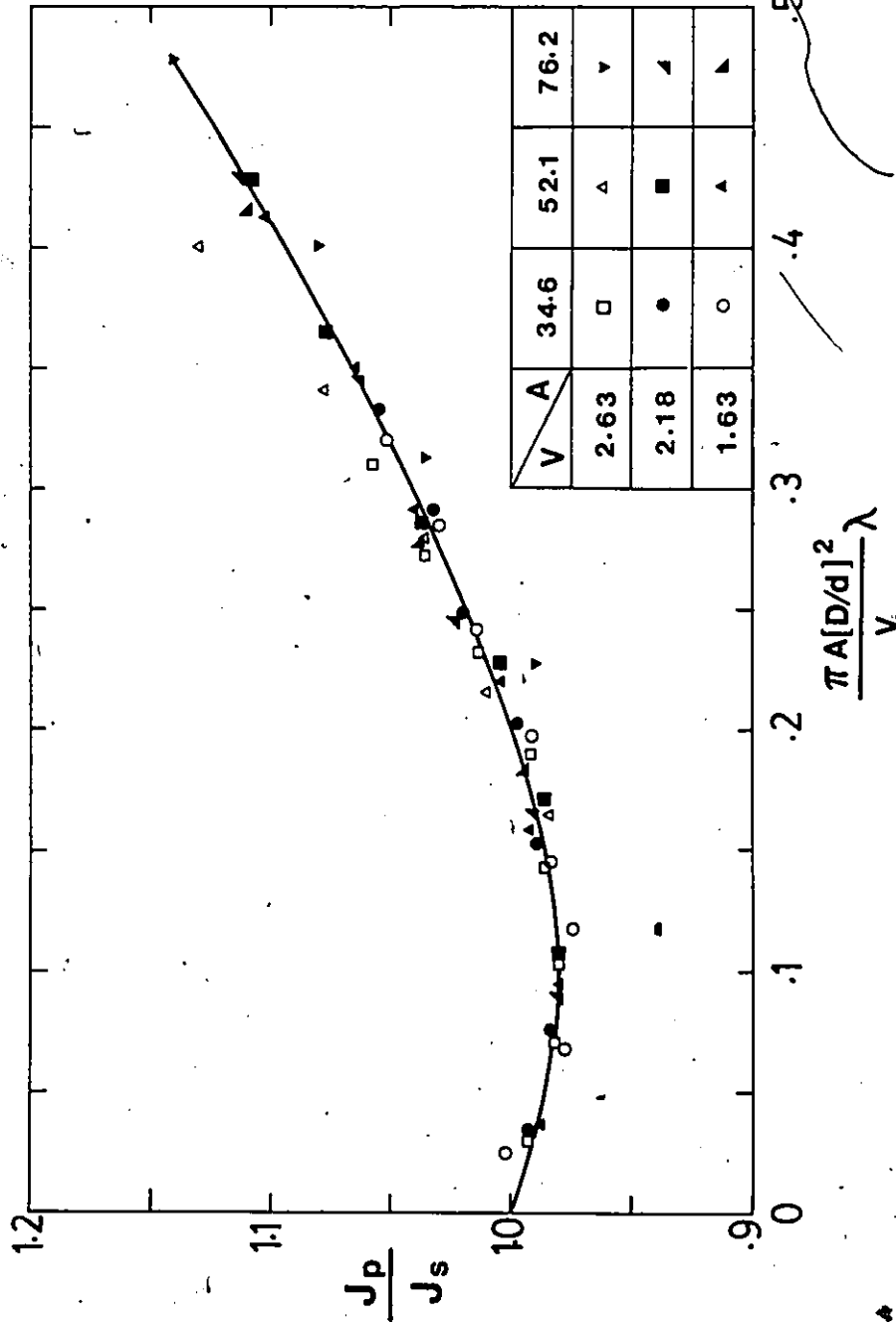


Figure 7.5 Hydraulic power ratio of pulsating to steady flow vs. dimensionless velocity amplitude. Experimental results for bentonite clay-water suspension ($C_w = 4.47\%$).

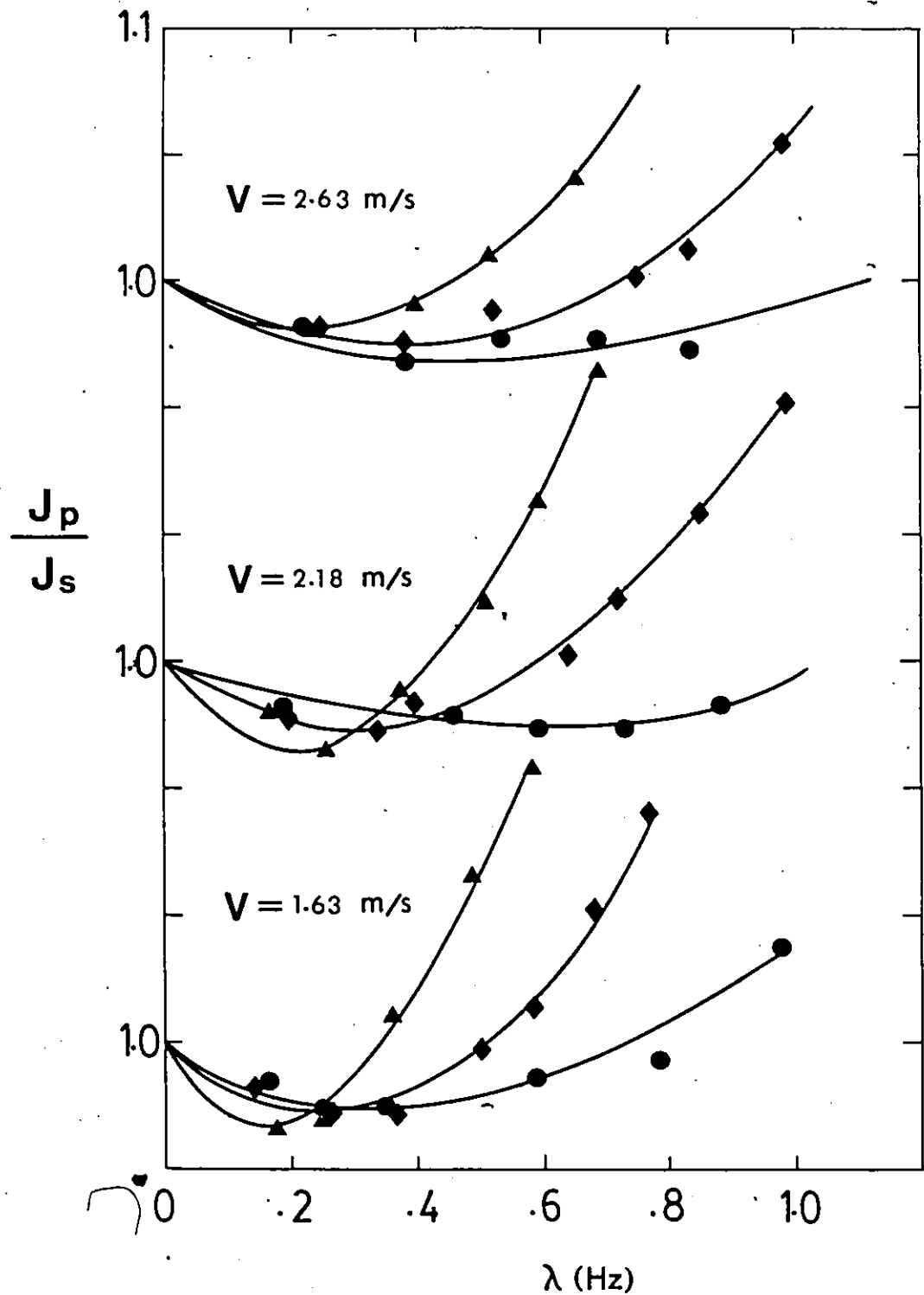


Figure 7.6

Hydraulic power ratio of pulsating to steady flow vs. pulsing frequency. Experimental results for bentonite clay-water suspension ($C_w = 7.63\%$).

\bullet $A = 34.6$ mm, \blacklozenge $A = 52.1$ mm, \blacktriangle $A = 76.2$ mm.

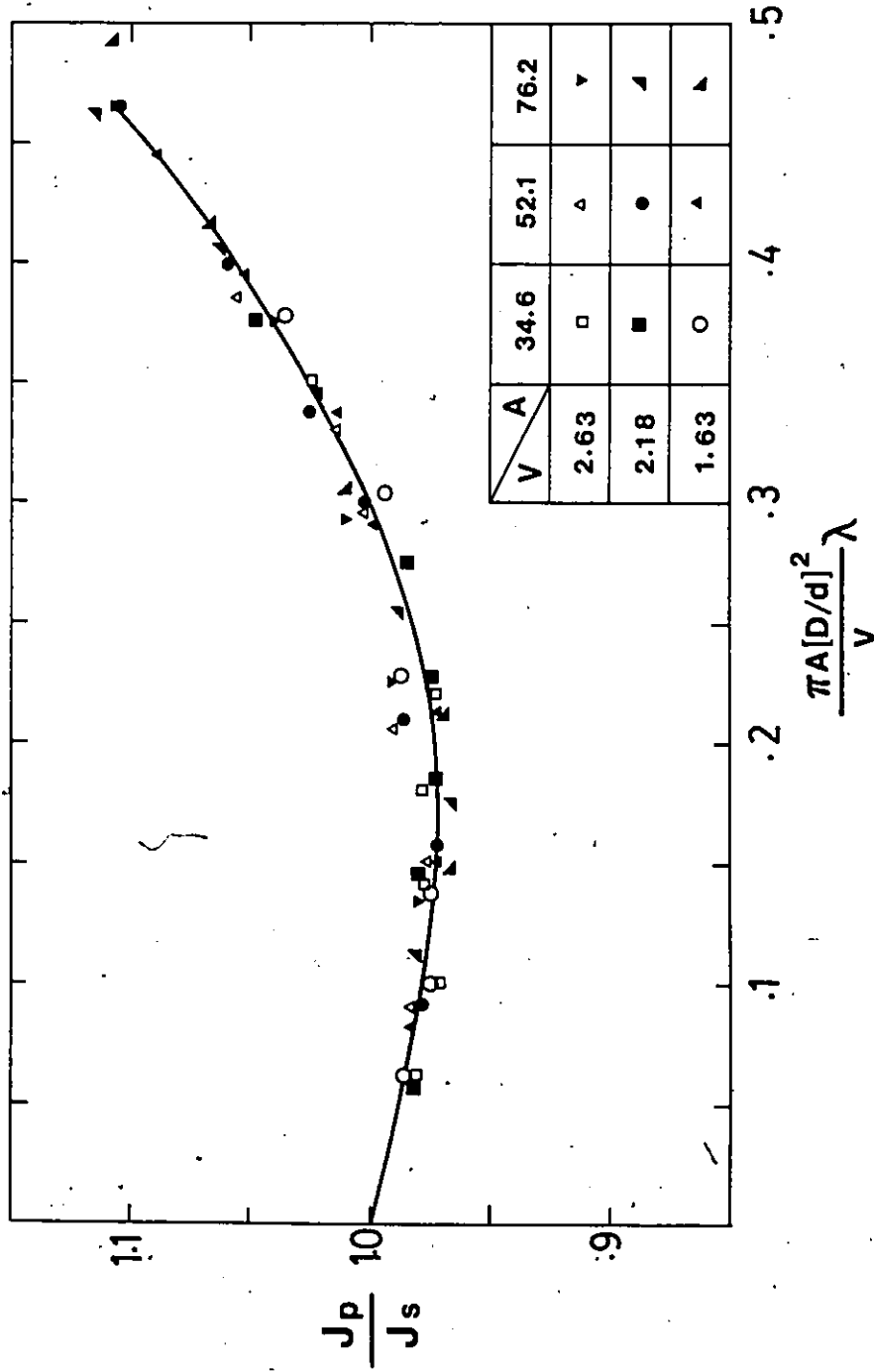


Figure 7.7 Hydraulic power ratio of pulsating to steady flow vs. dimensionless velocity amplitude. Experimental results for bentonite clay-water suspension ($C_w = 7.63\%$).

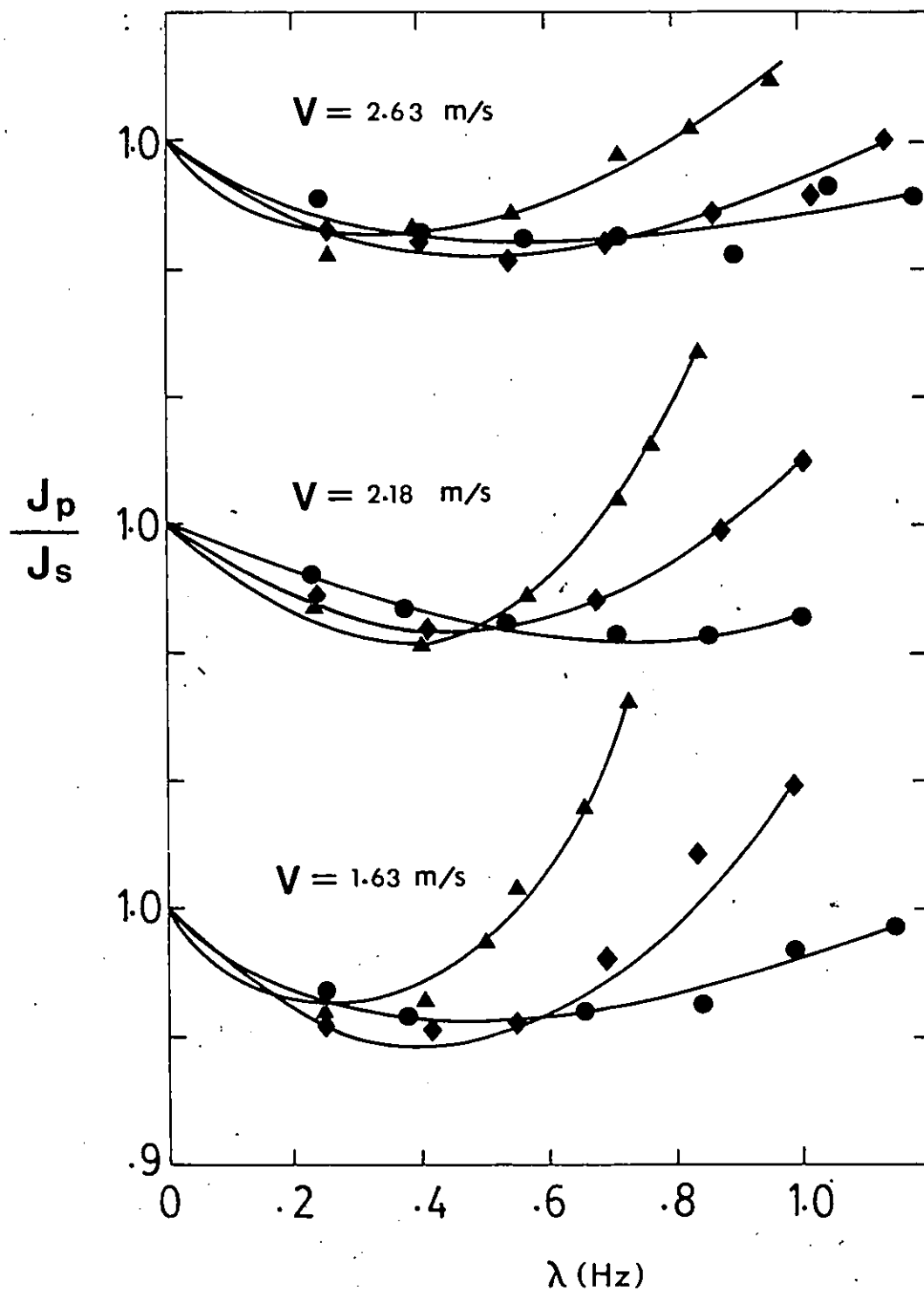


Figure 7.8

Hydraulic power ratio of pulsating to steady flow vs. pulsing frequency. Experimental results for bentonite clay-water suspension ($C_w = 11.2\%$).

● $A = 34.6$ mm, ◆ $A = 52.1$ mm, ▲ $A = 76.2$ mm.

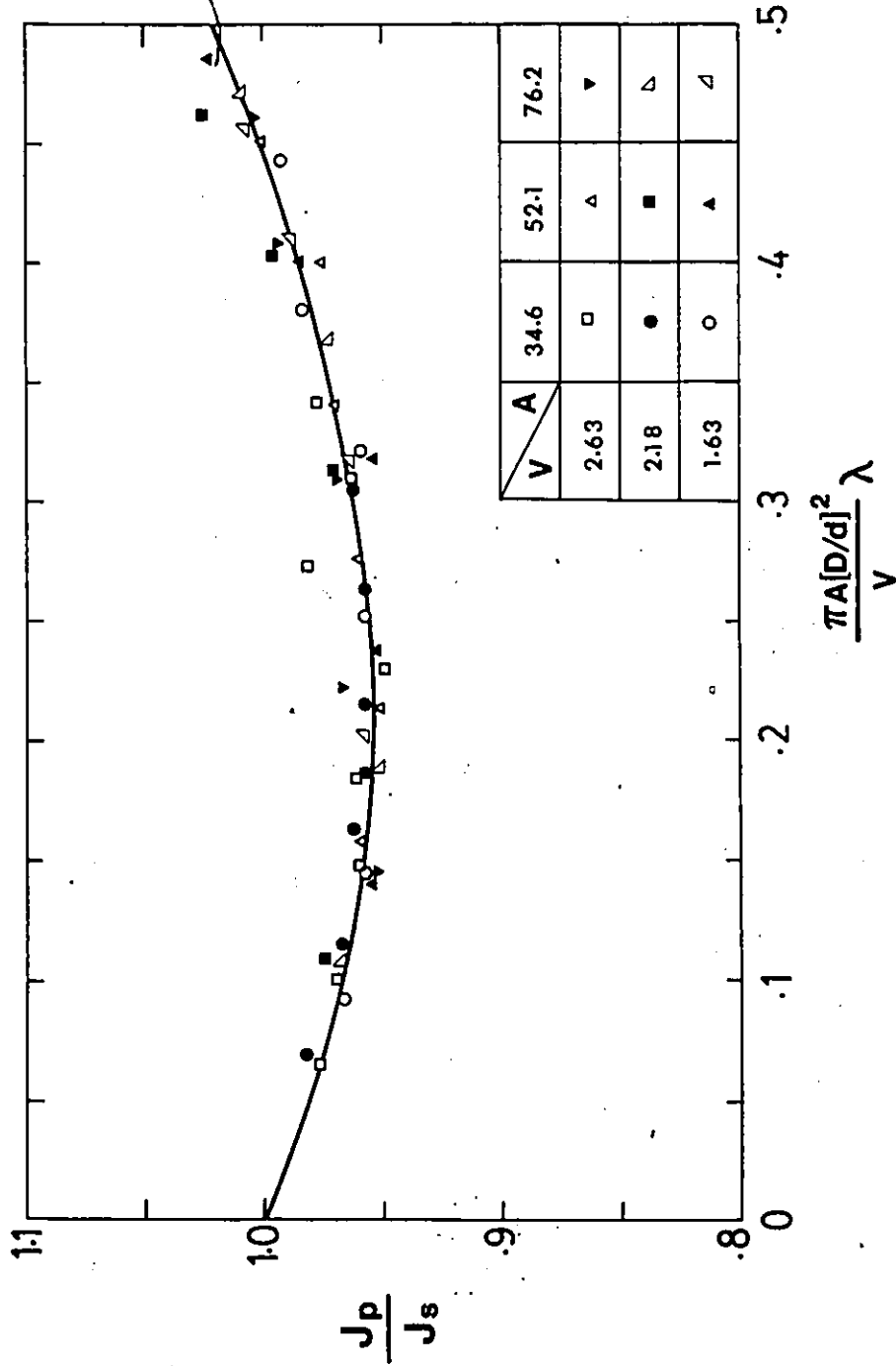


Figure 7.9 Hydraulic power ratio of pulsating to steady flow vs. dimensionless velocity amplitude. Experimental results for bentonite clay-water suspension ($C_w = 11.2\%$).

Figures 7.3, 7.5, 7.7, and 7.9 show the hydraulic power ratio J_p/J_s versus the dimensionless velocity amplitude, defined in equation (7.4), at different values of C_w . It can be seen that all the data points given at different values of A and V lie on one curve. Each curve represents J_p/J_s as a function of the velocity amplitude (or indirectly a function of the pressure amplitude) at certain solids concentration. This proves that equation (7.4) is valid. Also it shows that the velocity or the pressure amplitude is the major factor that should be considered and not the pulsing amplitude A . This conclusion agrees with the theoretical analysis in Chapter 4 and also with the works of Barnes et al. [1] and Walters and Townsend [2], but it is limited to suspensions which behave homogeneously or pseudohomogeneously. The situation is very different in the case of a coal-water slurry - as will be explained in section 7.2.

7.1.2 Effect of Solids Concentration:

Figure 5.3 shows typical viscometric flow curves obtained for bentonite clay-water suspensions at the concentrations used in the pulsating flow investigation. At low concentration ($C_w = 2.97\%$) the fluid behaved as Newtonian, it started to become increasingly non-Newtonian as C_w increased. At $C_w = 7.63\%$ and 11.2% the suspension was undoubtedly a general Bingham.

In Figures 7.2 and 7.3 the minimum value of J_p/J_s is unity and it occurs at $\lambda = 0$. This is the exact behaviour of a Newtonian fluid under pulsating flow conditions. As weights of the solids concentration increase in Figures 7.4 to 7.9, the minimum value of J_p/J_s becomes less than unity and shifts from the position of $\lambda = 0$ toward higher values of λ . The values of J_p/J_s below unity result from a decrease in the apparent viscosity of the suspension in the region near the pipe wall. This region is dominated by high viscous forces - particularly in the

accelerating phase of each pulse. Consequently, this may result in a decrease in the frictional pressure drop for the same flowrate below that for steady flow.

In Chapter 4 it has been explained that a central core or a plug flow situation always occurs in the case of flowing Bingham-like materials. It follows, therefore, that the highest shear rate is concentrated in the annular layer between the plug and the pipe wall. Consequently a structure breakdown may occur in this layer depending upon the magnitude of the shear rate. This results in a considerable decrease in the apparent viscosity. Because this type of suspension has a finite relaxation time, there is no structure build-up expected to occur, this is particularly so at high frequencies. At low values of λ , and depending on the solids concentration, the drop in hydraulic energy consumption due to the decrease in the apparent viscosity is more than the energy required to maintain the oscillating flow component. At higher frequencies, i.e. when λ exceeds its critical value at which J_p/J_s is minimum, the structure is already broken down and the decrease in the fluid apparent viscosity becomes insignificant. Therefore, no further decrease in the hydraulic power can be achieved, while the energy required for the oscillating flow becomes higher and higher.

It is conceivable from the foregoing that as the solids concentration increases (in the limit), the effect of the oscillating flow component becomes more and more pronounced, and therefore the minima in J_p/J_s are expected to reduce and the critical values of λ and the velocity amplitude are expected to increase.

7.1.3 Effect of Average Flow Velocity:

The majority of the present results are in the turbulent flow region. In some cases, where the apparent viscosity is high due to high solids concentration and where the average flow velocity is low, the flow is laminar or transient/laminar. Table 7.1 shows values of the time-averaged Reynolds number Re corresponding to each value of V and each value of C_w .

Table 7.1

Values of Reynolds number and plasticity number at different flow velocities and solids weight concentrations

V(m/s) \ C _w %		2.97	4.47	7.63	11.20
1.63	R _e '	43,697	34,457	10,728	2,996
	P _l '	0.0	14.7	18.5	36.0
2.18	R _e '	58,442	46,083	14,617	4,075
	P _l '	0.0	11.0	14.1	27.3
2.63	R _e '	70,505	55,596	17,847	4,969
	P _l '	0.0	9.2	11.8	22.9

The effect of variable average flow velocity on the ratio J_p/J_s can be seen in Figures 7.2, 7.4, 7.6 and 7.8. In the first two figures, $C_w = 2.97\%$ and 4.47% , the flow is turbulent. At the lowest average flow velocity, the value of the velocity amplitude is the highest for fixed values of λ and A . Thus, the energy required to maintain the oscillating flow component is accordingly the highest. While at the highest flow velocity, the velocity amplitude is the lowest, for the same values of λ and A , and therefore the energy required for the oscillating flow component is the lowest. This may explain the reason why as the average flow velocity increases, the curves - at each value of A - tend to shift downward indicating values of J_p/J_s lower than those at the lowest value of V .

Transition from laminar to turbulent flow in steady flow of Bingham fluids occurs at critical values of Reynolds number higher than that of Newtonian and power law fluids [9,91]. Such values are a function of fluid yield stress, i.e. plasticity number. Higher critical Reynolds numbers usually correspond to higher plasticity numbers. Moreover, it has been shown, in Figures 2.3 and 2.4 by Gilbrech and Combs [42,43] and by Sarpkaya [44], respectively, that transition from laminar to turbulent may possibly be delayed to much higher values of Reynolds number if the flow is oscillated harmonically. Accordingly there is a strong possibility that the flow is laminar or nearly laminar, at the high solids concentration investigated here.

Figures 7.6 and 7.8 show the results of pulsating flows at high solids concentrations. In the first parts of the curves, where $\lambda = 0-0.4$ Hz, as the velocity increases, values of J_p/J_s increase accordingly for the same value of λ and A . This must be due to the decrease of velocity amplitude which is already small in this range of λ . As λ then increases, the situation is reversed, higher flow velocities indicate lower values of J_p/J_s . Again this must be a result of lower magnitude of the velocity amplitude which is relatively high at such values of λ .

It is possible to support the above explanation referring to Figures 7.7 and 7.9. In these figures it is clear that the velocity amplitude has a critical value at which a minimum in J_p/J_s occurs. The point at which the effect of the flow velocity on J_p/J_s is reversed, as discussed above, is in good agreement with the point of critical velocity amplitude.

7.2 Coal-Water Slurry

The results of pulsating flow experiments of coal-water slurry are presented in Figures 7.10 to 7.18. The ratio J_p/J_s is presented as a function of the pulsing frequency λ , at different values of A , V and C_w . Tables of all the data points are included in Appendix C. Similar to the case of bentonite clay-water suspension, all the curves start from $\lambda = 0$, at $J_p/J_s = 1$.

Although the general appearance of the ratio J_p/J_s against the pulsing frequency, at different average flow velocities and different pulsing amplitudes, is very similar to the case of clay-water suspensions, the physical phenomena in the two cases are fundamentally different. The clay-water suspension is in fact a pseudohomogeneous suspension exhibiting generalized Bingham characteristics. While in the case of coal-water slurry, the flow is heterogeneous and the distribution of the coal particles across the pipe cross-section is not uniform. In heterogeneous suspensions there are two possible advantages of applying an oscillating flow component superimposed on the steady flow. This can yield a particle-free region at the pipe wall which acts as a lubricating layer and, in the limit, produces plug flow of the suspension - particularly at high solids concentration [6,13,67,68]. The first advantage due to this phenomenon is the reduction in pipe wear especially when solid particles are very angular and irregular in shape, while the second and most important is the possible reduction in the hydraulic power required to maintain flow.

In steady flows, when particle Reynolds number is high ($Re_p > 10^4$), appreciable inward radial migration of solid particles from the pipe wall and outward radial migration from the pipe axis occurs [67,69,92]. This radial migration in steady flow of suspensions has been observed also with rods, discs, ellipsoids, and particles of other shapes [68,92]. It is believed that inward radial migration is due to a "spin lift" force resulting from particle rotation [72,74,75,93] and a "shear lift" force resulting from translation slip or relative velocity between the solid particle and the liquid [76,93]. On the other hand there is no clear explanation why radial migration may occur outwards.

It has been indicated in Section 2.5 that the rate of radial migration of solid particles in suspensions can be increased by oscillating the flow. Shizgal et al. [13] have reported that the rates of inward radial migration can be increased by increasing the oscillation frequency and amplitude as well as the mean particle size relative to the pipe diameter. Additionally they reported that the radial distance of the equilibrium position from the pipe wall, i.e. the thickness of the particle-free layer, varies with frequency and amplitude. Other conclusions reported included, the rate of radial migration increased with increased solids concentration (in the range 5-20%) and with increased particle Reynolds number to values higher than 10^4 .

By analogy to the foregoing discussion, the effect of the different parameters on pulsating flow behaviour is illustrated below.

7.2.1 Effect of Pulsing Frequency:

The results given in Figures 7.10 to 7.18 are for solids weight concentration ranges from 5.34% to 53.7%. The average flow velocities are 1.63 m/sec, 2.18 m/sec, and 2.63 m/sec, while the pulsing amplitudes are 34.6 mm, 52.1 mm, and 76.2 mm. Each single curve in these

Figures represent the variation of J_p/J_s corresponding to variations in the pulsing frequency λ at different combinations of the three parameters abovementioned.

At very low solids concentration (Figure 7.10), the curves are similar to those of Newtonian fluids. The hydraulic power in pulsating flow at all values of λ is higher than that in steady flow, irrespective of the amplitude and flow velocity. As the concentration increases, a minimum in J_p/J_s occurs < 1 at a certain value of λ . Examination of all the curves in Figures 7.11 to 7.16 demonstrates that the value of λ at which the minimum J_p/J_s occurs is somewhere between 0.25 Hz and 0.4 Hz. Variations in pulsing amplitude and average flow velocity seem to have very weak influence on the critical value of λ .

Hydraulic power in pulsatile flow, within certain range of λ , is less than that for steady flow at the same throughput. One of the possible mechanistic explanations for this may be an inward radial migration of coal particles and the formation of a particle-free layer adjacent to the pipe wall which acts as a lubricant. Another mechanism such as turbulence modification may also be of importance (see Section 8.2). As far as the effect of pulsing frequency on the power ratio is concerned, it follows from the preceding discussion that in the range of $\lambda = 0 - 0.45$ Hz increasing the pulsing frequency increases the inward (and upward) radial particle migration from the wall and consequently increases the thickness of the particle-free layer at the wall. The inward radial migration, as discussed before, is believed to result from two lift forces. Due to the shape of the velocity profile, the viscous force is not uniform on the particle surface. This causes the particle to rotate and, therefore, a spin lift force perpendicular to the main flow direction is generated causing the particle to travel inwards away from the wall. As the pulsing frequency increases, the radial velocity gradient increases accordingly and causes the particle to rotate at higher angular velocity which is proportional to the spin lift. The other force is the shear lift which results from the difference between the axial velocity of the liquid and the actual velocity of the particle. As the velocity

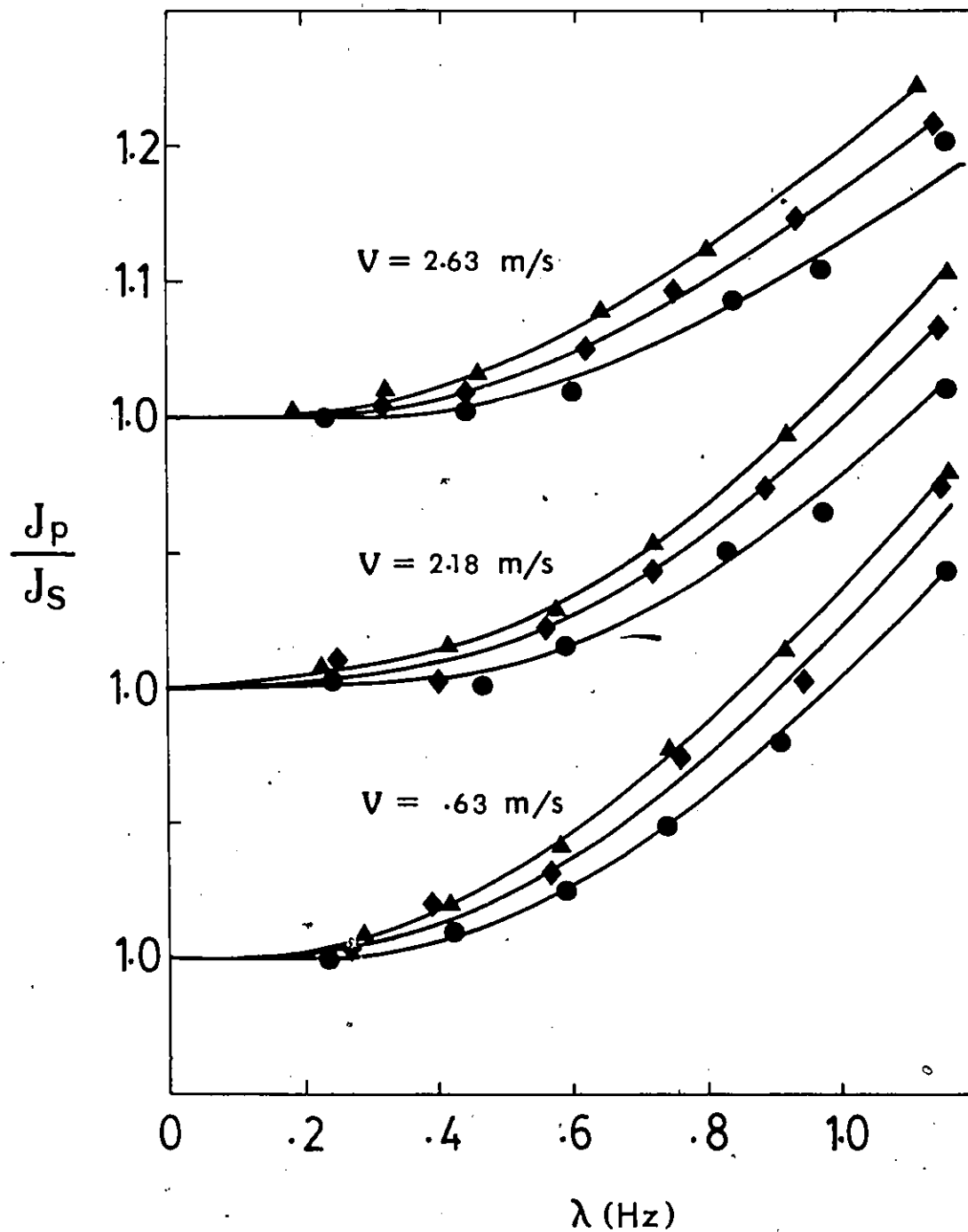


Figure 7.10

Hydraulic power ratio of pulsating to steady flow vs. pulsing frequency. Experimental results for coal-water slurry ($C_w = 5.34\%$).

● $A = 34.6$ mm, ◆ $A = 52.1$ mm, ▲ $A = 76.2$ mm.

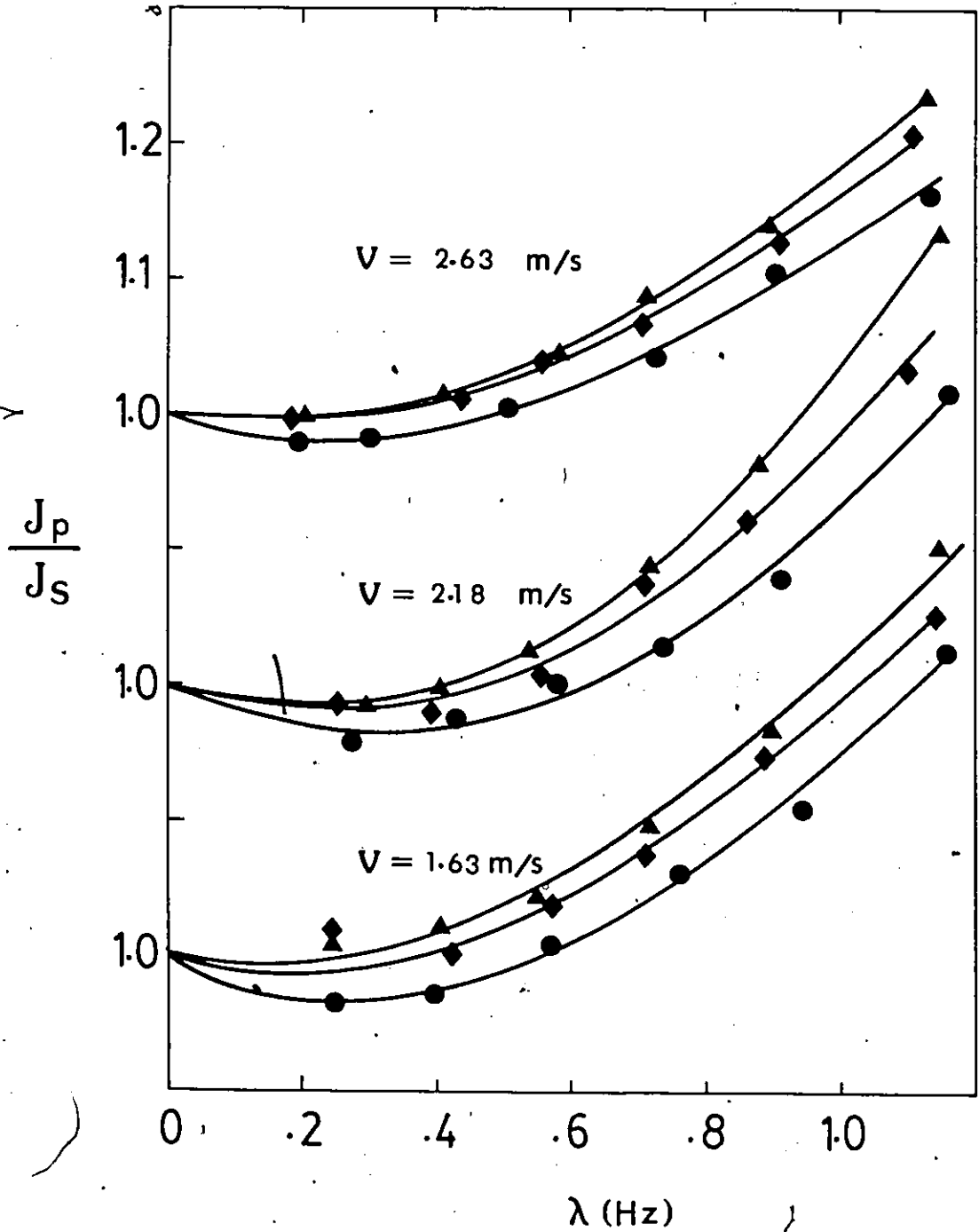


Figure 7.11 Hydraulic power ratio of pulsating to steady flow vs. pulsing frequency. Experimental results for coal-water slurry ($C_w = 8.9\%$).
 ● $A = 34.6$ mm, ◆ $A = 52.1$ mm, ▲ $A = 76.2$ mm.

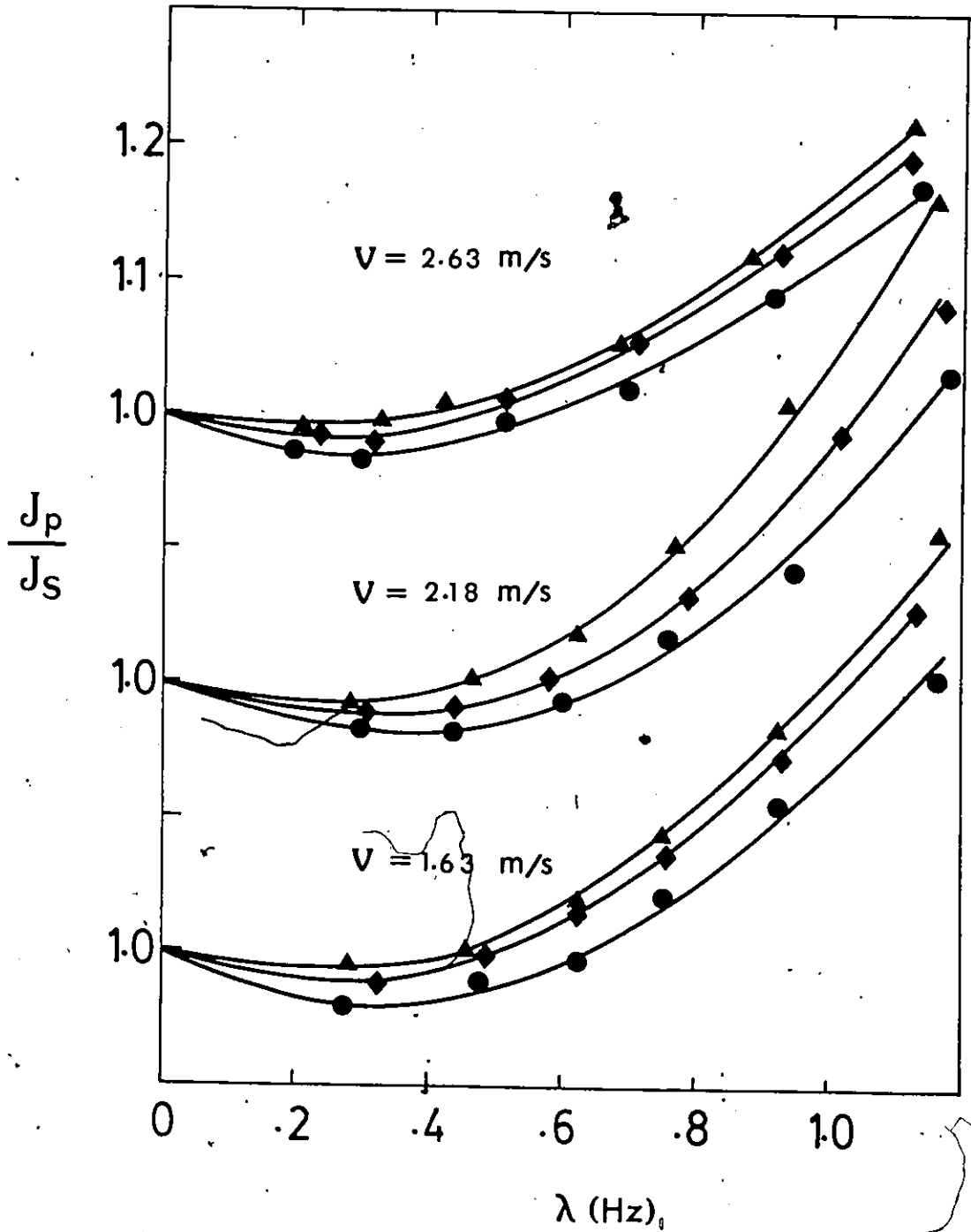


Figure 7.12 Hydraulic power ratio of pulsating to steady flow vs. pulsing frequency. Experimental results for coal-water slurry ($C_w = 14.25\%$).
 \bullet $A = 34.6$ mm, \blacklozenge $A = 52.1$ mm, \blacktriangle $A = 76.2$ mm.

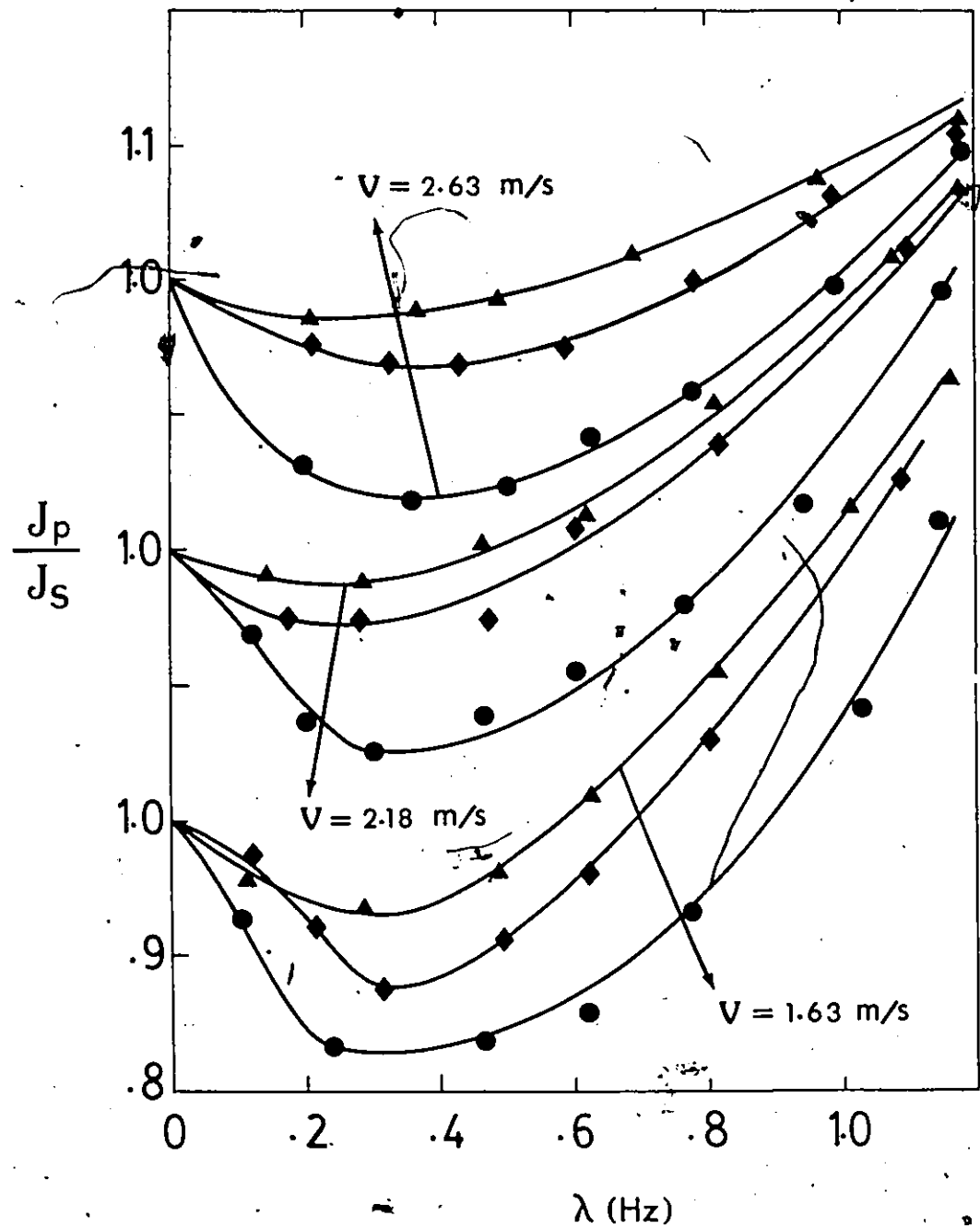


Figure 7.13

Hydraulic power ratio of pulsating to steady flow vs. pulsing frequency. Experimental results for coal-water slurry ($C_w = 19.59\%$).

● $A = 34.6$ mm, ◆ $A = 52.1$ mm, ▲ $A = 76.2$ mm.

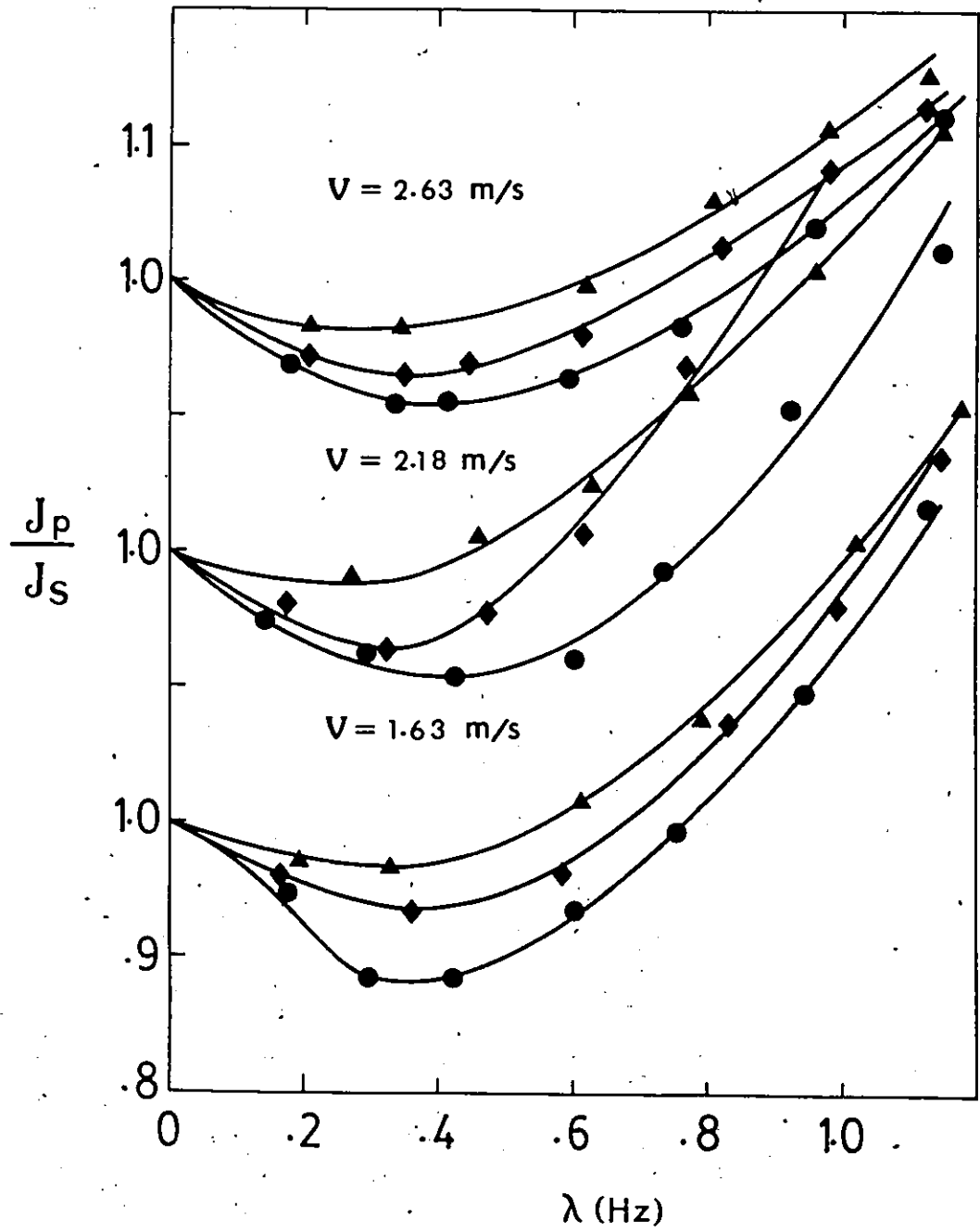


Figure 7.14

Hydraulic power ratio of pulsating to steady flow vs. pulsing frequency. Experimental results for coal-water slurry ($C_w = 24.93\%$).

● $A = 34.6$ mm, ◆ $A = 52.1$ mm, ▲ $A = 76.2$ mm.

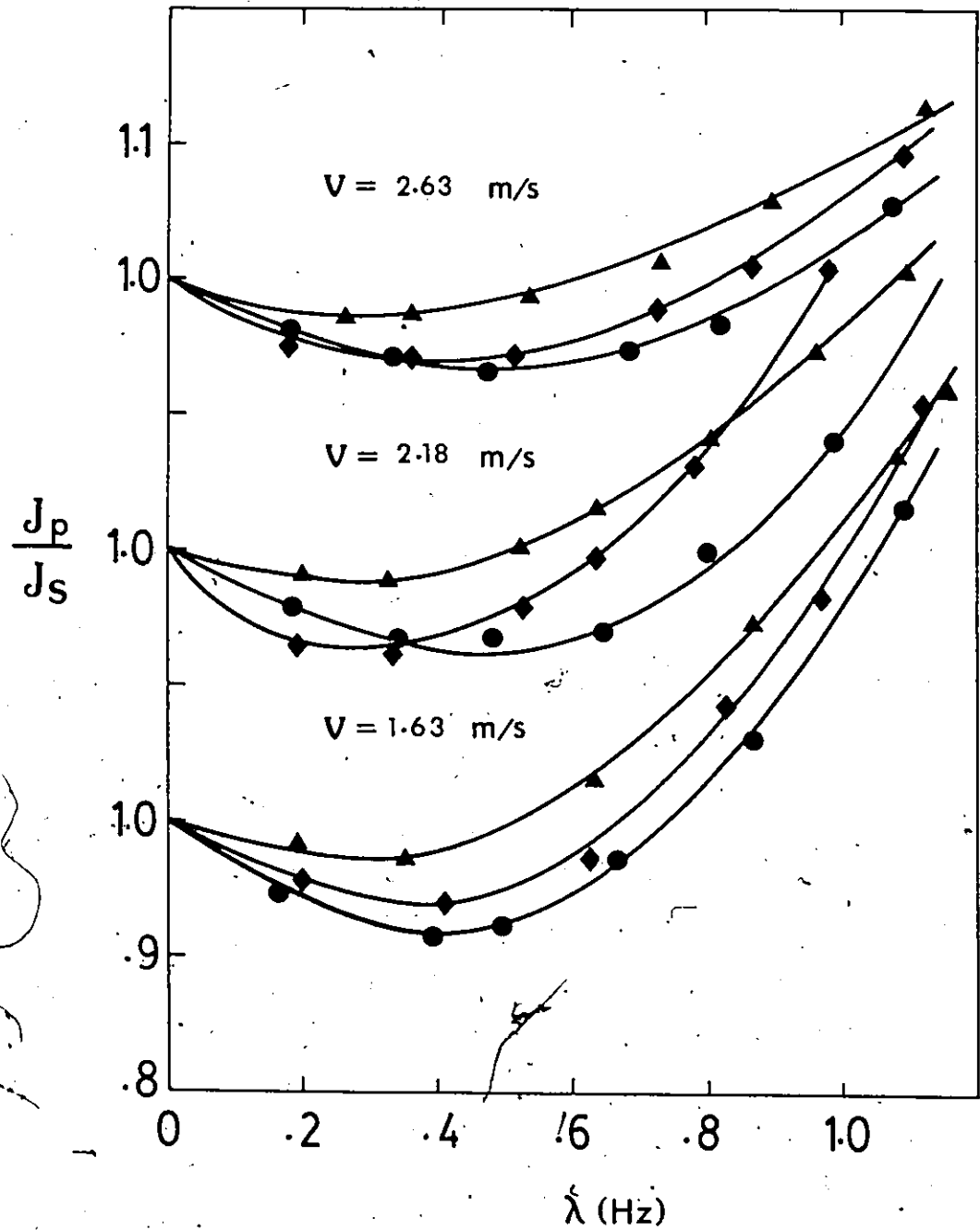


Figure 7.15 Hydraulic power ratio of pulsating to steady flow vs. pulsing frequency. Experimental results for coal-water slurry ($C_w = 30.27\%$).
 \bullet $A = 34.6$ mm, \blacklozenge $A = 52.1$ mm, \blacktriangle $A = 76.2$ mm.

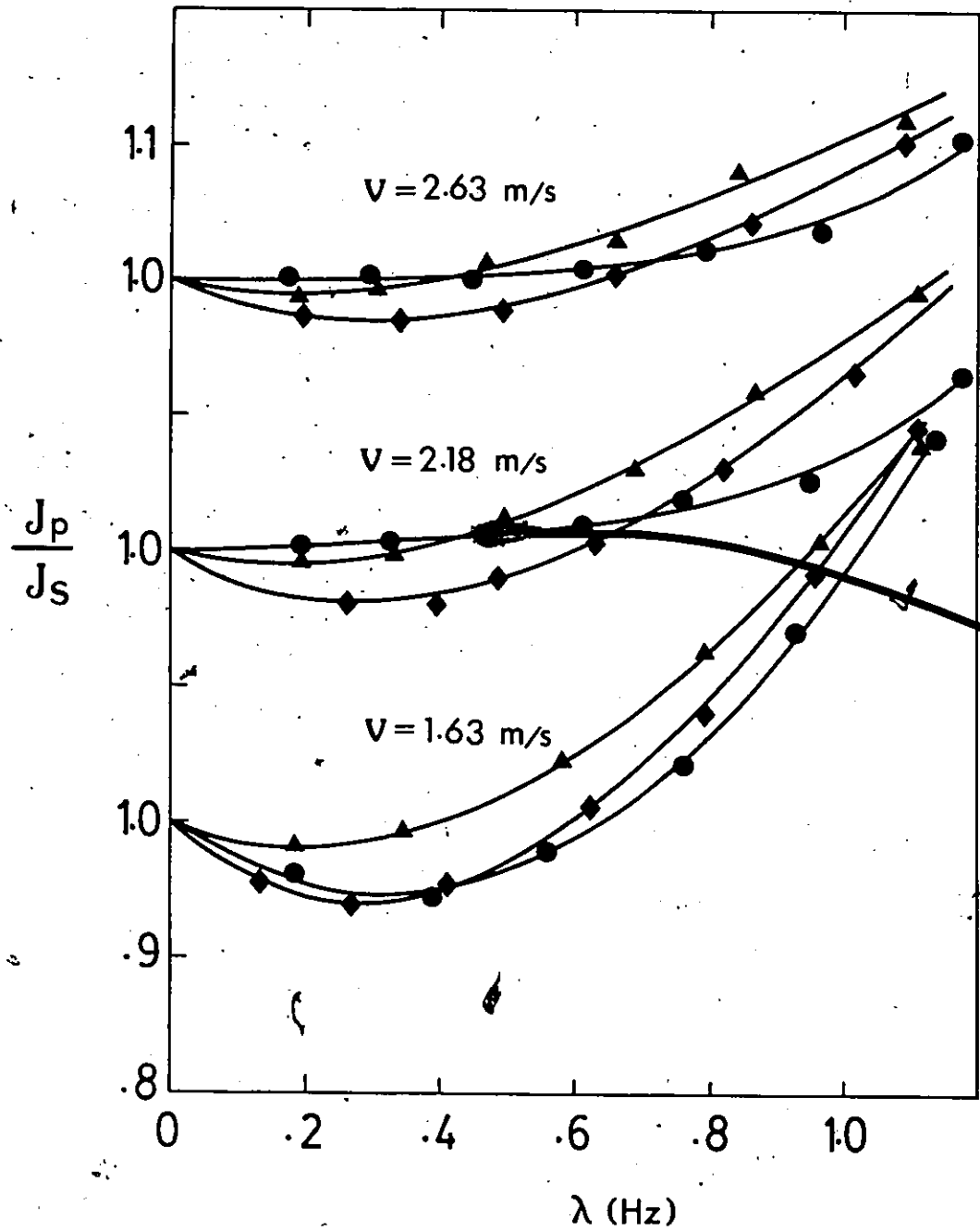


Figure 7.16

Hydraulic power ratio of pulsating to steady flow vs. pulsing frequency. Experimental results for coal-water slurry ($C_w = 37.5\%$).

● $A = 34.6$ mm, ◆ $A = 52.1$ mm, ▲ $A = 76.2$ mm.

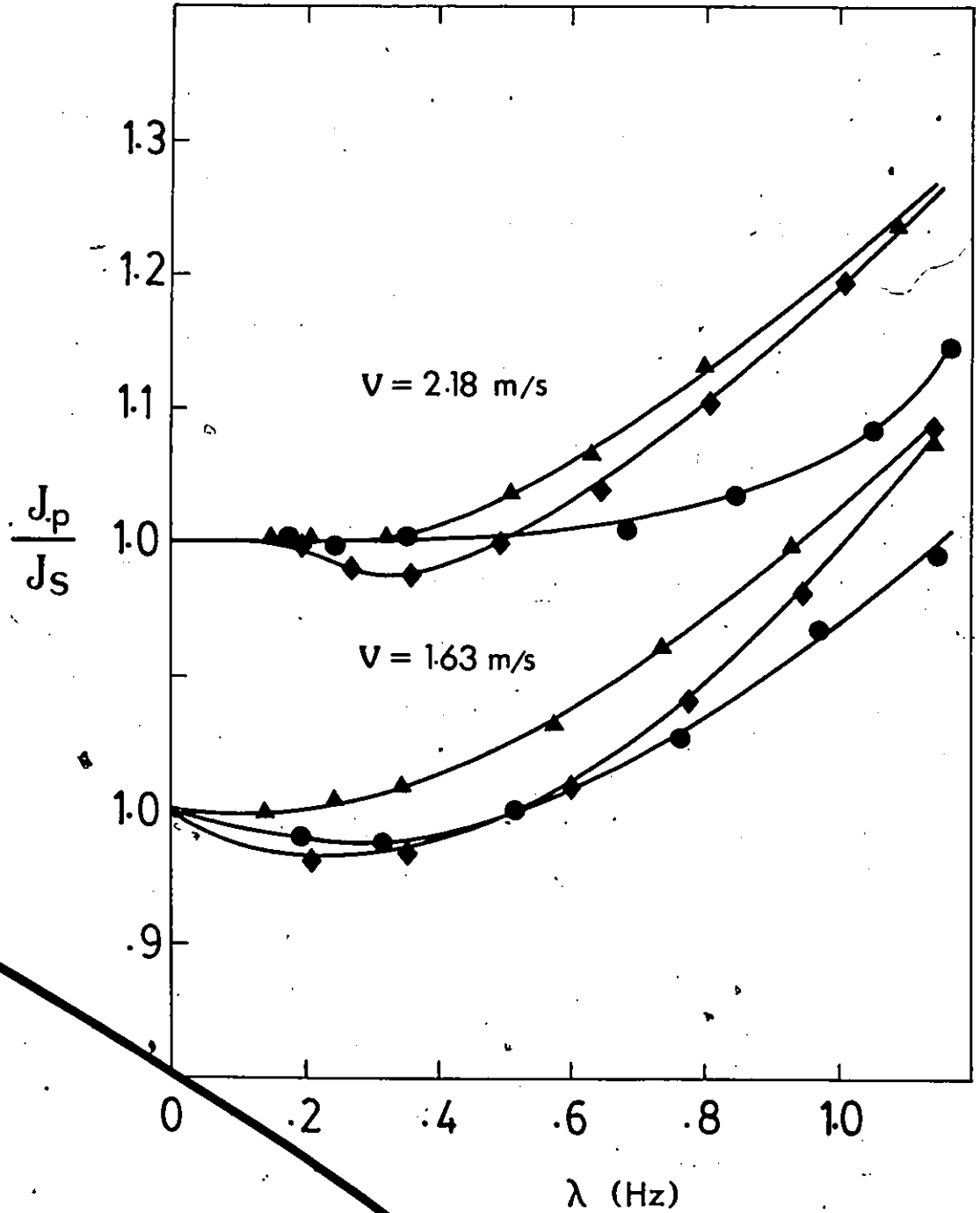


Figure 7.17

Hydraulic power ratio of pulsating to steady flow vs. pulsing frequency. Experimental results for coal-water slurry ($C_w = 44.64\%$).

● $\lambda = 34.6$ mm, ◆ $\lambda = 58.1$ mm, ▲ $\lambda = 76.2$ mm.

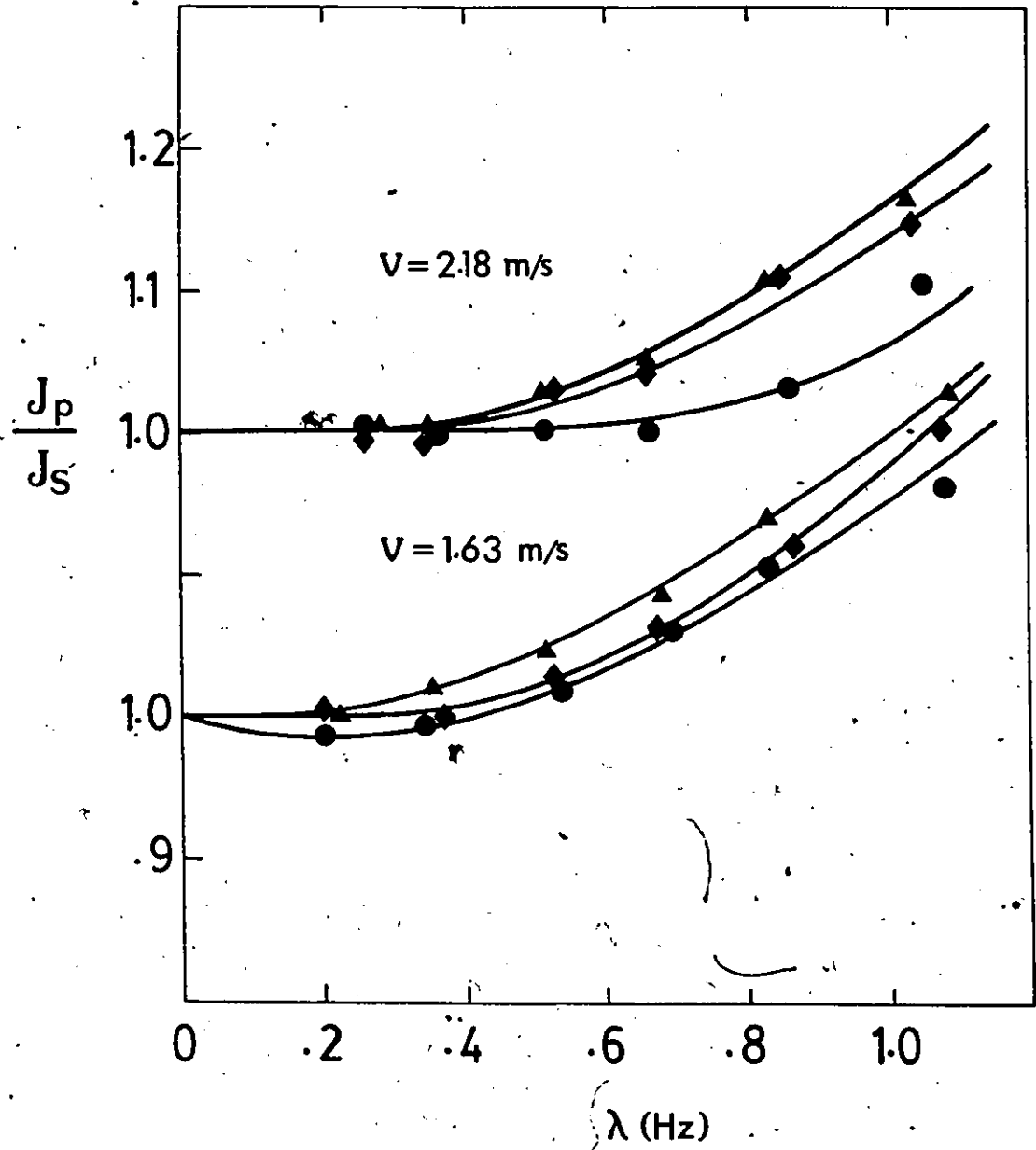


Figure 7.18 Hydraulic power ratio of pulsating to steady flow vs. pulsing frequency. Experimental results for coal-water slurry ($C_w = 53.7\%$).
 ● $A = 34.6$ mm, ◆ $A = 52.1$ mm, ▲ $A = 76.2$ mm.

increases over the accelerating phase of each pulse, the difference between the liquid velocity and the particle velocity increases and the particle gains momentum because it is dragged by the liquid. This causes the particle to move to a new radial position at which the momentum level is higher. In the given range of λ , it appears from the experimental results that the above situation is not reversible over the decelerating phase. This agrees with the observations of Shizgal et al. [13].

Further increase in λ beyond its critical value results in an undesirable increase in the power ratio J_p/J_s . This may be explained by one or by a combination of two reasons. The first is that as λ increases more and more, the rate of inward radial migration becomes less than before because the transient time, available for the particle to travel under the effect of lift forces, is less than the actual required time. The other reason is that even if the rate of the inward radial migration remains unchanged, the energy required for maintaining the oscillatory flow component increases with increasing frequency. Therefore, there must be a situation at which this extra energy exceeds the value of energy saved by the growth of the particle-free layer adjacent to the pipe wall.

7.2.2 Effect of Pulsing Amplitude:

Unlike the case of bentonite clay-water suspension, plotting the measured values of the hydraulic power ratio J_p/J_s as a function of the velocity amplitude ($\pi A [D/d]^2 \Delta V$) does not combine all the data points on one curve. On the other hand, pulsing frequency λ , which represents the volume of fluid injected into the test section, i.e. the instantaneous change in the flowrate and the flow velocity, has direct effect on the magnitude of J_p/J_s . It is clear from Figures 7.10 to 7.18 that an increase in λ , shifts all the curves upward to a higher level of J_p/J_s . This, perhaps, can be explained by referring to equation (2.14). In this equation the hydraulic power is proportional to square the oscillating velocity component, while it is

proportional to the inverse of the particle-free layer thickness. This means that the value of A has a greater effect on the hydraulic power than the particle-free layer thickness has. It appears, however, from the experimental results and from equation (2.14) that there is a situation in which the particle-free layer thickness reaches its optimum value. This occurs at $A = 34.6$ mm.

In Figure 7.13, it can be seen that the effect of A on the ratio J_p/J_s is much more pronounced in the middle range of λ . This is because in this range the amount of energy saved by pulsating flow has reached its maximum value, i.e. J_p has reached its minimum possible value and, therefore, any change in A has greater effect on J_p/J_s . In a higher range of λ , J_p is already far beyond its minimum value and, consequently, variation in A has much less effect on J_p/J_s .

7.2.3 Effect of Average Flow Velocity:

As far as hydraulic energy is concerned, the maximum beneficial effect of pulsating flow in heterogeneous solid-liquid slurry can be achieved as long as the steady flow of such a slurry is in its complete or partial saltation regime, Figure 2.12. According to Durand [59,94,95], the lowest average flow velocity investigated here (1.63 m/sec) is less than the critical deposit velocity of coal particle of the given mean size of 260 microns. Considering the fact that there are coal particles of sizes up to 800 microns and more, this may bring the middle velocity investigated here (2.18 m/sec) into the critical region where partial saltation occurs. While the highest velocity is just above the critical region where the effect of pulsating flow on the hydraulic power requirement is significantly less. However, it must be understood that solids concentration has a great influence on the critical velocity, and therefore, it is very difficult to determine definitely whether saltation or partial saltation occurs or not.

In Figures 7.10 to 7.18, where $\lambda > 0.6$ Hz, at a given pulsing frequency and amplitude, an increase in the average flow velocity results in a slight decrease in the ratio J_p/J_s . This can be explained by the fact that in such frequency range J_p is already higher than its minimum value, and in some cases higher than J_s . In steady flow, the hydraulic power is proportional to the velocity cubed, which means that an increase in the average flow velocity results in much greater increase in J_s . On the other hand, increasing the flow velocity reduces the beneficial effect of pulsating flow, i.e. J_p increases, but not as much as J_s increases. Therefore, the ratio of J_p/J_s appears to be decreasing as V increases, but only where $\lambda > 0.6$ Hz.

Over the first part of the curves, the influence of the average flow velocity on the hydraulic power ratio is opposite to the above. In the range of $\lambda = 0 - 0.5$ Hz the beneficial effect of pulsating flow reaches its maximum, since J_p is near its minimum value. Therefore, any change in J_p relative to its small value is highly pronounced. As the flow velocity increases, more coal particles are suspended in the liquid due to the increasing turbulence, while the pulsating flow has less significance. This means that the energy required to maintain pulsating flow is relatively higher as V increases.

7.2.4 Effect of Solids Concentration:

Solids concentration is a critical and important parameter simply because it has a great effect on the physical properties of the slurry such as density and viscosity. Additionally, the 'shear rate-shear stress' response is fundamentally dependent on the solids concentration.

The effect of solids concentration on the ratio J_p/J_s is illustrated in Figure 7.19. In this Figure, values of J_p/J_s are plotted versus C_w for certain values of λ , A and V . More precisely, the curve given in the figure represents the ratio J_p/J_s as a function of C_w at the

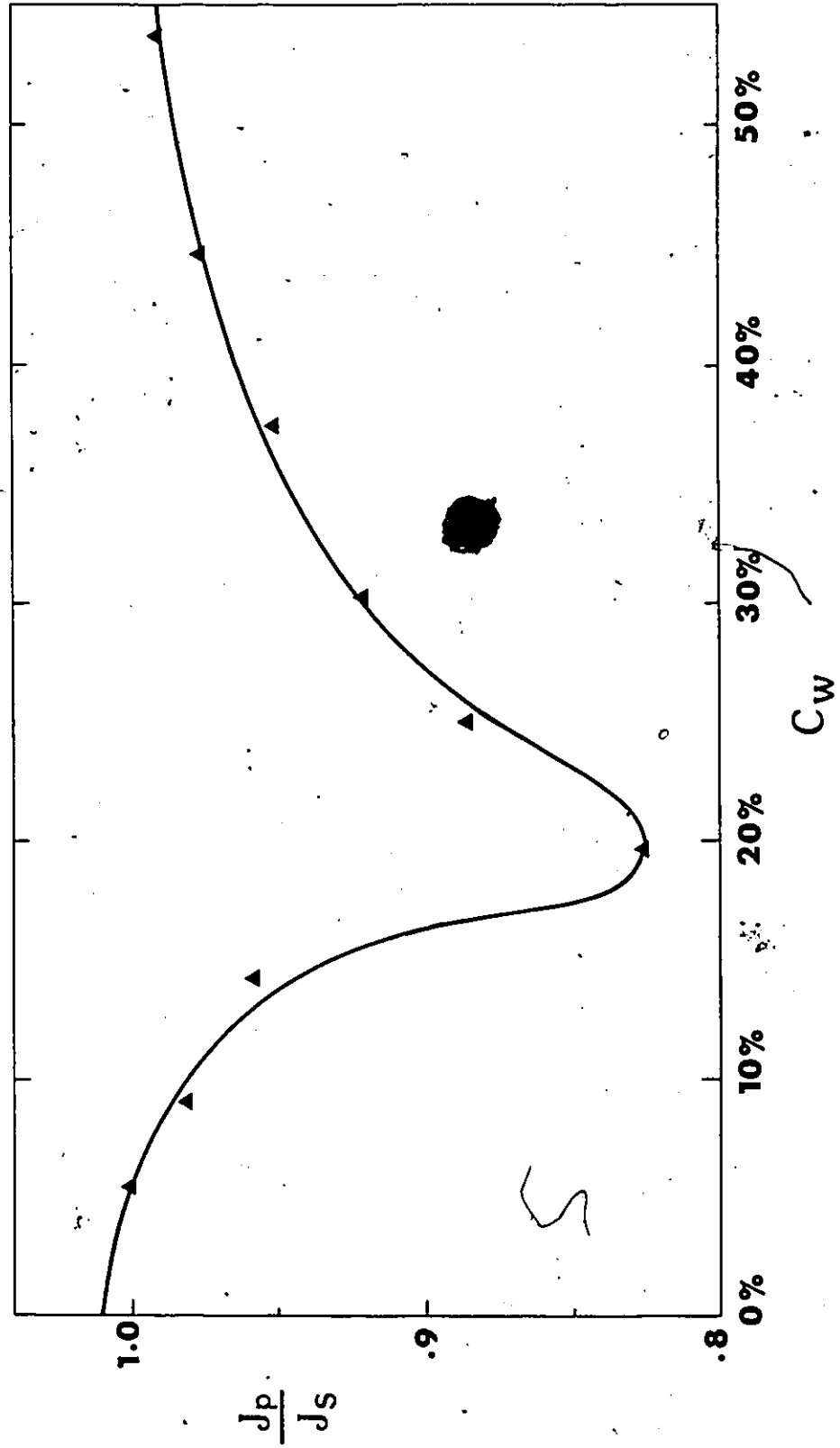


Figure 7.19 Power ratio of pulsating to steady flow versus slurry concentration. Experimental results at pulser amplitude $A = 34.6$ mm, average flow velocity $v = 1.63$ m/sec and pulsating frequency $\lambda = .3$ Hz.

S

S

3

optimum pulsing frequency and amplitude, and at the lowest flow velocity investigated here. It is obvious that there is an optimum value for C_w at which the maximum beneficial effect of pulsating flow occurs, or in other words, at which minimum J_p/J_s is achieved. This minimum is found to be at about $C_w = 20\%$ and its magnitude is about $J_p/J_s = 0.82$.

In the range of $C_w = 0-20\%$, as C_w increases the ratios J_p/J_s drop toward their minima. This agrees with the observations of Shizgal et al. [13]. It has been found that as C_w increases from 5% to 20%, the rate of inward radial particle migration increases significantly, particularly where $C_w > 10\%$. Also, the thickness of the particle-free layer adjacent to the pipe wall increases with the increasing rate of inward radial migration. As it has been discussed before, the formation of a particle-free layer, which acts as a lubricant, is one possible mechanism for the observed reductions in the hydraulic power in pulsating flow.

It follows from the preceding that there is a limit at which the particle-free layer has reached its maximum thickness and a plug flow of the suspension is established.

Further increase of solids particle concentration beyond its optimum value may result in a dramatic change in the shape of the actual velocity profile. Due to the plug flow situation, the radial velocity gradient may differ very little from zero and therefore more uniform viscous forces over the particle surface result in less rotation which cause significant reduction in the spin lift, it may even vanish. Also, the shear lift will be reduced because of the major change in the relative velocity between the solid particles and the liquid. The reduction in the total lift will naturally result in a great change in the inward radial migration. This series of events is confirmed by the dramatic increase in J_p/J_s in the range of $C_w = 20\% - 35\%$. For solids concentration higher than 35%, J_p/J_s continues to increase as C_w increases, but at a much slower rate.

7.3 Limitations

The theoretical results presented in Chapter 6 are quite general. Unfortunately, a fully detailed comparison between these results and the experimental results obtained for the bentonite clay-water suspension is not possible due to some limitations:

1. In the mathematical solution presented in Chapter 4 and from the results presented and discussed in Chapter 6, it has been proven that the flowrate can be increased by superimposing an oscillating flow component over the steady flow for non-Newtonian fluids at the same pressure gradient. According to the assumption of constant mean pressure gradient, the solution is actually forced to a situation in which due to the high shear stress generated over the accelerating phase during each pulse, increase in the velocity is achieved. This fact agrees well with Barnes et al. [1] and with Walters and Townsend [2]. There is, however, another situation which is possible, but may not be necessary. This is, as the fluid is dominated by the high viscous forces near the pipe wall in the accelerating phase, the fluid apparent viscosity decreases and the frictional pressure drop accordingly decreases, while the velocity or the flowrate remain unchanged. The values of the hydraulic power resulting from both situations are not necessarily equal.
2. Bentonite clay-water suspension is in fact a thixotropic material and it has a finite relaxation time, while the theoretical solution presented in Chapters 4 and 6 are for non-thixotropic non-Newtonian fluids where the relaxation time is zero.
3. Typical viscometric flow curves given in Figure 5.3 show that at high concentration of bentonite clay in water, the suspension behaves as a general Bingham fluid. The actual flow curve shows a slight deviation from the constitutive equation (4.1) which assumes inelastic behaviour where $|\tau_r| < \tau_0$. It appears from Figure 5.3 that

there is a very small value of shear rate corresponds to the point of breakdown, i.e. the point of $|\tau_{\dot{\gamma}}| = \tau_0$.

4. It has been shown in Section 7.1 that the velocity amplitude $(\pi A [D/d]^2 \lambda / V)$ is function of the pulsing amplitude. Any change in λ will result in a corresponding change in the velocity amplitude, and consequently in the pressure amplitude,

$$\varepsilon \propto (\pi A [D/d]^2 \lambda / V)^n.$$

On the other hand, in the theoretical treatment to the problem of pulsating flow, it has been assumed that the pulsing frequency and the pulsing amplitude are non-interdependent parameters. This limitation arises from the physical design of the pulse generating equipment.

CHAPTER 8

CONCLUSIONS AND RECOMMENDATIONS

8.1 Conclusions

The study that has been presented allows one to bring out a certain number of important results on the unsteady state flow of non-Newtonian fluids. Distinguishing between two types of solid-liquid suspensions in terms of homogeneous flow and heterogeneous flow, it was possible to characterize the influence of pulsating flow parameters on each type separately.

Experiments were carried out with two markedly different types of slurries or suspensions, and were principally based on measuring the instantaneous flowrate and the instantaneous pressure drop over a defined length. The use of a computer was obviously needed for calculating the hydraulic power requirements under different flow conditions.

On the other hand, in order to expand the range of the present investigation, a mathematical formulation was developed for homogeneous non-Newtonian fluids using the generalized Bingham model. An explicit finite difference scheme was used to treat the equations governing the flow.

Attention was mainly focussed on the evolution of the predicted velocity profiles when the fluid underwent a periodic axial pressure gradient or a suddenly imposed constant pressure gradient. Attention was also focussed on the ratio of pulsating flow energy to steady flow energy as a function of frequency, amplitude, average flow velocity and solids weight concentration.

The following general conclusions can be drawn:

1. The numerical solution allowed a systematic study of the influence of different parameters and in particular, the rheological ones. The experiments by themselves

cannot achieve these results because one parameter cannot be varied without affecting another.

2. Typical velocity profiles are presented for different pulsating flows for values of $n = 0.7$ and 1.0 , and values of $\tau_0/\tau_w = 0.32$ and 0.44 . The influence of all the major variables is demonstrated. Significant flow reversal could not be achieved for the investigated values of frequency parameter and pressure amplitudes but it may be achieved however, at low frequencies and higher amplitudes.

3. In the theoretical part, for values of frequency parameter ζ less than about 20, pulsations are seen to increase the flowrate of Bingham fluids. The maximum increase in the flowrate occurs in the region $2 \leq \zeta \leq 4$. The existence of a peak in the flowrate agrees with other experimental investigations.

4. It has been demonstrated theoretically that the hydraulic power requirement in pulsating flow of power law fluids is never less than that of steady flow at the same flowrate. The hydraulic power requirement in pulsating flow of Bingham fluids may possibly be lower than that for steady flow at the same flowrate. This, however, depends on the yield stress of the fluid and on the value of n .

5. Typical velocity profiles predicted for start-up flow are presented for the same values of n and τ_0/τ_w mentioned in no. 2. It has been seen that the transient time of Bingham materials is much less than that of Newtonian or power law fluids.

6. On the experimental side, pulsating flow appears to be advantageous in the transport of solid-liquid mixtures. This advantageous situation results in the reduction of hydraulic power. This reduction is accentuated when the fluid deviates considerably from Newtonian behaviour.

7. There are at least two kinds of phenomena in pulsating flow of solid-liquid mixtures.

These are:

- I) the formation of a low viscosity layer near the pipe walls in homogeneous non-Newtonian fluid for power law and Bingham fluids;
- II) the formation of a particle-free layer adjacent to the pipe wall - this occurs in heterogeneous slurries due to inward radial migration of solid particles from the wall.

8. Reductions in hydraulic energy are possible only with certain combinations of pulsing frequency, pulsing amplitude, average flow velocity, and most importantly solids concentration. The optimum frequency in most cases was found to be of the order of 0.3 Hz, while the lowest amplitude investigated here indicated that it is the best.

It should be emphasized, however, that these results are very much dependent on the pulse generating mechanism and the flow phenomena may vary according to the applied pulsations. There is no question however that the effect of flow parameters on the power ratio J_p/J_s remains the same irrespective of what piece of equipment being used.

9. It has been experimentally observed that the ratio of hydraulic power J_p/J_s is strongly dependent on the solids concentration. In the case of clay-water suspensions increasing solids concentration enhances the non-Newtonian nature of the fluid and increases the yield stress significantly. The consequence is a lower value of J_p/J_s . On the other hand, in the case of coal-water slurry the flow is heterogeneous and increasing the solids concentration may make the effect of inward particle migration, due to flow pulsations, more and more pronounced until

eventually a point is reached ($C_w = 20\%$) where increasing the concentration causes an opposite effect on the power ratio. This may result from fundamental changes in the lift forces which are responsible for inward radial migration.

10. Although the amount of possible savings in hydraulic energy in the case of Bingham materials by pulsation is not significant from the practical hydrotransport point of view, the theoretical analysis presented here is very useful in the field of hemodynamics and to many industrial areas in particular heat/mass transfer.
11. In view of the potential industrial applications of pulsating flow to coal slurry pipelines, it would appear that hydraulic energy requirements can be lowered by at least 20%. Although additional capital equipment will be required to produce pulsating flow, this should be minimal since the values of frequency and amplitude are quite low. There is no doubt from the study that further work is justified so that the effect of pulsations on overall costs can be assessed.

8.2 Suggestions for Further Studies

As suggestions for further studies, the following are presented.

1. Laser Doppler anemometers provide a method for measuring local velocities without insertion of a disturbance-producing probe into the flow field. Detailed velocity measurements in pulsating flows of Bingham materials, using such techniques, would be very useful as a comparison with the theoretical predictions presented in Chapter 6 and others which can be obtained by extending these predictions. Additionally such a study can provide detailed information about the flow stability and occurrence of turbulence as well as relaminarization of the flow of Bingham fluids.

2. The present theoretical investigation is quite general and comprehensive, but yet it was limited to one kind of wave shape which was a uniform, symmetric, periodic sinusoidal form. An extension of this should be done to include other kinds of pressure waves to investigate other possibilities of energy saving by pulsation.
3. In the present experimental investigation, only four parameters were studied, these were pulsing frequency, amplitude, average flow velocity, and solids concentration. However, the existing experimental rig with some modification facilitates further experiments which may include the effects of wave shape, mean particle size and size distribution, different carrier fluids, solids density, particle shape and pipe geometry.
4. The behaviour of individual solid particles under different pulsating flow conditions is still unknown. Further experimental study of radial migration of solid particles and other phenomena such as mixing effect or destratification of the flow due to turbulence changes is necessary for understanding and exploring the advantages of pulsating flows of heterogeneous slurries.
5. Before any industrial application to coal slurry transport by pulsation, an overall evaluation from economical viewpoint is necessary. This will require consideration of item 3 above.
6. The present theoretical and experimental models can be modified to include the problem of heat transfer which has potential applications in many areas of industry.

7. The theoretical formulation presented in Chapter 4 was based on the constitutive equation of generalized Bingham fluid which does not allow viscoelasticity into account. Hence, further theoretical work on pulsating flows of viscoelastic materials is recommended.



REFERENCES

- [1] Barnes, H.A.; Townsend, P.; and Walters, K., "Flow of Non-Newtonian Liquids Under a Varying Pressure Gradient", *Nature*, 224, 585 (1969).
- [2] Walters, K.; and Townsend, P., "The Flow of Viscous and Elastico-Viscous Liquids in Straight Pipes Under a Varying Pressure Gradient", *Proc. 5th Intl. Cong. Rheol.*, Kyoto, pp. 471-483, North Holland Pub. Co., Amsterdam (1969).
- [3] Round, G.F., "Pulsating Flows - Applications to the Pipeline Flow of Solid-Liquid Suspensions", *Proc. Hydrotransport 3*, Colorado, paper B3 (1974).
- [4] Round, G.F.; Latto, B.; and Lau, K.Y., "Pulsating Flows of Solid-Liquid Suspensions", *Proc. Hydrotransport 4*, Banff, Canada, paper D.1 (1976).
- [5] Round, G.F., "Pulsed Slurry Flow in Pipelines", *J. Pipelines*, 1, 307 (1981).
- [6] Hameed, A., "Pipeline Pulsing Flow of Slurries", Ph.D. Thesis, McMaster University (1983).
- [7] Round, G.F., "Pulsing Flow Applied to Slurry Transport: A Review", *Proc. Interfacial Phenomena in Mineral Processing*, Rindge, NH (Aug. 2-7, 1981).
- [8] Metzner, A.B.; and Reed, J.C., "Flow of Non-Newtonian Fluids - Correlation of the Laminar, Transition and Turbulent Flow Regions", *A.I.Ch.E.J.*, 1, no. 4, 435 (1955).
- [9] Hedström, B.O.A., "Flow of Plastic Materials in Pipes", *Ind. Eng. Chem.*, 44, 651 (1952).
- [10] Edwards, M.F.; and Wilkinson, W.L., "Review of Potential Applications of Pulsating Flow in Pipes", *Trans. Instn. Chem. Engrs.*, 49, 85 (1971).
- [11] Edwards, M.F.; Nellist, D.A.; and Wilkinson, W.L., "Unsteady Laminar Flows of Non-Newtonian Fluids in Pipes", *Chem. Engng. Science*, 27, 295 (1972).
- [12] Edwards, M.F.; Nellist, D.A.; and Wilkinson, W.L., "Pulsating Flow of Non-Newtonian Fluids in Pipes", *Chem. Engng. Science*, 27, 545 (1972).
- [13] Shizgal, B.; Goldsmith, H.L.; and Mason, S.G., "The Flow of Suspensions Through Tubes IV. Oscillating Flow of Rigid Spheres", *Can. J. Chem. Eng.*, 43, 97 (1965).
- [14] Schlichting, H., "Boundary Layer Theory", 4th edition, McGraw-Hill (1968).
- [15] Charles, M.E.; and Stevens, G.S., "The Pipeline Flow of Slurries - Transition Velocities", 2nd Intl. Conf. on Hyd. Transport of Solids in Pipes, BHRA Fluid Engng., Cranfield, U.K., paper E3 (1972).

- [16] Bird, R.B.; Stewart, W.E.; and Lightfoot, E.N., "Transport Phenomena", John Wiley (1960).
- [17] Alves, G.E.; Boucher, D.F.; and Pigford, R.L., "Pipe-Line Design for Non-Newtonian Solutions and Suspensions", Chem. Eng. Progr., 48, 385 (1952).
- [18] Unknown, "Industrial Rheology and Rheological Structures", John Wiley (1949).
- [19] Metzner, A.B., loc. cit., 50, 27 (1954).
- [20] Reiner, M., "Ten Lectures on Theoretical Rheology", Rubin-Mass, Jerusalem (1943).
- [21] Unknown, "Deformation and Flow", H.K. Lewis and Co., London (1949).
- [22] Reed, J.C., M.Ch.E. Thesis, University of Delaware (1954).
- [23] Scott Blair, G.W., "Introduction to Industrial Rheology", J. and A. Churchill, Ltd., London (1938).
- [24] Salt, D.L., M.S. Thesis, University of Utah (1949)
- [25] Stevens, W.E., Ph.D. Thesis, University of Utah (1953).
- [26] Harris, J., "The Correlation of Non-Newtonian Turbulent Pipe-Flow Data", Rheol. Acta, 7, 228 (1968).
- [27] Wilkinson, W.L., Ind. Chemist, 34, 79 (1958).
- [28] Mooney, M., J. Rheol., 2, 210 (1931).
- [29] Hanks, R.W., "The Not So "Generalized" Reynolds Number", Proc. 4th Intl. Tech. Conf. Slurry Transportation, Las Vegas, Nevada, 91 (1979).
- [30] McMillen, E.L., "Simplified Pressure-Losses Calculations for Plastic Flow", Chem. Eng. Prog., 44, 537 (1948).
- [31] Womersley, J.R., Appl. Physiol., 127, 553 (1955).
- [32] Uchida, S., "The Pulsating Viscous Flow Superposed on the Steady Laminar Motions of Incompressible Fluid in a Circular Pipe", Z. Engew. Math. U. Phys., 7(5), 403 (1956).
- [33] Sexl, T., "Annulareffekt", Z. Phys., 61, 349 (1930),
- [34] Linford, R.G.; and Ryan, N.W., Appl. Physiol., 20, 1078 (1965).
- [35] Bettner, L., Ph.D. Thesis, Purdue University, School of Mechanical Engineering (1965).

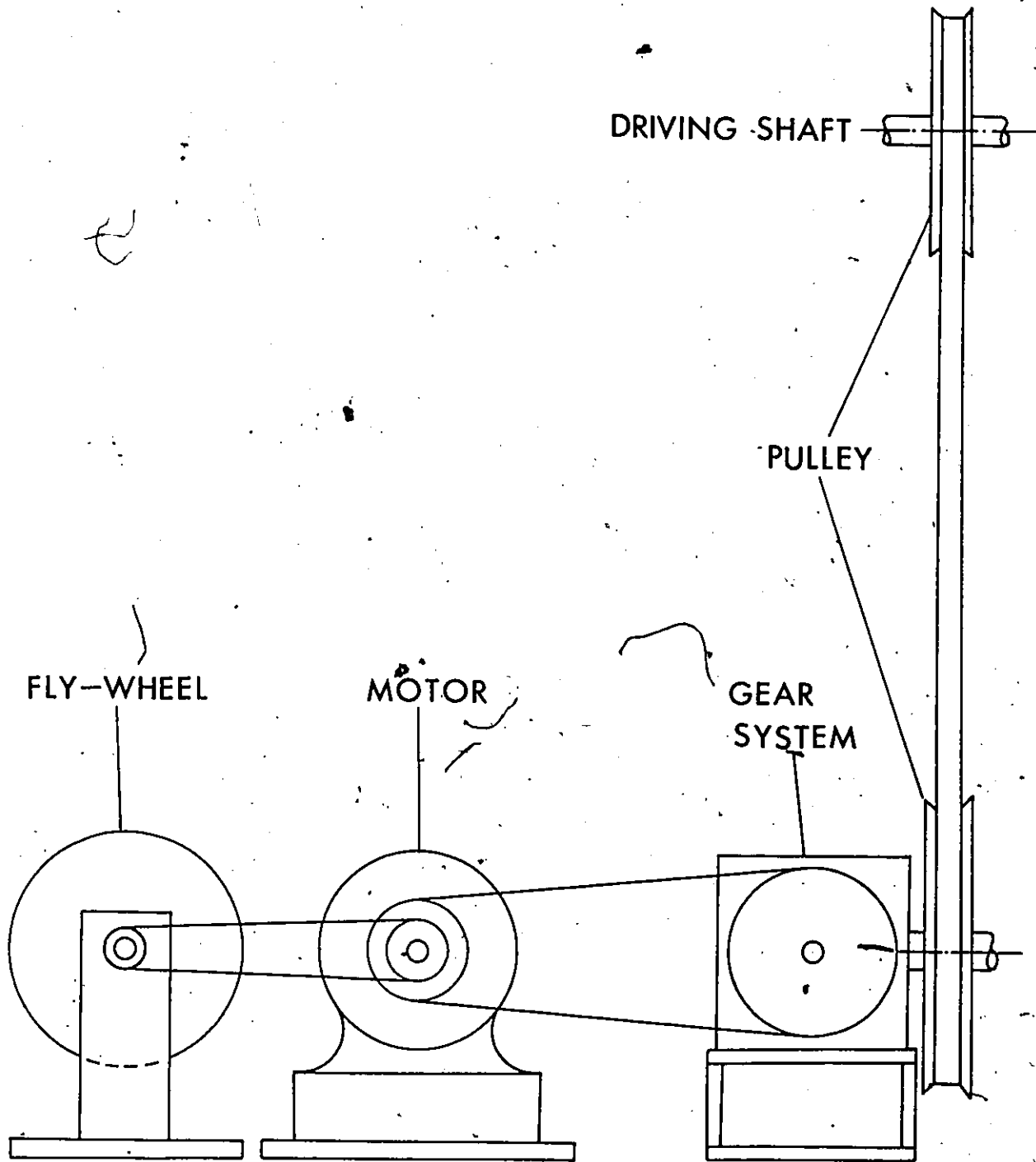
- [36] Chang, C.C.; and Atabek, H.B., "The Entry Length for Oscillating Flow and Its Effects on the Determination of the Rate of Flow in Arteries", *Phys. Med. and Bio.*, 6, 303 (1961).
- [37] Muto, T.; and Nakane, K., "Unsteady Flow in Circular Tube (Velocity Distribution of Pulsating Flow)", *Bull. JSME*, 23 (186), 1990 (1980).
- [38] Klimes, F.; Korenar, J.; and Toman, J., "Experimental Verification of Theoretical Velocity Profiles of Oscillatory and Pulsatory Flow by Means of LDA", *Communications*, 12, 113 (1983), Institute of Hydrodynamics, Podbabska 13, 16612 Praha 6.
- [39] Binnie, A.M., "A Double-Refraction Method of Detecting Turbulence in Liquids", *Proc. Phys. Soc. London, London, England*, 57, 390 (1945).
- [40] Darling, G.B., "Heat Transfer to Liquids in Intermittent Flow", *Petroleum*, 22, 177 (1959).
- [41] Kastner, L.J.; and Shih, S.H., "Critical Reynolds Numbers for Steady and Pulsating Flow", *Engineering*, 172, 385 (1951).
- [42] Gilbrech, D.A.; and Combs, G.D., "Critical Reynolds Numbers for Incompressible Pulsating Flow in Tubes", *Developments in Theoretical and Applied Mechanics*, Plenum Press, New York, NY, 1, 292 (1963).
- [43] Combs, G.D.; and Gilbrech, D.A., "Pulsating Flow Research", University of Arkansas, Engineering Experiment Station, Research Papers, no. 4, April (1964).
- [44] Sarpkaya, T., "Experimental Determination of the Critical Reynolds Number for Pulsating Poiseuille Flow", *Trans. ASME, Series D (J. of Basic Engng.)*, 88, 589 (1966).
- [45] Ohmi, M.; Iguchi, M.; Usui, T.; and Minami, H., "Flow Pattern and Frictional Losses in Pulsating Pipe Flow, Part 1: Effect of Pulsating Frequency on the Turbulent Flow Pattern", *Bull. JSME*, 23(186), 2013 (1980).
- [46] Ohmi, M.; and Iguchi, M., "Flow Pattern and Frictional Losses in Pulsating Pipe Flow, Part 2: Effect of Pulsating Frequency on the Turbulent Frictional Losses", *Bull. JSME*, 23(186), 2021 (1980).
- [47] Ohmi, M.; and Iguchi, M., "Flow Pattern and Frictional Losses in Pulsating Pipe Flow, Part 3: General Representation of Turbulent Flow Pattern", *Bull. JSME*, 23(186), 2029 (1980).
- [48] Ohmi, M.; Iguchi, M.; Kakehashi, K.; and Masuda, T., "Transition to Turbulence and Velocity Distribution in an Oscillating Pipe Flow", *Bull. JSME*, 25(201), 365 (1982).
- [49] Ohmi, M.; Iguchi, M.; and Urahata, I., "Flow Patterns and Frictional Losses in an Oscillating Pipe Flow", *Bull. JSME*, 25(202), 536 (1982).

- [50] Ohmi, M.; Iguchi, M.; and Urahata, I., "Transition to Turbulence in a Pulsatile Pipe Flow, part 1: Wave Forms and Distribution of Pulsatile Velocities Near Transition Region", *Bull. JSME*, 25(200), 182 (1982).
- [51] Ohmi, M.; and Iguchi, M., "Transition to Turbulence in a Pulsatile Pipe Flow, part 2: Characteristics of Reversing Flow", *Bull. JSME*, 25(208), 1529 (1982).
- [52] Hino, M.; Sawamoto, M.; and Takasu, S., "Experiments on Transition to Turbulence in an Oscillatory Pipe Flow", *J. Fluid Mech.*, 75(2), 193 (1976).
- [53] Ly, D.P.; Bellet, D.; and Bousquet, A., "Non-Permanent Flow of Ostwald Fluids", *Rheol. Acta*, 14, 783 (1975).
- [54] Ly, D.P.; and Bousquet, A., "Determination of Velocity Profiles by Laser-Doppler-Anemometry in Pulsating Laminar Flow of Non-Newtonian Fluids", *Proceedings of the LDA-Symposium, Copenhagen* (1975).
- [55] Vela, S.; Kalb, J.W.; and Fredrickson, A.G., "On Stress-Relaxing Solids, part 3: Simple Harmonic Deformation", *A.I.Ch.E.J.*, 11, 288 (1965).
- [56] Etter, I.; and Schowalter, W.R., *Trans. Rheol. Soc.*, 9, 351 (1965).
- [57] Jones, J.R.; and Walters, T.S., "Flow of Elastic-Viscous Liquids in Channels Under the Influence of a-Periodic Pressure Gradient, Part 1", *Rheol. Acta*, 6, 240 (1967).
- [58] Wasp, E.J.; *et al.*, "Deposition Velocities, Transition Velocities, and Spatial Distribution of Solids in Slurry Pipelines", 1st Intl. Conf. On Hyd. Transport of Solids in Pipes, BHRA Fluid Engng., Cranfield, UK, Paper H4 (Sept. 1970).
- [59] Durand, R., "The Hydraulic Transportation of Coal and Other Materials in Pipes", *Colloq. of National Coal Board, London* (Nov. 1952).
- [60] Thomas, D.G., "Transport Characteristics of Suspensions, Part IV", *A.I.Ch.I.J.*, 8, 373 (1962).
- [61] Graf, W.H.; Robinson, M.; and Yucel, O., "The Critical Deposit Velocity of Solid-Liquid Mixtures", 1st Intl. Conf. on Hydr. Transport of Solids in Pipes, BHRA Fluid Engng., Cranfield, UK, Paper H5 (Sept. 1970).
- [62] Sinclair, C.G., "The Limit-Deposit Velocity of Heterogeneous Suspensions", *Interaction Between Fluid and Particles, Inc. Chem. Eng., London* (1962).
- [63] Zandi, I.; and Govatos, G., "Heterogeneous Flow of Solids in Pipeline", *Proceedings Hydraulics Division, ASCE*, 93, 145 (1967).
- [64] Charles, M.E.; and Stevens, G.S., "The Pipeline Flow of Slurries - Transition Velocities", 2nd Intl. Conf. on Hydr. Transport of Solids in Pipes, BHRA Fluid Engng., Cranfield, UK, Paper E3 (Sept. 1972).
- [65] Condolios, E.; and Chapus, E.E., "Solids Pipelines - 2: Designing Solids Handling Pipelines", *Chem. Eng.*, 70, 131 (1963).

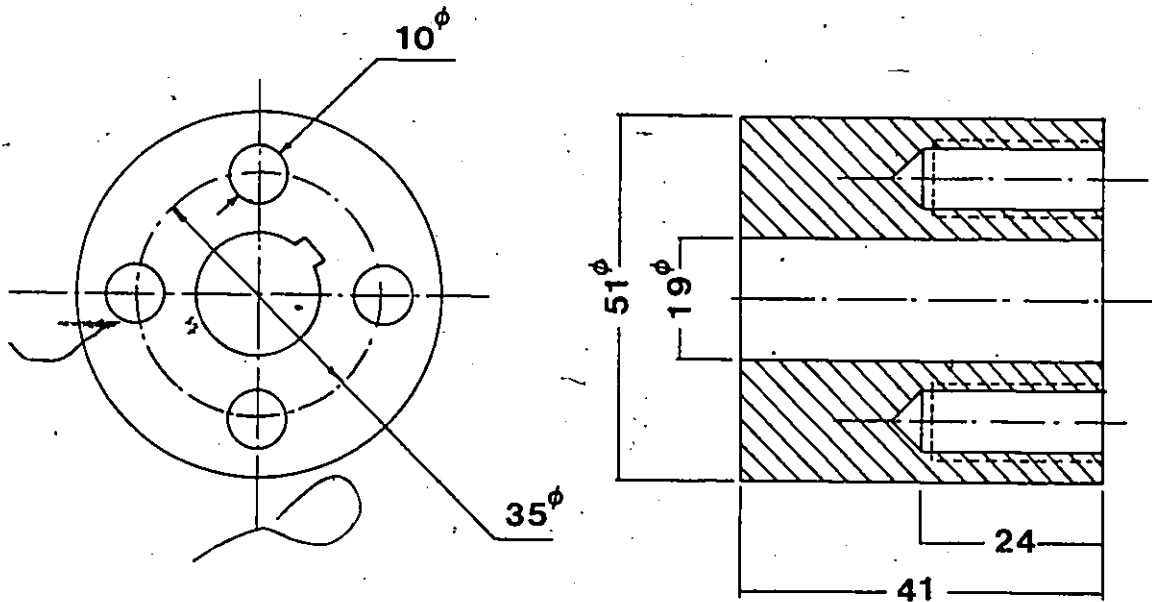
- [66] Young, D.F., "The Coring Phenomenon in the Flow of Suspensions in Vertical Tubes", ASME Paper No. 60-HYD-12 (1960).
- [67] Segré, G.; and Silberberg, A., "Radial Particle Displacements in Poiseuille Flow of Suspensions", *Nature*, 189, 209 (1961). See also *J. Fluid Mech.*, 14, 136 (1962).
- [68] Goldsmith, H.L.; and Mason, S.G., "The Flow of Suspensions Through Tubes", *I.J. Colloid Sci.*, 17, 448 (1962).
- [69] Oliver, D.R., "Influence of Particle Rotation on Radial Migration in the Poiseuille Flow of Suspensions", *Nature*, 194, 1269 (1962).
- [70] Jeffrey, R.C., "Particle Motion in Poiseuille Flow", Ph.D. Thesis, Cambridge University (1964). See also: Jeffrey, R.C. and Pearson, J.R.A., *J. Fluid Mech.*, 22, 721 (1965).
- [71] Theodore, L., "Sidewise Force Exerted on a Spherical Particle in a Poiseuille Flow", Eng. Sc.D. Dissertation, New York University (1964).
- [72] Repetti, R.V.; and Leonard, E.F., "Segré-Silberberg Annulus Formation: A Possible Explanation", *Nature*, 203, 1346 (1964).
- [73] Brandt, A.; and Bugliarello, G., "Concentration Redistribution Phenomena in the Shear Flow of Monolayers of Suspended Particles", presented at 1965 Soc. of Rheol. Meeting.
- [74] Denson, C.D., "Particle Migration in Shear Fields", Ph.D. Thesis, University of Utah (1965).
- [75] Denson, C.D.; Christiansen, E.B.; and Salt, D.L., "Particle Migration in Shear Fields", *A.I.Ch.E.J.*, 12 (3), 589 (1966).
- [76] Saffman, P.G., "The Lift on a Small Sphere in a Slow Shear Flow", *J. Fluid Mech.*, 22, 385 (1965).
- [77] Ariman, T.; Turk, M.A.; and Sylvester, N.D., "On Steady and Pulsatile Flow of Blood", *Trans. ASME, Series E (J. Appl. Mech.)*, 41, 1 (1974).
- [78] Tait, R.J.; Moodie, T.B.; and Haddow, J.B., "Wave Propagation in a Fluid-Filled Elastic Tube", *Acta Mechanica*, 38, 71 (1981).
- [79] Womersley, J.R., *Wright Air Development Centre Tech. Repts.*, 56, 614 (1958).
- [80] Lambert, J.W., *J. Franklin Institute*, 266, (2) (1958).
- [81] Evans, R.L., "A Unifying Approach to Blood Flow Theory", *J. Theor. Biol.*, 3, 392 (1962).
- [82] Streeter, V.L.; Keitzer, W.F.; and Bohr, D.F., *Circul. Res.*, 13, 3 (1963).

- [83] Olsen, J.H.; and Shapiro, A.H., "Large-Amplitude Unsteady Flow in Liquid-Filled Elastic Tubes", *J. Fluid Mech.*, 29, 513 (1967).
- [84] Barnard, A.C.L.; Hunt, W.A.; Timlake, W.P.; and Varley, E., "A Theory of Fluid Flow on Compliant Tubes", *Proc. 4th Am. Symp. Biomath Comp. Sci.*, Houston, Texas (1966).
- [85] Cokelet, G.R., "The Rheology of Human Blood", *Biomechanics - Its Foundation and Objectives*, ed. Fung, Y.C.; Perrone, N.; and Anliker, M., Prentice-Hall, Englewood Cliffs, NJ, 63-103 (1972).
- [86] Davidson, G.A., "The Pumping of Bentonite Clays", M.Eng. Thesis, McMaster University (1979).
- [87] Prager, W., "Introduction to Mechanics of Continua", Ginn and Co., Boston (1961).
- [88] Forsythe, G.E., "Finite-Difference Methods for Partial Differential Equations", John Wiley (1960).
- [89] Smith, G.D., "Numerical Solution of Partial Differential Equations", Oxford University Press (1965).
- [90] Szymanski, P., *J. Math. Pure Appl.*, Series 9, 11, 67 (1932).
- [91] Wasp, E.J.; Kenny, J.P.; and Gandhi, R.L., "Solid-Liquid Flow Slurry Pipeline Transportation", Gulf Publishing Co. (1979).
- [92] Karnis, A.; Goldsmith, H.L.; and Mason, S.G., "Axial Migration of Particles in Poiseuille Flow", *Nature*, 200, 159 (1963).
- [93] Rubinow, S.J.; and Keller, J.B., "The Transverse Force on a Spinning Sphere Moving in a Viscous Fluid", *J. Fluid Mech.*, 11, 447 (1961).
- [94] Durand, R., "Basic Relationships of the Transportation of Solids in Pipes - Experimental Research", *Proc. Intl. Assoc. Hydraulic Research*, Minneapolis, MN (1953).
- [95] Durand, R., "Hydraulic Transport of Solid Material in Pipes", *Abs. Chem. Eng. and Mining Review*, 60, 225 (1953).

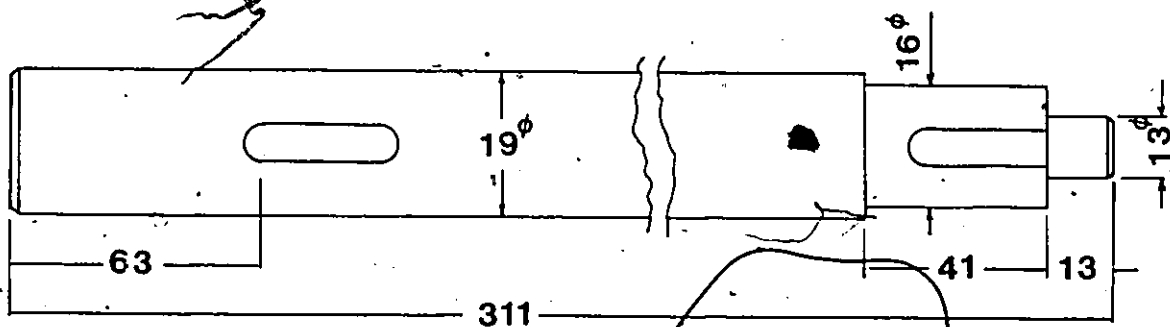
APPENDIX A
DETAILS OF PULSING EQUIPMENT



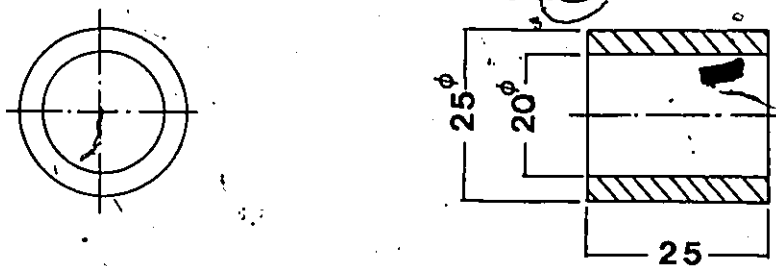
DRIVING SYSTEM [schematic]



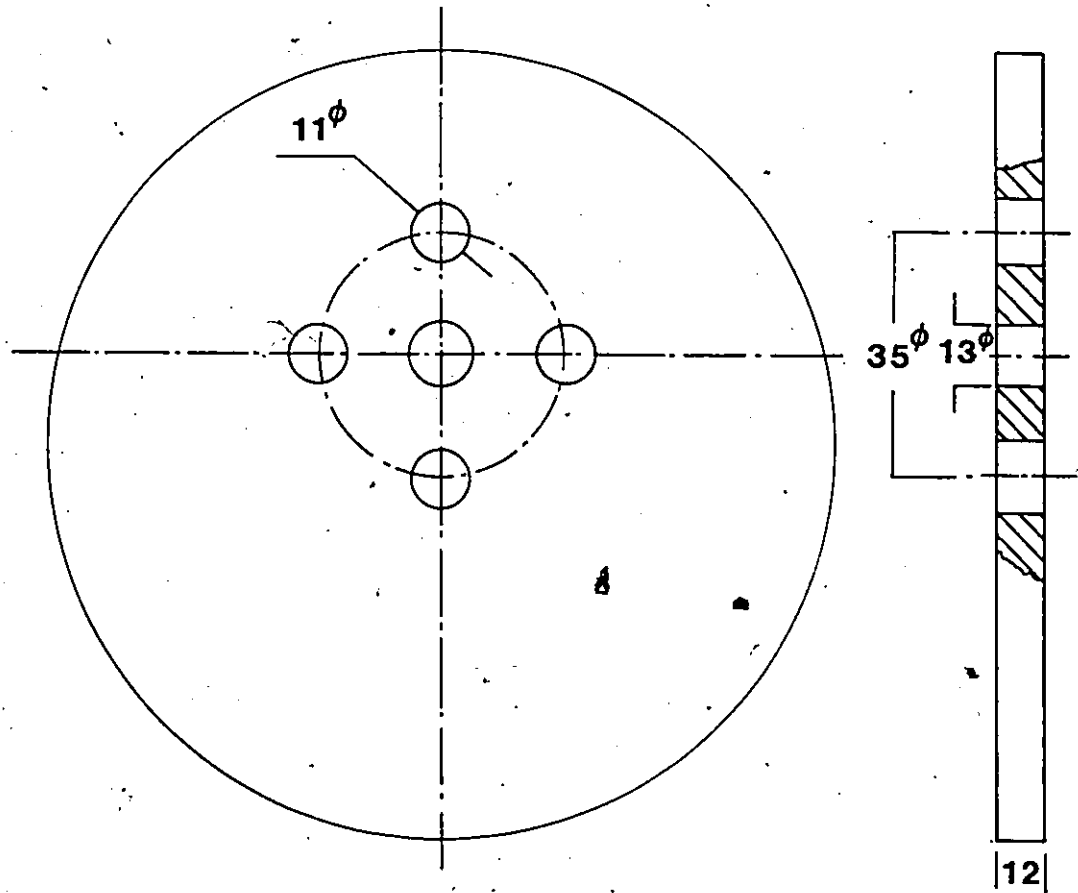
COUPLING



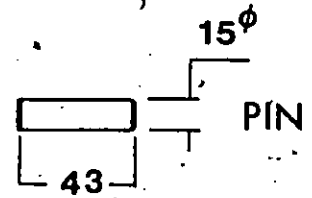
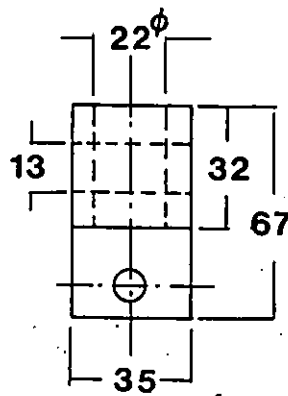
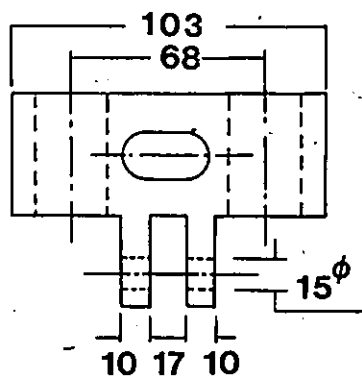
DRIVING SHAFT



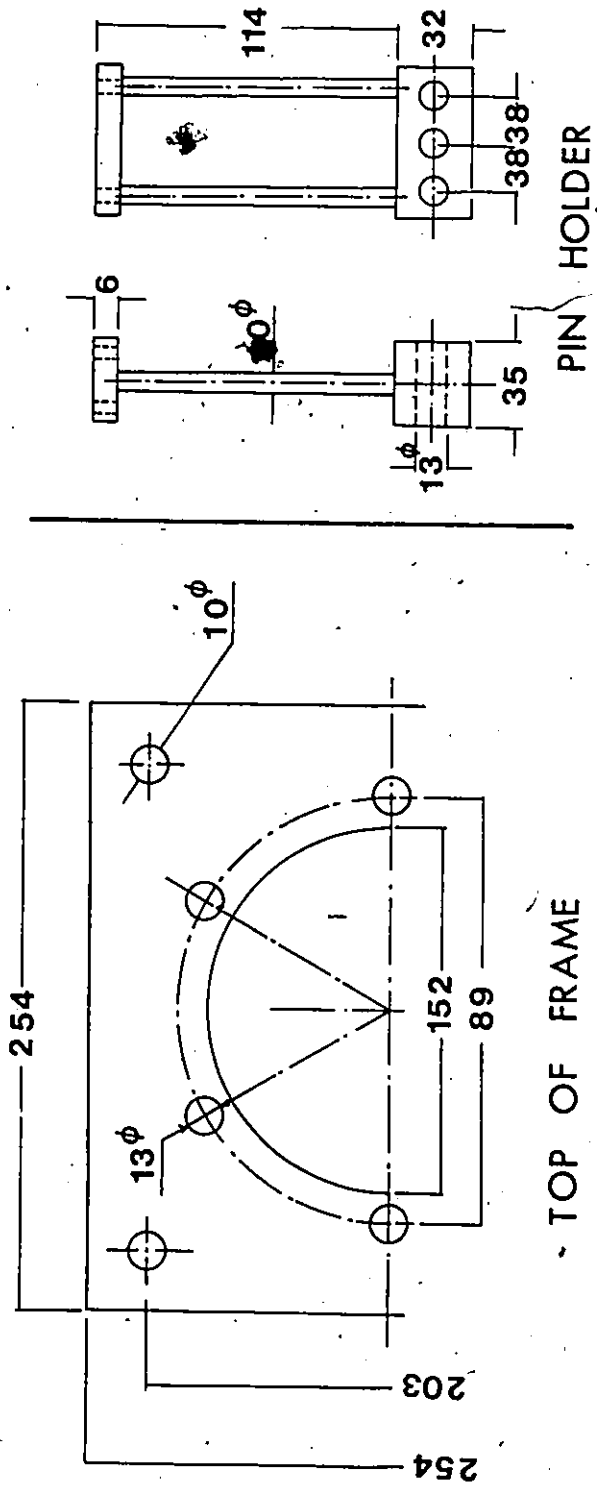
BEARING SLEEVE



CAM

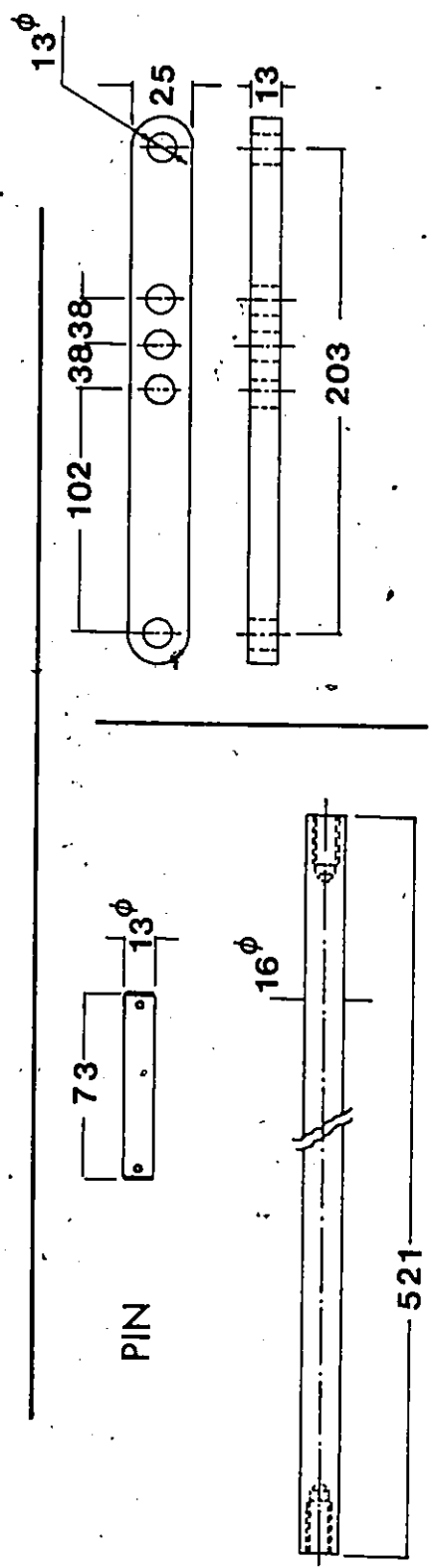


CAM FOLLOWER



TOP OF FRAME

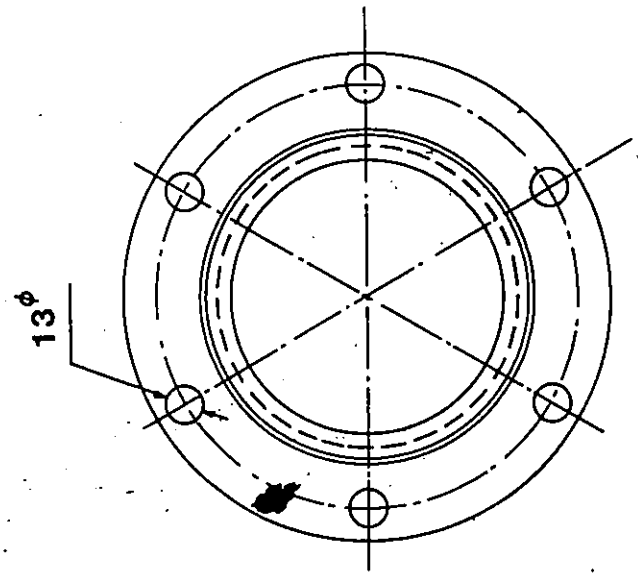
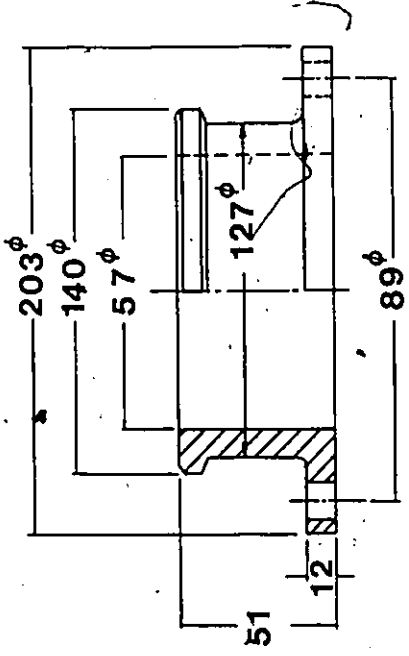
PIN HOLDER



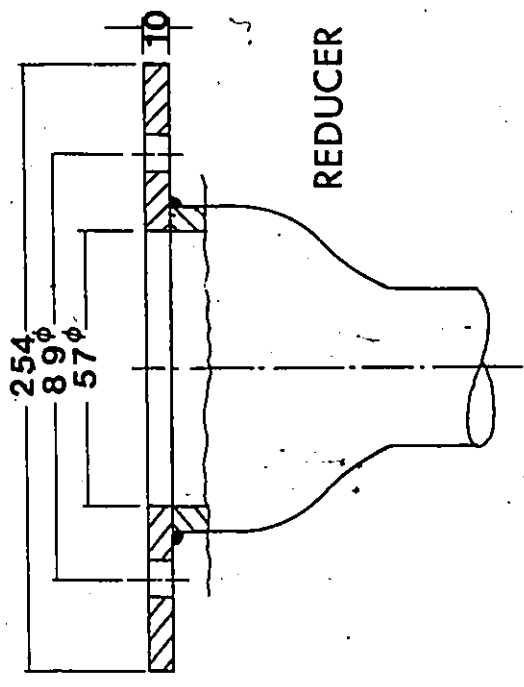
PIN

SUPPORTING ROD

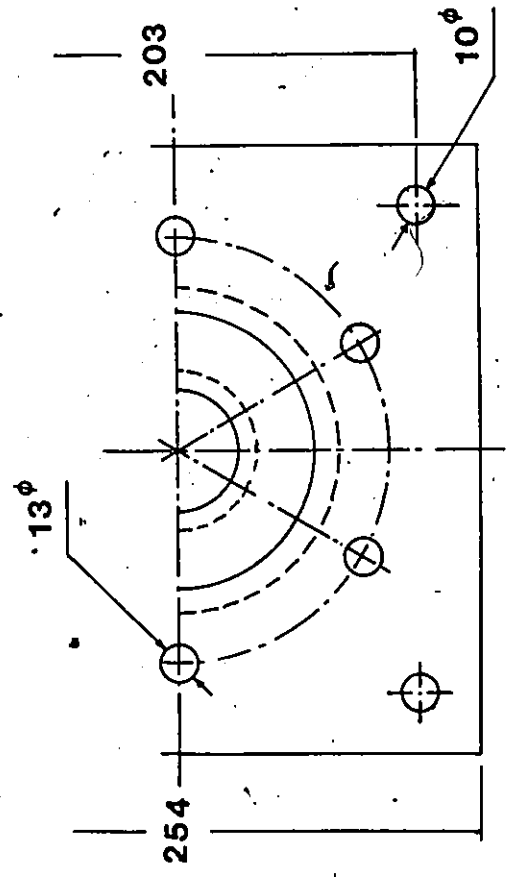
CONNECTING ROD



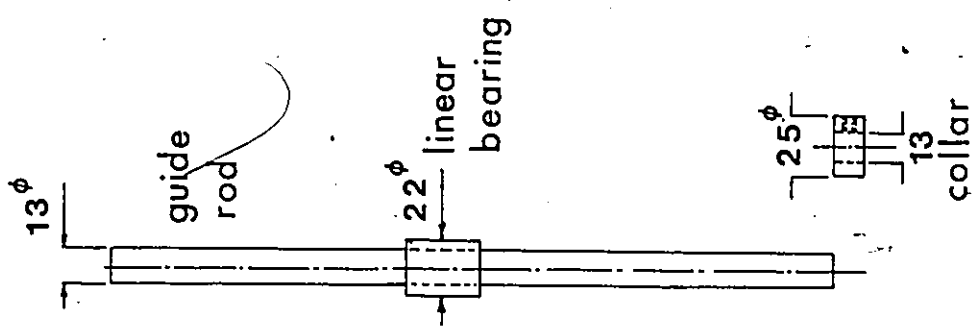
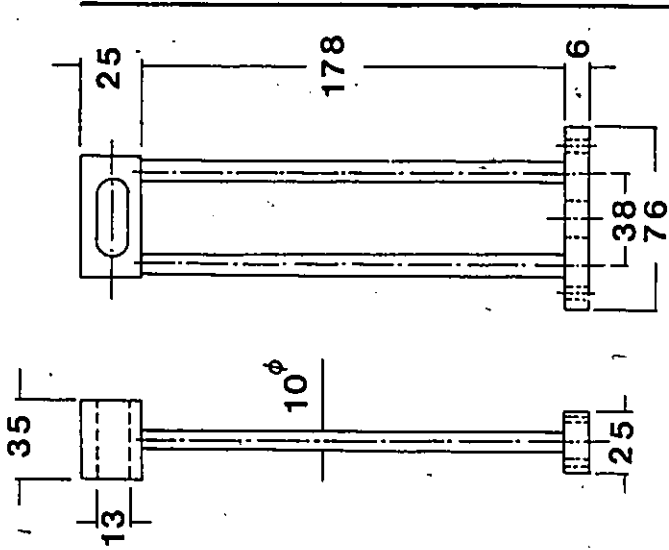
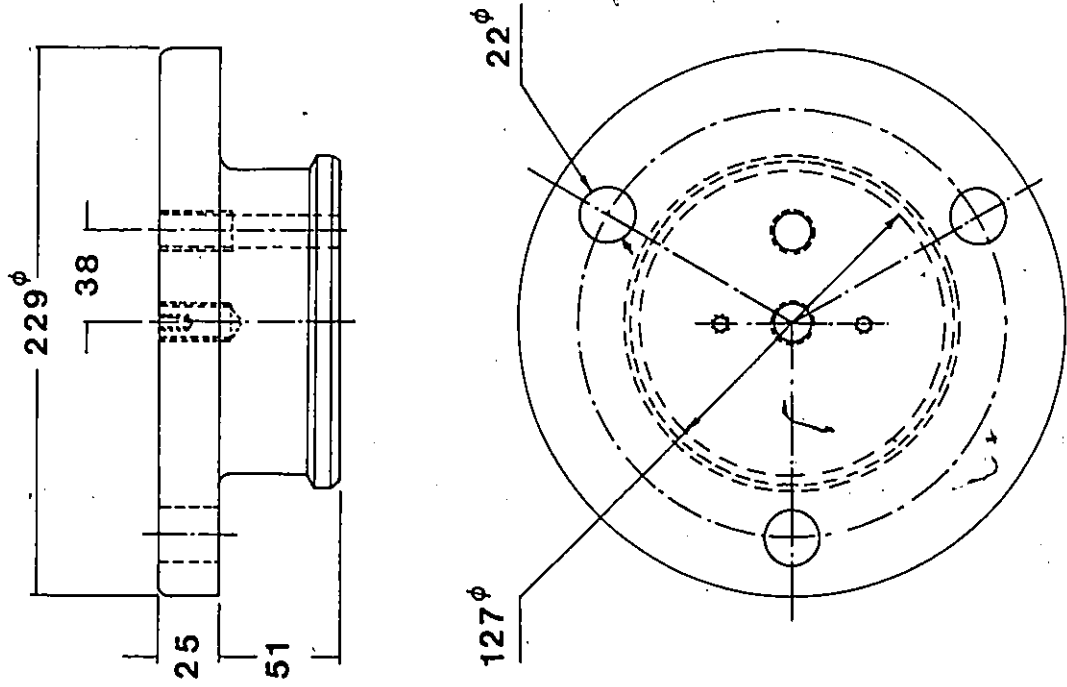
FLANGE



REDUCER



BOTTOM OF FRAME



PISTON

PISTON ARM

GUIDE SYSTEM

APPENDIX B
PULSATING FLOW DATA OF
BENTONITE CLAY-WATER SUSPENSION

Table (B1):

$\bar{C}_w = 2.97\%$,

Mean Temp. = 26°C

$V = 1.63 \text{ m/s}$,

$J_s = 7.695 \text{ Watt}$

λ (Hz)	J_p (Watt)	J_p/J_s	A (mm)	$n.A[D/d]^2 \Delta V$
.164	7.687	.999	34.6	.06835
.360	7.710	1.002		.15004
.446	7.757	1.008		.18589
.536	7.803	1.014		.22340
.686	8.041	1.045		.28592
.770	8.211	1.067		.32093
.831	8.311	1.080		.34635
.146	7.649	.994	52.1	.09163
.222	7.703	1.001		.13933
.352	7.849	1.020		.22091
.451	8.026	1.043		.28305
.554	8.326	1.082		.34769
.621	8.603	1.118		.38974
.152	7.787	1.012	76.2	.13952
.249	7.780	1.011		.22856
.323	8.295	1.078		.29648
.452	8.757	1.138		.41489
.576	9.442	1.227		.52045
.687	9.988	1.298		.63060

Table (B2):

 $C_w = 2.97\%$

Mean Temp. = 26°C

 $V = 2.18 \text{ m/s}$ $J_s = 16.321 \text{ Watt}$

λ (Hz)	J_p (Watt)	J_p/J_s	A (mm)	$\pi A[D/d]^2 \lambda V$
.152	16.174	.991	34.6	.04737
.465	16.452	1.008		.14491
.578	16.745	1.026		.18013
.742	17.153	1.051		.23123
.838	17.333	1.062		.26115
.934	17.790	1.090		.29107
1.054	18.247	1.118		.32847
.195	16.239	.995	52.1	.09151
.278	16.403	1.005		.13045
.412	16.664	1.021		.19333
.535	16.990	1.041		.25105
.673	17.676	1.083		.31581
.757	18.328	1.123		.35523
.175	16.452	1.008	76.2	.12011
.293	16.762	1.027		.20109
.387	16.860	1.033		.26561
.494	17.643	1.081		.33904
.606	18.785	1.151		.41591
.721	20.287	1.243		.49484

Table (B3):

 $C_w = 2.97\%$,

Mean Temp. = 26°C

 $V = 2.63 \text{ m/s}$, $J_s = 25.273 \text{ Watt}$

λ (Hz)	J_p (Watt)	J_p/J_s	A (mm)	$\pi \cdot A[D/d]^2 \text{ } \mu\text{V}$
.228	25.105	.993	34.6	.05890
.358	24.601	.973		.09248
.513	25.389	1.005		.13252
.654	25.870	1.024		.16894
.800	26.165	1.035		.20665
.952	26.518	1.049		.24592
1.116	27.214	1.077		.28828
.240	25.363	1.004	52.1	.09335
.343	25.260	.999		.13342
.501	25.707	1.017		.19487
.654	26.410	1.045		.25438
.810	27.435	1.086		.31506
.949	27.730	1.097		.36913
.211	24.830	.982	76.2	.12004
.343	25.060	.992		.19513
.462	25.506	1.009		.26283
.633	27.494	1.088		.36011
1.084	35.859	1.419		.61668

Table (B4):

 $C_w = 4.47\%$,

Mean Temp. = 27°C

 $V = 1.63 \text{ m/s}$, $J_s = 12.013 \text{ Watt}$

λ (Hz)	J_p (Watt)	J_p/J_s	A (mm)	$\pi A[D/d]^2 \mu V$
.065	12.043	1.002	34.6	.02709
.175	11.749	.978		.07294
.304	11.701	.974		.12670
.373	11.809	.983		.15546
.511	11.917	.992		.21298
.628	12.169	1.013		.26174
.737	12.373	1.030		.30718
.828	12.614	1.050		.34510
.064	11.863	.988	52.1	.04017
.163	11.773	.980		.10230
.272	11.919	.992		.17071
.378	12.313	1.025		.23723
.483	12.494	1.040		.30313
.601	12.788	1.065		.37719
.709	13.238	1.102		.44497
.215	11.953	.995	76.2	.19735
.326	12.469	1.038		.29924
.489	13.334	1.110		.44886
.599	13.995	1.165		.54982
.702	14.368	1.196		.64437

Table (B5):

 $C_w = 4.47\%$

Mean Temp. = 28°C

 $V = 2.18 \text{ m/s}$ $J_s = 19.156 \text{ Watt}$

λ (Hz)	J_p (Watt)	J_p/J_s	A (mm)	$\pi \cdot A [D/d]^2 \cdot V$
.230	18.773	.980	52.1	.10793
.370	18.888	.986		.17363
.494	19.213	1.003		.23181
.618	19.788	1.033		.29000
.790	20.612	1.076		.37071
.928	21.608	1.128		.43517
.111	12.022	.993	34.6	.03459
.248	18.830	.983		.07729
.498	19.012	.992		.15520
.809	19.539	1.020		.25211
.951	19.769	1.032		.29637
1.087	20.190	1.054		.33875
.131	18.792	.981	76.2	.08991
.241	18.964	.990		.16540
.356	19.577	1.022		.24433
.501	20.401	1.065		.34383
.624	21.301	1.112		.42827
.789	22.355	1.167		.54151
.867	22.796	1.190		.59504

Table (B6):

 $C_w = 4.47\%$,

Mean Temp. = 30°C

 $V = 2.63 \text{ m/s}$, $J_s = 26.275 \text{ Watt}$

λ (Hz)	J_p (Watt)	J_p/J_s	Λ (mm)	$\pi \cdot A[D/d]^2 \Delta V$
.271	26.314	1.001	52.1	.10541
.420	25.890	.985		.16337
.544	26.698	1.016		.21160
.709	27.587	1.050		.27578
.867	28.300	1.077		.33723
1.011	29.660	1.129		.39324
.249	26.349	1.003	76.2	.14165
.396	26.005	.990		.22528
.543	27.201	1.035		.30891
.691	28.322	1.078		.39310
.830	30.032	1.143		.47218
.985	33.130	1.261		.56036
.122	26.108	.994	34.6	.03151
.273	25.821	.983		.07052
.393	25.729	.979		.10152
.547	26.175	.996		.14130
.721	26.662	1.015		.18625
.892	27.005	1.028		.23042
1.035	27.684	1.054		.26736
1.182	29.455	1.121		.30533

Table (B7):

 $C_w = 7.63\%$,

Mean Temp. = 27°C

 $V = 1.63 \text{ m/s}$, $J_s \cong 12.226 \text{ Watt}$

λ (Hz)	J_p (Watt)	J_p/J_s	A (mm)	$\pi \cdot A [D/d]^2 \lambda/V$
.162	12.043	.985	34.6	.06752
.259	11.920	.975		.10795
.355	11.908	.974		.14796
.589	12.055	.986		.24549
.787	12.141	.993		.32801
.978	12.654	1.035		.40762
.142	12.006	.982	52.1	.08912
.258	11.896	.973		.16192
.366	11.884	.972		.22970
.499	12.202	.998		.31317
.581	12.385	1.013		.36463
.680	12.862	1.052		.42677
.767	13.326	1.090		.48137
.912	14.084	1.152		.57237
.173	11.810	.966	76.2	.15880
.248	11.835	.968		.22764
.361	12.348	1.010		.38136
.487	13.021	1.065		.44702
.578	13.546	1.108		.53055
.697	14.427	1.180		.63978

Table (B8):

 $C_w = 7.63\%$,

Mean Temp. = 29°C

 $V = 2.18 \text{ m/s}$, $J_s = 20.083 \text{ Watt}$

λ (Hz)	J_p (Watt)	J_p/J_s	A (mm)	$n.A[D/d]^2 \lambda/V$
.185	19.782	.985	34.6	.05765
.457	19.681	.980		.14242
.594	19.541	.973		.18511
.730	19.561	.974		.22750
.882	19.742	.983		.27486
1.203	21.027	1.047		.37490
.194	19.641	.978	52.1	.09104
.336	19.541	.973		.15767
.392	19.785	.985		.18395
.639	20.123	1.002		.29986
.719	20.585	1.025		.33740
.850	21.248	1.058		.39887
.991	22.152	1.103		.46503
.165	19.701	.981	76.2	.11324
.254	19.380	.965		.17433
.372	19.822	.987		.25531
.504	20.525	1.022		.34591
.593	21.328	1.062		.40699
.688	22.393	1.115		.47219
.775	23.598	1.175		.53190

Table (B9):

 $C_w = 7.63\%$,Mean Temp. = 32°C $V = 2.63 \text{ m/s}$, $J_s = 30.555 \text{ Watt}$

λ (Hz)	J_p (Watt)	J_p/J_s	A (mm)	$n.A[D/d]^2 \text{ } \mu\text{V}$
.238	30.068	.984	34.6	.06148
.379	29.690	.972		.09790
.535	30.520	.999		.13820
.687	30.891	1.011		.17746
.835	31.490	1.031		.21569
1.362	35.456	1.160		.35183
.228	30.103	.985	52.1	.08868
.381	29.819	.976		.14820
.520	30.750	1.006		.20226
.747	32.039	1.049		.29056
.835	33.029	1.081		.32479
.979	34.683	1.135		.38080
.232	30.633	1.003	76.2	.13198
.394	30.525	.999		.22414
.510	30.835	1.009		.29013
.654	31.887	1.044		.37205
.807	35.193	1.152		.45910
.925	34.587	1.132		.52622

Table (B10):

 $C_w = 11.2\%$,

Mean Temp. = 27°C

 $V = 1.63 \text{ m/s}$, $J_s = 12.426 \text{ Watt}$

λ (Hz)	J_p (Watt)	J_p/J_s	A (mm)	$\pi A [D/d]^2 \dot{N}/V$
.241	12.028	.968	34.6	.10045
.375	11.904	.958		.15630
.651	11.917	.959		.27133
.832	11.929	.960		.34677
.984	12.215	.983		.41012
1.144	12.339	.993		.47681
.240	11.867	.955	52.1	.15062
.408	11.830	.952		.25606
.547	11.842	.953		.34329
.687	12.240	.985		.43116
.832	12.699	1.022		.52216
.979	13.022	1.048		.61442
.240	11.904	.958	76.2	.22030
.398	11.966	.963		.36533
.545	12.252	.986		.50026
.721	12.525	1.008		.66181
.494	12.909	1.038		.45344
.649	13.408	1.079		.59572

Table (B11):

 $C_w = 11.2\%$,

Mean Temp. = 29°C

 $V = 2.18 \text{ m/s}$, $J_s = 21.196 \text{ Watt}$

λ (Hz)	J_p (Watt)	J_p/J_s	A (mm)	$\pi \cdot A [D/d]^2 \cdot \Delta V$
.235	20.666	.975	52.1	.11028
.405	20.285	.957		.19005
.675	20.581	.971		.31675
.876	21.111	.996		.41107
1.006	21.726	1.025		.47207
.225	20.814	.982	34.6	.07012
.376	20.497	.967		.11718
.532	20.391	.962		.16579
.705	20.285	.957		.21970
.856	20.327	.959		.26676
1.000	20.391	.962		.31164
.231	20.499	.967	76.2	.15854
.401	20.179	.952		.27522
.560	20.603	.972		.38434
.715	21.387	1.009		.49072
.761	21.874	1.032		.52229
.840	22.616	1.067		.57651

Table (B12):

 $C_w = 11.2\%$,Mean Temp. = 30°C $V = 2.63 \text{ m/s}$, $J_s = 33.730 \text{ Watt}$

λ (Hz)	J_p (Watt)	J_p/J_s	A (mm)	$\pi \cdot A [D/d]^2 \cdot \Delta V$
.255	32.145	.953	76.2	.14507
.388	32.617	.967		.22073
.542	32.752	.971		.30834
.709	33.561	.995		.40334
.826	33.865	1.004		.46990
.955	34.506	1.023		.54329
.253	32.549	.965	52.1	.09841
.399	32.381	.960		.15520
.544	32.111	.952		.21160
.700	32.448	.962		.27228
.870	32.718	.970		.33840
1.018	32.988	.978		.39597
1.135	33.764	1.001		.44148
.246	33.000	.978	34.6	.06355
.393	32.546	.965		.10152
.561	32.377	.960		.14491
.706	32.415	.961		.18237
.885	32.145	.953		.22861
1.041	33.123	.982		.26891
1.183	32.954	.977		.30559

APPENDIX C
PULSATING FLOW DATA OF
COAL-WATER SLURRY

Table (C1): $C_w = 5.342\%$,
 $V = 1.63 \text{ m/s}$,

Mean Temp. = 26°C
 $J_s = 7.882 \text{ Watt}$

λ (Hz)	J_p (Watt)	J_p/J_s	A (mm)
.243	7.890	1.001	34.6
.425	8.054	1.023	
.588	8.277	1.050	
.740	8.656	1.098	
.915	9.570	1.214	
1.160	10.149	1.288	
.270	7.933	1.006	52.1
.392	8.203	1.041	
.567	8.359	1.061	
.759	9.074	1.151	
.947	9.455	1.200	
1.149	10.774	1.367	
.283	8.008	1.016	76.2
.414	8.197	1.040	
.589	8.520	1.081	
.741	9.096	1.154	
.916	9.663	1.226	
1.162	10.676	1.366	

Table (C2): $C_w = 5.342\%$ Mean Temp. = 26°C $V = 2.18 \text{ m/s}$ $J_s = 16.347 \text{ Watt}$

λ (Hz)	J_p (Watt)	J_p/J_s	A (mm)
.242	16.462	1.007	34.6
.470	16.274	.996	
.597	16.877	1.032	
.831	17.205	1.052	
.971	18.429	1.127	
1.160	19.970	1.222	
.252	16.739	1.024	52.1
.407	16.374	1.002	
.563	17.089	1.045	
.722	17.761	1.086	
.888	18.774	1.148	
1.148	20.705	1.267	
.228	16.494	1.009	76.2
.415	16.837	1.030	
.576	17.279	1.057	
.718	18.421	1.109	
.918	19.379	1.185	
1.159	21.316	1.307	

Table (C3): $C_w = 5.342\%$,

Mean Temp. = 29°C

 $V = 2.63 \text{ m/s}$, $J_s = 25.880 \text{ Watt}$

λ (Hz)	J_p (Watt)	J_p/J_s	A (mm)
.229	25.905	1.001	34.6
.441	26.032	1.006	
.599	26.294	1.016	
.835	28.103	1.086	
.969	28.700	1.109	
1.159	31.288	1.209	
.321	26.087	1.008	52.1
.444	26.268	1.015	
.622	27.173	1.050	
.752	28.312	1.094	
.939	29.632	1.145	
1.143	31.444	1.215	
.189	25.957	1.003	76.2
.321	26.395	1.020	
.460	26.656	1.030	
.645	27.898	1.078	
.803	29.322	1.133	
1.118	32.220	1.245	

Table (C4): $C_w = 8.903\%$,

Mean Temp. = 28°C

 $V = 1.63 \text{ m/s}$, $J_s = 8.020 \text{ Watt}$

λ (Hz)	J_p (Watt)	J_p/J_s	A (mm)
.243	8.149	1.016	52.1
.420	8.027	1.001	
.564	8.351	1.041	
.707	8.605	1.073	
.882	9.266	1.155	
1.137	10.026	1.250	
.245	7.711	.961	34.6
.401	7.779	.970	
.557	8.059	1.005	
.758	8.532	1.064	
.939	8.894	1.109	
1.151	9.870	1.231	
.247	8.076	1.007	76.2
.405	8.196	1.022	
.544	8.353	1.042	
.716	8.758	1.092	
.895	9.343	1.165	
1.144	10.442	1.302	

Table (C5): $C_w = 8.903\%$

Mean Temp. = 30°C

 $V = 2.18 \text{ m/s}$ $J_s = 16.807 \text{ Watt}$

λ (Hz)	J_p (Watt)	J_p/J_s	A (mm)
.248	16.664	.991	52.1
.393	16.429	.978	
.549	16.925	1.007	
.707	18.132	1.079	
.861	18.845	1.120	
1.100	20.731	1.233	
.272	16.045	.955	34.6
.429	16.428	.977	
.573	16.839	1.002	
.737	17.275	1.028	
.915	18.161	1.081	
1.163	20.500	1.220	
.292	16.521	.983	76.2
.405	16.740	.996	
.533	17.227	1.025	
.716	18.252	1.086	
.879	19.530	1.162	
1.142	22.488	1.338	

Table (C6):

 $C_w = 8.903\%$,

Mean Temp. = 31°C

 $V = 2.63 \text{ m/s}$, $J_s = 26.783 \text{ Watt}$

λ (Hz)	J_p (Watt)	J_p/J_s	A (mm)
.201	26.193	.978	34.6
.295	26.247	.980	
.506	26.943	1.006	
.722	27.906	1.042	
.900	29.595	1.105	
1.132	31.148	1.163	
.189	26.729	.998	52.1
.429	27.077	1.011	
.561	27.968	1.044	
.708	28.497	1.064	
.907	30.233	1.129	
1.105	32.407	1.210	
.204	26.756	.999	76.2
.410	27.131	1.013	
.577	27.988	1.045	
.710	29.166	1.089	
.894	30.492	1.138	
1.123	33.132	1.237	

Table (C7): $C_w = 14.245\%$,

Mean Temp. = 27°C

 $V = 1.63 \text{ m/s}$, $J_s = 8.479 \text{ Watt}$

λ (Hz)	J_p (Watt)	J_p/J_s	Λ (mm)
.276	8.157	.962	34.6
.475	8.31	.980	
.623	8.428	.994	
.750	8.846	1.043	
.921	9.390	1.107	
1.161	10.200	1.203	
.318	8.259	.974	52.1
.457	8.484	1.001	
.597	8.722	1.029	
.762	9.064	1.069	
.913	9.715	1.146	
1.132	10.645	1.255	
1.159	11.192	1.320	76.2
.921	9.886	1.166	
.750	9.208	1.086	
.624	8.793	1.037	
.458	8.487	1.001	
.274	8.393	.990	

Table (C8): $C_w = 14.245\%$,

Mean Temp. = 27°C

 $V = 2.18 \text{ m/s}$, $J_s = 17.133 \text{ Watt}$

λ (Hz)	J_p (Watt)	J_p/J_s	A (mm)
.300	16.554	.966	34.6
.435	16.496	.963	
.594	16.913	.987	
.753	17.778	1.038	
.945	18.572	1.084	
1.174	21.072	1.230	
.273	16.850	.983	76.2
.460	17.190	1.003	
.619	17.768	1.037	
.760	18.920	1.104	
.925	20.686	1.207	
1.153	25.783	1.505	
.301	16.773	.979	52.1
.431	16.756	.978	
.576	17.476	1.020	
.780	18.195	1.062	
1.090	20.303	1.185	
1.171	21.930	1.280	

Table (C9): $C_w = 14.245\%$,Mean Temp. = 36°C $V = 2.63 \text{ m/s}$, $J_s = 26.863 \text{ Watt}$

λ (Hz)	J_p (Watt)	J_p/J_s	A (mm)
.196	26.165	.974	34.6
.295	25.923	.965	
.507	26.702	.994	
.694	27.320	1.017	
.914	29.281	1.090	
1.134	31.482	1.172	
.230	26.514	.987	52.1
.312	26.245	.977	
.508	27.239	1.014	
.708	28.394	1.057	
.921	30.087	1.120	
1.119	31.967	1.190	
.208	26.527	.987	76.2
.324	26.662	.993	
.418	27.103	1.009	
.684	28.260	1.052	
.879	30.033	1.118	
1.118	32.692	1.217	

Table (C10): $C_w = 19.587\%$,Mean Temp. = 26°C $V = 1.63 \text{ m/s}$, $J_s = 9.437 \text{ Watt}$

λ (Hz)	J_p (Watt)	J_p/J_s	A (mm)
.217	8.697	.922	52.1
.315	8.255	.875	
.489	8.618	.913	
.618	9.133	.968	
.799	10.004	1.060	
.988	11.819	1.252	
1.248	12.057	1.278	
.109	8.776	.930	34.6
.241	7.846	.831	
.465	7.898	.837	
.622	8.091	.857	
.772	8.799	.932	
.924	10.192	1.080	
1.140	11.536	1.222	
.119	9.003	.954	76.2
.284	8.819	.935	
.484	9.050	.959	
.619	9.625	1.020	
.813	10.466	1.109	
1.015	11.607	1.230	
1.152	12.504	1.325	

Table (C11): $C_w = 19.587\%$,Mean Temp. = 27°C $V = 2.18 \text{ m/s}$, $J_s = 18.278 \text{ Watt}$

λ (Hz)	J_p (Watt)	J_p/J_s	A (mm)
.172	17.366	.950	52.1
.283	17.320	.948	
.468	17.228	.943	
.601	18.644	1.020	
.814	20.128	1.101	
.993	22.341	1.222	
1.200	22.906	1.253	
.120	17.145	.938	34.6
.198	15.948	.873	
.294	15.531	.850	
.459	16.147	.883	
.597	16.703	.914	
.756	17.539	.960	
.946	18.883	1.033	
1.155	21.785	1.192	
.139	17.913	.980	76.2
.288	17.821	.975	
.460	18.350	1.004	
.616	18.735	1.025	
.809	20.250	1.108	
1.075	22.208	1.215	
1.176	23.150	1.267	

Table (C12): $C_w = 19.587\%$,

Mean Temp. = 35°C

 $V = 2.63 \text{ m/s}$, $J_s = 27.716 \text{ Watt}$

λ (Hz)	J_p (Watt)	J_p/J_s	A (mm)
.195	23.919	.863	34.6
.358	23.143	.835	
.498	23.392	.844	
.627	24.488	.884	
.777	25.388	.916	
.991	27.523	.993	
1.174	30.403	1.097	
.210	26.358	.951	52.1
.323	26.012	.939	
.429	25.914	.935	
.588	26.275	.948	
.778	27.661	.998	
.984	29.407	1.061	
1.169	30.627	1.105	
.212	26.746	.965	76.2
.361	27.079	.977	
.488	27.218	.982	
.689	28.268	1.020	
.962	29.768	1.074	
1.173	30.959	1.117	

Table (C13): $C_w = 24.93\%$,Mean Temp. = 36°C $V = 1.63 \text{ m/s}$, $J_s = 9.536 \text{ Watt}$

λ (Hz)	J_p (Watt)	J_p/J_s	A' (mm)
.171	9.074	.952	34.6
.296	8.439	.885	
.421	8.411	.882	
.600	8.916	.935	
.757	9.479	.994	
.946	10.413	1.092	
1.126	11.767	1.234	
.161	9.135	.958	52.1
.361	8.907	.934	
.580	9.155	.960	
.826	10.232	1.073	
.989	11.043	1.158	
1.171	12.443	1.305	
.189	9.240	.969	76.2
.330	9.212	.966	
.609	9.703	1.018	
.791	10.251	1.075	
1.009	11.510	1.207	
1.141	12.092	1.268	

Table (C14): $C_w = 24.93\%$,

Mean Temp. = 39°C

 $V = 2.18 \text{ m/s}$, $J_s = 18.253 \text{ Watt}$

λ (Hz)	J_p (Watt)	J_p/J_s	A (mm)
.139	17.249	.945	34.6
.293	16.956	.929	
.426	16.511	.905	
.602	16.610	.910	
.732	18.019	.987	
.923	20.164	1.105	
1.149	22.322	1.223	
.171	17.556	.962	52.1
.320	16.923	.927	
.470	17.301	.948	
.615	18.605	1.019	
.768	20.865	1.143	
.977	23.380	1.281	
.269	17.887	.980	76.2
.456	18.454	1.011	
.623	19.093	1.046	
.770	20.361	1.115	
.956	22.013	1.206	
1.144	23.912	1.310	

Table (C15): $C_w = 24.93\%$,

Mean Temp. = 34°C

 $V = 2.63 \text{ m/s}$, $J_s = 27.809 \text{ Watt}$

λ (Hz)	J_p (Watt)	J_p/J_s	A (mm)
.182	26.891	.967	34.6
.332	25.223	.097	
.418	25.348	.912	
.590	25.751	.926	
.759	26.808	.964	
.954	28.880	1.039	
1.148	31.049	1.117	
.207	26.307	.946	52.1
.346	25.862	.930	
.441	26.057	.937	
.611	26.696	.960	
.814	28.504	1.025	
.974	30.062	1.081	
1.119	31.341	1.127	
.208	26.822	.965	76.2
.340	26.808	.964	
.618	27.642	.994	
.805	29.380	1.056	
.976	30.896	1.111	
1.122	31.980	1.150	

Table (C16): $C_w = 30.271\%$,Mean Temp. = 31°C $V = 1.63 \text{ m/s}$, $J_s = 9.655 \text{ Watt}$

λ (Hz)	J_p (Watt)	J_p/J_s	A (mm)
.160	9.143	.947	34.6
.389	8.841	.916	
.494	8.921	.924	
.664	9.389	.972	
.863	10.225	1.059	
1.091	11.875	1.230	
.197	9.134	.946	52.1
.410	9.056	.938	
.624	9.380	.972	
.829	10.476	1.085	
.970	11.243	1.164	
1.116	12.638	1.309	
.189	9.510	.985	76.2
.350	9.365	.970	
.628	9.911	1.027	
.863	11.060	1.146	
1.080	12.243	1.268	
1.154	12.716	1.317	

Table (C17): $C_w = 30.271\%$,

Mean Temp. = 32°C

 $V = 2.18 \text{ m/s}$, $J_s = 19.061 \text{ Watt}$

λ (Hz)	J_p (Watt)	J_p/J_s	A (mm)
.191	17.973	.943	52.1
.329	17.910	.940	
.528	18.508	.971	
.633	19.298	1.012	
.777	20.534	1.077	
.977	22.906	1.202	
1.206	23.355	1.225	
.180	18.543	.973	34.6
.335	18.089	.949	
.479	18.140	.952	
.644	18.147	.952	
.801	19.369	1.016	
.98	20.917	1.097	
1.221	23.466	1.231	
.190	18.708	.981	76.2
.322	18.604	.976	
.518	19.042	.999	
.634	19.652	1.031	
.805	20.624	1.082	
.957	21.882	1.148	
1.090	22.969	1.205	

Table (C18): $C_w = 30.271\%$,Mean Temp. = 32°C $V = 2.634 \text{ m/s}$, $J_s = 29.452 \text{ Watt}$

λ (Hz)	J_p (Watt)	J_p/J_s	A (mm)
.266	28.568	.970	76.2
.364	28.684	.974	
.534	29.010	.985	
.727	29.732	1.010	
.896	31.131	1.057	
1.119	33.281	1.130	
.174	27.978	.950	52.1
.354	27.743	.942	
.512	27.744	.942	
.726	28.775	.977	
.868	29.717	1.009	
1.089	32.221	1.094	
.181	28.362	.963	34.6
.338	27.744	.942	
.476	27.449	.932	
.683	27.891	.947	
.821	28.421	.965	
1.070	31.072	1.055	

Table (C19): $C_w = 37.5\%$,

Mean Temp. = 37°C

 $V = 1.63 \text{ m/s}$, $J_s = 9.712 \text{ Watt}$

λ (Hz)	J_p (Watt)	J_p/J_s	A (mm)
.179	9.576	.986	76.2
.343	9.634	.992	
.587	10.146	1.045	
.790	10.945	1.127	
.959	11.722	1.207	
1.111	12.421	1.279	
.129	9.255	.953	52.1
.270	9.114	.938	
.411	9.246	.952	
.626	9.809	1.010	
.794	10.489	1.080	
.954	11.508	1.185	
1.109	12.567	1.294	
.175	9.338	.961	34.6
.389	9.178	.945	
.560	9.498	.978	
.761	10.124	1.042	
.924	11.072	1.140	
1.130	12.479	1.285	

Table (C20): $C_w = 37.5\%$,
 $V = 2.18 \text{ m/s}$,

Mean Temp. = 36°C

$J_s = 19.361 \text{ Watt}$

λ (Hz)	J_p (Watt)	J_p/J_s	A (mm)
.187	19.461	1.005	34.6
.322	19.488	1.007	
.468	19.552	1.010	
.616	19.773	1.021	
.757	20.110	1.039	
.948	20.337	1.050	
1.180	21.484	1.110	
.258	18.598	.961	52.1
.393	18.588	.960	
.486	19.013	.982	
.630	19.461	1.005	
.818	20.568	1.062	
1.016	21.943	1.133	
.187	19.187	.991	76.2
.331	19.342	.999	
.489	19.826	1.024	
.685	20.494	1.059	
.867	21.684	1.120	
1.111	22.972	1.187	

Table (C21): $C_w = 37.5\%$,

Mean Temp. = 40°C

 $V = 2.63 \text{ m/s}$, $J_s = 29.903 \text{ Watt}$

λ (Hz)	J_p (Watt)	J_p/J_s	A (mm)
.171	30.052	1.005	34.6
.291	30.023	1.004	
.445	29.906	1.000	
.609	30.205	1.010	
.793	30.651	1.025	
.964	30.950	1.035	
1.175	33.043	1.105	
.189	29.155	.975	52.1
.334	29.006	.970	
.491	29.245	.978	
.659	30.053	1.005	
.861	31.189	1.043	
1.090	33.013	1.104	
.182	29.514	.987	76.2
.301	29.694	.993	
.466	30.262	1.012	
.659	30.740	1.028	
.841	32.325	1.081	
1.092	33.402	1.117	

Table (C22): $C_w = 44.64\%$,

Mean Temp. = 38°C

 $V = 1.63 \text{ m/s}$, $J_s = 9.766 \text{ Watt}$

λ (Hz)	J_p (Watt)	J_p/J_s	Λ (mm)
.189	9.571	.980	34.6
.322	9.522	.975	
.514	9.756	.999	
.761	10.303	1.055	
.965	11.084	1.135	
1.150	11.622	1.190	
.208	9.434	.966	52.1
.346	9.453	.968	
.597	9.922	1.016	
.769	10.567	1.082	
.946	11.329	1.160	
1.140	12.530	1.283	
.139	9.742	.998	76.2
.244	9.844	1.008	
.340	9.922	1.016	
.571	10.396	1.065	
.731	10.948	1.121	
.924	11.700	1.198	
1.141	12.452	1.275	

Table (C23): $C_w = 44.64\%$,

Mean Temp. = 40°C

 $V = 2.18 \text{ m/s}$, $J_s = 19.367 \text{ Watt}$

λ (Hz)	J_p (Watt)	J_p/J_s	A (mm)
.189	19.310	.997	52.1
.266	18.963	.979	
3.59	18.884	.975	
.495	18.997	.981	
.645	20.128	1.039	
.805	21.374	1.104	
1.014	23.101	1.193	
1.233	24.864	1.284	
.163	19.478	1.006	34.6
.239	19.253	.994	
.349	19.421	1.003	
.669	19.481	1.006	
.842	20.050	1.035	
1.052	21.000	1.084	
1.169	22.175	1.145	
.144	19.409	1.002	
.205	19.378	1.001	
.319	19.406	1.002	76.2
.506	20.045	1.035	
.630	20.626	1.065	
.792	21.943	1.133	
1.089	23.918	1.235	

Table (C24): $C_w = 53.7\%$,Mean Temp. = 41°C $V = 1.63 \text{ m/s}$, $J_s = 10.005 \text{ Watt}$

λ (Hz)	J_p (Watt)	J_p/J_s	A (mm)
.200	9.855	.985	34.6
.349	9.945	.994	
.536	10.185	1.018	
.694	10.625	1.062	
.831	11.046	1.104	
1.078	11.626	1.162	
.199	10.080	1.007	52.1
.368	10.009	1.000	
.528	10.275	1.027	
.673	10.655	1.065	
.866	11.206	1.120	
1.074	12.026	1.202	
.223	.998	.999	76.2
.352	10.205	1.020	
.516	10.455	1.045	
.680	10.855	1.085	
.829	11.416	1.141	
1.085	12.276	1.227	

Table (C25): $C_w = 53.7\%$,

Mean Temp. = 43°C

$V = 2.18 \text{ m/s}$,

$J_s = 20.237 \text{ Watt}$

λ (Hz)	J_p (Watt)	J_p/J_s	A (mm)
.262	20.326	1.004	34.6
.352	20.204	.998	
.519	20.317	1.004	
.658	20.157	.996	
.855	20.845	1.030	
1.047	22.362	1.105	
1.266	23.824	1.177	
.259	20.158	.996	52.1
.339	20.117	.994	
.523	20.831	1.029	
.658	21.155	1.045	
.834	22.475	1.111	
1.029	23.188	1.146	
1.269	23.966	1.184	
.275	20.253	1.001	76.2
.349	20.318	1.004	
.511	20.763	1.026	
.655	21.330	1.054	
.829	22.362	1.105	
1.024	23.536	1.163	


```

VN=((1+3*EN)/(4*EN)**EN
A=DELT/(FREQ*VN)
C=2*PL*VN
*****
*
* CALL SUBROUTINE START1 TO CALCULATE THE VELOCITY PROFILE *
* AND TO INITIATE THE FINITE DIFFERENCE SOLUTION FOR START *
* UP FLOW. OR, CALL SUBROUTINE PULSG1 TO CALCULATE THE *
* VELOCITY PROFILE AND TO INITIATE THE FINITE DIFFERENCE *
* SOLUTION FOR PULSATING FLOW. *
*****
IF(NCONT.EQ.0)CALL START1(RN,PL,EN,F,NR,IR,DELR,U0,UF)
IF(NCONT.EQ.1)CALL PULSG1(RN,PL,EN,F,NR,IR,DELR,AMP,FREQ,U0,UF)
DO 200 I=1,NR
200 V(I,I)=UF(I)
L=1
J=0
MC=0
IQ=0
SUMQ2=0.0
SUMQ4=0.0
SUMP2=0.0
SUMP4=0.0
NFACIR=0
300 J=J+1
MC=MC+1
T=J*DELT
IF(T.GT.TMAX)GO TO 900
IF(NCONT.EQ.0)B=0.3*F*RN*VN
IF(NCONT.EQ.1)B=0.3*F*RN*VN*(1+AMP*SIN(2*PI*T))
*****
*
* CALL START2 TO CALCULATE THE INSTANTANEOUS VELOCITIES *
* AT NODAL POINTS FOR START-UP FLOW. OR, CALL PULSG2 TO *
* CALCULATE THE INSTANTANEOUS VELOCITIES AT NODAL POINTS *
* FOR PULSATING FLOW. *
*****
IF(NCONT.EQ.0)CALL START2(A,B,C,EN,NR,DELR,U0,U)
IF(NCONT.EQ.1)CALL PULSG2(A,B,C,EN,NR,DELR,U0,U)
DO 400 I=1,NR
400 UO(I)=U(I)
IF(NCONT.EQ.0)GO TO 500
*****
*
* CALL AINTGR TO CALCULATE THE INSTANTANEOUS FLOWRATE USING *
* NUMERICAL INTEGRATION. *
*****
CALL AINTGR(U,NR,DELR,Q)

```

000119
000120
000121
000122
000123
000124
000125
000126
000127
000128
000129
000130
000131
000132
000133
000134
000135
000136
000137
000138
000139
000140
000141
000142
000143
000144
000145
000146
000147
000148
000149
000150
000151
000152
000153
000154
000155
000156
000157
000158
000159
000160
000161
000162
000163
000164
000165
000166
000167
000168
000169
000170
000171
000172
000173
000174
000175


```

C
C
SUBROUTINE START1(RN,PL,EN,F,NR,IR,DELR,U,UF)
=====
DIMENSION U(21),RR(11),UF(21)
WRITE(6,1)RN,PL,EN
1 FORMAT(//,40X,"*****SOLUTION FOR START-UP FLOW*****",
+//,10X,"RN=",F8.1,/,10X,"PL=",F8.1,/,10X,"N=",F4.2)
RATIO=3*PL/(F*RN)
DO 200 I=1,NR
R=1.-(I-1)*DELR
IF(R.LT.RATIO)R=RATIO
200 UF(I)=(1+3*EN)*(F*RN/64)**(1/EN)*((1-RATIO)**(1+1/EN)-(R-RATIO)
+**(1+1/EN))/(1+EN)
DO 300 I=1,NR,IR
300 RR(I)=1.-(I-1)*DELR
WRITE(6,2)(RR(I),I=1,NR,IR)
2 FORMAT(////,10X,"VELOCITY PROFILE OF FULLY DEVELOPED FLOW",//,
+13X,11(5X,"R=",F3.1),//)
WRITE(6,3)(UF(I),I=1,NR,IR)
3 FORMAT(17X,11(F8.4,2X))
DO 400 I=1,NR
400 U(I)=0.0
T=0.0
WRITE(6,4)T,(U(I),I=1,NR,IR)
4 FORMAT(////,10X,"NUMERICAL SOLUTION OF THE PROBLEM STARTING ",
+"AT TIME ZERO",//,3X,"T=",F7.5,5X,11(F8.4,2X))
RETURN
END
000224
000225
000226
000227
000228
000229
000230
000231
000232
000233
000234
000235
000236
000237
000238
000239
000240
000241
000242
000243
000244
000245
000246
000247
000248
000249
000250
000251

```

```

SUBROUTINE PULSG1(RN, PL, EN, F, NR, IR, DELR, AMP, FREQ, U, UF)
=====
C
C
DIMENSION U(21), RR(11), UF(21)
WRITE(6, 1) RN, PL, EN, AMP, FREQ
1 FORMAT(//, 40X, "*****SOLUTION FOR PULSING FLOW*****", //,
+10X, "RN=", F8.1, /, 10X, "PL=", F8.1, /, 10X, "N=", F4.2, /, 10X, "AMP.=",
+F5.2, /, 10X, "FREQUENCY=", F3.2)
RATIO=0*PL/(F*RN)
DO 200 I=1, NR
R=1.-(I-1)*DELR
IF(R.LT.RATIO) R=RATIO
UF(I)=(1+3*EN)*(F*RN/64)**(1/EN)**((1-RATIO)**(1+1/EN)-(R-RATIO)**
+(1+1/EN))/(1+EN)
200 U(I)=0.0
DO 300 I=1, NR, IR
300 RR(I)=1.-(I-1)*DELR
WRITE(6, 2) (RR(I), I=1, NR, IR)
2 FORMAT(////, 10X, "VELOCITY PROFILE OF PULSING FLOW AT TIME ZERO",
+//, 13X, 11(5X, "R=", F3.1), //)
T=0.0
WRITE(6, 3) T, (U(I), I=1, NR, IR)
3 FORMAT(3X, "T=", F7.3, 5X, 11(F8.4, 2X))
RETURN
END
000252
000253
000254
000255
000256
000257
000258
000259
000260
000261
000262
000263
000264
000265
000266
000267
000268
000269
000270
000271
000272
000273
000274
000275
000276

```

C C	<pre> SUBROUTINE START2(A,B,C,EN,NR,DELR,U0,U) ===== DIMENSION U0(21),U(21) U(1)=0.0 D=(U0(1)-U0(2))/DELR IF(C.EQ.0.0)RATIO=0.0 IF(C.NE.0.0.AND.D.EQ.0.0)RATIO=1.0 IF(C*D.NE.0.0)RATIO=C/(C-4**(2-EN)*D*(ABS(D))**(EN-1)) DO 300 I=2,NR R=1.-(I-1)*DELR IF(R.GT.RATIO)GO TO 200 IF(RATIO.NE.0.0)GO TO 100 D=(U0(I-1)-U0(I))/DELR E=2*D/DELR IF(D.EQ.0.0)U(I)=U0(I)+A*B IF(D.EQ.0.0)GO TO 300 U(I)=U0(I)+A*(B+4**(2-EN)*E*((ABS(D))**(EN-1))*(1+(EN-1)* +(D/ABS(D))*(ABS(E)/E))*2.) GO TO 300 100 U(I)=U0(I)+A*(B-2*C/RATIO) GO TO 300 200 D=(U0(I-1)-U0(I+1))/(DELR*2.) E=(U0(I-1)+U0(I+1)-2.*U0(I))/DELR**2) IF(C.EQ.0.0)H=C/R IF(C.NE.0.0)H=C/RATIO IF(D.EQ.0.0.AND.RATIO.EQ.0.0)U(I)=U0(I)+A*B IF(D.EQ.0.0.AND.RATIO.NE.0.0)U(I)=U0(I)+A*(B-H) IF(D.NE.0.0.AND.E.EQ.0.0)U(I)=U0(I)+A*(B-H+(4.**((2.-EN)* +D*((ABS(D))**(EN-1))/R)) IF(D.NE.0.0.AND.E.NE.0.0)U(I)=U0(I)+A*(B-H+ +(4.**((2.-EN)*E*((ABS(D))**(EN-1))*(1+(EN-1)*(D/ABS(D)) +(ABS(E)/E)))+(4.**((2.-EN)*D*((ABS(D))**(EN-1))/R)) 300 CONTINUE RETURN END </pre>	<pre> 000277 000278 000279 000280 000281 000282 000283 000284 000285 000286 000287 000288 000289 000290 000291 000292 000293 000294 000295 000296 000297 000298 000299 000300 000301 000302 000303 000304 000305 000306 000307 000308 000309 000310 000311 000312 </pre>
--------	--	--

SUBROUTINE PULSG2(A,B,C)EN,NR,DELR,UO,U)

=====

DIMENSION UO(21),U(21)

DW=(UO(1)-UO(2))/DELR

IF(C.EQ.0.0)RATIO=0.0

IF(DW.GE.0.0.AND.C.NE.0.0)RATIO=.95

IF(DW.LT.0.0)RATIO=C/(C+4.**((2.-EN)*(-DW)*(ABS(DW))**(EN-1.)))

U(1)=0.0

DO 300 I=2,NR

R=1.-(I-1)*DELR

IF(R.GT.RATIO)GO TO 200

IF(RATIO.NE.0.0)GO TO 100

D=(UO(I-1)-UO(I))/DELR

E=2*D/DELR

IF(D.EQ.0.0)U(I)=UO(I)+A*B

IF(D.EQ.0.0)GO TO 300

U(I)=UO(I)+A*(B+4.**((2.-EN)*E*(ABS(D))**(EN-1.))*(1+(EN-1)*

+D*ABS(D))*(ABS(E)/E))*2.)

GO TO 300

100 IF(RATIO-R.LT.DELR)GO TO 150

U(I)=U(I-1)

GO TO 300

150 D=(UO(I-1)-UO(I))/DELR

E=(UO(I-1)+UO(I+1)-2.*UO(I))/(DELR**2)

IF(D.EQ.0.0)U(I)=UO(I)+A*(B-2*C/RATIO)

IF(D.NE.0.0)U(I)=UO(I)+A*(B-C/RATIO+(4.**((2.-EN)*E*(ABS(D))**

+(EN-1.))*(1+(EN-1.)*(D/ABS(D))*(ABS(E)/E)))+(4.**((2.-EN)*

+D*(ABS(D)**(EN-1.))/RATIO))

GO TO 300

200 D=(UO(I-1)-UO(I+1))/(2.*DELR)

E=(UO(I-1)+UO(I+1)-2.*UO(I))/(DELR**2)

IF(C.EQ.0.0)H=C/R

IF(C.NE.0.0)H=C/R

IF(D.EQ.0.0.AND.RATIO.EQ.0.0)U(I)=UO(I)+A*B

IF(D.EQ.0.0.AND.RATIO.NE.0.0)U(I)=UO(I)+A*(B-C/RATIO)

IF(D.NE.0.0.AND.E.EQ.0.0)U(I)=UO(I)+A*(B-H+(4.**((2.-EN)*D*((ABS(D)

))*((EN-1)/R))

IF(D.NE.0.0.AND.E.NE.0.0)U(I)=UO(I)+A*(B-H+(4.**((2.-EN)

)*E*((ABS(D))**(EN-1))*(1+(EN-1)*(D/ABS(D))*(ABS(E)/E)))+

+(4.**((2.-EN)*D*((ABS(D))**(EN-1)/R))

300 CONTINUE

RETURN

END

000313

000314

000315

000316

000317

000318

000319

000320

000321

000322

000323

000324

000325

000326

000327

000328

000329

000330

000331

000332

000333

000334

000335

000336

000337

000338

000339

000340

000341

000342

000343

000344

000345

000346

000347

000348

000349

000350

000351

000352

000353

000354

000355

000356

	SUBROUTINE NEWTON (RN,PL,EN,F)	
	=====	
C	IF (PL.NE.0.0) GO TO 5	000357
C	F=64/RN	000358
	GO TO 20	000359
5	CONTINUE	000360
	A1=1+EN	000361
	A2=1+2*EN	000362
	A3=1+3*EN	000363
	C1=2*EN*EN/(A1*A2)	000364
	C2=2*EN/A2	000365
	C3=(4*EN/A3)**EN	000366
	PLRN=RN*PL*8	000367
	FRN2=PLRN	000368
100	CONTINUE	000369
	FRN2=FRN2*1.01	000370
	S=PLRN/FRN2	000371
	B1=(C1*S*S+C2*S+1)**EN	000372
	B2=(1-S)**(EN+1)	000373
	RNP=FRN2*B1*B2/64	000374
	ERROR=ABS(RNP-RN)/RN	000375
	IF (ERROR.GT.0.02) GO TO 100	000376
	F=FRN2/RNP**2	000377
20	RETURN	000378
	END	000379
		000380
		000381
		000382

```
C
C
SUBROUTINE AINTGR(U, NR, D, Q)
=====
DIMENSION U(21), R(21)
NNR=NR-1
DO 100 I=1, NR
100 R(I)=1.0-(I-1)*D
SUM1=0.0
SUM2=0.0
DO 200 I=2, NNR, 2
SUM1=SUM1+U(I)*R(I)
SUM2=SUM2+U(I+1)*R(I+1)
200 CONTINUE
Q=2*D*(SUM1*4.+SUM2*2.)/3.0
RETURN
END
```

```
000383
000384
000385
000386
000387
000388
000389
000390
000391
000392
000393
000394
000395
000396
000397
000398
```

```

C      SUBROUTINE GRAPHS(XMIN, XMAX, YMIN, YMAX, XFRAM, YFRAM, XU, YU, NM, NC,
C      =====
C      +NX, NY, IXX, NHX, HY, NHY, HP1, NHP1, HP2, NHP2, HP3, NHP3, WX, WY)
C      =====
C
C      DIMENSION X(1), Y(1), XTM(2), YTM(2), HX(1), HY(1), XU(NC, 1), YU(NC, 1),
C      +NM(1), WX(1), WY(1)
C      DIMENSION HP1(1), HP2(1), HP3(1)
C
C      *****
C      * SET UP THE PLOTTING AREA FOR ALL THE DATA POINTS *
C      *****
C
C      NP=NC
C      XTM(1)=XMIN
C      XTM(2)=XMAX
C      YTM(1)=YMIN
C      YTM(2)=YMAX
C      DATA XH, YH, XL, YL/2.,4.,9.,8./
C
C      *****
C      * POSITION THE GRAPH IN THE SPECIFIED AREA *
C      *****
C
C      XL=XFRAM+XM
C      YL=YFRAM+YM
C      XX=(XL-FLOAT(NHX))*1
C      ZZ=(YL-FLOAT(NHY))*1
C      CALL PLOT(0.03, 0.03, -3)
C
C      *****
C      * LABEL THE Y-AXIS *
C      *****
C
C      CALL LETTER(NHY, .1, 90., .8, ZZ, HY)
C
C      *****
C      * COMPUTE THE SCALING FACTOR FOR ALL THE DATA POINTS *
C      *****
C
C      CALL FACTOR(2, XTM, YTM, XL, YL, XM, YD)
C
C      *****
C      * PLOT THE BOUNDARY OF THE FRAME *
C      *****
C
C      CALL PLOT(XH, YH, 3)
C      CALL PLOT(XL, YH, 2)
C      CALL PLOT(XL, YL, 1)
C      CALL PLOT(XH, YL, 4)
C      CALL PLOT(XH, YH, 5)

```

```

000389
000400
000401
000402
000403
000404
000405
000406
000407
000408
000409
000410
000411
000412
000413
000414
000415
000416
000417
000418
000419
000420
000421
000422
000423
000424
000425
000426
000427
000428
000429
000430
000431
000432
000433
000434
000435
000436
000437
000438
000439
000440
000441
000442
000443
000444
000445
000446
000447
000448
000449
000450
000451
000452
000453
000454
000455
000456
000457
000458
000459

```



```

C *****
C *
C * LABEL THE X-AXIS: *
C *
C *****
C
CALL LETTER(NHX,.1,0.,XX,2.7,HD)
DO 3 I=1,NXI
CALL PLOT(XI,YM+.07,3)
CALL PLOT(XII,YM,2)
CALL INCHTO(XII,YM,XW,YW)
ENCODE(10,2,XD) XW
CALL LETTER(10.,1,90.,XH+.05,2.9,XD)
5 XI=XII-XS
  XII=XII
  DO 6 I=1,NP
    MZ=MI(I)
    DO 7 J=1,MZ
      WX(J)=XU(I,J)
7 WY(J)=YU(I,J)
C *****
C *
C * PLOT ALL DATA POINTS BY JOINING SMOOTH LINES *
C * THROUGH ALL DATA POINTS *
C *
C *****
C
CALL NEWPEN(2)
CALL PLTMPL(WX,WY,MZ)
6 CONTINUE
  NHPMAX=NHP1
  IF (NHPMAX.LT.NHP1) NHPMAX=NHP1
  IF (NHPMAX.LT.NHP2) NHPMAX=NHP2
  IF (NHPMAX.LT.NHP3) NHPMAX=NHP3
  XHP=XL-FLOAT(NHPMAX)*0.12
  CALL NEWPEN(2)
  CALL LETTER (NHP1,0.1,0.,XHP,YL-0.4,HP1)
  CALL LETTER (NHP2,0.1,0.,XHP,YL-0.6,HP2)
  CALL LETTER (NHP3,0.1,0.,XHP,YL-0.8,HP3)
  XEND=XL+3.
  CALL PLOT(XEND,0.,-3)
  RETURN
  END
000514
000515
000516
000517
000518
000519
000520
000521
000522
000523
000524
000525
000526
000527
000528
000529
000530
000531
000532
000533
000534
000535
000536
000537
000538
000539
000540
000541
000542
000543
000544
000545
000546
000547
000548
000549
000550
000551
000552
000553
000554
000555
000556
000557

```

APPENDIX E

MIMCROCOMPUTER PROGRAM FOR DETERMINATION OF
THE HYDRAULIC POWER

PROGRAM PLFLOW
=====

DIMENSION IARRYX(2), IARRY(2), IARRYZ(2)

COMMON IPPUL(150), IPDIF(150), IFLOW(150)

2000 WRITE(1,2100)

READ(1,2110)ICOMM

IF(ICOMM.EQ.Z'4554')GO TO 1010

IF(ICOMM.EQ.Z'6574')GO TO 1010

IF(ICOMM.EQ.Z'4650')GO TO 1

IF(ICOMM.EQ.Z'6670')GO TO 1

WRITE(1,2120)

GO TO 2000

2100 FORMAT(' ENTER COMMAND (Pulse Flow or Test) - ')

2110 FORMAT(A2)

2120 FORMAT(' ** COMMAND ERROR ** TYPE 'PF' or 'TE'')

* TEST PROGRAM *

1010 WRITE(1,1100)

READ(1,1110)ISAM

IF(ISAM.EQ.0)GO TO 1030

DO 1020 I=1, ISAM

ITIME=10

INUM=1

CALL PFLOW(IARRY(1), IARRYZ(1), ITIME, INUM)

Y=(FLOAT(IARRY(1))*10.)/512.

Z=(FLOAT(IARRYZ(1))*10.)/512.

WRITE(1,1120)Y,Z

1020 CONTINUE

GO TO 1010

1030 CALL PERD1(IPER)

PERIOD=FLOAT(IPER)/1000.

CALL PERD2(IPOW)

WRITE(1,1130)PERIOD

POWER=FLOAT(IPOW)/1000.

WRITE(1,1140)POWER

GO TO 1030

1100 FORMAT(' ENTER # OF SAMPLES (1-20). ENTER 0 TO READ PERIOD -')

1110 FORMAT(I5)

1120 FORMAT(' Y= ',F10.3,' Z= ',F10.3)

1130 FORMAT(' CYCLE TIME = ',F10.3)

1140 FORMAT(' POWER STROKE TIME = ',F10.3)

```

52      C
53      C *****
54      C *
55      C *
56      C *
57      C * AMP.....AMPLITUDE
58      C * NSYC.....NUMBER OF CYCLES
59      C * ICONT.....CONTROL VARIABLE.EQUALS 0 IF PULSING FLOW,
60      C *          EQUALS 1 IF STEADY FLOW
61      C * FACT1.....CONVERSION FACTOR FOR THE UNITS
62      C * NTSAMP....NUMBER OF TOTAL SAMPLES IN ONE CYCLE
63      C * ITMAX....,MAXIMUM TIME ALLOWED BETWEEN TWO SAMPLES
64      C * ITMIN....MINIMUM TIME ALLOWED BETWEEN TWO SAMPLES
65      C * FREQ.....FREQUENCY
66      C * IWTIME....TIME BETWEEN TWO SAMPLES
67      C * IPDIF....PRESSURE DIFFERENTIAL SIGNAL
68      C * IFLOW....FLOWMETER SIGNAL
69      C * PIPWR....HYDRAULIC POWER IN THE TEST SECTION
70      C *
71      C *****
72      C
73      1   WRITE(1,100)
74          READ(1,101)AMP
75          WRITE(1,200)
76          READ(1,201)NSYC
77          WRITE(1,300)
78          READ(1,301)ICONT
79          WRITE(1,300)
80          READ(1,301)FACT1
81      3   WRITE(1,300)
82          READ(1,301)NTSAMP
83          AREA=0.0
84          NODD=NTSAMP-2
85          NEVEN=NTSAMP-1
86          IF(ICONT.NE.0)GO TO 666
87          ITMAX=32000
88          ITMIN=1
89          SYCT=0.0
90          DO 11 K=1,3
91      C
92      C *****
93      C * CALL ASSEMBLY ROUTINE PERD1 TO CALCULATE THE TIME OF ONE PULSE *
94      C *****
95      C
96          CALL PERD1(ITIME)
97      11  SYCT=SYCT+FLOAT(ITIME)/1000
98          SYCT=SYCT/3.
99          FREQ=1/SYCT
100         WRITE(1,400)FREQ,AMP
101         IWTIME=1000/(NTSAMP*FREQ)
102         IF(IWTIME.LE.ITMAX.OR.IWTIME.GE.ITMIN)GO TO 5
103         WRITE(1,500)
104         GO TO 3
105         CONTINUE

```

```

106      DO 10 L=1,NSYC
107      SUM=0.0
108      C
109      C *****
110      C * CALL ASSEMBLY ROUTINE START1 TO SET THE TIME AT ZERO FOR THE *
111      C * BEGINNING OF A NEW CYCLE *
112      C *****
113      C
114      CALL START1
115      C
116      C *****
117      C * CALL ASSEMBLY ROUTINE PFLOW TO READ SIGNALS FROM THE PRESSURE *
118      C * TRANSDUCER AND THE FLOW METER *
119      C *****
120      C
121      CALL PFLOW(IPDIF,IFLOW,IWTIME,NTSAMP)
122      DO 6 K=2,NEVEN,2
123      6 SUM=SUM+4*(FLOAT(IPDIF(K))*FLOAT(IFLOW(K))*FACT1)
124      DO 7 K=3,NODD,2
125      7 SUM=SUM+2*(FLOAT(IPDIF(K))*FLOAT(IFLOW(K))*FACT1)
126      SUM=SUM+(FLOAT(IPDIF(1))*FLOAT(IFLOW(1))*FACT1)
127      SUM=SUM+(FLOAT(IPDIF(NTSAMP))*FLOAT(IFLOW(NTSAMP))*FACT1)
128      AREA=AREA+FLOAT(IWTIME)*SUM/3000
129      10 CONTINUE
130      PIPWR=AREA/(SYCT*NSYC)
131      WRITE(1,600)PIPPWR
132      GO TO 1
133      656 IWTIME=5
134      DO 999 L=1,NSYC
135      SUM=0.0
136      CALL PFLOW(IPDIF,IFLOW,IWTIME,NTSAMP)
137      DO 777 K=2,NEVEN,2
138      777 SUM=SUM+4*(FLOAT(IPDIF(K))*FLOAT(IFLOW(K))*FACT1)
139      DO 888 K=3,NODD,2
140      888 SUM=SUM+2*(FLOAT(IPDIF(K))*FLOAT(IFLOW(K))*FACT1)
141      SUM=SUM+(FLOAT(IPDIF(1))*FLOAT(IFLOW(1))*FACT1)
142      SUM=SUM+(FLOAT(IPDIF(NTSAMP))*FLOAT(IFLOW(NTSAMP))*FACT1)
143      999 AREA=AREA+FLOAT(IWTIME)*SUM/3
144      PIPWR=AREA/(IWTIME*NTSAMP*NSYC)
145      WRITE(1,700)PIPPWR
146      GO TO 1
147      100 FORMAT(/,' ENTER AMPLITUDE = ')
148      101 FORMAT(F6.2)
149      200 FORMAT(/,' ENTER NUMBER OF CYCLES REQUIRED = ')
150      201 FORMAT(I3)
151      300 FORMAT(/,' ENTER NUMBER OF SAMPLES PER CYCLE = ')
152      301 FORMAT(I4)
153      400 * FORMAT(/,3X,' FREQ = ',F6.3,3X,' AMP = ',F6.2)
154      500 FORMAT(/,' ***** RESET FREQUENCY *****')
155      600 FORMAT(/,' HYDRAULIC POWER IN TEST SECTION = ',F15.3)
156      900 FORMAT(/,' ENTER CONVERSION FACTOR = ')
157      901 FORMAT(1F10.5)
158      800 FORMAT(/,' IF PULSING FLOW TEST ENTER 0 , IF STEADY FLOW',
159      1 ' TEST ENTER 1 ??? ')
160      801 FORMAT(I2)
161      700 FORMAT(/,' HYDRAULIC POWER IN TEST SECTION = ',F15.3)
162      STOP
163      END

```

APPENDIX F
ERROR ANALYSIS OF EXPERIMENTAL DATA

Basic Measurements:

$$\Delta P = \pm 5 \text{ m.v}/1.0 \text{ v} = \pm 0.05\%$$

$$Q = \pm 0.1/30.0 = \pm 0.3\%$$

$$\lambda = \pm 5 \text{ ms}/1.0 \text{ s} = \pm 0.5\%$$

$$A = \pm 1 \text{ mm}/34.6 \text{ mm} = \pm 3\%$$

$$C_w = \pm 1.0\%$$

$$d = \pm 0.5\%$$

$$D = \pm 1.0\%$$

Derived Groups:

$$V = \pm 1.3\%$$

$$\frac{\pi A \left[\frac{D}{d} \right]^2}{V} \lambda = \pm 7.8\%$$

$$J_p = \pm 6.3\%$$

$$J_s = \pm 1.8\%$$

$$J_p/J_s = \pm 8.25\%$$